QUANTUM MECHANICAL STUDIES OF MOLECULAR SCATTERING

Thesis by

John Patrick Dwyer

In Partial Fulfillment of the Requirements
For the Degree of
Doctor of Philosophy

California Institute of Technology
Pasadena, California

1978
(Submitted June 27, 1977)

To John A. Ricketts

ACKNOWLEDGEMENTS

I gratefully acknowledge the help and advice of my advisor, Professor Aron Kuppermann. His genuine interest in my research and his seemingly endless store of ideas made my studies at Caltech challenging and exciting. He encouraged me to work independently, but he was always available and eager to listen to my half-formed ideas. It has been a pleasure to work with him.

I wish to thank the present and past members of the Kuppermann group for the years of scientific interaction. In particular, I am grateful to Professors George Schatz and Joel Bowman for their patience and insights during my first two years here. I would also like to thank Dr. Henry Suzukawa, Dr. Gregory Parker, and Mr. Jack Kaye for many useful discussions and many hours of assistance this past year. Equally as important, they have been good friends. I would especially like to thank Mr. Mark Keil. Although our many scientific discussions were valuable to my thinking and my research, I value his friendship most highly.

I would like to thank Adria McMillan, the Kuppermann group secretary. Her expert typing of the manuscript in this thesis (including all of her grammatical and scientific corrections) has been invaluable.

I am indebted to other members of the Caltech community, most notably Professor William A. Goddard III and his group. Their collective patience in explaining the eccentricities of the MQM programs was boundless.

I thank the National Science Foundation for a fellowship which supported me during my first three years. I thank Ambassador College

for the use of their computer facilities.

The past three months have been, at times, difficult and depressing (as future thesis writers will someday discover). Were it not for Francie Levitt's constant love and encouragement, I would have had a more difficult time persevering. Thank you, Francie.

My parents have been wonderful. Never losing faith, they watched their eldest son stumble through his early twenties, painfully aware that each of us must make his own mistakes and triumphs. I think that we all have grown and are now a bit wiser for the experiences.

This thesis is dedicated to my undergraduate advisor, Professor John A. Ricketts. He has been a true friend and a superb teacher. He has challenged me, prodded me, and helped me. His grasp of the subject and his willingness to learn, his critical attitude and his affection for his students have made him the best teacher I have ever known. His inimitable style and wit will never be forgotten. More than any other person, he is responsible for my entering Caltech. Any accomplishments I have made here are to some extent a product of his continued interest in my welfare.

"The philosophers have only interpreted the world in various ways; the point is, to change it."

Karl Marx

ABSTRACT

This thesis is not about changing the world. Its scope is much more modest; we wish only to describe a very small part of it. In fact, we will usually restrict ourselves to only three or four atoms at any one time.

This thesis is a collection of seven theoretical studies on elementary chemical processes. In each of the studies we have used a quantum mechanical framework to describe a particular chemical system. In nearly every case we have formulated the problem exactly. That is, we have made no mathematical approximations to the governing equations. Because these problems are too complex to be solved analytically, we have turned to computers to solve them numerically. Once the appropriate equations have been derived, each study becomes an exercise in numerical techniques and computer programming. The crucial step, interpretation of the numbers, comes last.

In the first chapter we examine a model that describes energy transfer in the collinear collision of two diatomic molecules. In this system the diatomics are homonuclear Morse oscillators and interact through an exponentially repulsive potential. We compare our results with previous quantum calculations and find that the older results were not converged with respect to the number of basis functions. A comparison with the adiabatic approximation of Clarke and Thiele shows that the approximate results are reasonably accurate at all but the highest collision energies.

The second chapter is a study of the importance of low energy reaction probabilities in calculating low temperature rate constants. It

is limited to the collinear H + H_2 reactive system using a realistic potential energy surface. We show that the integral which relates probabilities to rate constants must be calculated carefully in order to avoid numerical errors. We show that this was not done by other workers and has probably led to an incorrect conclusion concerning the isotope dependence of the transmission coefficient.

The third chapter is a survey of resonances in the reactive scattering of collinear H + H_2 and its symmetric isotopic variants. From the survey we note trends and differences in the resonance strengths and positions caused by the various mass combinations. This leads us to propose a simple model for collinear scattering which should predict resonances. In fact, it correctly predicts their relative strengths and their positions to better than 0.08 eV.

The fourth chapter is an extensive study of the effect of barrier heights on vibrational deactivation in collinear scattering. The five surfaces used were for the H + FH system with barriers ranging from 1.5 kcal/mole to 40 kcal/mole. The motivation for the study comes from recently published work which indicates that the correct barrier in the HFH arrangement channel is much closer to 40 kcal/mole than the often used 1.5 kcal/mole. The results indicate that the large barriers significantly reduce the rate of collisional deactivation via reaction, but that nonreactive deactivation is roughly constant for a wide range of barrier heights.

In Chapter 5 we propose a method to describe collinear breakup collisions of the form A + BC $\rightarrow$ A + B + C. The method is general and can be applied to systems in which the energy is too low to allow

dissociation. It has been applied to the H + H_2 reaction and found to accurately reproduce reaction probabilities at low energies. The central idea is to use a discrete pseudo-vibrational basis set which can describe both bound and continuum states naturally. This preliminary work points the way to further calculations.

In the last two chapters we move to three-dimensional collisions. Chapter 6 is a comparison of two independent calculations of reactive scattering in an actual chemical system, one by Elkowitz and Wyatt (EW) and the other by Schatz and Kuppermann (SK). The comparison shows that the results are qualitatively and quantitatively different. It further shows that differences lie in the separate formulations of the problem and that the SK method is numerically converged while the EW is not. We note that the EW method used certain approximations that were not investigated and conclude that their results are in error.

In the last chapter we consider the difficulty of doing exact quantum calculations for even simple reactive systems and propose a mathematical approximation that preserves the accuracy of the exact results. The approximation arises from the neglect of certain off-diagonal angular momentum terms in the Hamiltonian and thus reduces the number of coupled equations to be solved simultaneously. We find that the computation time can be reduced by as much as a factor of 20.

TABLE OF CONTENTS

CHAPTER 1.

Validity of the Adiabatic Approximation for Vibrational Energy Transfer in Collisions Between Diatomic Molecules

VALIDITY OF THE ADIABATIC APPROXIMATION FOR VIBRATIONAL ENERGY TRANSFER IN COLLISIONS BETWEEN DIATOMIC MOLECULES[†]

John P. DWYER[*] and Aron KUPPERMANN
Arthur Amos Noyes Laboratory of Chemical Physics,[‡]
California Institute of Technology, Pasadena, California 91125, USA

(Received)

Accurate quantum mechanical transition probabilities for vibrational to vibrational and vibrational to translational energy transfer in collinear collisions of two hydrogen molecules were calculated for a model potential by numerical integration of the Schrödinger equation. The accuracy of these calculations was checked by conservation of flux and convergence tests and by verifying that they satisfied a rigorous theorem proven by Clarke and Thiele. These accurate results were then used to determine the range of validity of the adiabatic approximation of Thiele and Katz as applied to this model system by Clarke and Thiele. This approximation yielded probabilities which agreed with the accurate ones to 10% or better for total energies E up to 6.1 (in units of diatom vibrational quanta). However, at E = 7.9 these approximate results could be off by a factor of 1.5 or higher.

[†]Research supported in part by the Air Force Office of Scientific Research, Grant AFOSR 73-2539.

[*]In partial fulfillment of the requirements for the Ph.D. degree in Chemistry at the California Institute of Technology.

[‡]Contribution No. 5395.

1. Introduction

In a recent paper [1] (hereafter called I) Clarke and Thiele studied energy transfer in the collinear collision of two diatomic molecules. After reducing the problem to a pseudo atom-diatom collision (using a method developed by Zelechow et al. [2], they used the adiabatic approximation of Thiele and Katz [3] and the first order distorted wave $\underline{\underline{T}}$ and $\underline{\underline{K}}$ matrix methods to calculate vibrational-vibrational (V-V) and translational-vibrational (T-V) transition probabilities. In a previous paper [4] (hereafter called II), Riley and Kuppermann calculated the exact quantum transition probabilities for the same system. Because of the special form of the interaction potential used, (exponentially repulsive), part of the calculation can be done analytically. From this information, Clarke and Thiele were able to show that some of the probabilities calculated in II must be inaccurate. We have redone the Riley and Kuppermann calculations and have found that the number of basis functions which had been used was insufficient for convergence. Using larger basis sets we have obtained converged results which also satisfy the conditions derived in I.

2. Theory

We will briefly examine the equations to be solved. A more complete treatment is given by Riley [5]. The diatomic molecules are assumed to be harmonic oscillators, confined to move on a space-fixed straight line while the intermolecular potential is

exponentially repulsive and dependent only on the nearest end-atom separation. The Schrödinger equation to be solved is

$$\left[\left(-\frac{\partial^2}{\partial y^2} + y^2\right) + \omega\left(-\frac{\partial^2}{\partial x^2} + x^2\right) - \frac{1}{\mu}\frac{\partial^2}{\partial r^2} + e^{-\alpha(r-y-\beta x)} - E\right]\psi(x,y,r) = 0 \tag{1}$$

where r describes the intermolecular separation, x and y are related to the intramolecular separations, μ is an effective mass of the system, E is the total energy, ω and β are measures of the relative frequencies of the oscillators,and α is a length which describes the nearest end-atom repulsion. All of these parameters are in reduced units. Following I and II we treated the case of identical homonuclear diatomics, which results in $\mu = \frac{1}{2}$, $\beta = 1$, and $\omega = 1$. The value of α was taken to be 0.2973 as before, which is appropriate for describing a collision between two hydrogen molecules. We define the reference hamiltonian H_0 by

$$H_0(x,y) = \left(-\frac{\partial^2}{\partial y^2} + y^2\right) + \omega\left(-\frac{\partial^2}{\partial x^2} + x^2\right), \tag{2}$$

whose eigenfunctions and eigenvalues are denoted by $\Phi_{ij}(x,y)$ and W_{ij}, respectively, i and j being the vibrational quantum numbers of the isolated molecules. The separability of the x and y coordinates in eq. (2) permits us to write

$$\Phi_{ij}(x,y) = \phi_i(y)\,\phi_j(x) \tag{3}$$

and

$$W_{ij} = (2i + 1) + \omega\,(2j + 1). \tag{4}$$

The solutions $\psi^{n'm'}(x,y,r)$ of eq. (1) can be expanded in the $\Phi_{ij}(x,y)$ basis set to give

$$\psi^{n'm'}(x,y,r) = \sum_{n=0}^{N-1} \sum_{m=0}^{M-1} f_{nm}^{n'm'}(r)\, \Phi_{nm}(x,y) \tag{5}$$

$$n' = 0, \ldots, N-1$$
$$m' = 0, \ldots, M-1$$

where N and M are the number of eigenstates in the expansion for coordinates y and x, respectively. For the present case N = M, and the transition probabilities are considered converged when increasing N produces in them an acceptably small change.

Substituting eq. (5) into eq. (1) gives the following set of coupled differential equations

$$[f_{nm}^{n'm'}(r)]'' = [V_{nm}^{n'm'}(r) - k_{nm}^2]\, f_{nm}^{n'm'}(r) \tag{6}$$

where

$$V_{nm}^{n'm'}(r) = \mu < \Phi_{nm}(x,y) \left| e^{-\alpha(r-y-\beta x)} \right| \Phi_{n'm'}(x,y) > \tag{7}$$

and

$$k_{nm} = [\mu(E - W_{nm})]^{\frac{1}{2}}, \tag{8}$$

the integrations implied in eq. (7) being performed over the x and y coordinates. These equations are solved by a method described previously [5].

3. Results and Discussion

The results for N = 5 and N = 6 are presented in tables 1 and 2 for a variety of transitions and of total energies (in units of diatom vibrational quanta). Included are the values of Riley and Kuppermann (N = 3) and those of Clarke and Thiele. In I, Clarke and Thiele present a partial decoupling scheme which reduces the problem to a pseudo atom-diatom collision. Although they used approximate methods to calculate transition probabilities, they showed rigorously that

$$\frac{P_{00 \to 11}}{P_{00 \to 02}} = 2$$

where $P_{ij \to k\ell}$ is the probability of going from the i, j states of the initial molecules to the corresponding k, ℓ states of the final ones. On the basis of this result they were able to conclude that certain of the transition probabilities calculated in II are incorrect. Table 3 lists this ratio for various choices of N. First note that the results in tables 1 and 2 are nearly identical for N = 5 and N = 6. The largest discrepancy is 1 part in 2000. In addition, table 3 shows that the ratio $P_{00 \to 11}/P_{00 \to 02}$ has converged to 2 to within this accuracy, in agreement with Clarke and Thiele's predictions. From this and the fact that flux conservation is satisfied in these calculations to six significant digits, we conclude that our results have not only converged but are also accurate. At the lowest energies (4.1 and 4.5) the Clarke and Thiele approximate results agree with our accurate ones to better than

1%. In general, the inaccuracy is less than 10% for all transitions at $E \leq 6.1$. However, at $E = 7.9$, their result for the $01 \rightarrow 20$ transition is too large by a factor of about 2.

For V-V transitions, the results of Riley and Kuppermann are in good agreement with ours for the transition involving the lowest internal excitation ($01 \rightarrow 10$). As expected, the agreement is somewhat worse for higher internal excitation transitions. For T-V transitions, the agreement is good only for the lowest four energies of the $00 \rightarrow 01$ transition.

We conclude that the adiabatic method of Thiele and Katz gives results for this model problem in good agreement with the exact quantum probabilities for all but the highest energies considered.

Table 1. Transition probabilities for the V-V energy transfer of 1 and 2 quanta.

Transition	E[a]	Riley and Kuppermann[b] M = N = 3	Clarke and Thiele[c]	M = N = 5	M = N = 6
01 → 10	4.1	0.4100×10^{-2}	0.4100×10^{-2}	0.4100×10^{-2}	0.4100×10^{-2}
	4.5	0.2109×10^{-1}	0.2094×10^{-1}	0.2109×10^{-1}	0.2109×10^{-1}
	5.0	0.4376×10^{-1}	0.4285×10^{-1}	0.4376×10^{-1}	0.4376×10^{-1}
	5.5	0.6805×10^{-1}	0.6545×10^{-1}	0.6808×10^{-1}	0.6808×10^{-1}
	6.1	0.9894×10^{-1}	0.9319×10^{-1}	0.9924×10^{-1}	0.9924×10^{-1}
	7.0	0.1459	0.1371	0.1483	0.1483
	7.9	0.1875	0.1780	0.1957	0.1957
02 → 11	6.1	0.7821×10^{-2}	0.7843×10^{-2}	0.7850×10^{-2}	0.7850×10^{-2}
	7.0	0.7609×10^{-1}	0.7882×10^{-1}	0.8033×10^{-1}	0.8033×10^{-1}
	7.9	0.1317	0.1480	0.1544	0.1544
02 → 20	6.1	0.1695×10^{-4}	0.1710×10^{-4}	0.1711×10^{-4}	0.1711×10^{-4}
	7.0	0.1571×10^{-2}	0.1707×10^{-2}	0.1780×10^{-2}	0.1780×10^{-2}
	7.9	0.5165×10^{-2}	0.6508×10^{-2}	0.7248×10^{-2}	0.7248×10^{-2}

a) Total energy in units of diatom vibrational quanta.

b) References [4] and [5].

c) References [1], using the adiabatic method of Thiele and Katz [3].

Table 2. Transition probabilities for the T-V energy transfer of 1 and 2 quanta.

Transition	E[a]	Riley and Kuppermann[b] M = N = 3	Clarke and Thiele[c]	M = N = 5	M = N = 6
00 → 01	4.1	0.169×10^{-5}	0.167×10^{-5}	0.1665×10^{-5}	0.1665×10^{-5}
	4.5	0.784×10^{-4}	0.802×10^{-4}	0.7883×10^{-4}	0.7884×10^{-4}
	5.0	0.650×10^{-3}	0.672×10^{-3}	0.6503×10^{-3}	0.6503×10^{-3}
	5.5	0.231×10^{-2}	0.244×10^{-2}	0.2325×10^{-2}	0.2325×10^{-2}
	6.1	0.641×10^{-2}	0.701×10^{-2}	0.6568×10^{-2}	0.6568×10^{-2}
	7.0	0.174×10^{-1}	0.207×10^{-1}	0.1879×10^{-1}	0.1879×10^{-1}
	7.9	0.326×10^{-1}	0.439×10^{-1}	0.3854×10^{-1}	0.3854×10^{-1}
01 → 11	6.1	0.195×10^{-5}	0.169×10^{-5}	0.1691×10^{-3}	0.1691×10^{-5}
	7.0	0.826×10^{-3}	0.675×10^{-3}	0.6513×10^{-3}	0.6512×10^{-3}
	7.9	0.653×10^{-2}	0.514×10^{-2}	0.4745×10^{-2}	0.4745×10^{-2}
01 → 02	6.1	0.111×10^{-5}	0.324×10^{-5}	0.3238×10^{-5}	0.3237×10^{-5}
	7.0	0.152×10^{-3}	0.128×10^{-2}	0.1168×10^{-2}	0.1188×10^{-2}
	7.9	0.444×10^{-3}	0.122×10^{-1}	0.8269×10^{-2}	0.8270×10^{-2}
01 → 20	6.1	0.560×10^{-7}	0.115×10^{-6}	0.1216×10^{-6}	0.1216×10^{-6}
	7.0	0.455×10^{-4}	0.629×10^{-4}	0.1139×10^{-3}	0.1139×10^{-3}
	7.9	0.413×10^{-3}	0.258×10^{-2}	0.1314×10^{-2}	0.1314×10^{-2}
00 → 11	6.1	0.150×10^{-7}	0.998×10^{-8}	0.1128×10^{-7}	0.1128×10^{-7}
	7.0	0.224×10^{-4}	0.989×10^{-5}	0.1262×10^{-4}	0.1262×10^{-4}
	7.9	0.397×10^{-3}	0.120×10^{-3}	0.1945×10^{-3}	0.1944×10^{-3}
00 → 02	6.1	0.350×10^{-8}	0.494×10^{-8}	0.5638×10^{-8}	0.5639×10^{-8}
	7.0	0.189×10^{-5}	0.494×10^{-5}	0.6308×10^{-5}	0.6309×10^{-5}
	7.9	0.181×10^{-4}	0.599×10^{-4}	0.9720×10^{-4}	0.9722×10^{-4}

a) Total energy in units of diatom vibrational quanta.

b) References [4] and [5].

c) Reference [1], using the adiabatic method of Thiele and Katz [3] except for the 00 → 11 and 00 → 02 transitions, for which the "corrected" adiabatic results are given.

Table 3. Ratio of $P_{00 \rightarrow 11}$ and $P_{00 \rightarrow 02}$ probabilities.

E[a]	Riley and Kuppermann[b] M = N = 3	M = N = 4	M = N = 5	M = N = 6
6.1	4.314	1.998	2.000	2.000
7.0	11.84	2.012	2.001	2.000
7.9	21.96	2.185	2.000	2.000

a) Total energy in units of diatom vibrational quanta.

b) From the data of references [4] and [5].

References

[1] J. Clarke and E. Thiele, Chem. Phys. 4 (1974) 447.

[2] A. Zelechow, D. Rapp and T. Sharp, J. Chem. Phys. 48 (1968) 286.

[3] E. Thiele and R. Katz, J. Chem. Phys. 55 (1971) 3195.

[4] M. Riley and A. Kuppermann, Chem. Phys. Lett. 1 (1968) 537.

[5] M. Riley, Ph.D. Thesis, California Institute of Technology (1968).

CHAPTER 2.

The Importance and Treatment of Low Energy Reaction Probabilities for Low Temperature Rate Constants

Two papers have been published [1, 2] in which the authors reach conflicting conclusions on the importance of transmission coefficients in calculating isotope effects, especially at low temperatures. Each of the studies was limited to the collinear $H + H_2$ reactive system and its deuterium-substituted variants.

In the first paper [1], Wu, Johnson, and Levine calculated exact quantum transmission probabilities using a close-coupling method formulated in natural collision coordinates. The potential energy surface used was the semi-empirical Porter-Karplus [3] (PK) H_3 surface. The reactions they studied on this surface were the deuterium substitutes of $H + H_2$:

$$H + H_2 \rightarrow H_2 + H \qquad \text{(a)}$$

$$D + D_2 \rightarrow D_2 + D \qquad \text{(b)}$$

$$D + H_2 \rightleftharpoons DH + H \qquad \text{(c and d)}$$

$$H + D_2 \rightleftharpoons HD + D \qquad \text{(e and f)}$$

$$H + DH \rightarrow HD + H \qquad \text{(g)}$$

$$D + HD \rightarrow DH + D \qquad \text{(h)}$$

From the exact transmission probabilities, one can calculate the exact rate constant, which is given by (in the notation of Wu, Johnson, and Levine)

$$k_{rate}(T) = (2\pi\mu kT)^{-\frac{1}{2}} \frac{1}{Q_I^{int}(T)} \sum_i f_i \exp(-E_i/kT) \int_0^\infty P_r(E_R^i, i) \times \exp(-E_R^i/kT) dE_R^i , \qquad (1)$$

where E_R^i is the relative translational energy, k is Boltzmann's constant,

E_i is the internal energy of state i (with degeneracy f_i), Q_I^{int} is the reactant partition function, P_r is the reaction probability from state i to all possible final states, and $\mu = m_A m_{BC}/(m_A + m_{BC})$ is the reduced mass of the initial A + BC system. In the temperature range considered (200-1250°K), only the ground vibrational state is significantly populated and eq.(1) reduces to (assuming no ground state degeneracy)

$$k_{rate}(T) = (2\pi\mu kT)^{-\frac{1}{2}} \int_0^\infty P_r(E_R, 0)\exp(-E_R/kT)dE_R \,, \qquad (2)$$

where $E_R^0 = E_R$. One can write an analogous equation for the classical hard sphere model of reactive scattering where the classical transmission probability $P_C(E_R) = 1$ for $E_R \geq E^0$ and $P_C(E_R) = 0$ for $E_R < E^0$ and where E^0 is the barrier height along the reaction coordinate corrected for the difference in the zero-point energies between the activated complex and the reactant. This correction is important because the barrier height is not equal to the minimum energy necessary to clear the barrier. That energy is actually equal to the difference between the activated complex zero-point energy (measured relative to the bottom of the diatom potential) and the asymptotic zero-point energy. The ratio of the quantum rate constant to the classical rate constant is called the transmission coefficient, $\kappa(T)$, and is given by

$$\kappa(T) = \frac{\int_0^\infty P_r(E_R)\exp(-E_R/kT)dE_R}{\int_0^\infty P_C(E_R)\exp(-E_R/kT)dE_R}$$

$$= \frac{\exp(E^0/kT)}{kT}\int_0^\infty P_r(E_R)\exp(-E_R/kT)dE_R$$

$$= \left(\frac{2\pi\mu}{kT}\right)^{\frac{1}{2}} \exp(E^{0}/kT) k_{rate}(T). \qquad (3)$$

The transmission coefficient is a measure of the deviation of the chemical system from classical mechanics. The isotope effect is measured by the ratio of the rate constants (at a temperature T) for two isotopically different reactions. In transition state theory, this ratio is directly proportional to the ratio of the transmission coefficients and inversely proportional to the square root of the reduced masses.

Using the exact quantum transmission probabilities for each of reactions (a)-(h), Wu et al. calculated the transmission coefficients corresponding to each reaction. They found that at each temperature, the transmission coefficients for all eight reactions were roughly comparable, differing at most by 45%. From this they concluded that the isotope effect is dominated by other factors (differences in zero-point energies and differences in reduced masses) and is not strongly affected by transmission coefficients. In other words, in calculating the ratios of rate constants of two reactions, the ratio of transmission coefficients may be set to unity. This conclusion, if correct, allows one to neglect the transmission coefficient calculations (which requires exact probabilities) in determining the isotope effect.

In a more recent paper [2], Truhlar, Kuppermann, and Adams also studied the isotope effect in the collinear $H + H_2$ exchange reaction in the 200-1250°K temperature range. The potential energy surface that they used [4] was a Wall-Porter [5] fit to the SSMK surface [6], which is a surface different from the one used by Wu et al. They used a modified version [4] of the finite-difference

boundary-value method of Diestler and McKoy [7] to calculate exact quantum transmission probabilities for reactions (a)-(f). They found, however, that by setting the ratio of transmission coefficients to unity (i.e., isotope independent), transition state theory predicted ratios of rate constants in error by as much as a factor of 4.6 at 200°K and 0.56 at 300°K. This is a contradiction to the conclusions of Wu et al. at low temperatures.

The discrepancy could be attributed to a couple of factors (assuming no simple arithmetic error is involved). One, the potential surfaces used in the two studies are not identical. This could be critical for low temperature studies, because small changes in the barrier (thickness, height), for example, could significantly affect transmission probabilities calculated at or below the classical threshold. Two, the difference could arise from the way low energy probabilities were treated in calculating rate constants. At very low translational energies, P_r changes by orders of magnitude. The method by which low energy probabilities are interpolated may be important for low temperature rate constants.

In order to resolve the contradictory conclusions of Wu et al. and Truhlar et al., it is important to remove the possibility of the first type of error. To do this we have calculated exact quantum transmission probabilities for the H + H_2 exchange reaction using the close-coupling method of Kuppermann [8] as applied to the PK surface. Using these results, we have calculated both rate constants and transmission coefficients in the range 200-1000°K. These results can be compared with those of Wu et al.

As mentioned above, the method by which low energy probabilities are interpolated is critical. In an earlier study, Truhlar and Kuppermann [4] found that the transmission probability could be accurately represented at classically forbidden energies (0.043 eV < E_R < 0.151 eV) by

$$P_r(E_R) = \exp[\beta(E_R - V_0)],$$

where V_0 = 0.286 eV and β = 51.1 eV^{-1}. However, this expression extrapolates to an incorrect value for E_R = 0. The small deviation ($\sim 5 \times 10^{-7}$) produces large errors in the rate constant at 250°K. They found a more accurate fit at very low energies (0.005 eV < E_R < 0.083 eV) to be

$$P_r(E_R) = e^{-\beta V_0}[\exp(\beta E_R) - 1],$$

where V_0 = 45.9 eV and β = 0.309 eV^{-1}. This expression extrapolates to the correct value of $P_r(0)$. The conclusion to be drawn is that when calculating rate constants from eq.(2), one should not interpolate probabilities but rather logarithms of probabilities.

In this present work, we calculated transmission probabilities at energies as low as 10^{-6} eV, where the reaction probability is 9.5×10^{-20}. We have found that it is much more accurate to interpolate $\log P_r(E_R)$ than $P_r(E_r)$. Low temperature rate constants calculated from linearly interpolated probabilities can be in error by as much as an order of magnitude. Linear and quadratic interpolation of $\log P_r$ gave rate constants which agreed to within 2%. Figure 1 is a plot of $P_r(E_R)$ on a log scale versus translational energy. The linearity of the plot demonstrates the need to interpolate $\log P_r(E_R)$ at low energies. In our rate constant

calculation we employed both a Simpson rule and a trapezoidal rule integration method. The results agreed to within 2% at all temperatures. For all the results presented here we have used the Simpson rule method.

It is difficult to compare directly the work of Wu et al. with our results for two reasons. One, Wu et al. did not publish their rate constants, only their transmission probabilities and transmission coefficients. Two, the transmission probabilities that they published are given to only three decimal places, precluding any values smaller than 10^{-3}. The latter makes an accurate calculation of low temperature rate constants difficult or impossible.

In our rate constant calculation we found that neglecting probabilities smaller than 3.2×10^{-5} ($E_R < 0.09$ eV) lowered the rate constant at 200°K by only 1%. Because Wu et al. considered translational energies as low as 0.078 eV, neglect of lower energy probabilities should not have significantly affected their rate constant calculation at the temperatures considered. Figure 2 is a comparison of $P_r(E_R)$ from our results and from Wu et al. We can see that there are no gross differences between the two. In Table 1 we have listed the rate constants of Wu et al. which we calculated using eq.(3) and their published values of the transmission coefficients. In calculating their rate constants, we have used their value of the zero-point energy, 0.2689 eV. For comparison we have listed rate constants calculated from our transmission probabilities using a more accurate [9] value for the zero-point energy of 0.258 eV. One can see that only at very high temperatures is there reasonable ($\sim 10\%$) agreement between the results; at low temperatures

our results are larger by as much as a factor of two. In Table 2 we have listed transmission coefficients as published by Wu et al. and those calculated from our rate constants using two values for E^0, one from Wu et al. and the more accurate one. The agreement at very low temperatures is poor, with the differences as large as a factor of two. While this does not pinpoint the source of any possible error, it does show that the contradictions that existed between Wu et al. and Truhlar et al. continue to exist between our results and those of Wu et al., even though we are using the same potential energy surface.

To resolve this, we calculated rate constants from the published transmission probabilities of Wu et al. Because their published probabilities are not sufficiently precise, we have repeated the calculations using $P_r(E_R) \pm 0.0005$. Another difficulty is that Wu et al. listed their probabilities by total energy, whereas rate constants must be calculated using translational energy. Thus we calculated rate constants from their probabilities using both their inaccurate value for the zero-point energy and the accurate value [9]. All of these calculations are in Table 3. Two things are noteworthy. One, none of the low temperature rate constants are close to the Wu, Johnson and Levine results in Table 1. At or below 400 °K, the difference is greater than 23%. Two, our rate constants (column two of Table 1) lie between the corresponding values in the last two columns of Table 3, indicating that their probabilities may be good enough to calculate accurate rate constants if the correct zero-point energy is used.

For a final comparison we have calculated transmission coefficients from the rate constants in Table 4. Columns one through three

use the (inaccurate) values of zero-point energy and E^0 given by Wu et al. Columns four through six use the more accurate values. One can see that none of the low temperature transmission coefficients agree with the results published by Wu, Johnson, and Levine. Our results, in column two of Table 2, generally are outside the possible range of their transmission coefficients calculated using inaccurate values for E^0 and zero-point energy. Using their probabilities as published and using accurate values for zero-point energy and E^0, their transmission coefficients (column four of Table 4) differ from ours (column two of Table 2) by only 7.8% at the lowest temperature and 1% or less at all higher temperatures.

Concluding Remarks

We have seen the importance of low energy probabilities in calculating low temperature rate constants. Equally important, however, is the way in which the probabilities are interpolated for the integral in eq.(2). Care must be taken to ensure that the probabilities are interpolated in a manner consistent with their analytical representation. In light of these results, the conclusions of Wu, Johnson, and Levine regarding isotope-independent transmission coefficients should be reexamined. Because Truhlar et al. used an interpolation procedure similar to ours, their rate constants seem to be accurate. Unless the two potential surfaces (the Wall-Porter fit to the SSMK and the PK) are quite different, transmission coefficients will not be isotope-independent at temperatures below 400°K.

Table 1

Comparison of rate constants for $H + H_2$

T(°K)	$k_{rate}(T)$[a]	
	WJL[b]	present work[c]
200	4.64(-1)[d]	9.42(-1)
300	2.07(1)	3.16(1)
400	1.61(2)	2.23(2)
500	5.98(2)	7.73(2)
800	4.83(3)	5.66(3)
900	7.27(3)	8.37(3)
1000	1.02(4)	1.15(4)

a) The units are cm/(molec•sec).

b) Wu, Johnson and Levine, ref. [1]; zero-point energy: 0.2689 eV.

c) Zero-point energy: 0.2727 eV.

d) Numbers in parentheses are powers of ten by which entries should be multiplied.

Table 2

Comparison of transmission coefficients for $H + H_2$

T(°K)	$\kappa(T)$[a] WJL[b]	present work[c]	present work[d]
200	30.2	47.6	61.5
300	6.79	8.88	10.52
400	3.68	4.47	5.08
500	2.66	3.11	3.44
800	1.73	1.90	2.03
900	1.61	1.75	1.85
1000	1.52	1.64	1.72

a) Unitless.

b) Wu, Johnson and Levine, ref. [1]; $E^0 = 0.2624$ eV.

c) $E^0 = 0.258$ eV.

d) $E^0 = 0.2624$ eV.

Table 3

Rate constants for $H + H_2$ using reaction probabilities of Wu, Johnson and Levine

T(°K)	k_{rate} (cm molec^{-1} sec^{-1})					
200	6.97(-1)[a]	6.92(-1)	8.70(-1)	8.68(-1)	8.62(-1)	1.08
300	2.70(1)	2.70(1)	2.80(1)	3.13(1)	3.13(1)	3.25(1)
400	1.99(2)	1.99(2)	2.01(2)	2.22(2)	2.22(2)	2.24(2)
500	7.06(2)	7.06(2)	7.10(2)	7.71(2)	7.71(2)	7.75(2)
800	5.35(3)	5.35(3)	5.36(3)	5.65(3)	5.65(3)	5.66(3)
900	7.96(3)	7.96(3)	7.97(3)	8.36(3)	8.36(3)	8.37(3)
1000	1.10(4)	1.10(4)	1.10(4)	1.15(4)	1.15(4)	1.15(4)
reaction probabilities[b]	published	r.d.	r.u.	published	r.d.	r.u.
zero-point energy	0.2689[c]	0.2689	0.2689	0.2727[d]	0.2727	0.2727

[a] Numbers in parentheses are powers of ten by which entries should be multiplied.

[b] Published: uses published probabilities of Wu, Johnson and Levine; r.d.: round down by 0.0005 (except for values of 0.000 which were taken as published); r.u.: round up by 0.0005.

[c] Wu, Johnson and Levine.

[d] Accurate value.

Table 4

Transmission coefficients for $H + H_2$ calculated from the reaction probabilities of Wu, Johnson and Levine

T (°K)	κ(T)					
200	45.1	45.1	56.7	43.9	43.6	54.6
300	8.99	8.99	9.32	8.79	8.79	9.13
400	4.54	4.54	4.58	4.45	4.45	4.49
500	3.14	3.14	3.16	3.10	3.10	3.11
800	1.92	1.92	1.92	1.90	1.90	1.90
900	1.76	1.76	1.76	1.75	1.75	1.75
1000	1.65	1.65	1.65	1.64	1.64	1.64
reaction probabilities [a]	published	r.d.	r.u.	published	r.d.	r.u.
zero-point energy (eV)	0.2689 [b]	0.2689	0.2689	0.2727 [c]	0.2727	0.2727
E^0 (eV)	0.2624 [b]	0.2624	0.2624	0.258 [c]	0.258	0.258

[a] r.d.: round down; r.u.: round up (see footnote b), Table 3).

[b] Wu, Johnson and Levine. [c] Accurate.

References

[1] S.-f. Wu, B. R. Johnson and R. D. Levine, Mol. Phys. 25 (1973) 609.

[2] D. G. Truhlar, A. Kuppermann and J. T. Adams, J. Chem. Phys. 59 (1973) 395.

[3] R. N. Porter and M. Karplus, J. Chem. Phys. 40 (1964) 1105.

[4] D. G. Truhlar and A. Kuppermann, J. Chem. Phys. 56 (1972) 2232.

[5] F. T. Wall and R. N. Porter, J. Chem. Phys. 36 (1962) 3256.

[6] I. Shavitt, R. M. Stevens, F. L. Minn and M. Karplus, J. Chem. Phys. 48 (1968) 2700.

[7] D. J. Diestler and V. McKoy, J. Chem. Phys. 48 (1968) 2951.

[8] A. Kuppermann, Proceedings of a Conference on Potential Energy Surfaces in Chemistry, W. A. Lester, Jr., Ed. (IBM Research Laboratory, San Jose, California, 1971), pp. 121-134; Abstracts of Papers, VIIth International Conference on the Physics of Electronic and Atomic Collisions (North-Holland Publishing Co., Amsterdam, The Netherlands, 1971), p. 3.

[9] J. W. Duff and D. G. Truhlar, Chem. Phys. Lett. 23 (1973) 327.

Figure Captions

Fig. 1. A plot of the transmission probability as a function of translational energy. The energy range is from 0.07 eV to 0.13 eV. The probabilities range from 10^{-6} to 10^{-2}.

Fig. 2. A plot of the transmission probability as a function of total energy in the range of 0.35 eV to 0.50 eV. The solid line represents results from the present calculation. The squares are taken from Wu et al., ref. [1].

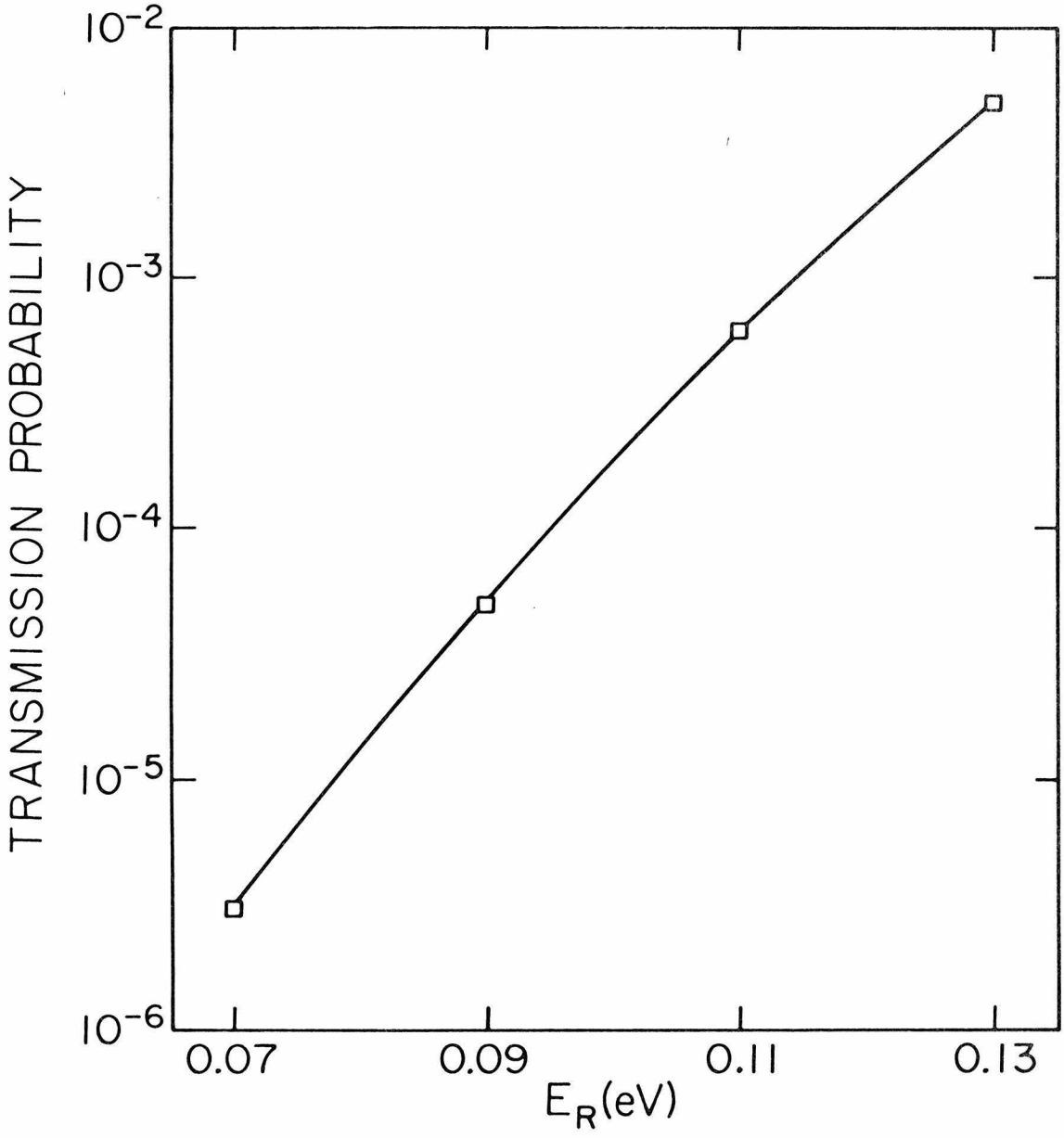
TRANSMISSION PROBABILITY
10^{-2}
10^{-3}
10^{-4}
10^{-5}
10^{-6}
0.07
0.09
0.11
0.13
E_R(eV)

Fig. 1.

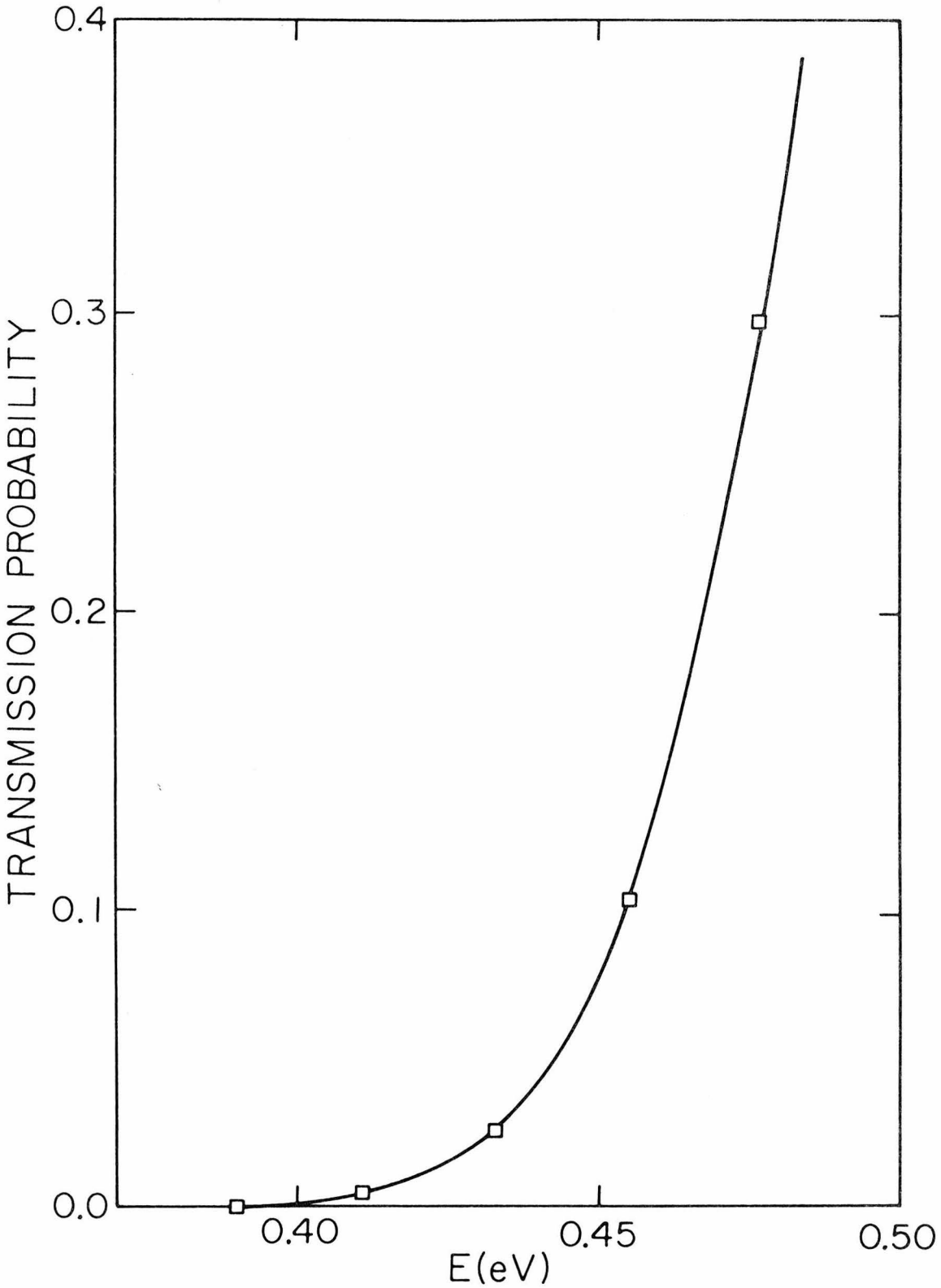

Fig. 2.

CHAPTER 3.

Resonances in Collinear Reactive Scattering: A Simple Model

I. INTRODUCTION

Resonances are well established in theoretical quantum studies of collinear chemical reactions. Exact quantum results on the H + H_2 system, reported by Truhlar and Kuppermann,[1] show both transmission and reflection probabilities to be strongly oscillatory. Bowman and Kuppermann[2] compare the quantum results with semi-classical and quasi-classical results and find that the oscillations are not reproduced. Schatz and Kuppermann[3] argue that it is the interference of direct and compound mechanisms which contributed to these resonances. That is, the oscillations are strictly quantum mechanical phenomena and are difficult to produce with quasi-classical and semi-classical methods. Schatz[4] later discusses the types of resonances which occur in the H + H_2 reaction, using the SSMK surface.[5] He points out that the first resonance at 0.6 eV (total energy) is largely adiabatic (and therefore a shape resonance) but that the next two at 0.9 eV and 1.276 eV have nonadiabatic behavior (and therefore are internal or Feshbach resonances). However, they find that the 1.276 eV resonance is not associated with just one virtual state, and they were not able to easily separate adiabatic and nonadiabatic effects. The 0.9 eV resonance was associated primarily with the second vibrational state of H_3.

Central to understanding the physical origin of resonant processes is the development of simple models that mimic the real system. Using natural collision coordinates and a close-coupling technique to solve the Schrödinger equation for the Porter-Karplus[6] H_3 surface, Levine and Wu[7] calculate transmission and reflection probabilities for the collinear H + H_2 reaction. Then they define static channel potentials to be

$$V_n(s) = V(s) + \epsilon_n(s) ,$$

where V(s) is the potential along the reaction pathway and $\epsilon_n(s)$ is the local eigenvalue of the eigenfunction calculated in the transverse direction. At the saddle point (s = 0), the ϵ_n are eigenvalues of the symmetric stretch of H_3, and V_n has a relative minimum for n = 2 and 3. Levine and Wu maintain that these static potentials can hold bound or quasi-bound states. They conclude that internal excitations to these states are possible and represent Feshbach resonances. They maintain that vibration in the s-direction (corresponding to the approach of the atom and diatom, and therefore asymmetric stretch) is "drained" into the transverse direction (symmetric stretch mode), thus trapping the H_3 molecule for a couple of vibrational periods. Eventually, the vibration drains back into the s-motion and the reaction proceeds to its conclusion. In a later paper, Wu, Johnson, and Levine[8] argue that the resonances are due to a dynamic channel potential. As an example they write the dynamic channel potential for the one-vibration approximation. The result is just the static potential V_0 plus an energy-dependent matrix element. They remark that the dynamics may be altered by the inclusion of closed states. In that same paper, Wu et al. examine resonances of one isotopic variant, $D + D_2$. They note that the dynamic potentials for $D + D_2$ are not as deep as those for $H + H_2$ (in the one-state approximation) and that the $D + D_2$ resonance is not as strong as the $H + H_2$. They do not consider any other isotopic variants in their discussion of resonances, and they do not use their model to predict quantitatively resonance strengths or positions.

The analysis by Wu et al. provides some insight into the origin of resonances in chemical systems, but it does not provide a simple method to predict their strength and position. While it is clear that the difference between resonance strengths in the H + H_2 and D + D_2 systems is caused by the mass differences, it is not clear whether the difference is caused by a change in the reduced mass, the mass of the central atom, the masses of the end atom, or something else.

In this paper we analyze the results of close-coupling calculations on several collinear chemical systems. From the analysis we develop a simple model which predicts the relative strengths and positions of Feshbach resonances in collinear systems.

II. CLOSE-COUPLING CALCULATION

Because there are very few two-dimensional (2-D) and three-dimensional (3-D) results available,[9] we have restricted this study to collinear reactive systems. In order to study systematically the origin of resonances in several systems, we have limited this work to the following symmetric isotopic variants of the $H + H_2$ system;

$$H + H_2 \rightarrow H_2 + H \quad (1)$$

$$D + HD \rightarrow DH + D \quad (2)$$

$$T + HT \rightarrow TH + T \quad (3)$$

$$H + DH \rightarrow HD + H \quad (4)$$

$$D + D_2 \rightarrow D_2 + D \quad (5)$$

$$H + TH \rightarrow HT + H \quad (6)$$

In all cases the potential surface used was the Porter-Karplus[6] H_3 surface.

To calculate reaction probabilities, we used a close-coupling technique that has been described elsewhere[10,16] and applied to other systems.[11,12]

We will denote P_{ij}^N and P_{ij}^R as the nonreactive and reactive transition probabilities from reactant state $v = i$ to product state $v = j$, respectively. E_i is the translational energy relative to initial state $v = i$. Figure 1 shows a spectrum of P_{00}^R for reaction (1). The rapid oscillation at $E_0 = 0.60$ eV was analyzed by Schatz[4] to be a Feshbach (internal excitation) resonance. Figures 2-6 show the corresponding spectra for reactions (2)-(6). In all of the figures there is an oscillation or inflection in the reactive probability near $E_0 = 0.60$ eV.

What is striking is that for the first three chemical systems the oscillation is quite rapid, for the next two systems, relatively weak, and for the last, HTH, there seems to be no resonance at all. Another interesting feature of the spectra is the grouping by resonance strength. The systems with the strongest resonances always have hydrogen as the central atom. Deuterium is the central atom in the weaker resonances and tritium is the central atom in the weakest. For a given central atom, the strength of the resonance seems to be independent of the masses of the end atoms, the reduced masses of the diatoms, the system reduced mass, and the system skew angle. (These last two quantities are described in Appendix A.) Table I summarizes this information. This is not meant to imply that a strong resonance will occur only if hydrogen is the central atom. Both the H + FH and D + FH reactions have strong resonances[4] in the P_{00}^{R} spectrum (see Fig. 7). What is important to note is that doubling the masses of the end atoms in the H + FH system does not significantly affect the strength of the resonance near 0.4 eV. We can conclude that for given potential surfaces the isotope effect on resonances is not caused by the masses of the end atoms.

III. MODEL

In this section we will develop a crude model that is able to predict the relative strengths of resonances for different model systems. The model will be applied to a symmetric collinear reactive chemical system (A + BA).

In Appendix A we developed a mass scaled coordinate system that transformed the Hamiltonian to a form involving only one reduced mass, μ. We can define polar coordinates in this system as follows,

$$\alpha = \tan^{-1} \frac{x_2'}{x_2'}$$

$$\rho = (x_2'^2 + x_1'^2)^{\frac{1}{2}} .$$

As shown in Appendix A, $0 \leq \alpha \leq \tan^{-1}(m_B/\mu)$. Figure 8 is a contour plot of the H + H_2 surface in the mass-scaled coordinates. At the beginning of the reaction, when A is far from BC, x_1' is large and (because BC is bound) x_2' is small. As the reaction progresses, x_1' becomes smaller. In order to proceed to reaction, the system must begin to "turn the corner". If this were viewed in polar coordinates, ρ would remain relatively constant and α would be changing rapidly. Because the α motion is much faster than the ρ motion, there is a crude decoupling of the two coordinates. The decoupling approximation is best near the symmetric stretch line, or $\alpha = \alpha_{max}/2$. This approximation is analogous to the Born-Oppenheimer approximation where electronic motion is much faster than nuclear motion. In that case, the nuclei are said to move in the field of the electrons, or to move on electronic potential surfaces. In our present case, the decoupling of

the two motions is not that complete, but it may be possible to develop α-potentials that are parameterized by different values of ρ.

At the minimum and maximum values of α the potential diverges because each of those two points correspond to the middle atom superimposed on each of the end atoms. A cut of the potential at constant ρ, which spans all values of α, is a one-dimensional box with infinitely high walls. At large ρ (and for symmetric systems) the box has a symmetric double well. Asymptotically the eigenvalues of the double well are pairwise degenerate and correspond to AB eigenvalues, one for each arrangement channel. At small ρ there is only a single well, whose corresponding eigenvalues are much greater than the asymptotic values because $V(\rho_1, \alpha) > V(\rho_2, \alpha)$ for $\rho_1 \ll \rho_2$. We can define eigenpotentials, $\epsilon_i(\rho)$, to be the eigenvalues of the constant ρ cuts for all $\rho > 0$. These are, in effect, the α-fields in which the ρ motion takes place. Each of these eigenpotentials are a function of ρ only, and therefore in this approximation determine the ρ motion. We can now solve the one-dimensional Schrödinger equation on each surface (eigenpotential). If the decoupling idea is an accurate reflection of the reaction near the barrier and if resonances result from motion near the barrier, then one would expect the one-dimensional wavefunctions to exhibit resonance behavior near the resonance energies.

The eigenpotentials are found by solving the Schrödinger equation for a particle in a cut at constant ρ,

$$-\frac{\hbar^2}{2\mu\rho^2}\frac{d\phi_i(\rho,\alpha)}{d\alpha^2} + V(\rho,\alpha)\phi_i(\rho,\alpha) = \epsilon_i(\rho)\phi_i(\rho,\alpha) , \qquad (7)$$

where ϕ_i is the eigenfunction solution of that equation. Figure 9 shows

some eigenpotentials for i = 0-7 of the H + H_2 systems. Note that the eigenpotentials become pairwise degenerate for large ρ. Some of the even eigenpotentials (i = 2, 4, 6), which are eigenvalues of symmetric eigenfunctions, exhibit shallow wells whose minima are about 0.10 eV below the asymptotic values of $\epsilon_i(\rho)$. These same eigenpotentials have small barriers of about 0.05 eV. None of the odd eigenvalues (corresponding to antisymmetric eigenfunctions) have either wells or barriers. The eigenpotentials of the other symmetric hydrogen systems have similar trends. One other fact, which is not apparent from the graphs, is that some of the eigenpotentials are deep enough and wide enough to hold bound states.

Because the eigenpotentials were developed analogously to electronic adiabatic surfaces, we conclude that, in the approximation, there is no coupling between the surfaces. Because there is no coupling, the Schrödinger equation in polar coordinates (see Appendix B) reduces to

$$-\frac{\hbar^2}{2\mu}\frac{d^2 g_i(\rho)}{d\rho^2} + \left[\epsilon_i(\rho) - \frac{\hbar^2}{8\mu\rho^2} - E\right] g_i(\rho) = 0 , \qquad (8)$$

where E is the total energy and $g_i(\rho)$ is the scattering wavefunction describing ρ-motion. This equation may be easily solved for any $E > \epsilon_i(\infty)$, using the Numerov[15] method of integration. For each eigenpotential, the equation was integrated from small ρ [$\epsilon_i(\rho) \gg E$] to large ρ ($\sim$ 12 bohr) where the solutions had become periodic. Equation (8) was solved at 100 equally spaced [$E - \epsilon_i(\infty) \sim 0.005$ eV] energies for each eigenpotential. The phase shift, $\delta_i(E)$, and its derivative, $[d\delta_i(E)/dE]$, were calculated and plotted as a function of energy. The solutions were converged, i.e., beginning at smaller ρ and

integrating further did not change the phases by more than 0.001 radians.

The phases calculated from the odd eigenpotentials (which were calculated from antisymmetric eigenfunctions) show no unusual behavior for any of the hydrogen systems; they decrease monotonically with energy. Figure 10 shows the phase, $\delta_3(E)$, resulting from $\epsilon_3(\rho)$ of the $H + H_2$ system. $(d\delta_3/dE)$, which is related to the lifetime by $\tau = \hbar(d\delta_i/dE)$ is shown in Fig. 11. For all energy values, $d\delta/dE < 0$ and seems to have $d\delta/dE = 0$ as the asymptotic limit. Figures 10 and 11 are typical of all of the eigenpotentials except for $\epsilon_2(\rho)$ of each hydrogen system. In a couple of cases $d\delta/dE$ does not increase monotonically (see Fig. 12), but it is always negative unless calculated from $\epsilon_2(\rho)$. Figures 13 and 14 show $\delta_2(E)$ and $d\delta_2(E)/dE$ for the $H + H_2$ system. One should note that the peak of the $d\delta_2(E)/dE$ curve is positive and gives a lifetime of 1.02×10^{-12} sec. This is a factor of 20 larger than the reported[4] lifetime. This resonance behavior of the ρ-motion corresponds to an internal excitation (Feshbach resonance) in the H_3 vibrational manifold. $d\delta_2(E)/dE$ has the same behavior in two other systems, D + HD and T + HT. From Figs. 4 and 5, one would expect the predicted lifetime to be much smaller for the H + DH and $D + D_2$ systems. Figures 15 and 16 show $d\delta_2(E)/dE$ for those systems. Two things are important. One, the derivatives of the phase shifts are the same order of magnitude, corresponding to similar resonance strengths in Figs. 4 and 5. Two, the peak of the $d\delta_2(E)/dE$ curve in the H + DH (or $D + D_2$) system is much smaller than the corresponding peak in the $H + H_2$ (or D + HD and T + HT) system, thus correctly predicting the relative strengths of the resonances. From Fig. 6, one can see that there is no resonance in

the H + TH system near 0.60 eV. Figure 17 shows that this is also the prediction of the model, the $d\delta_2(E)/dE$ curve is never positive. Table II is a summary of this information.

Equally important as the predictions of the relative strengths of resonances are the comparisons between the actual and predicted positions of the resonances in the energy spectrum. In every case (except H+TH, where there is no resonance) the resonances were predicted to be at a lower translationsl energy than exact calculations showed. The differences ranged from 0.019 eV (T+HT) to 0.080 eV (H+DH). These are summarized in Table II. It is interesting to note that the ordering of the exact resonance energies is nearly preserved in the predicted resonance energies.

In concluding this section we will look briefly at another resonance in the P^R_{00} spectrum of the H + H_2 system, this one at E_0 = 1.033 eV. A plot of $d\delta/dE$ for each of the H + H_2 eigenpotentials shows no oscillatory behavior. However, a closer examination reveals that $\epsilon_4(\rho)$ holds a bound state at E_0 = 0.949. This implies that the model predicts a resonance whenever an eigenpotential holds a bound state, or $d\delta/dE$ goes positive. The other systems for which we have close-coupling calculations of the second Feshbach resonance (D + D_2, H + DH, and D + HD) have bound states below the actual resonance (< 0.10 eV). Generally, the bound states predict the resonance energies less accurately than plots of $d\delta/dE$. The estimation of lifetimes is meaningless because a bound state has an infinite lifetime.

IV. SUMMARY

After transforming the Schrödinger equation into mass-scaled center-of-mass coordinates (Delves' coordinates), we defined the polar coordinates ρ and α. We then showed that ρ-motion and α-motion are roughly uncoupled near the symmetric stretch line, analogous to the uncoupling of electronic and nuclear motion in the Born-Oppenheimer approximation. We developed the idea of eigenpotentials (which are analogous to electronic adiabatic surfaces) and used them to solve the Schrödinger equation governing ρ-motion. When the phase shifts and their derivatives are calculated, most of them show no unusual behavior. A few, however, $[d\delta_2(E)/dE]$, were oscillatory and positive near the resonance energies ($\sim$ 0.050 eV) calculated by an exact close-coupling method. In the model calculation, these were interpreted to be resonances. The lifetime predicted by the model for the H + H_2 system was too large by a factor of 20. However, the relative strengths and the ordering of the resonance energies were preserved. In fact, for the H + TH system, the close-coupling calculation shows no resonance and the model predicts the same.

For the next resonance, the model has no oscillatory behavior in $d\delta/dE$ near the resonance energy. Instead, a bound state in $\epsilon_4(\rho)$ was identified with the resonance.

We found that the only simple correlation between the masses of the atoms involved and the strength of the resonances was with the central atom. Within the hydrogen system, the smaller the skew angle the more intense the resonance. Because the skew angle is given by $\alpha = \tan^{-1}(m_B/\mu)$, decreasing m_B (with constant μ) will produce a smaller

skew angle. As the skew angle is made smaller, the system must "turn" a sharper corner in proceeding from reactants to products. When the turn becomes too sharp, the system is trapped in the symmetric stretch region, and it produces a resonance.

APPENDIX A.

In center of mass coordinates, the Hamiltonian for a collinear atom-diatom system may be written as

$$\mathcal{H} = \frac{\hbar^2}{2\mu_{A,BC}} \frac{\partial^2}{\partial x_1^2} - \frac{\hbar^2}{2\mu_{BC}} \frac{\partial^2}{\partial x_2^2} + V(x_1, x_2). \qquad (A.1)$$

This is written in the coordinates which describe atom A incident on diatom BC, where B is the central atom. x_2 is just the BC internuclear distance and x_1 is the distance from A to the center of mass of BC. The reduced masses are defined as

$$\mu_{BC} = \frac{m_A \cdot m_B}{m_A + m_B}$$

and

$$\mu_{A,BC} = \frac{m_A(m_B + m_C)}{m_A + m_B + m_C} \quad ,$$

where m_A, m_B, and m_C are the masses of atoms A, B, and C, respectively. An analogous Hamiltonian may be written for atom C incident on diatom BA. Using the Hamiltonian in this form, with two different reduced masses in each arrangement channel, the associated Schrödinger equation would be difficult to solve. It is important to transform the Hamiltonian to a form involving only one reduced mass which is independent of arrangement channel. Such a transformation, first proposed by Delves[13] and Hirschfelder and Jepsen[14] is

$$x_1' = \left(\frac{\mu_{A,BC}}{\mu_{BC}}\right)^{\frac{1}{4}} x_1$$

$$x_2' = \left(\frac{\mu_{BC}}{\mu_{A,BC}}\right)^{\frac{1}{4}} x_2 .$$

The Hamiltonian becomes

$$\mathcal{H} = -\frac{\hbar^2}{2\mu}\left(\frac{\partial^2}{\partial x_1'^2} + \frac{\partial^2}{\partial x_2'^2}\right) + V(x_1', x_2'), \qquad (A.2)$$

where

$$\mu = (\mu_{A,BC} \cdot \mu_{BC})^{\frac{1}{4}}$$

$$= (\mu_{C,AB} \cdot \mu_{AB})^{\frac{1}{4}}$$

$$= [(m_A m_B m_C)/(m_A + m_B + m_C)]^{\frac{1}{2}} \qquad (A.3)$$

and is called the system reduced mass. If we define a polar angle α to be

$$\alpha = \tan^{-1}\left(\frac{x_2'}{x_1'}\right),$$

α is limited by $r_1 = 0$ and $r_2 = 0$, or $\alpha_{min} = 0$ and $\alpha_{max} = \tan^{-1}(m_B/\mu)$. α_{max} is called the skew angle of the system and is independent of arrangement channel. Systems with a relatively small central mass to μ ratio will have a small skew angle, and the system must "turn" a sharp corner to proceed to reaction.

The Hamiltonian in polar coordinates becomes

$$\mathcal{H} = -\frac{\hbar^2}{2\mu}\left(\frac{1}{\rho^2}\frac{\partial^2}{\partial\alpha^2} + \frac{\partial^2}{\partial\rho^2} + \frac{1}{\rho}\frac{\partial}{\partial\rho}\right) + V(\rho, \alpha).$$

APPENDIX B

In this appendix we will develop the Schrödinger equation in polar coordinates, which can be used to solve collinear scattering problems. As shown in Appendix A [Eq.(A.2)], the Hamiltonian in mass scaled polar coordinates may be written as

$$\mathcal{H} = -\frac{\hbar^2}{2\mu}\left(\frac{1}{\rho^2}\frac{\partial^2}{\partial\alpha^2} + \frac{\partial^2}{\partial\rho^2} + \frac{1}{\rho}\frac{\partial}{\partial\rho}\right) + V(\rho,\alpha) .$$

If the solution is written as $\rho^{-\frac{1}{2}}G_j(\rho,\alpha)$, the Schrödinger equation is

$$-\frac{\hbar^2}{2\mu}\left[\frac{\partial^2 G_j(\rho,\alpha)}{\partial\rho^2} + \frac{1}{\rho^2}\frac{\partial^2 G_j(\rho,\alpha)}{\partial\alpha^2}\right] + \left[V(\rho,\alpha) - \frac{\hbar^2}{8\mu\rho^2}\right]G_j(\rho,\alpha) = EG_j(\rho,\alpha) , \qquad (B.1)$$

where E is the total energy.

We now define a complete orthonormal basis set, $\{\phi_i\}$, such that

$$-\frac{\hbar^2}{2\mu\bar{\rho}^2}\frac{d^2\phi_i(\bar{\rho},\alpha)}{d\alpha^2} + V(\bar{\rho},\alpha)\phi_i(\bar{\rho},\alpha) = E_i(\bar{\rho})\phi_i(\bar{\rho},\alpha) , \qquad (B.2)$$

where $\phi_i(\bar{\rho},\alpha)$ is parametrically dependent on $\bar{\rho}$. If $G_j(\rho,\alpha)$ is expanded in terms of these basis functions, the Schrödinger equation becomes (after some manipulation)

$$-\frac{\hbar^2}{2\mu}\frac{d^2 g_{ij}}{d\rho^2}(\rho) + \left[\frac{\bar{\rho}^2}{\rho^2}E_i(\bar{\rho}) - \frac{\hbar^2}{8\mu\rho^2} - E\right]g_{ij}(\rho) + \sum_i \left[V_{ii'}(\rho) - \frac{\bar{\rho}^2}{\rho^2}V_{ii'}(\bar{\rho})\right]g_{i'j}(\rho) = 0 , \qquad (B.3)$$

where the g_{ij}'s are the coefficients of expansion and

$$V_{ii'}(\rho) = \int_0^{\alpha_{max}} \phi_i(\bar{\rho},\alpha)V(\rho)\phi_j(\bar{\rho},\alpha)d\alpha .$$

TABLE I.

Reaction	Resonance Strength	Central Atom Mass [a]	End Atom Mass	Diatom Reduced Mass	Delves' Reduced Mass	Skew Angle
$H + H_2 \rightarrow H_2 + H$	strong	1	1	0.50	0.58	60.0°
$D + HD \rightarrow DH + D$	strong	1	2	0.67	0.89	48.2°
$T + HT \rightarrow TH + T$	strong	1	3	0.75	1.13	41.4°
$H + DH \rightarrow HD + H$	weak	2	1	0.67	0.71	70.5°
$D + D_2 \rightarrow D_2 + D$	weak	2	2	1.00	1.15	60.0°
$H + TH \rightarrow HT + H$	none	3	1	0.75	0.77	75.5°

[a] All of the masses are relative to $m_H = 1$.

TABLE II. Resonance energies, E^{res}, exact and predicted.

Reaction	E^{res}_{exact} (eV)[a]	E^{res}_{pred} (eV)	ΔE (eV)
$H + H_2 \rightarrow H_2 + H$	0.598	0.544	0.54
$D + HD \rightarrow DH + D$	0.534	0.504	0.030
$T + HT \rightarrow TH + T$	0.510	0.491	0.019
$H + DH \rightarrow HD + H$	0.582	0.502	0.080
$D + D_2 \rightarrow D_2 + D$	0.508	0.452	0.56
$H + TH \rightarrow HT + H$	none	none	---

[a] All energies are measured relative to the ground vibrational state of the diatom in each system.

REFERENCES

1. D. G. Truhlar and A. Kuppermann, J. Chem. Phys. 56, 2232 (1972).

2. J. M. Bowman and A. Kuppermann, J. Chem. Phys. 59, 6524 (1973).

3. G. C. Schatz and A. Kuppermann, J. Chem. Phys. 59, 964 (1973).

4. G. C. Schatz, Ph.D. Thesis, California Institute of Technology, 1975.

5. I. Shavitt, R. M. Stevens, F. L. Minnan, and M. Karplus, J. Chem. Phys. 48, 2700 (1968).

6. R. N. Porter and M. Karplus, J. Chem. Phys. 40, 1105 (1964).

7. R. D. Levine and S.-F. Wu, Chem. Phys. Lett. 11, 557 (1971).

8. S.-F. Wu, B. R. Johnson, and R. D. Levine, Mol. Phys. 25, 609 (1973).

9. G. C. Schatz and A. Kuppermann, Phys. Rev. Lett. 35, 1266 (1975).

10. A. Kuppermann, Proceedings of the Conference on Potential Energy Surfaces in Chemistry, W. A. Lester, Jr., Ed. (IBM Research Laboratory, San Jose, California, 1971), pp. 121-134; Abstracts of Papers, VIIth International Conference on the Physics of Electronic and Atomic Collisions (North-Holland Publishing Co., Amsterdam, The Netherlands, 1971), p. 3.

11. G. C. Schatz and A. Kuppermann, J. Chem. Phys. 59, 964 (1973).

12. G. C. Schatz, J. M. Bowman, and A. Kuppermann, J. Chem.

Phys. 58, 4023 (1973).

13. (a) L. Delves, Nucl. Phys. 9, 391 (1959); (b) ibid. 20, 275 (1960).

14. D. Jepsen and J. O. Hirschfelder, Proc. Natl. Acad. Sci. USA 45, 249 (1959).

15. D. R. Hartree, The Calculation of Atomic Structure (John Wiley and Sonc, Inc., New York, 1957), p. 71.

16. Z. H. Top and M. Baer, J. Chem. Phys. 66, 1363 (1977).

FIGURE CAPTIONS

FIG. 1. The reactive v = 0 to v = 0 transition probability, P_{00}^{R}, for the H + H_2 system. The abscissa is translational energy in eV in the range 0.0 eV to 1.0 eV.

FIG. 2. P_{00}^{R} for the D + HD system in the translational energy range 0.0 eV to 1.0 eV.

FIG. 3. P_{00}^{R} for the T + HT system in the translational energy range from 0.0 eV to 1.0 eV.

FIG. 4. P_{00}^{R} for the H + DH system in the translational energy range from 0.0 eV to 1.0 eV.

FIG. 5. P_{00}^{R} for the D + D_2 system in the translational energy range from 0.0 eV to 1.0 eV.

FIG. 6. P_{00}^{R} for the H + TH system in the translational energy range from 0.0 eV to 1.0 eV.

FIG. 7. P_{00}^{R} for the H + FH system (dashed line) and D + FD system (solid line) in the translational energy range of each system from 0.0 eV to 0.5 eV.

FIG. 8. A contour plot of the H + H_2 surface in Delves' (mass scaled) coordinates. The spacing between contours is 0.3 eV beginning with 0.3 eV. The abscissa and ordinate are measured in units of bohr.

FIG. 9. The first eight eigenpotentials, $\epsilon_i(\rho)$ for the H + H_2 system. The ordinate is in eV and is measured from the bottom of the H_2 well. The abscissa is in bohr.

FIG. 10. The phase shift, $\delta_4(E)$, versus translational energy, calculated using $\epsilon_4(\rho)$ of the H + H_2 system. The ordinate is measured in radians and the abscissa in eV.

FIG. 11. The energy derivative of the phase shift, $[d\delta_4(E)/dE]$, versus translational energy, calculated using $\epsilon_4(\rho)$ of the H + H_2 system. The ordinate is in units of rad/eV and the abscissa in units of eV.

FIG. 12. $[d\delta_5(E)/dE]$ versus translational energy, calculated using $\epsilon_5(\rho)$ of the D + HD system. The units are the same as in Fig. 11.

FIG. 13. $\delta_2(E)$ versus translational energy, calculated using $\epsilon_2(\rho)$ of the H + H_2 system. Units are the same as in Fig. 10.

FIG. 14. $[d\delta_2(E)/dE]$ versus translational energy, calculated using $\epsilon_2(\rho)$ of the H + H_2 system. Units are the same as in Fig. 11.

FIG. 15. $[d\delta_2(E)/dE]$ versus translational energy, calculated using $\epsilon_2(\rho)$ of the H + DH system. Units are the same as in Fig. 11.

FIG. 16. $[d\delta_2(E)/dE]$ versus translational energy, calculated using $\epsilon_2(\rho)$ of the D + D_2 system. Units are the same as in Fig. 11.

FIG. 17. $[d\delta_2(E)/dE]$ versus translational energy, calculated using $\epsilon_2(\rho)$ of the H + TH system. Units are the same as in Fig. 11.

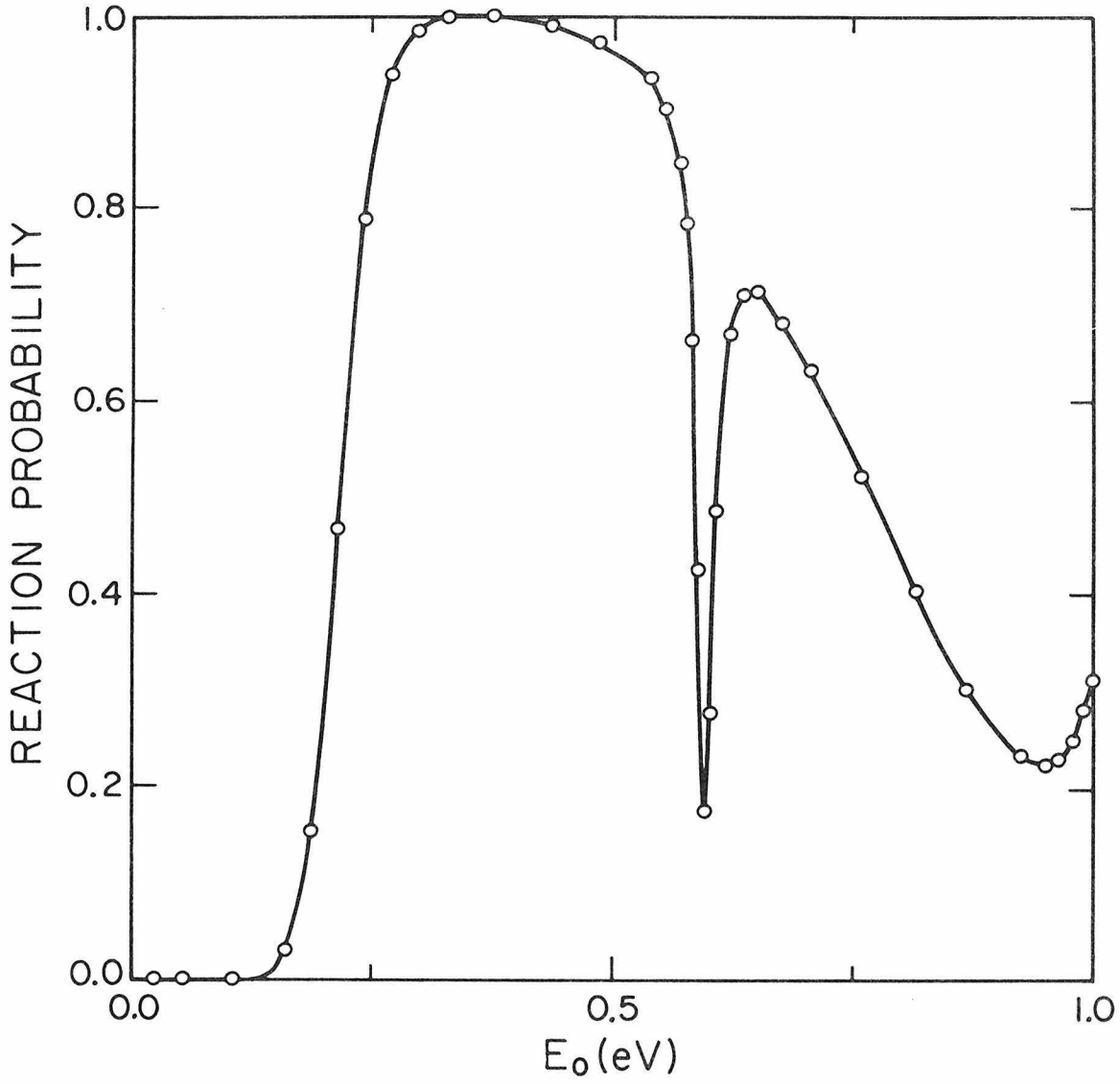

Fig. 1.

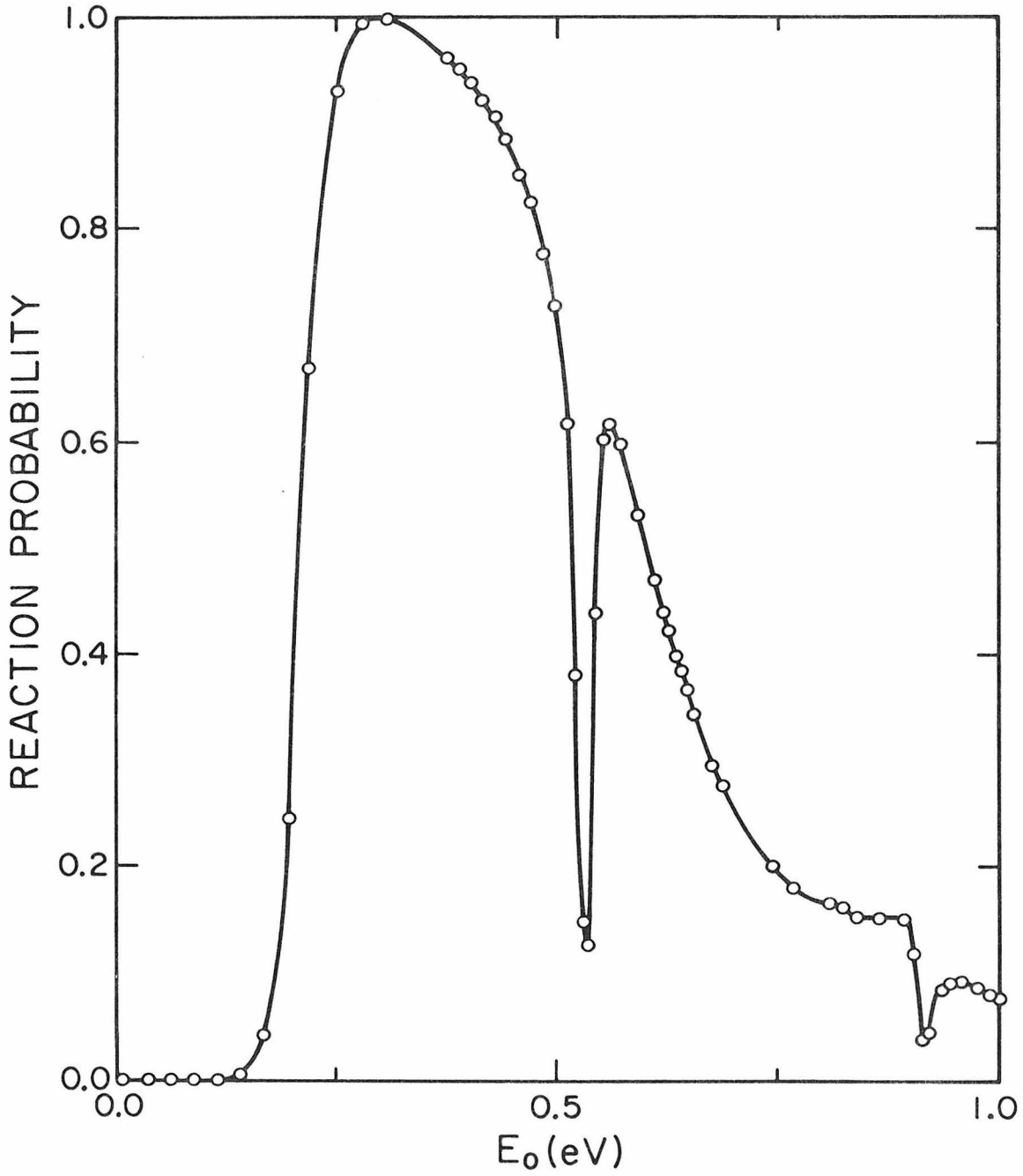

Fig. 2.

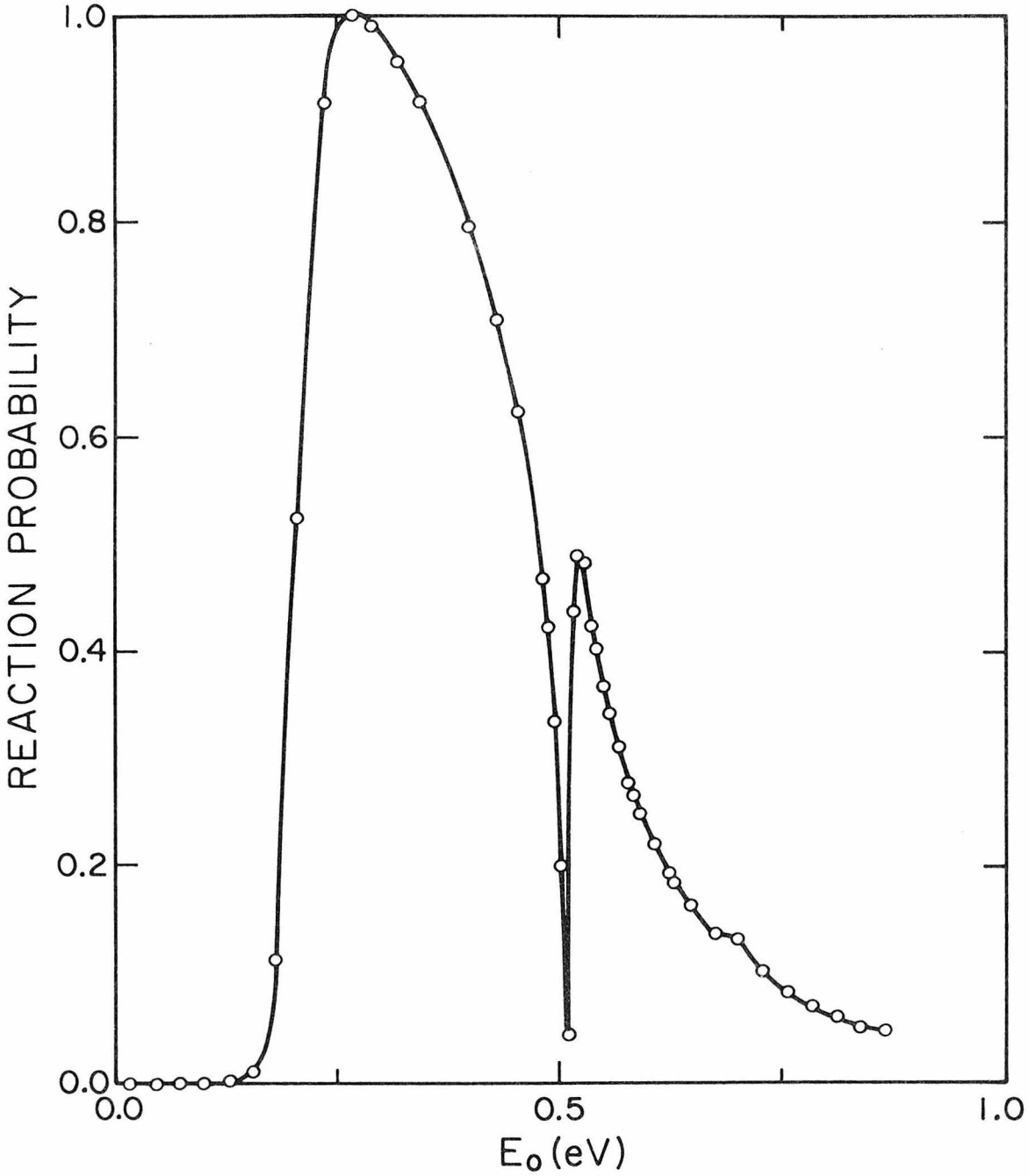

Fig. 3.

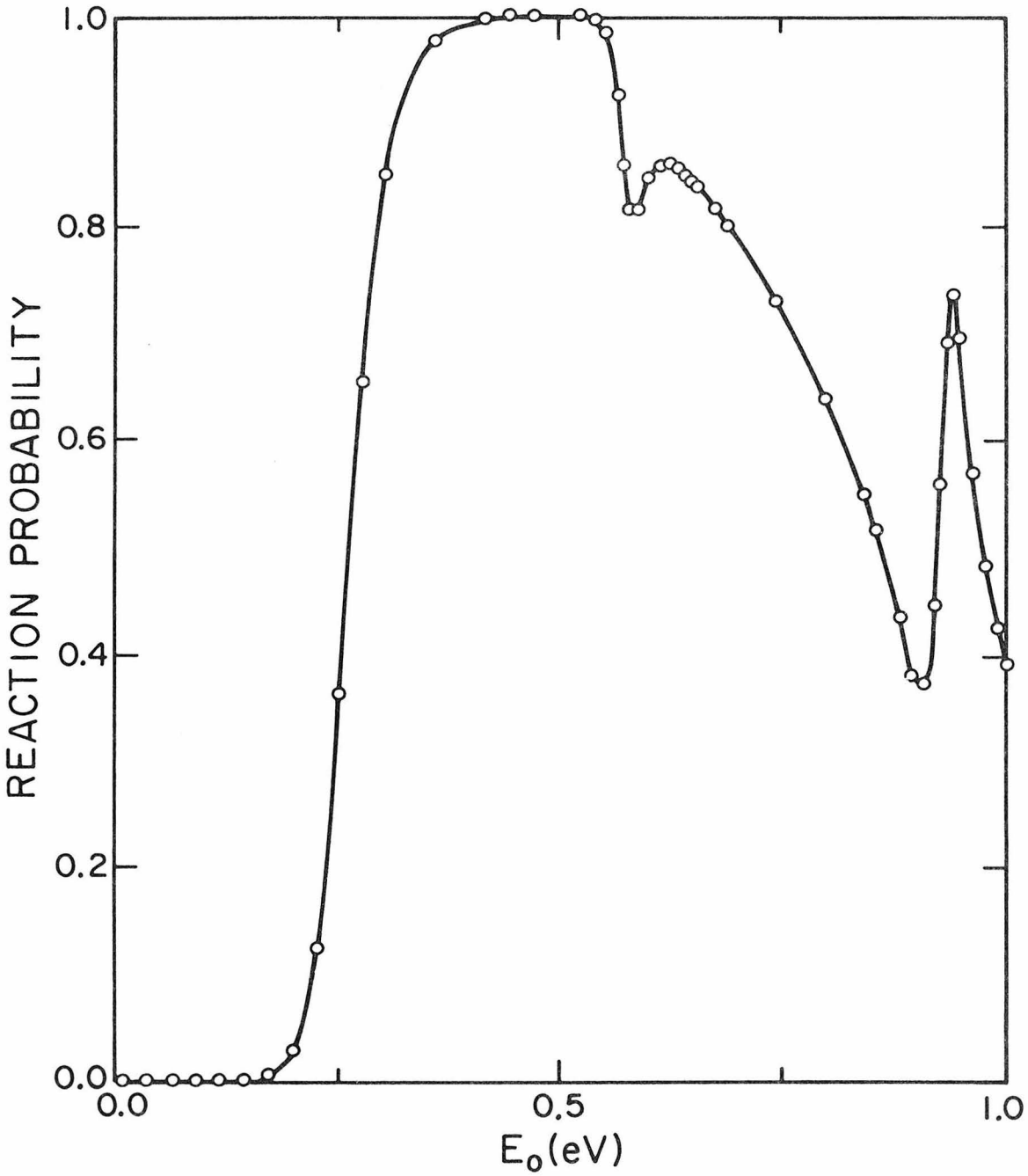

Fig. 4.

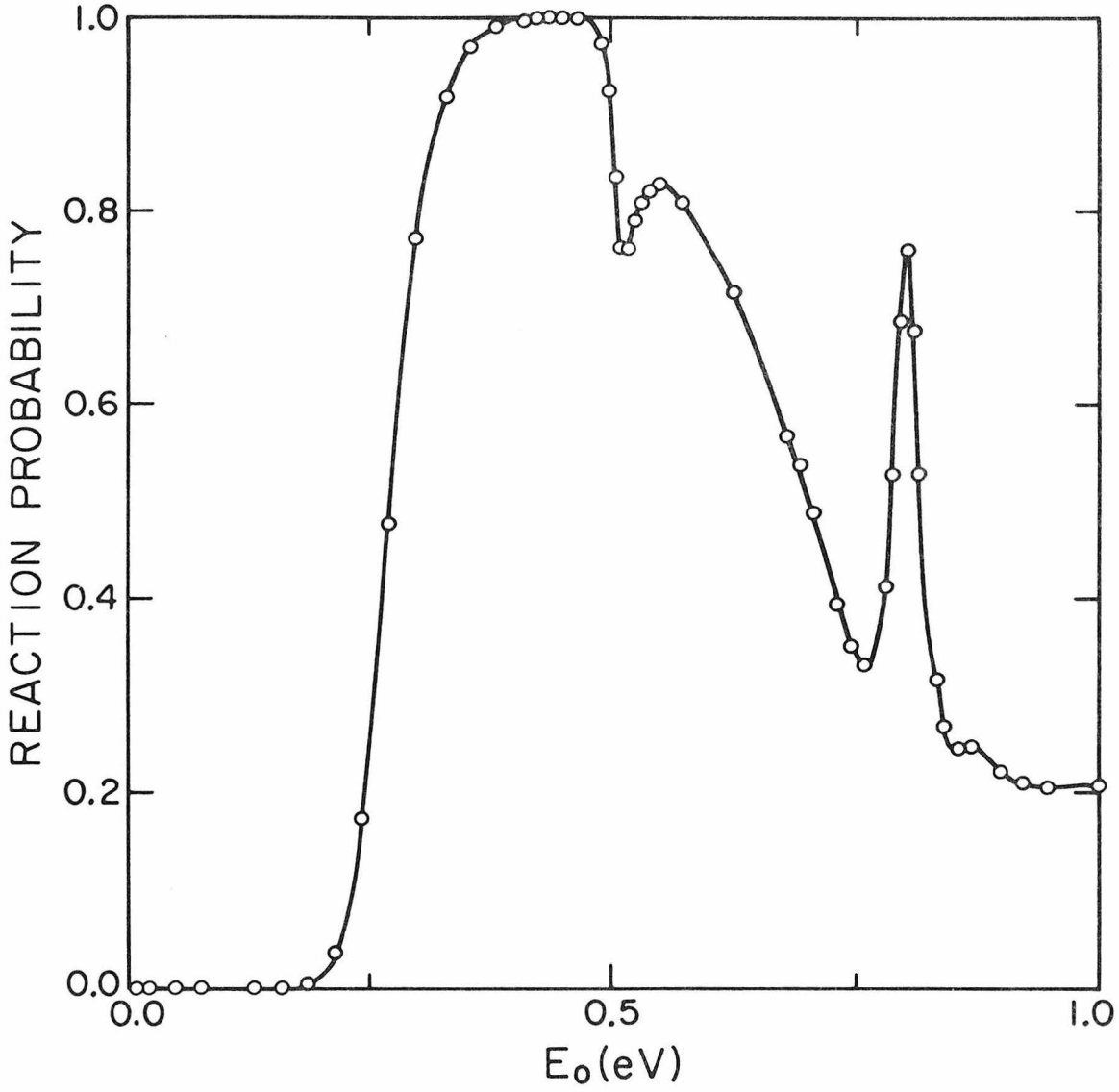

Fig. 5.

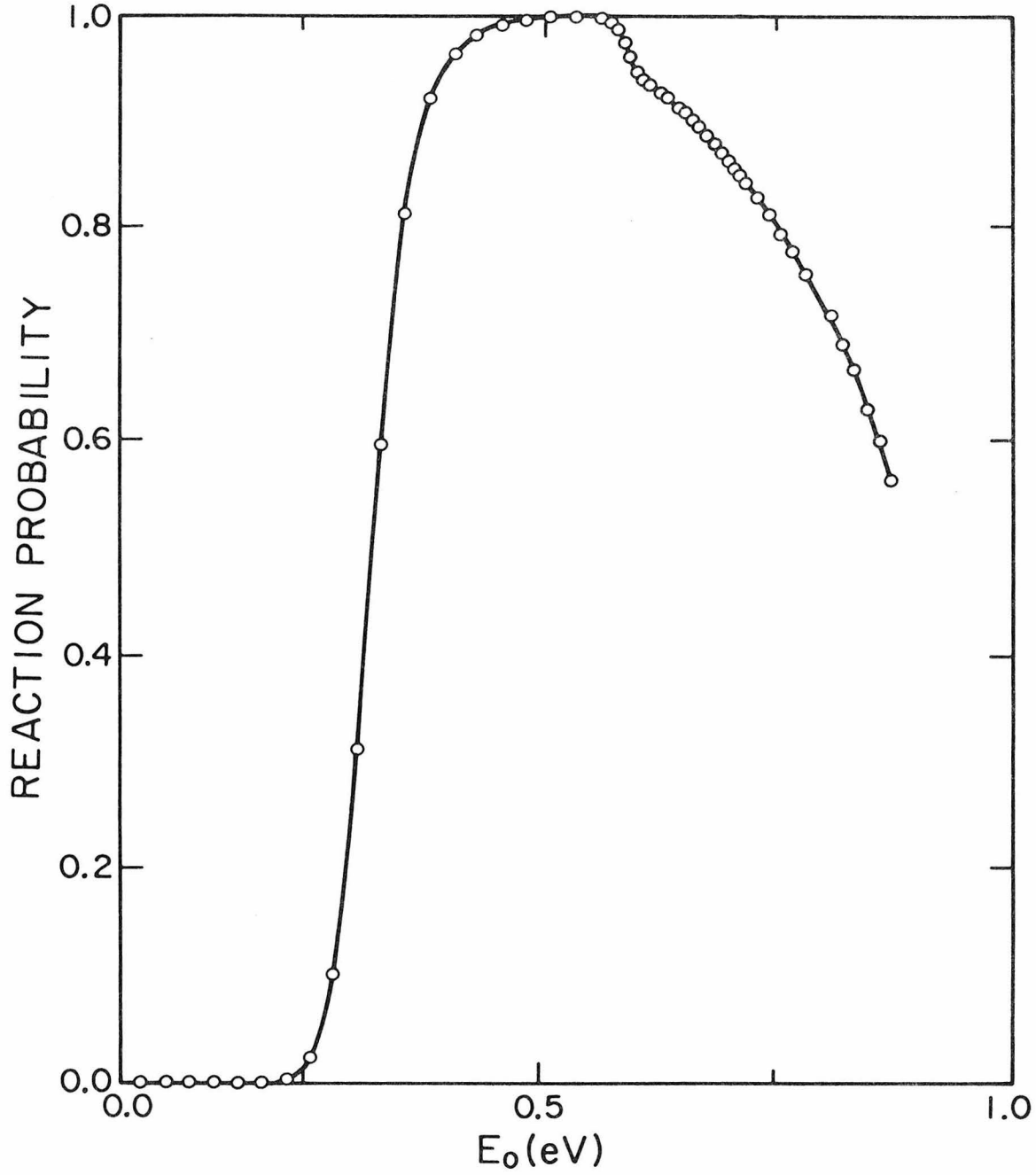

Fig. 6.

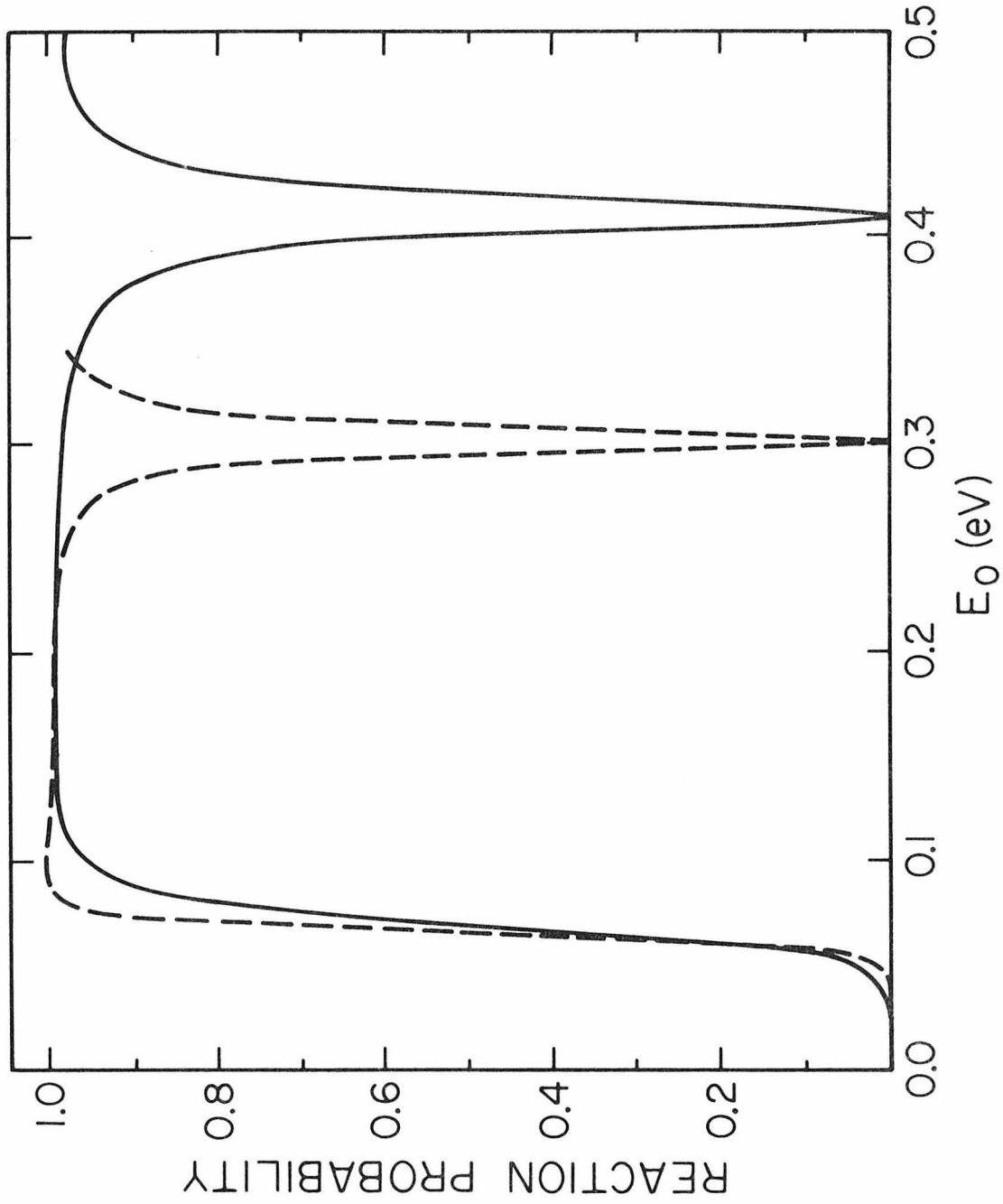

Fig. 7.

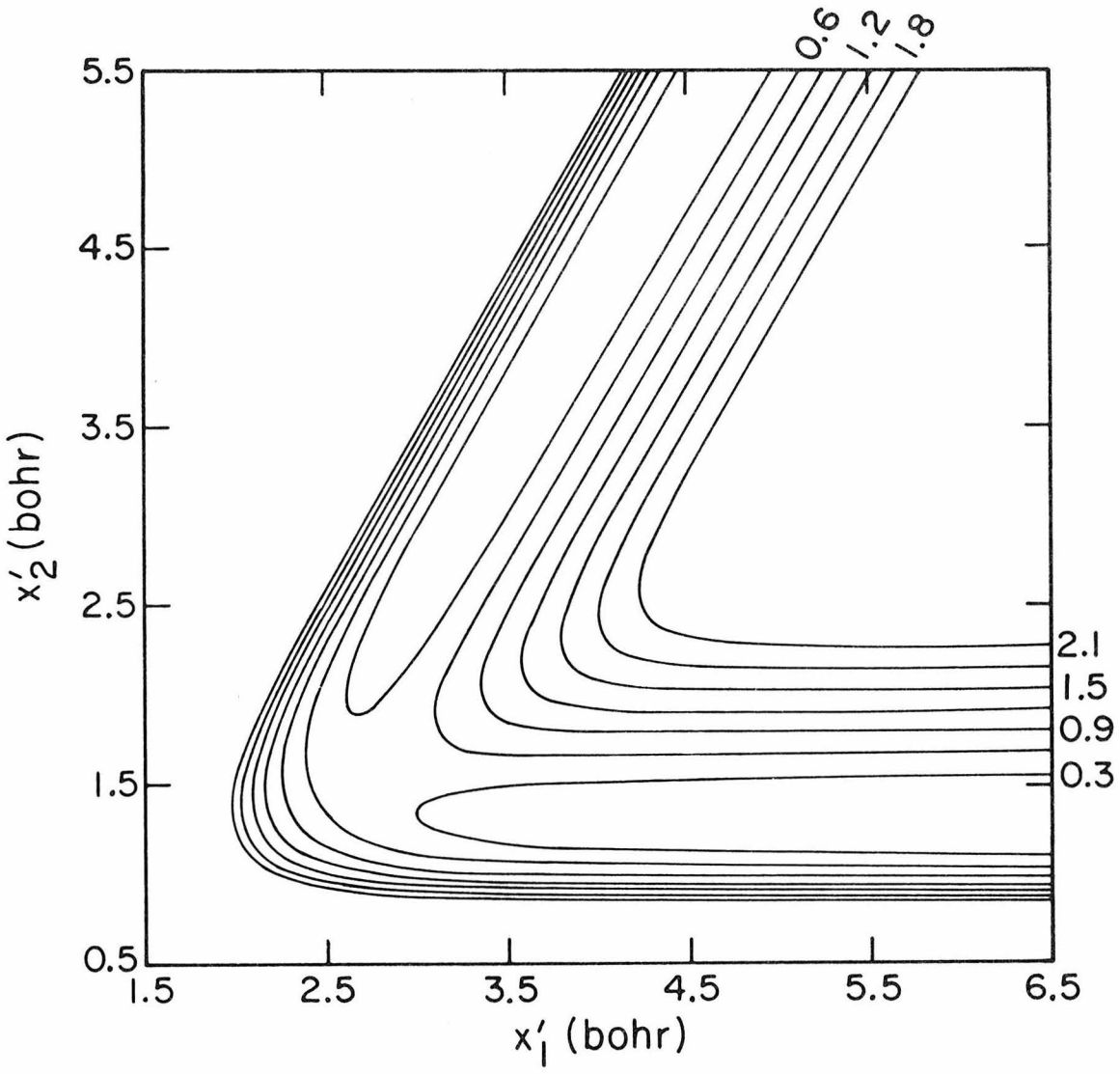
0.6
1.2
1.8
2.1
1.5
0.9
0.3
5.5
4.5
3.5
2.5
1.5
0.5
x'2 (bohr)
1.5
2.5
3.5
4.5
5.5
6.5
x'1 (bohr)

Fig. 8.

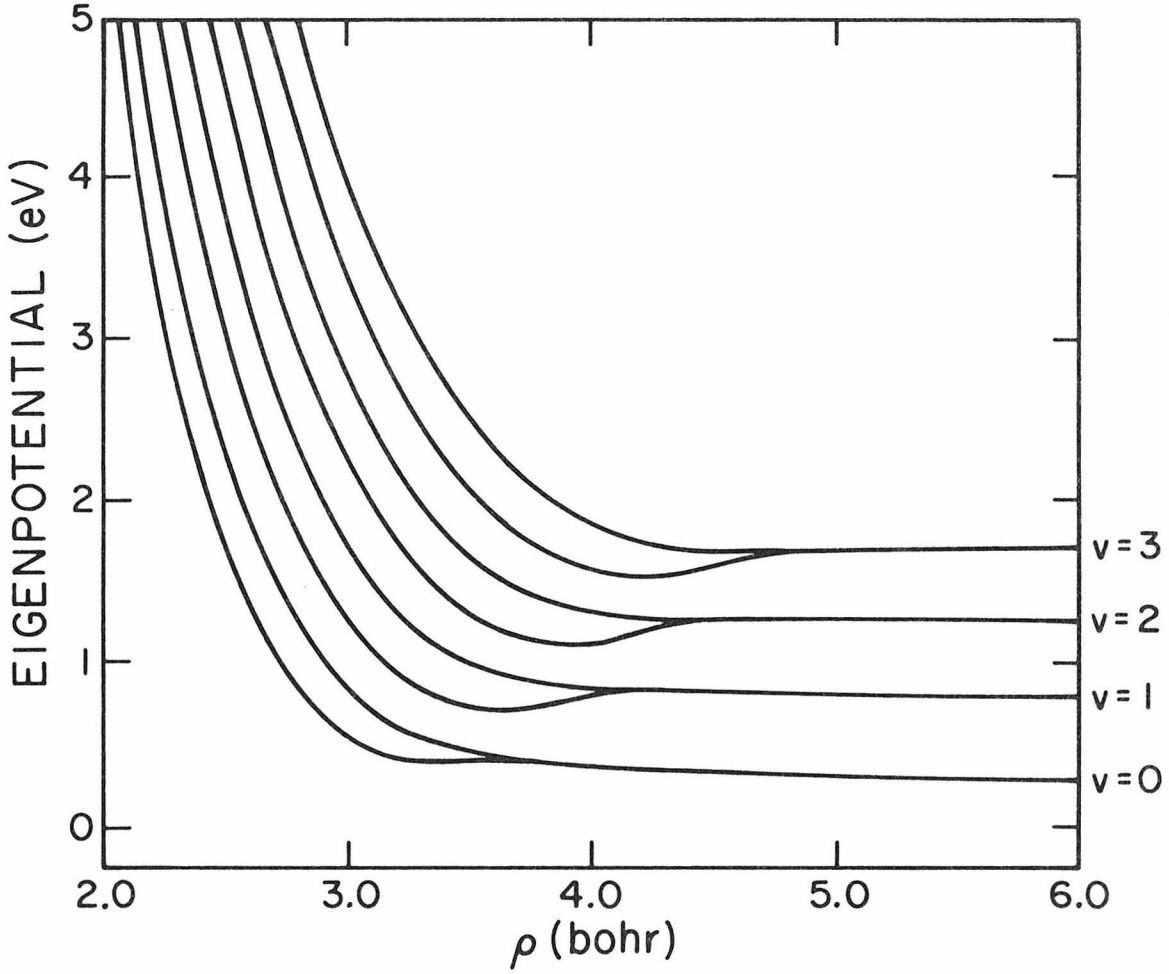

Fig. 9.

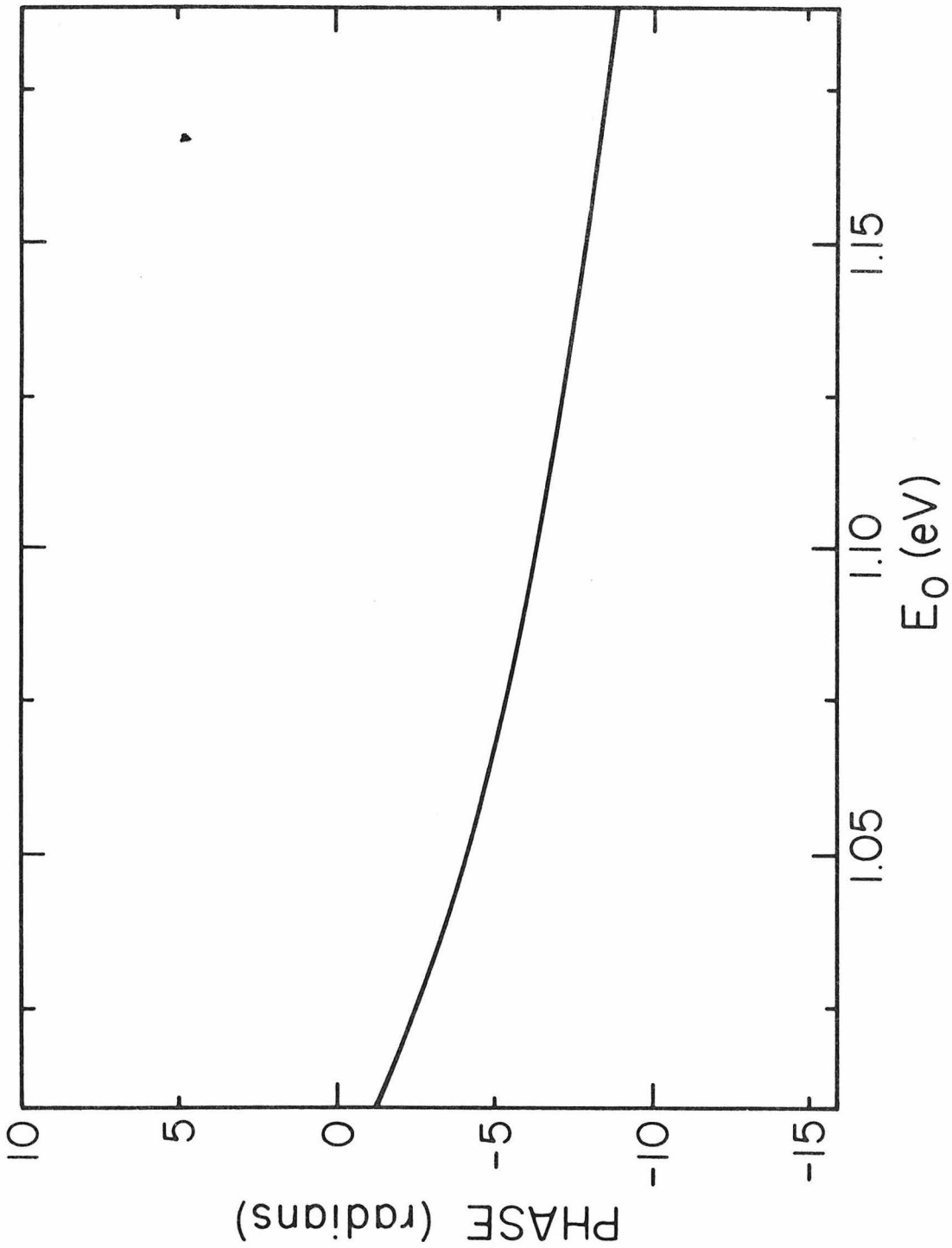

Fig. 10.

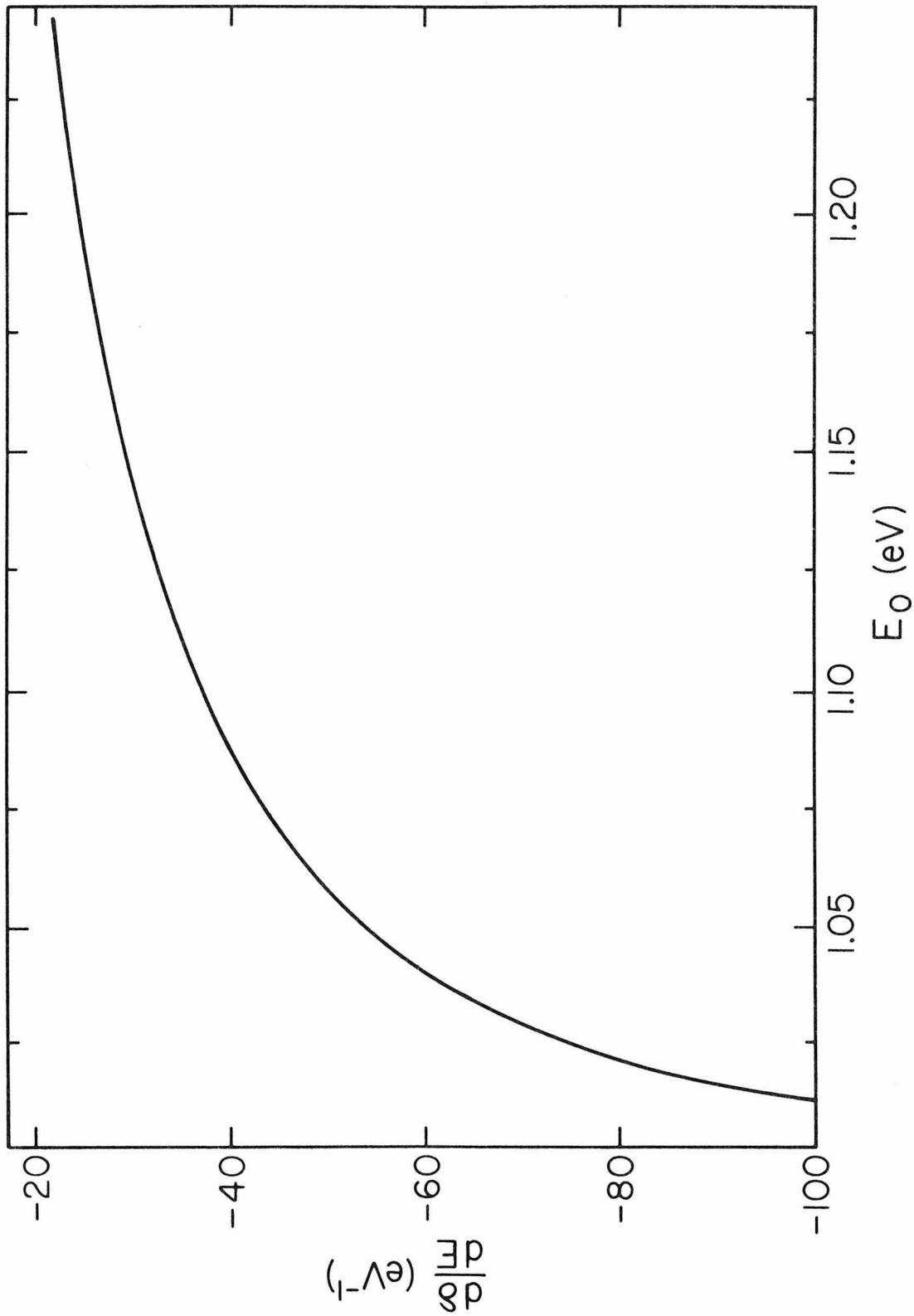

Fig. 11.

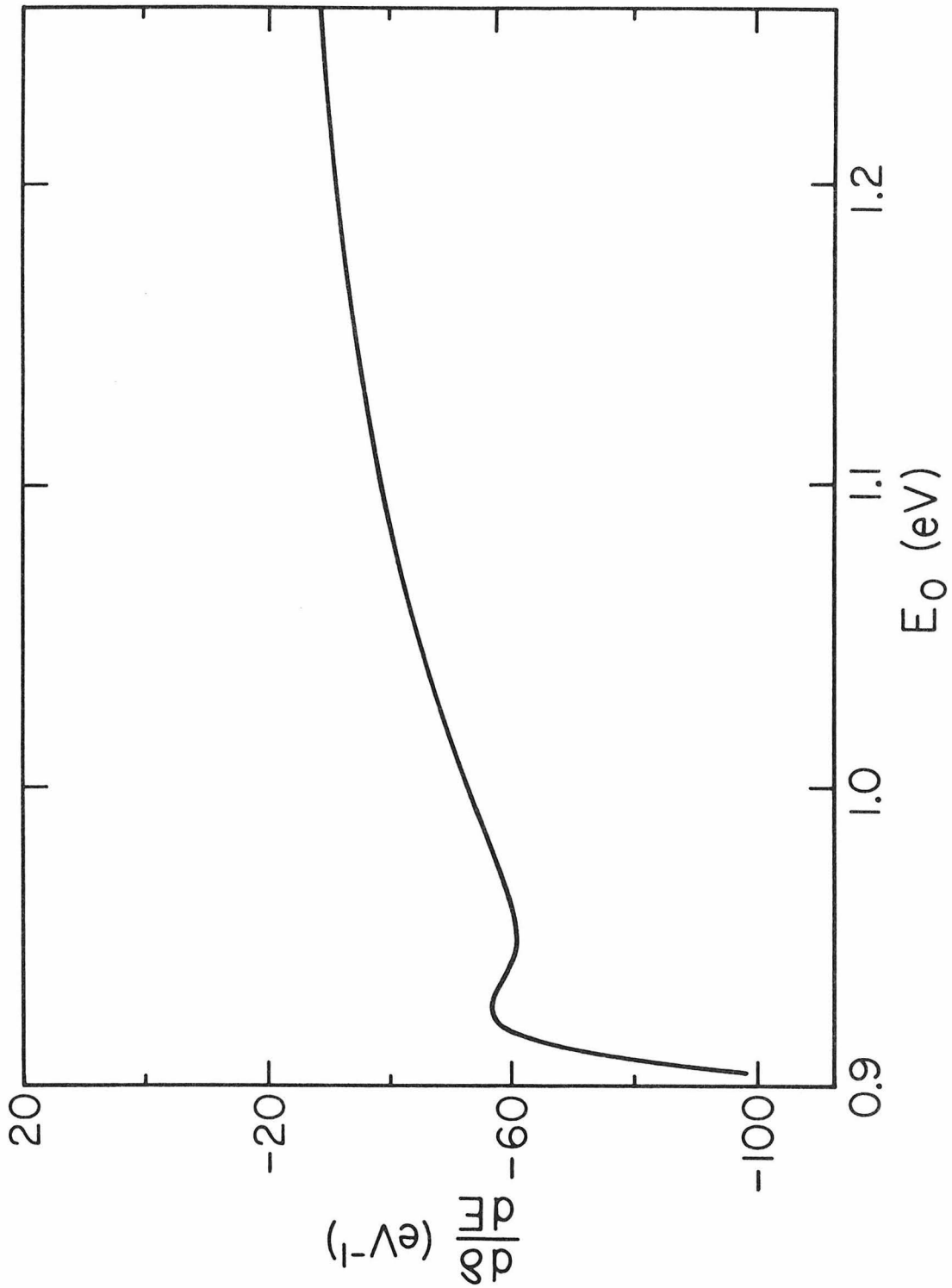

Fig. 12.

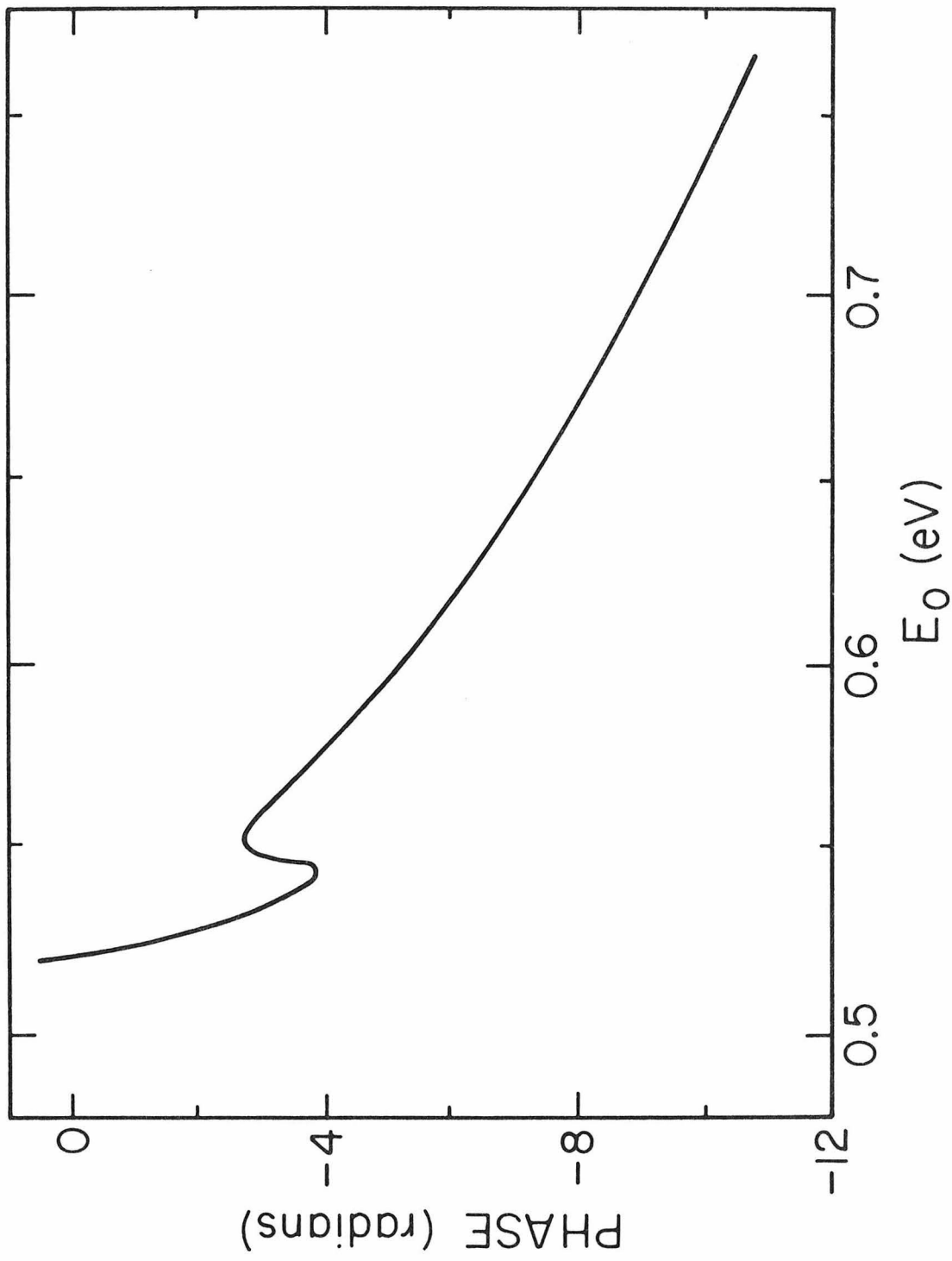

Fig. 13.

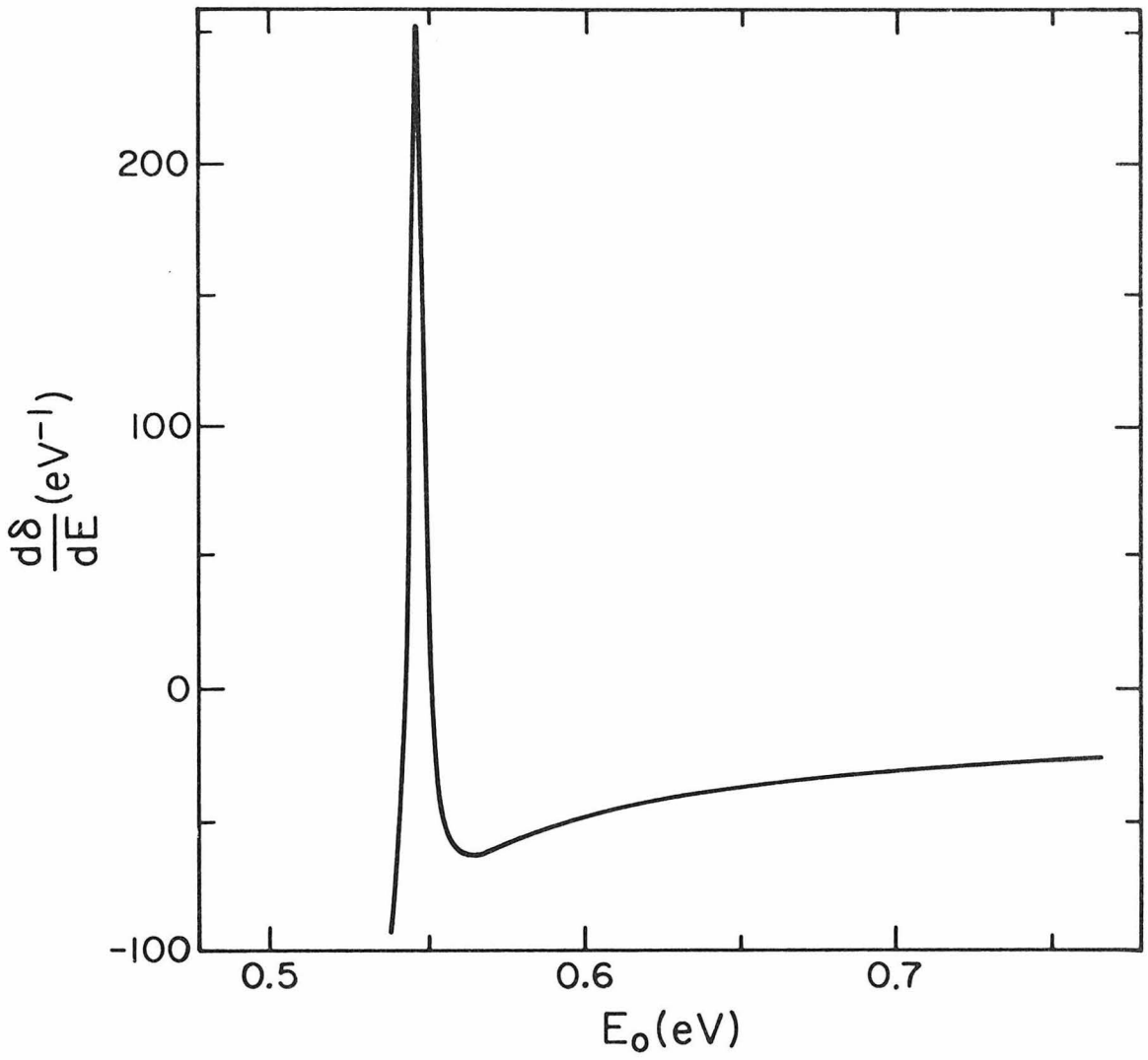

Fig. 14.

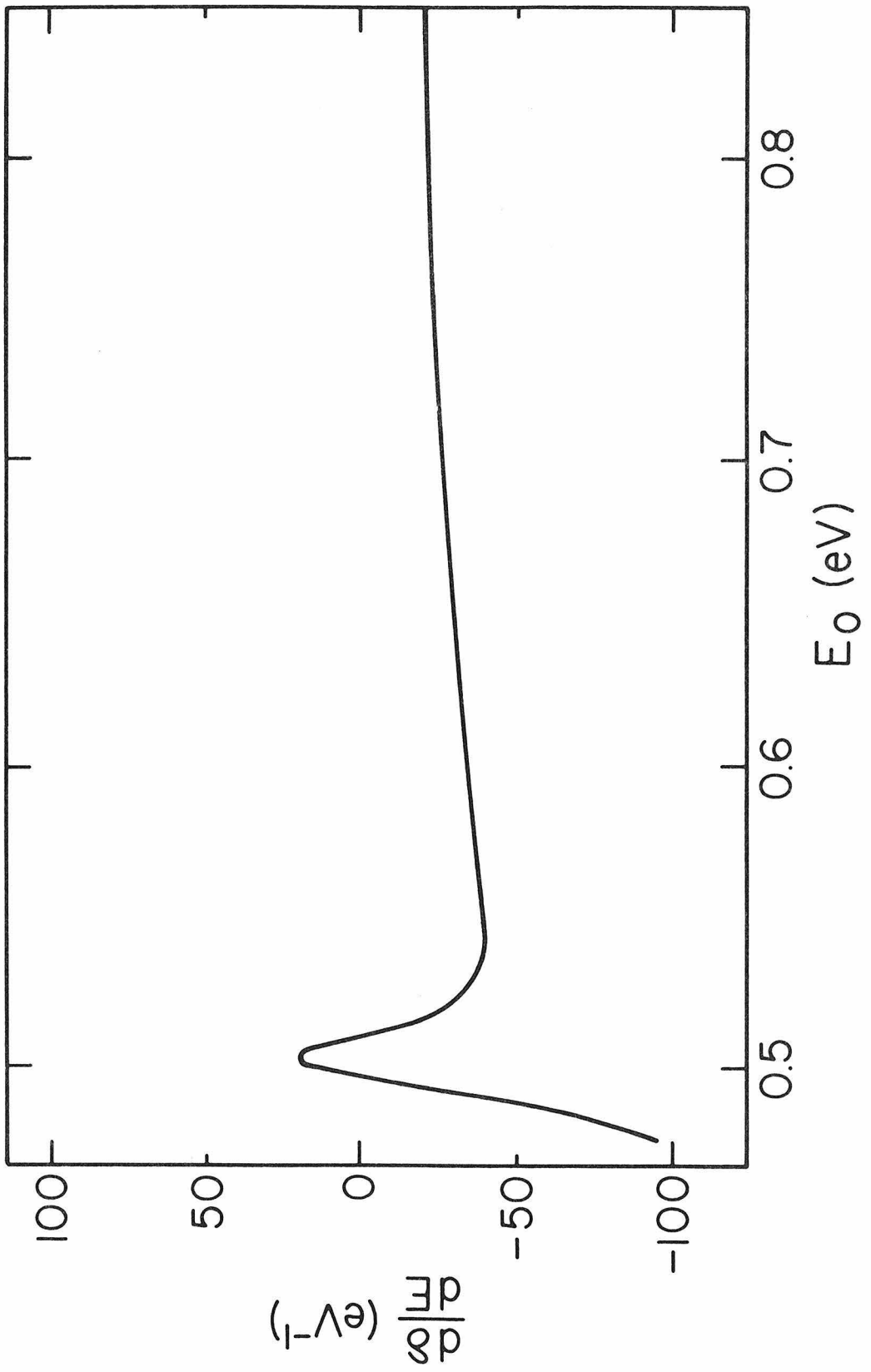

Fig. 15.

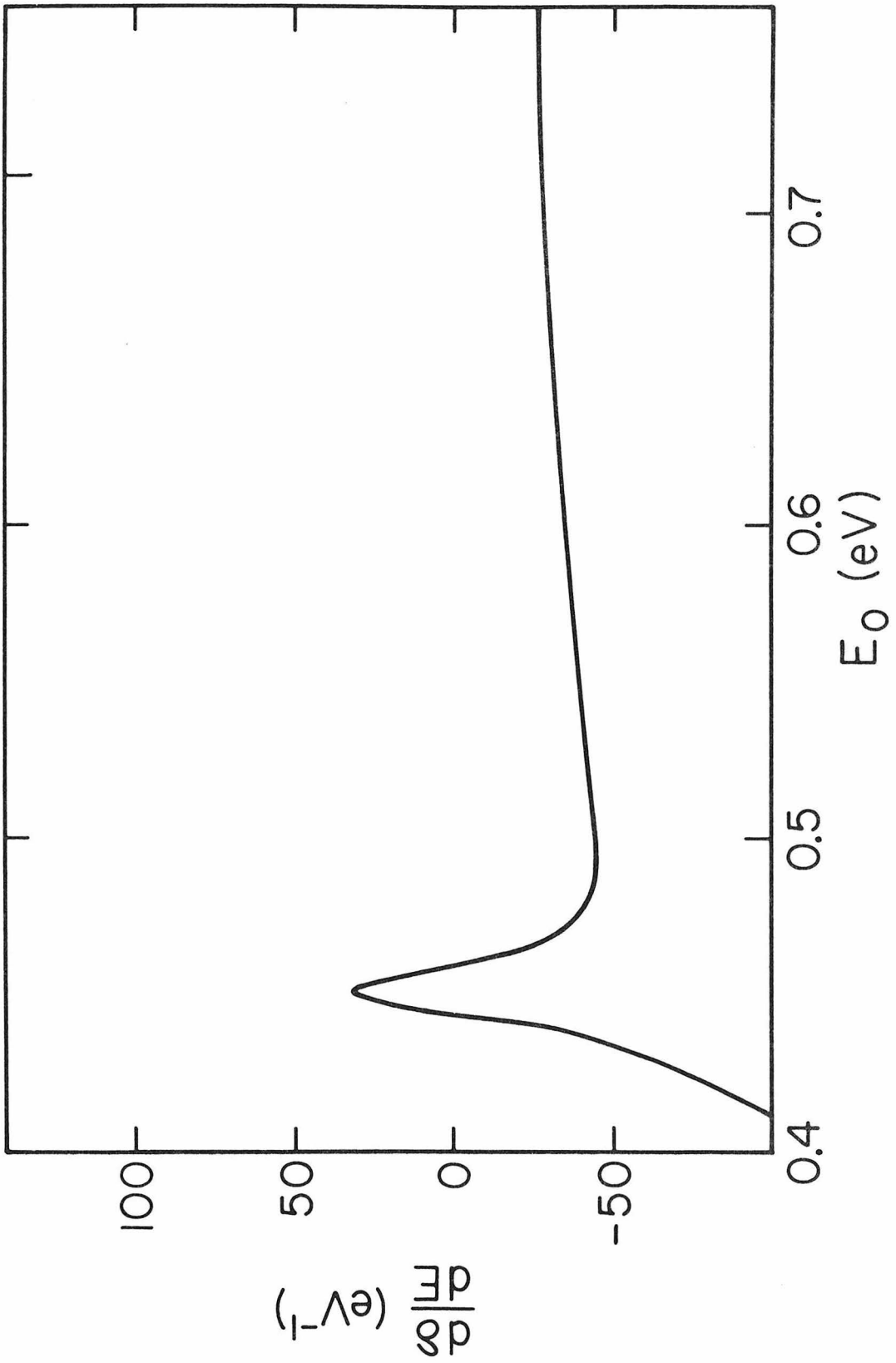

Fig. 16.

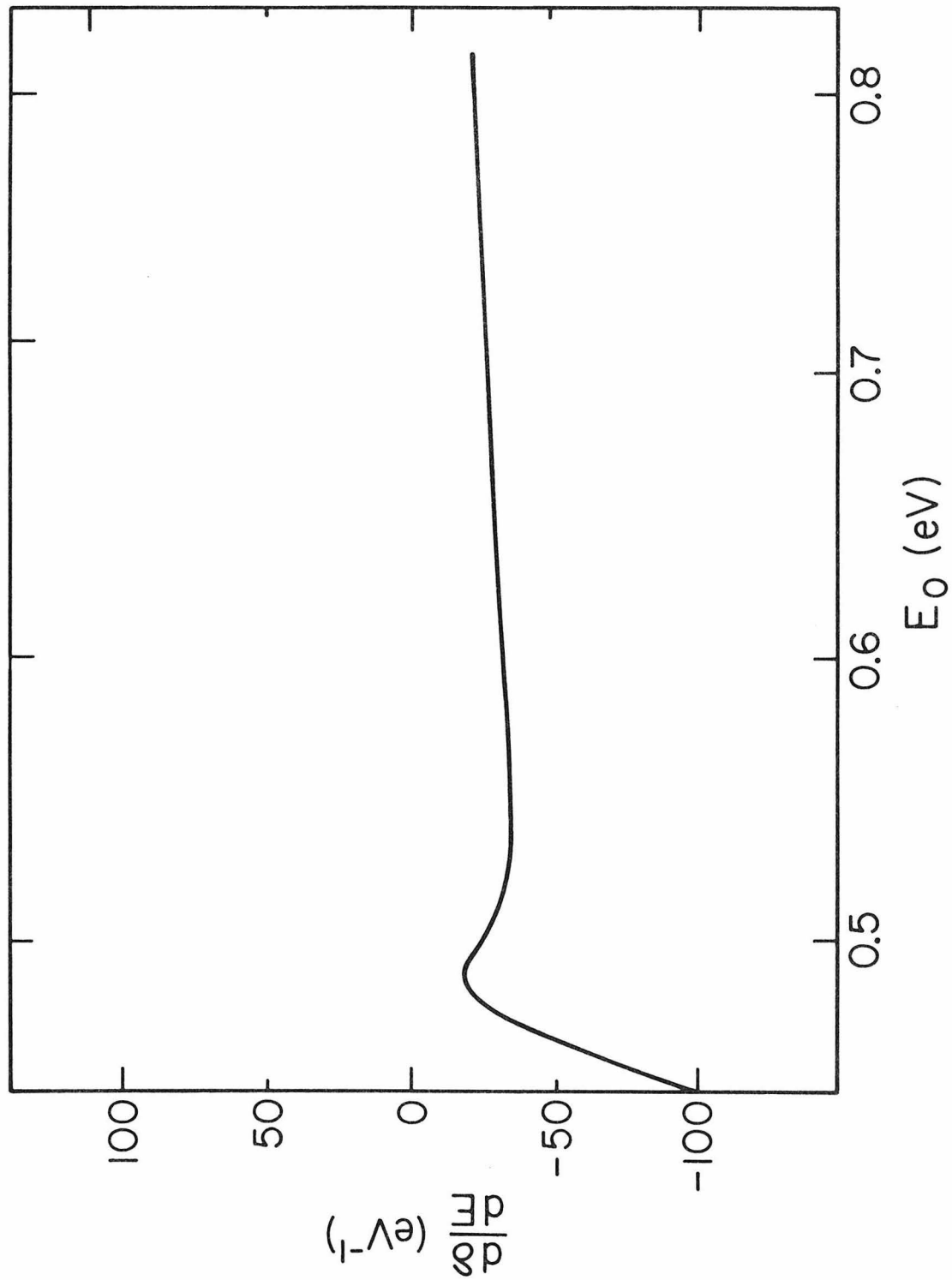

Fig. 17.

CHAPTER 4.

The Effect of Increasing the Barrier Height in Collisional Deactivation of Vibrationally Excited HF by H

I. Introduction

A central interest in chemical dynamics is energy transfer processes. These processes include electronic (de)excitation, vibrational-vibrational (V-V) energy transfer, vibrational-translational (V-T) energy transfer, and permutations with rotational energy. An immediate application of theoretical chemical dynamics is the chemical laser, the most important of which are the FH_2 and ClH_2 lasers.

Several theoretical approaches have been used to understand V-V and V-T processes in diatom-diatom systems. Shin[1] recently developed a model for the system

$$DF(v = n) + DF(v = 0) \rightarrow DF(v = n - 1) + DF(v = 1).$$

The model assumes dimer formation through hydrogen bonding. There is good agreement with experiment at $T < 300°K$, where there is little rotational motion.

Exact quantum calculations of diatom-diatom systems have generally been restricted to collinear collisions.

Riley and Kuppermann[2] and Dwyer and Kuppermann[3] calculated V-V and V-T probabilities for a model H_2-H_2 collinear system. The model assumed a harmonic oscillator potential for the diatomics and an exponential repulsive potential for the nearest end atoms.

Considerable work has been done in atom-diatom V-T reactions. Thompson[4-8] has used a quasi-classical trajectory technique to study systems of the type H + HX, X + HX, X + X_2, and X + H_2 where X is a halide atom. In his study[6] of vibrational deexcitation of HF by H (or D) atoms, Thompson found that both vibration-rotation (V-R) and V-T

processes were important. He also found that a number of multi-quantum V-V transitions were significant. In spite of this, he calculated rate constants on the assumption that only single quantum jumps occurred. The potential he used was a semi-empirical LEPS surface with a barrier of 28.6 kcal/mole in the collinear H + FH arrangement channel.

Schatz and Kuppermann[9] have done an exact quantum mechanical study of collinear H + FH systems. The surface used was Muckermann's number 5 LEPS potential.[10] The surface has a small well where the minimum reaction pathway intersects the symmetric stretch line, which is typical of LEPS surfaces. The well is 0.51 kcal/mole below the barrier height of 1.74 kcal/mole. They calculated reactive and nonreactive probabilities with initial translational energies between 0.01 eV and 1.5 eV and rate constants from 200 to 1000°K. Two important conclusions were drawn. One, reactive probabilities and rate constants were generally larger than nonreactive ones over a large range of energies and temperatures. Two, multi-quantum transitions were roughly as probable as single quantum jumps. Wilkins[11] reports very similar results in a three-dimensional (3-D) classical trajectory calculation on a different LEPS surface (but with roughly the same collinear barrier height, 1.4 kcal/mole). In addition, Wilkins found that V-T deactivation is more efficient than V-R deactivation.

It has been recently reported that the HFH collinear barrier height may be much higher than previously thought.[12,17] Bender et al.[12] report ab initio calculations (configuration interaction) which give a barrier height of 49 kcal/mole. They reason that the small error in their

calculation ($\sim$ 5 kcal/mole) implies that the true barrier is not lower than 40 kcal/mole. They conclude that F-atom exchange cannot be an important mechanism for vibrational deactivation of HF by H.

In a shock tube study of the reaction of H atoms with DF, Bott[16] estimated that the activation energy for F atom exchange was greater than 19 kcal/mole and probably close to 34 kcal/mole. He was certain that the LEPS surface was incapable of describing that reaction because of its small barrier.

The purpose of this study is to examine the effect of the barrier height on the dynamics of the H + FH collinear system; specifically, vibrational deactivation of HF by H atoms. We have used an exact quantum mechanical (close-coupling) formulation, which has been described elsewhere.[9] The potential energy surfaces (which will be described in detail in Sec. II) have barrier heights ranging from 1.5 kcal/mole to 40 kcal/mole. In Sec. III we present a discussion of the results.

II. Potential Energy Surfaces

For this study we need several potential energy surfaces which are alike except for the barrier height. Using surfaces which already exist is unsatisfactory. Even if one could find surfaces with the desired barrier heights, other aspects of the surfaces would differ and not allow a consistent comparison of the dynamics. Bowman and Kuppermann[13] have developed a simple method which allows one to design a surface to meet nearly any specification. It is a modification of the Wall-Porter method of rotating a Morse function (Fig. 1). The potential is given by

$$V(R_1, R_2) = D(\theta) \{[1 - \exp\{\beta(\theta)(\ell - \ell_{eq}(\theta))\}]^2 - 1\} + D(\theta = 0°) ,$$

where R_1 and R_2 are the two HF internuclear distances, β, D, and ℓ_{eq} are the Morse parameters, and θ and ℓ are given by

$$\tan \theta = (R_1 - R_1^0)/(R_2 - R_2^0),$$

and

$$\ell = [(R_1 - R_1^0)^2 + (R_1 - R_2^0)^1]^{\frac{1}{2}}.$$

The origin of the system, (R_1^0, R_2^0), is the point about which the Morse function rotates. The advantage of the Bowman-Kuppermann method over the Wall-Porter formulation is that β, D, and ℓ_{eq} are not necessarily analytical functions of θ. Instead, values for the parameters are chosen at several values of θ and then splined together to form a smooth curve.

The first surface developed was quite similar to Muckermann's surface 5. To do this we chose a swing point of $R_1^0 = R_2^0 = 7.0$ bohr

and used the Muckermann surface to calculate the Morse parameters as a function of θ. We chose enough points (11) on the ℓ_{eq} graph so that when splined together the $\ell_{eq}^{Muckermann}(\theta)$ and $\ell_{eq}^{spline}(\theta)$ were indistinguishable. The same procedure was used for $\beta(\theta)$.

For $D(\theta)$ we found it more convenient to assume

$$D(\theta) = D(\theta = 0°) - [A + Be^{-C(45° - \theta)^2}].$$

To solve for A, B, and C, we need to supply D at three angles, $\theta = 0°$, $\theta = 45°$, and an arbitrary choice of $\theta = 22°$. All of the values of D were taken from the Muckermann surface 5. To increase the barrier height, only D (45°) was changed. All other Morse parameters were held constant. Plots of the minimum reaction pathway for both Muckermann surface 5 and one created by the Bowman-Kuppermann method (with a 2.0 kcal barrier height) are shown in Fig. 2. For $R_1 > R_1^0$ (R_2 small), the surface was assumed to have the same value as at $R_1 = R_1^0$, and similarly for $R_2 > R_2^0$ (R_1 small). This produced a slight upward shift (~ 0.0168 kcal/mole = 0.7 mV) in the bottom of the well relative to HF dissociation. We have developed surfaces with 1.5, 10.0, 20.0, 30.0, and 40.0 kcal/mole barrier heights. The parameters for $D(\theta)$ are given in Table I for each of these surfaces. Figure 3 is a contour plot of the 20 kcal/mole surface.

The actual calculation uses a close-coupling technique which has been applied to several other systems.[14,15] For higher energies, the vibrational basis contained as many as 24 eigenfunctions in order to get converged results accurate to 2% or better.

III. Results

In this section we will present nonreactive and reactive transition probabilities for deactivation from excited vibrational states. Then we will examine rate constants for several transitions.

First let us define a few symbols. P_{ij}^{N} and P_{ij}^{R} are the nonreactive and reactive (in this case, F atom exchange) transition probabilities, respectively, from the i^{th} vibrational state to the j^{th} vibrational state. E_n is the translational energy relative to the n^{th} vibrational state of the reactant diatom.

The first spectrum (Fig. 4) is the P_{00}^{R} transition for two surfaces, Muckermann's surface 5 and the 1.5 kcal/mole barrier height surface. The results are quite similar over a range of 1.5 eV, which is expected as one surface (1.5 kcal/mole) was created from the other. The slight differences arise from the fact that "cuts" of the LEPS surface are not really Morse potentials and $D^{Gaussian}(\theta)$ and $D^{Muckermann}(\theta)$ are not identical. The next four figures depict transition probabilities P_{00}^{R} from each of the 10.0, 20.0, 30.0, and 40.0 kcal/mole surfaces, respectively. These spectra demonstrate the expected effect of increasing the barrier height on reactive probabilities. As the barrier is increased, it takes increasingly more translational energy to proceed to reaction. If we define the threshold energy, E_{th}, as the energy at which $P_{00}^{R} = 0.001$, Table II shows that for all but the smallest barrier height the threshold of reaction is about 75% of the barrier height.

Figures 9-13 show reactive and nonreactive deactivation probabilities from v = 3 to v = 2 for all five surfaces. Once the barrier

has been effectively surmounted by increasing the translational energy, the reactive probability is generally larger than the nonreactive probability. The figures also demonstrate that there is a threshold for reactive transitions (shown in Table II) that increases linearly with the barrier height. A comparison of the second and third columns of Table II indicates that except for the 1.5 kcal/mole surface the translational energy threshold for a reactive process from v = 3 is significantly lower ($\sim$ 40%) than the threshold for a reactive process from v = 0. This implies that vibrational energy is effective in overcoming the barrier. At low translational energies, which are the most important energies in determining rate constants, the nonreactive probabilities are larger than the reactive ones.

A significant conclusion from previous studies[6,9] of this system was that multiquantum transition probabilities were of the same magnitude as single quantum transitions. Although both of the studies were done on systems with very low barriers, we find that multiquantum transitions are still significant with larger barriers. Figures 14 and 15 illustrate this for the 1.5 kcal/mole and 20 kcal/mole surfaces. For the largest barrier (40.0 kcal/mole) the 3→0 transition probabilities are relatively small. The largest reactive probability is 0.06, which is about a factor of five smaller than the 3→2 probability.

Because multiquantum transitions are important, we will examine total reactive and nonreactive deactivation probabilities from v = 6 and 5, which we will denote as $\sum P_{6j}$ and $\sum P_{5j}$, respectively. The results indicate that there is almost no deactivation (reactive or nonreactive) from v = 6 on the 30 kcal/mole and 40 kcal/mole surfaces in the energy

range considered (0.0 eV < $E_6 \leq 0.32$ eV). Similarly, there is little deactivation from v = 5 on the 40 kcal/mole surface (0.0 eV $\leq E_5 \leq$ 0.7 eV). This probably resulted from the narrow translational energy range. In Figs. 16-18 we have plotted $\sum P_{5j}^{R,N}$ as a function of translational energy for the 1.5, 10, and 20 kcal/mole surfaces. As before, deactivation by reactive collisions is more probable than by nonreactive collisions for all surfaces and at all energies above a threshold energy. At energies greater than threshold, the total probability for deactivation (reactive plus nonreactive) is about 0.75. The probability of deactivation from v = 6 shows similar trends; once the effective barrier has been crossed, the probability of deactivation is quite high, between 0.8 and 0.9.

Using the transition probabilities presented in this paper, we have calculated rate constants from the equation

$$k_{ij}^{R(N)}(T) = \int_0^\infty P_{ij}^{R(N)} \exp(-E_i/kT) dE_i \ ,$$

where E_i is the translational energy of the reactant diatomic in vibrational state i, k is Boltzmann's constant, T is the temperature in K, and P is the transition probability. We will let $k_i^{R(N)}$ denote the reactive (nonreactive) rate constant of deactivation from state i to all other states.

Figure 19 is a plot of a reactive rate constant for a single quantum deactivation transition, k_{32}^R, and it demonstrates what we intuitively expect. As the barrier height is increased from 1.5 kcal/mole to 40 kcal/mole, k_{32}^R decreases for any temperature in the range 200 K to 1000 K. The corresponding nonreactive transitions do not show this trend, and in fact for temperatures below 300 K, the rate constants

slowly increase as the barrier height is increased. Whereas the reactive rate constants may differ by several orders of magnitude as the barrier is increased, the nonreactive rate constants differ by less than an order of magnitude at all temperatures and by a factor of 5.0 at 300 K.

Table II contains the Arrhenius parameters for the reactive $3 \rightarrow 2$ transition. For both low temperature and high temperature cases, the activation energy, E_a^{32}, increases with the barrier height. E_a^{32} is significantly smaller in the low temperature region, where low translational energies are important in calculating rate constants. This deviation from the high temperature linearity probably results from the importance of vibrational energy in overcoming the barrier. At higher temperatures, molecules are more likely to have a larger translational energy and the relative importance of vibrational energy is diminished. A comparison of Figs. 19 and 20 shows that the reactive and nonreactive rate constants from the low barrier height surfaces are of comparable magnitude. For the large barrier height surfaces (20.0, 30.0, and 40.0 kcal/mole) k_{32}^N is orders of magnitude larger than k_{32}^R.

In Fig. 21 we have plotted k_{30}^R and k_{30}^N as a function of temperature for the three surfaces, with 1.5, 20, and 40 kcal/mole barrier heights. In this figure one can see that multiquantum reactive rate constants are at least as large as the rate constants for single quantum transitions for all three surfaces. Rate constants for multiquantum nonreactive transitions, k_{30}^N, become much smaller than the corresponding single quantum rate constant k_{32}^N as the barrier is increased.

In Fig. 22 we have plotted rate constants for the collinear reactions

$$H + FD\ (v = 3) \rightarrow HF\ (v = 0) + D$$
$$H + FD\ (v = 3) \rightarrow H + FD\ (v = 0)$$
$$D + FH\ (v = 3) \rightarrow DF\ (v = 0) + H$$
$$D + FH\ (v = 3) \rightarrow D + FH\ (v = 0)$$

along with the H + FH results, all using the 20 kcal/mole surface. The figure indicates that substitution of H by D does not qualitatively affect the results; reactive rate constants are generally larger than the nonreactive rate constants. When D is substituted for H in the target diatom, both the reactive and nonreactive rate constants become smaller. This is a result of the difference in total energy available for reaction; even though the translational energies are equal, the vibrational energy of the v = 3 state in DF is 0.43 eV less than the vibrational energy of the same state in HF.

In Fig. 23 we examine k_5^R and k_5^N as a function of temperature for three surfaces. As with the individual reactive rate constants, k_5^R decreases steadily with increasing barrier height. Except for the smallest barrier height, the rate constants for total nonreactive deactivation are roughly constant as the barrier is increased.

From Fig. 23 we can conclude that below 1000 K there is no significant deactivation by a fluorine atom exchange mechanism for surfaces with large ($\sim$ 40 kcal/mole) barrier heights.

IV. Summary

We have shown that increasing the barrier height in a collinear chemical system affects the dynamics in several ways. There is a threshold above which reactive collisions are generally more probable than nonreactive ones. Below that threshold, nonreactive collisions are more probable for systems with barrier heights greater than 10.0 kcal/mole. This is reflected in the rate constants over a wide range of temperatures (200-1000 K). At the temperatures considered, F-atom exchange is not an efficient mode of deactivation for systems with the larger barrier heights. The translational energy threshold for F-atom exchange is generally lower than the barrier height, indicating that vibrational energy is effective in promoting the reaction. Finally, multiquantum transition probabilities are of the same magnitude as single quantum transitions for all barrier heights considered and must be considered in calculating deactivation rate constants.

TABLE I. $D(\theta)$ parameters for different barrier heights.

Barrier Height (kcal/mole)	A (kcal/mole)	B (kcal/mole)	C (rad^{-1})
1.5	0.01681	1.4832	13.434
10.	0.01681	9.9832	25.268
20.	0.01681	19.983	29.575
30.	0.01681	29.983	32.093
40.	0.01681	39.983	33.879

TABLE II. Threshold of P_{ij}^{R} with different barrier heights.

Barrier Height (kcal/mole)		E_{th}: Threshold of P_{ij}^{R} (eV) i=0, j=0	i=3, j=0
1.5	(0.065 eV)	0.022	0.025
10.	(0.43 eV)	0.31	0.18
20.	(0.87 eV)	0.69	0.39
30.	(1.30 eV)	1.05	0.68
40.	(1.73 eV)	1.43	0.79

TABLE III. Arrhenius rate constant parameters[a] for H + FH → HF + H for different surfaces.

	Temperature Range (K)	1.5 kcal/mole[b]	10 kcal/mole	20 kcal/mole	30 kcal/mole	40 kcal/mole
E_a^{32}	200-400	0.9403	1.0906	1.7978	1.9732	2.935
A_{32}	200-400	0.7242(4)	0.1384(3)	0.4492(4)	0.5445(-2)	0.2185(-5)
E_a^{32}	800-1000	2.2932	5.2326	8.543	16.272	21.944
A_{32}	800-1000	0.2577(5)	0.1665(5)	0.1075(5)	0.2454(5)	0.1052(5)

[a] $k_{ij}(T) = A_{ij} \exp(-E_a^{ij}/RT)$, where E_a^{ij} is in kcal/mole and A_{ij} is in cm/(molec-sec).

[b] The number in parentheses is the power of 10 by which the preceding number is to be multiplied.

References

1. H. K. Shin, J. Chem. Phys. 63, 2901 (1975).
2. M. Riley and A. Kuppermann, Chem. Phys. Lett. 1, 537 (1968).
3. J. Dwyer and A. Kuppermann, Chem. Phys. Lett. 44, 499 (1976).
4. D. L. Thompson, J. Chem. Phys. 56, 3570 (1972).
5. D. L. Thompson, J. Chem. Phys. 57, 4164 (1972).
6. D. L. Thompson, J. Chem. Phys. 57, 4170 (1972).
7. D. L. Thompson, J. Chem. Phys. 60, 4577 (1974).
8. J. M. White and D. L. Thompson, J. Chem. Phys. 61, 719 (1974).
9. G. Schatz and A. Kuppermann, unpublished results.
10. J. T. Muckermann, J. Chem. Phys. 54, 1155 (1971); ibid. 56, 2977 (1972).
11. R. L. Wilkins, J. Chem. Phys. 58, 3038 (1973).
12. C. F. Bender, B. J. Garrison, and H. F. Schaefer III, J. Chem. Phys. 62, 1188 (1975).
13. J. M. Bowman and A. Kuppermann, Chem. Phys. Lett. 34, 523 (1975).
14. G. C. Schatz and A. Kuppermann, J. Chem. Phys. 59, 964 (1973).
15. G. C. Schatz, J. M. Bowman, and A. Kuppermann, J. Chem. Phys. 58, 4023 (1973).
16. J. F. Bott, J. Chem. Phys. 65, 1976 (1976).
17. W. R. Wadt and N. W. Winter, "Ab Initio Potential Surface Calculations for the H + H_2O and H + HF Hydrogen Atom Exchange Reactions", 12th International Symposium on Free Radicals, Laguna Beach, California, January 1976.

FIGURE CAPTIONS

FIG. 1. Coordinate system used by the Bowman-Kuppermann method of creating potential energy surfaces with rotated Morse functions.

FIG. 2. The minimum reaction pathway as a function of swing angle θ. The dashed line is from Muckermann's surface 5; the solid line is from a 2 kcal/mole barrier height surface.

FIG. 3. A contour plot of the 20 kcal/mole barrier height HFH surface. The axes are the HF internuclear distances (in bohr) and the contours range from 0.3 eV to 1.5 eV in steps of 0.3 eV. 0.0 eV is defined as the bottom of the HF potential.

FIG. 4. P_{00}^{R} as a function of translational energy E_0. The solid line was calculated using the Muckermann surface (see Ref. 9) and the dashed line using the 1.5 kcal/mole surface. The energy range is from 0.0 eV to 1.5 eV.

FIG. 5. P_{00}^{R} as a function of translational energy E_0 in the range of 0.0 eV to 3.0 eV. It was calculated using the 10 kcal/mole surface. The arrow on the abscissa indicates the height of the barrier.

FIG. 6. P_{00}^{R} for the 20 kcal/mole surface. Units and markings are the same as in Fig. 5.

FIG. 7. P_{00}^{R} for the 30 kcal/mole surface. Units and markings are the same as in Fig. 5.

FIG. 8. P_{00}^{R} for the 40 kcal/mole surface. Units and markings are the same as in Fig. 5.

FIG. 9. The probability of deactivation from v = 3 to v = 2 using the 1.5 kcal/mole surface. The dashed line is the reactive probability and the solid line is the nonreactive probability. The abscissa

is the initial translational energy E_3 and is in the range 0.0 eV to 1.6 eV. The arrow indicates the opening to excited vibrational states of HF.

FIG. 10. P_{32}^N (solid line) and P_{32}^R (dashed line) calculated using the 10 kcal/mole surface. Units and markings are identical to Fig. 9.

FIG. 11. P_{32}^N (solid line) and P_{32}^R (dashed line) calculated using the 20 kcal/mole surface. Units and markings are identical to Fig. 9.

FIG. 12. P_{32}^N (solid line) and P_{32}^R (dashed line) calculated using the 30 kcal/mole surface. Units and markings are identical to Fig. 9.

FIG. 13. P_{32}^N (solid line) and P_{32}^R (dashed line) calculated using the 40 kcal/mole surface. Units and markings are identical to Fig. 9.

FIG. 14. P_{30}^N (solid line) and P_{30}^R (dashed line) calculated using the 1.5 kcal/mole surface. Units and markings are identical to Fig. 9.

FIG. 15. P_{30}^N (solid line) and P_{30}^R (dashed line) calculated using the 20 kcal/mole surface. Units and markings are identical to Fig. 9.

FIG. 16. The probability of deactivation from v = 5 to all other states calculated using the 1.5 kcal/mole surface. The solid line is the sum of all nonreactive transitions, the dashed line the sum of all reactive transitions, and the dashed-dotted line the sum of all transitions. The abscissa is initial translational energy E_5 in the range 0.0 eV to 0.8 eV. The arrow indicates the opening of the v = 6 vibrational state of HF.

FIG. 17. $\sum P_{5j}^{N}$ (solid line), $\sum P_{5j}^{R}$ (dashed line), and $\sum P_{5j}^{N} + \sum P_{5j}^{R}$ (dashed-dotted line) calculated using the 10 kcal/mole surface. Units and markings are the same as in Fig. 16.

FIG. 18. $\sum P_{5j}^{N}$ (solid line), $\sum P_{5j}^{R}$ (dashed line), and $\sum P_{5j}^{N} + \sum P_{5j}^{R}$ (dashed-dotted line) calculated using the 20 kcal/mole surface. Units and markings are the same as in Fig. 16.

FIG. 19. An Arrhenius plot of the rate constant for the reactive v = 3 to v = 2 transition for the 1.5, 10, 20, 30, and 40 kcal/mole surfaces. The units of k_{32}^{R} are (cm/molecule-sec). The abscissa is measured in units of 1000 K/T and T (200 K $\leq$ T $\leq$ 1000 K).

FIG. 20. k_{32}^{N} calculated using the 1.5, 10, 20, 30, and 40 kcal/mole surfaces. The units are the same as in Fig. 19.

FIG. 21. k_{30}^{N} and k_{30}^{R} using the 1.5, 20, and 40 kcal/mole surfaces. The units are the same as in Fig. 19.

FIG. 22. Arrhenius plots of k_{30} for the HFH and DFH systems using the 20 kcal/mole barrier height surface.

FIG. 23. Arrhenius plots of k_{5}^{N} and k_{5}^{R} for the 1.5, 20, and 40 kcal/mole surfaces.

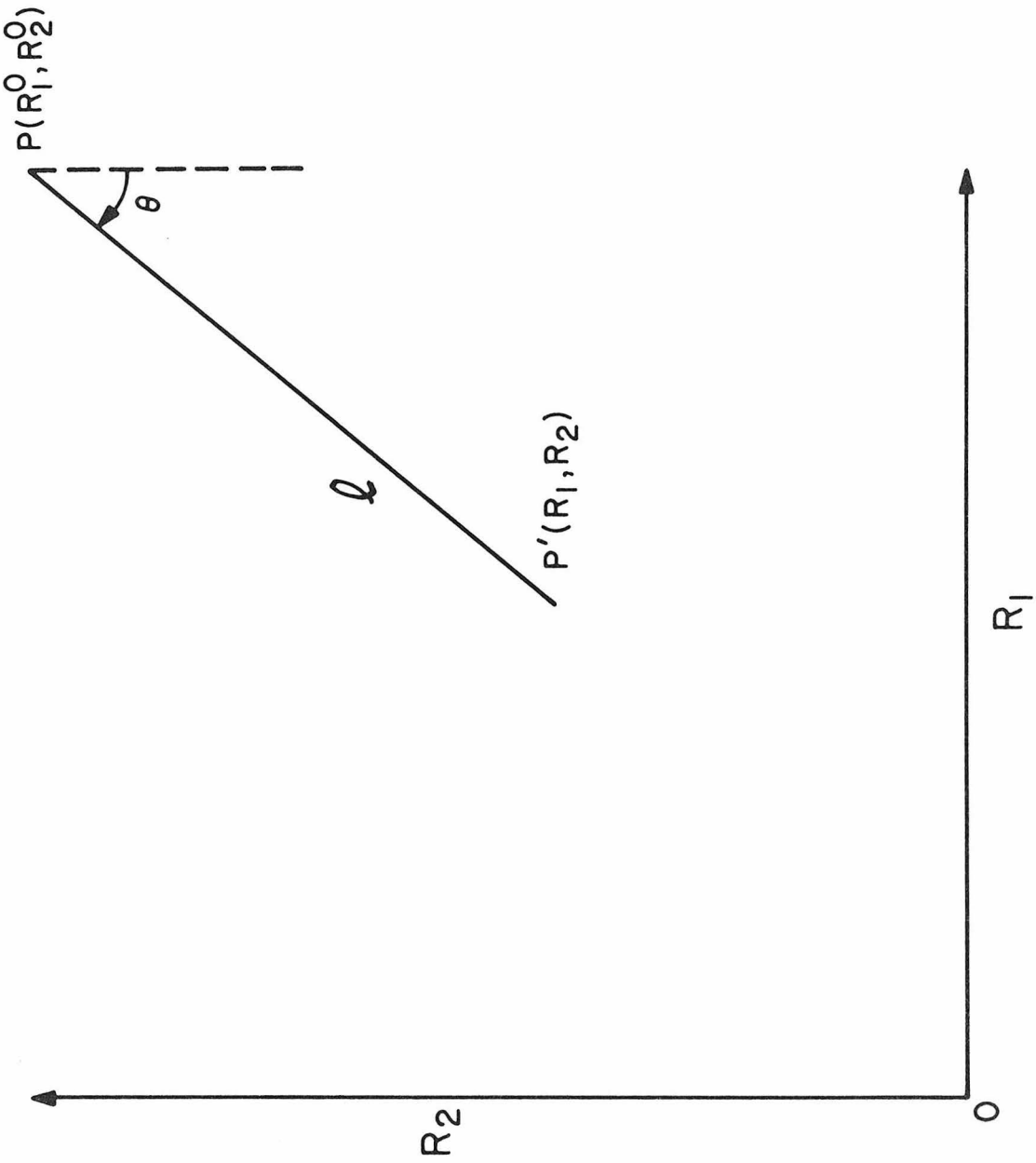

Fig. 1.

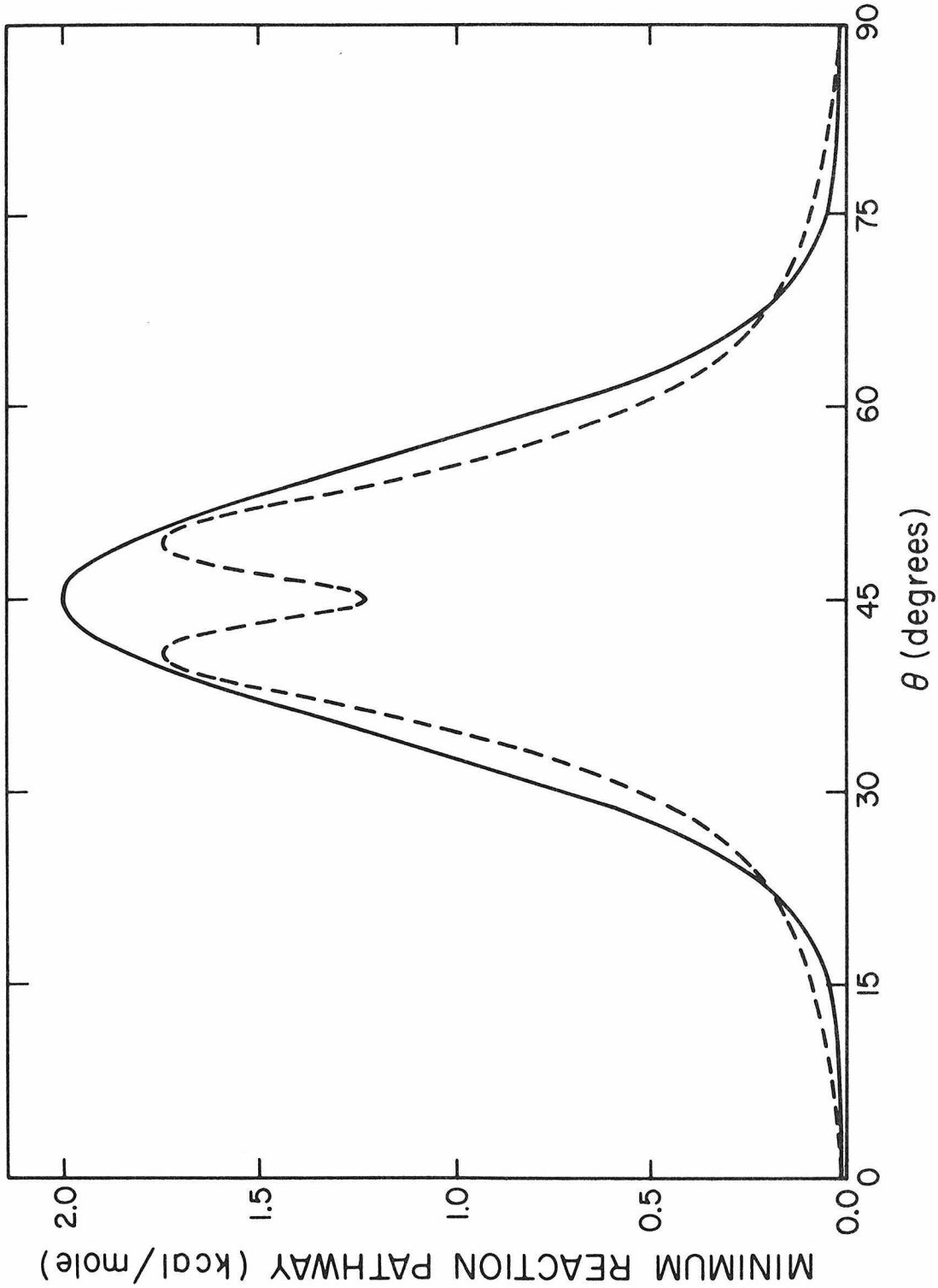
MINIMUM REACTION PATHWAY (kcal/mole)
2.0
1.5
1.0
0.5
0.0
0
15
30
45
60
75
90
θ (degrees)

Fig. 2.

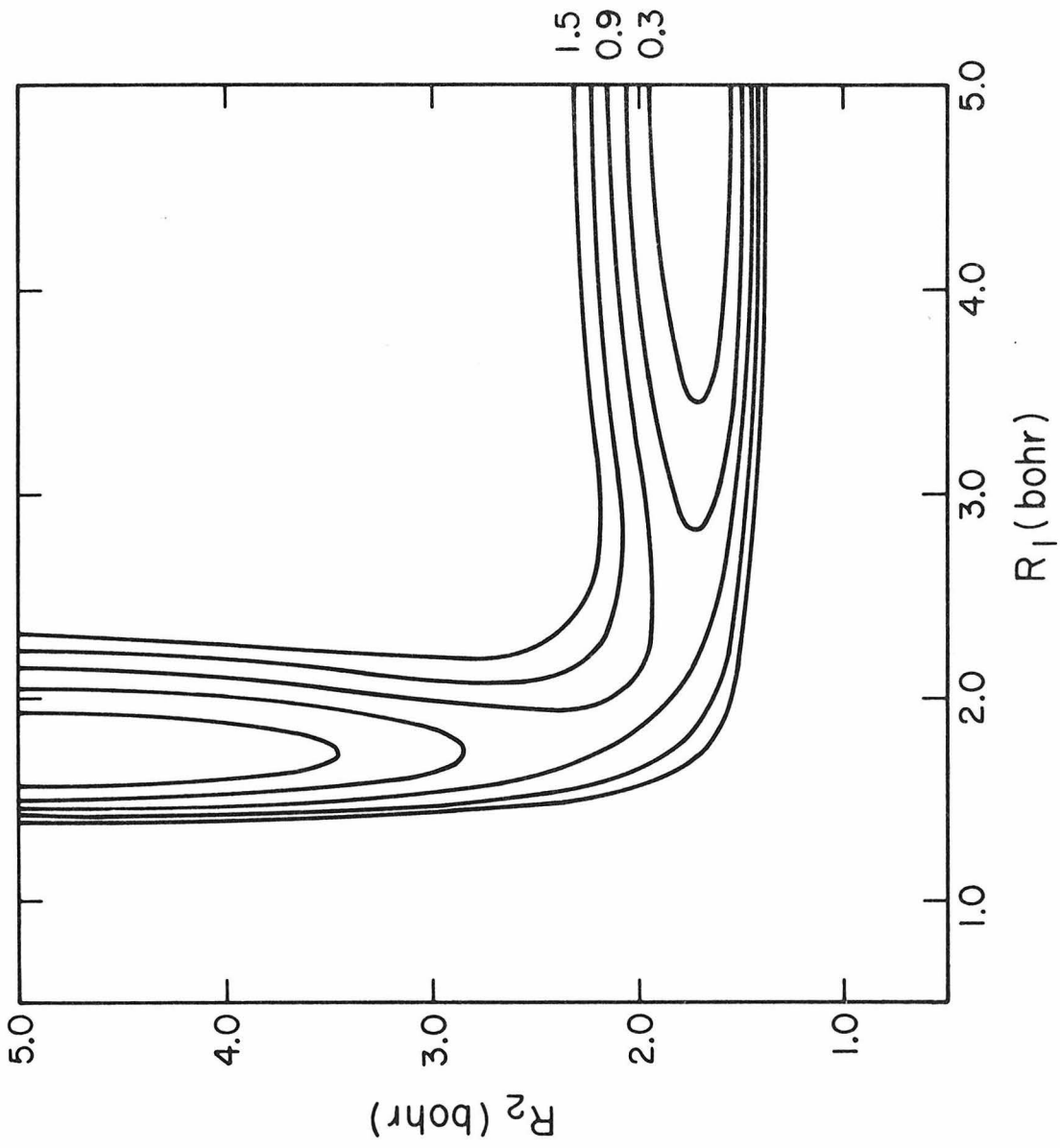

Fig. 3.

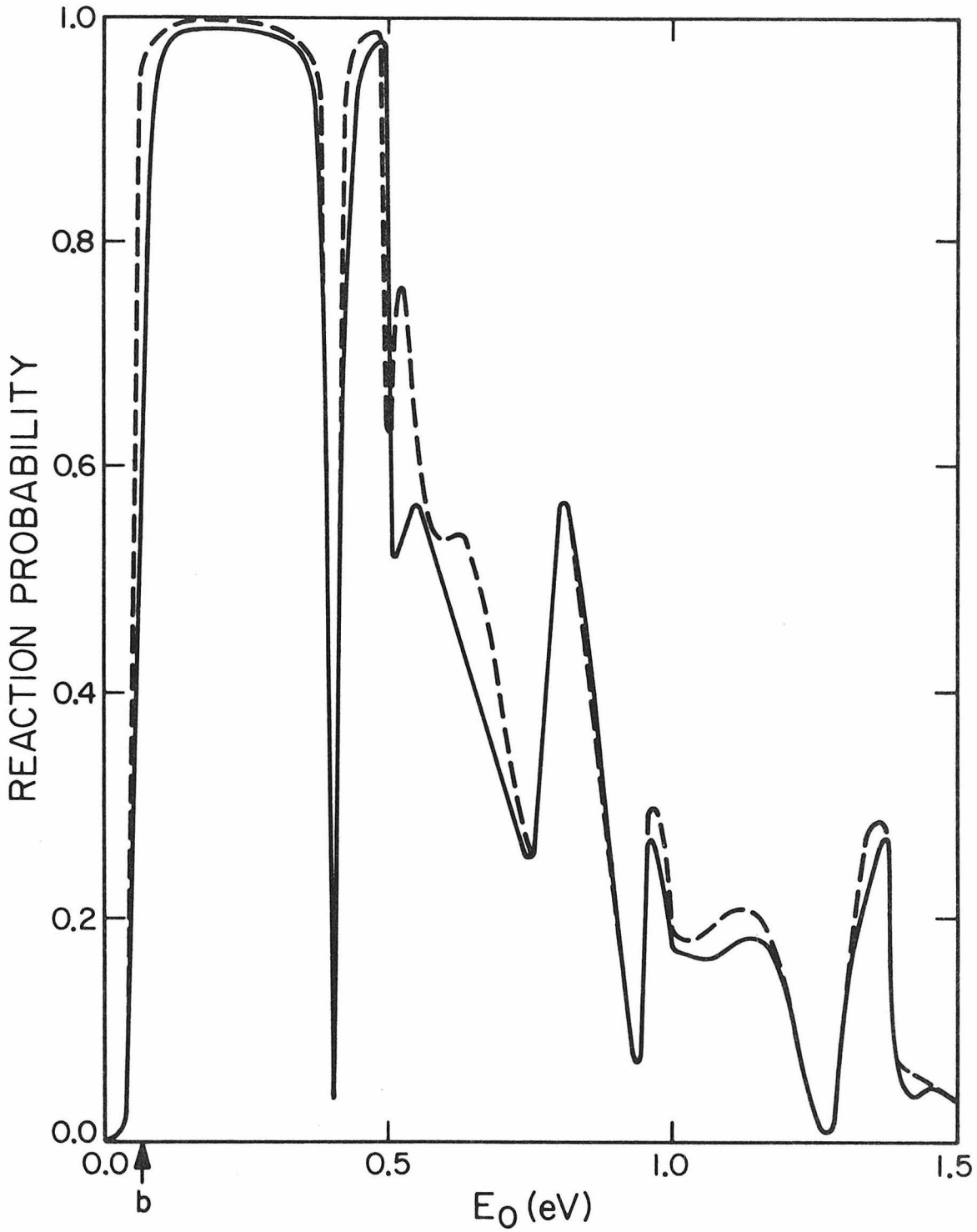

Fig. 4.

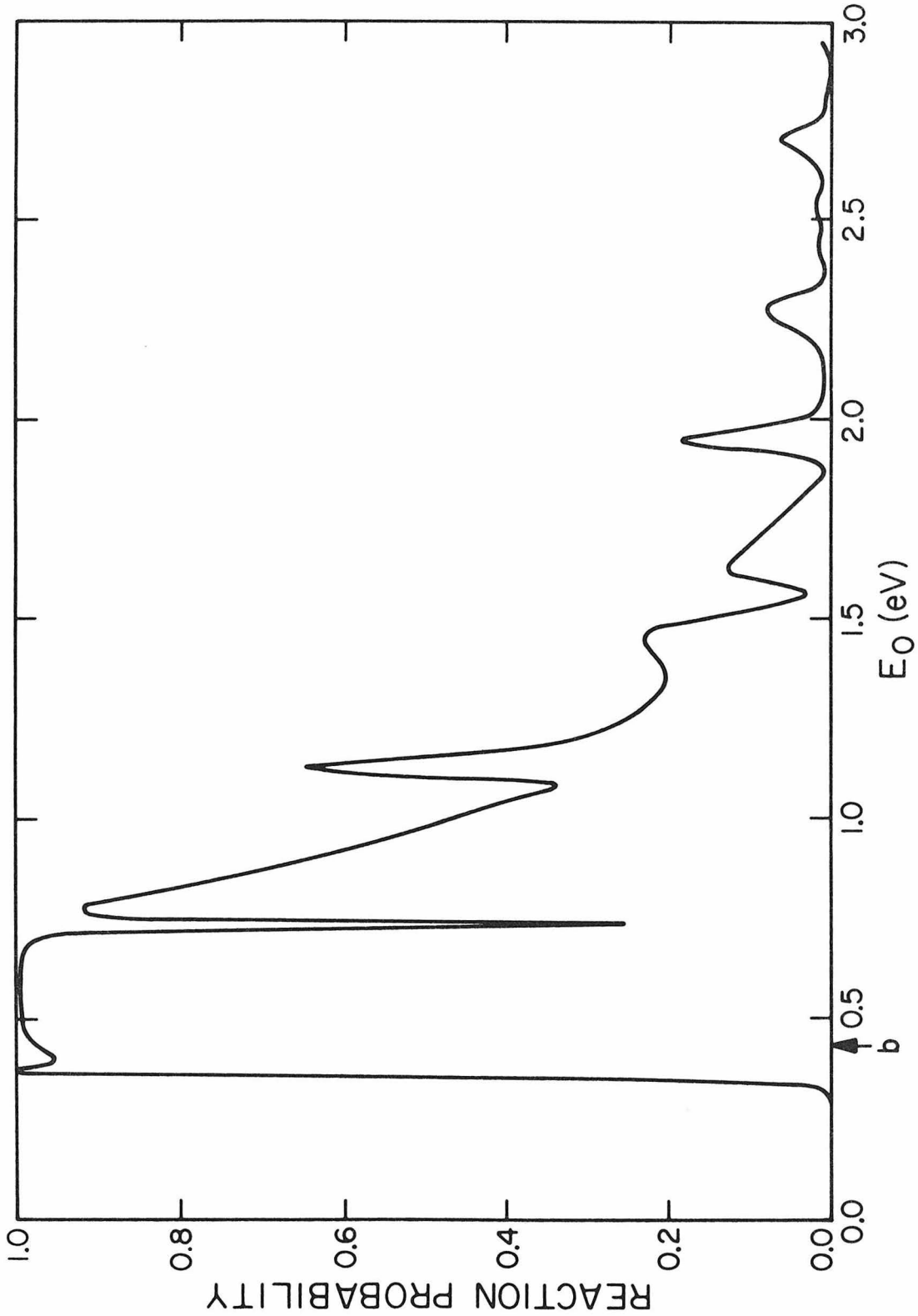
REACTION PROBABILITY
1.0
0.8
0.6
0.4
0.2
0.0
0.0
0.5
b
1.0
1.5
2.0
2.5
3.0
E_0 (eV)

Fig. 5.

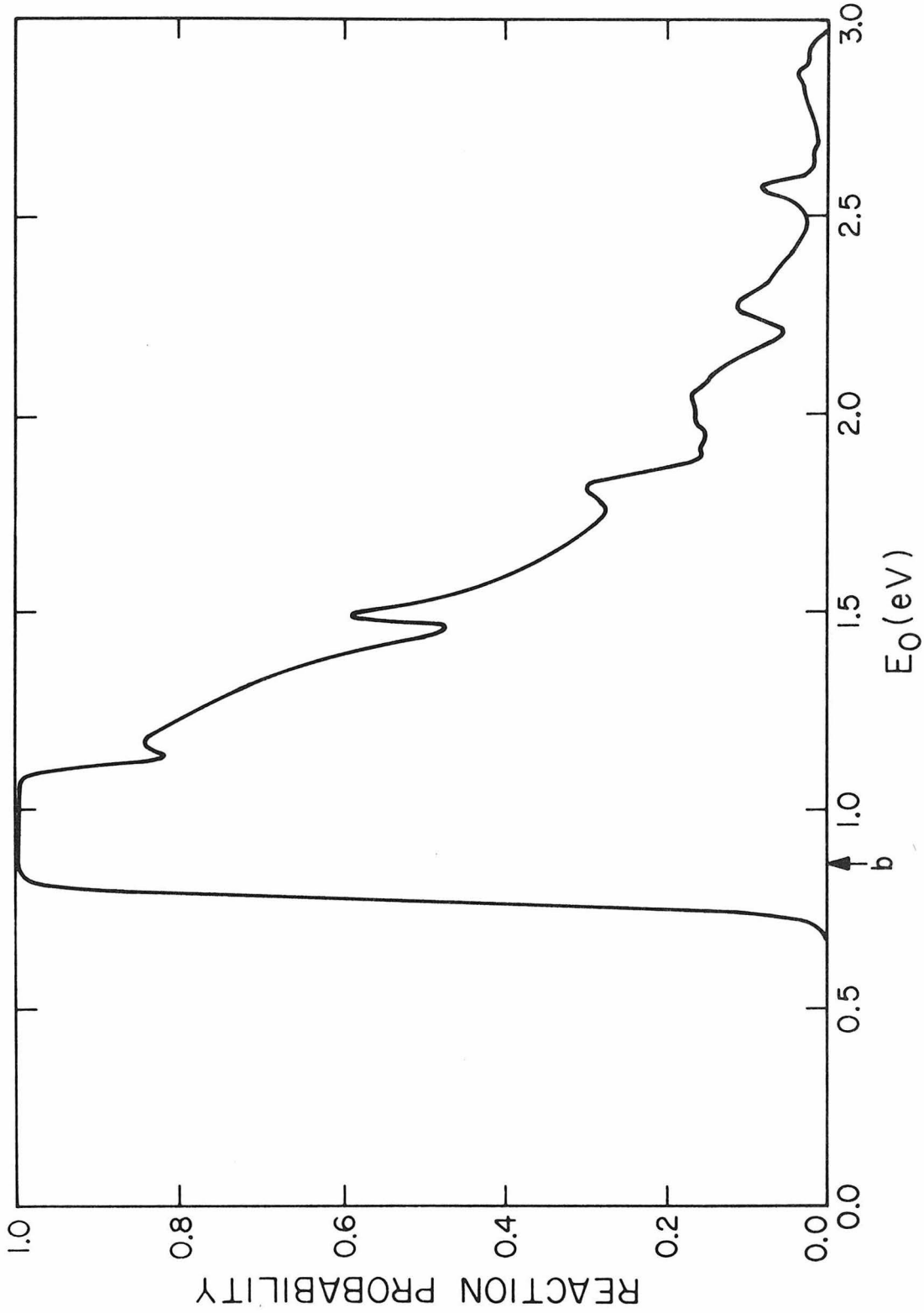
REACTION PROBABILITY
1.0
0.8
0.6
0.4
0.2
0.0
0.0
0.5
1.0
1.5
2.0
2.5
3.0
b
E_0(eV)

Fig. 6.

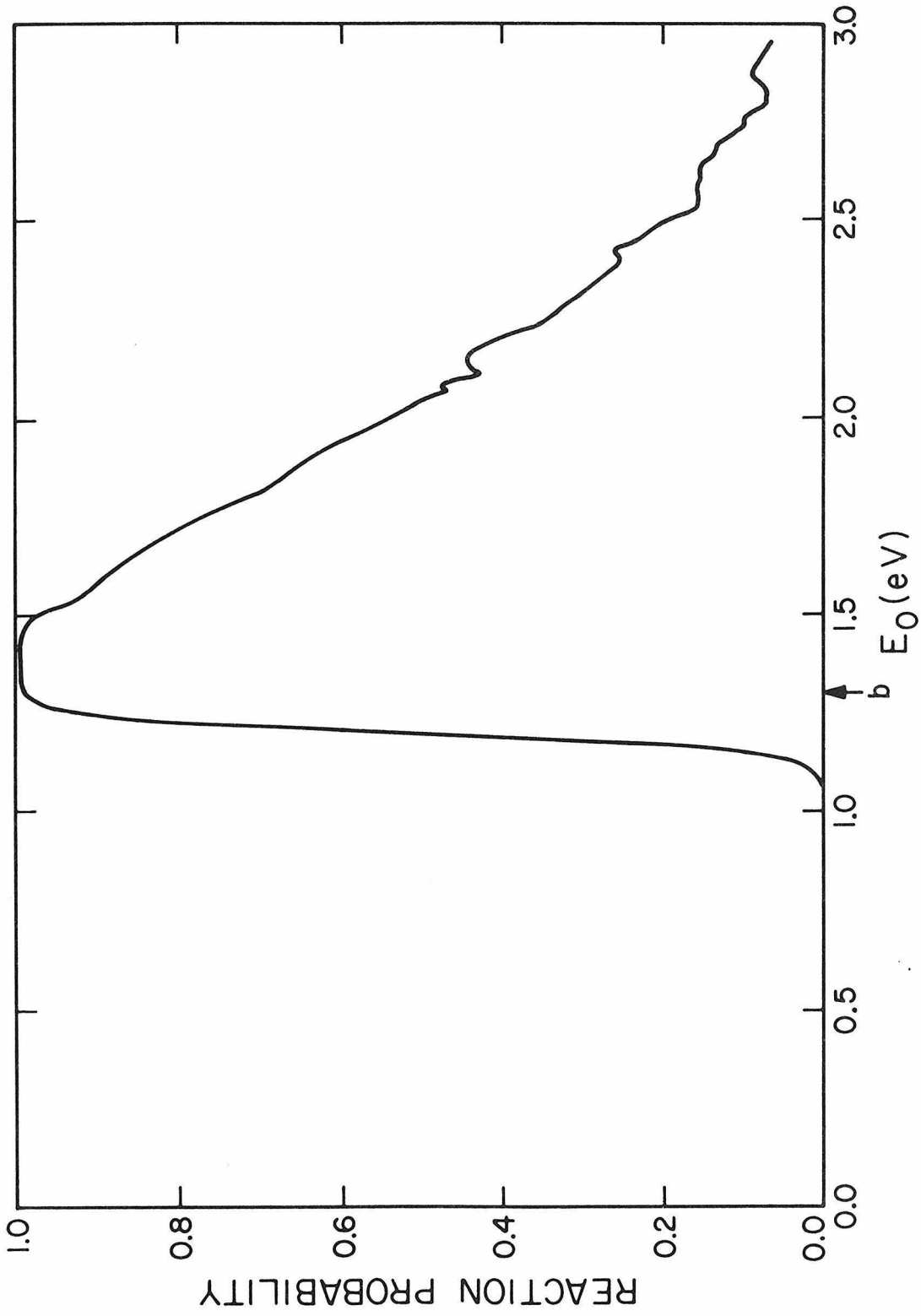
REACTION PROBABILITY
1.0
0.8
0.6
0.4
0.2
0.0
0.0
0.5
1.0
1.5
2.0
2.5
3.0
b
E_0(eV)

Fig. 7.

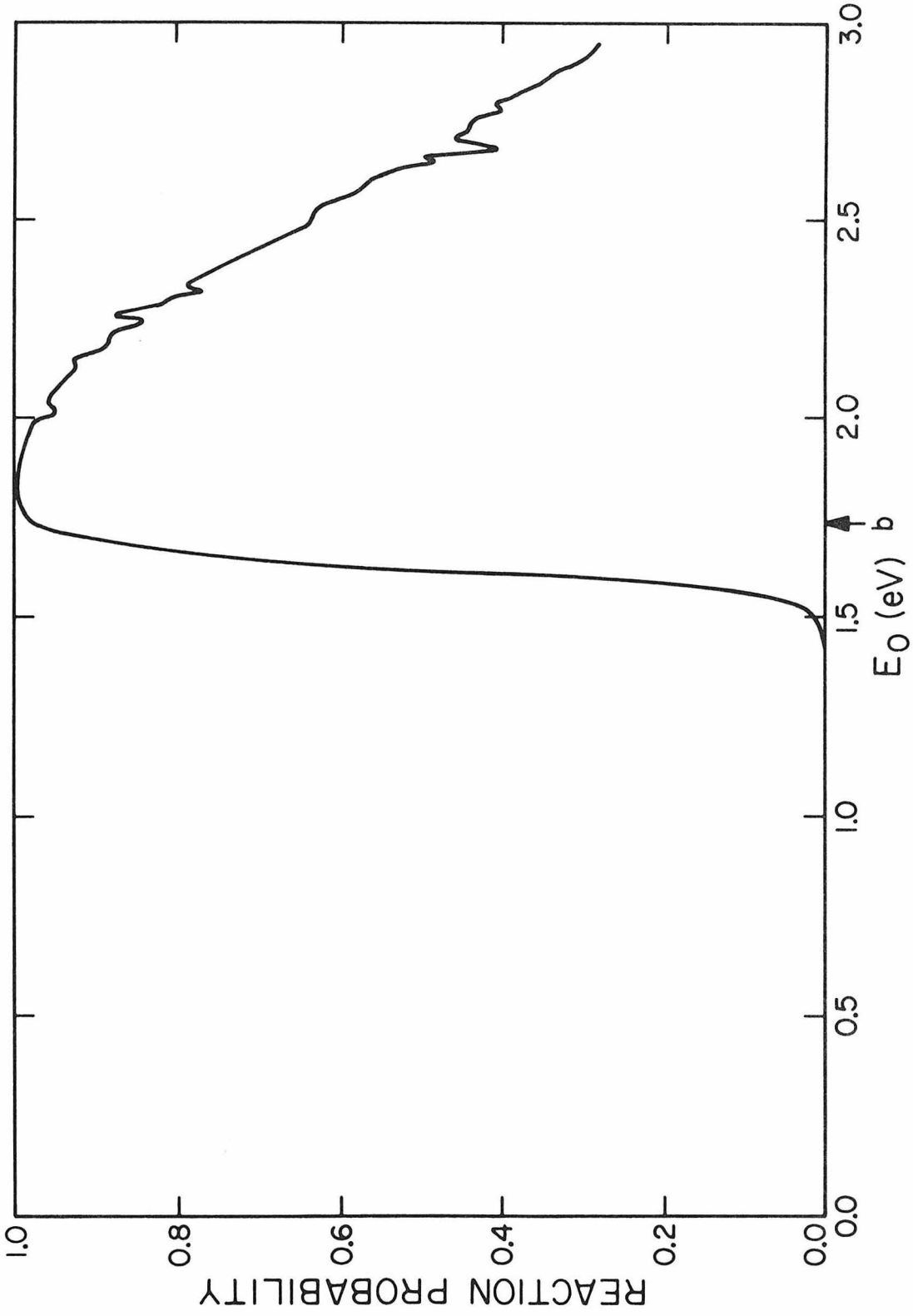
REACTION PROBABILITY
1.0
0.8
0.6
0.4
0.2
0.0
0.0
0.5
1.0
1.5
2.0
2.5
3.0
E_0 (eV)
b

Fig. 8.

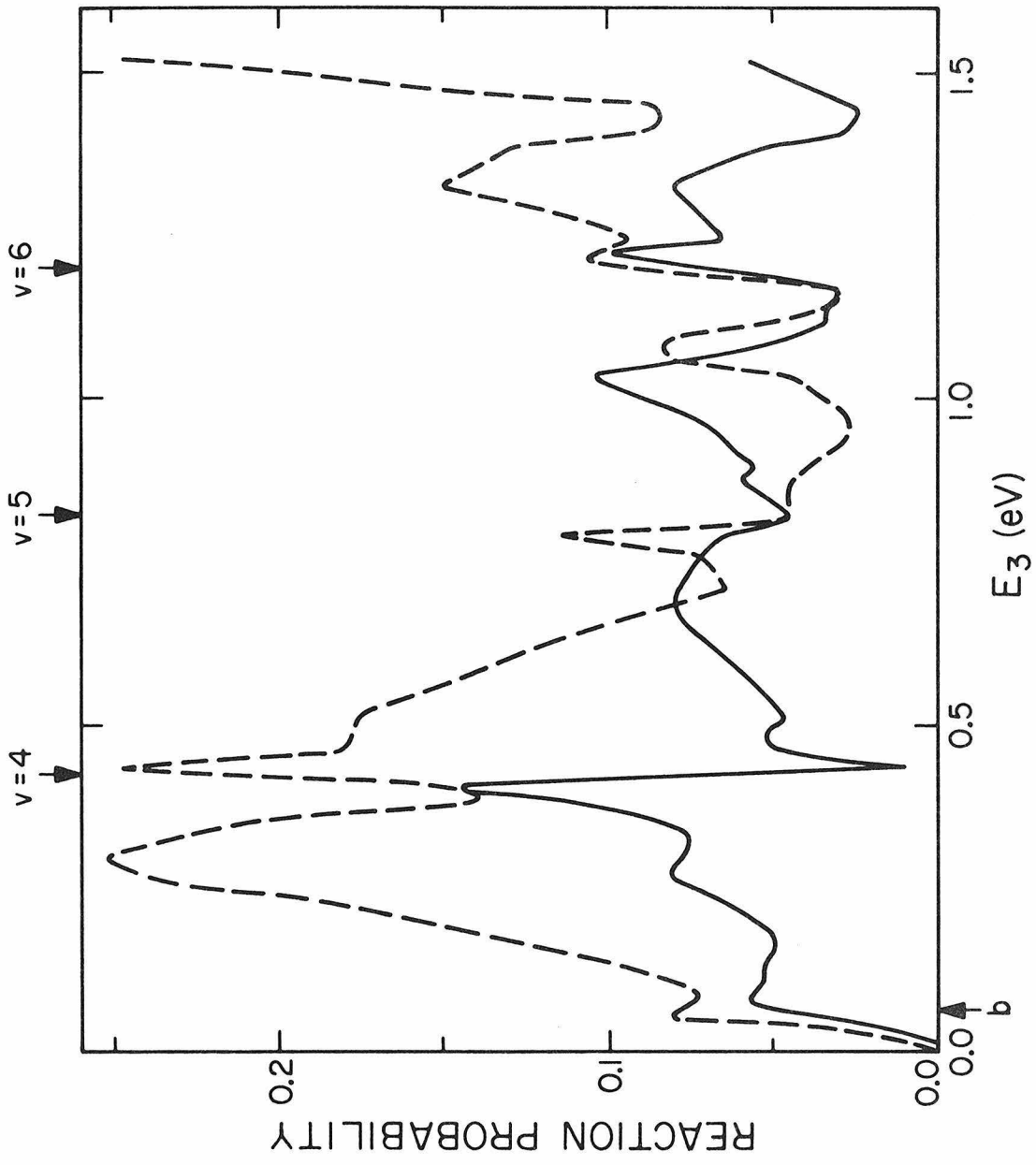

Fig. 9.

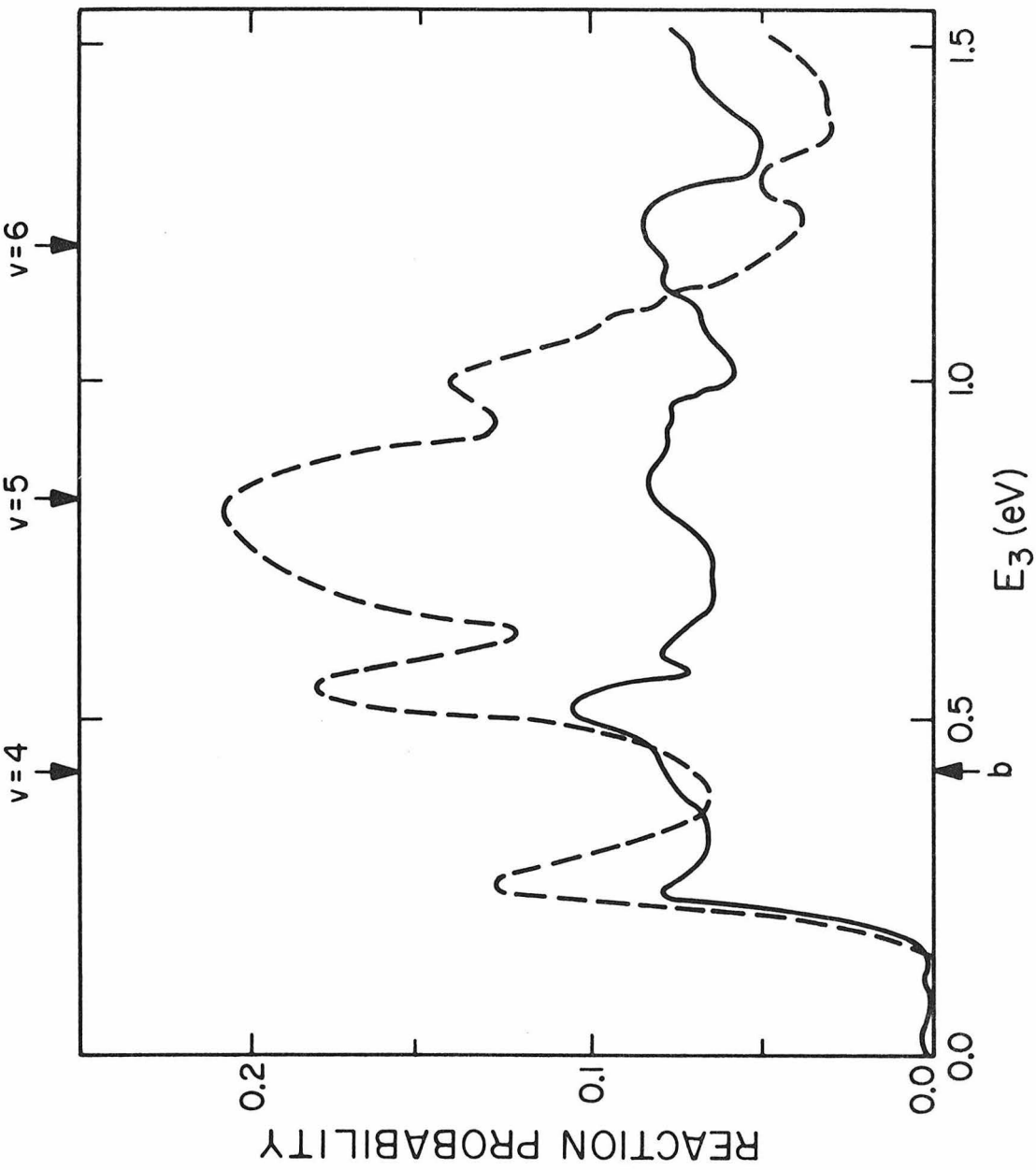

Fig. 10.

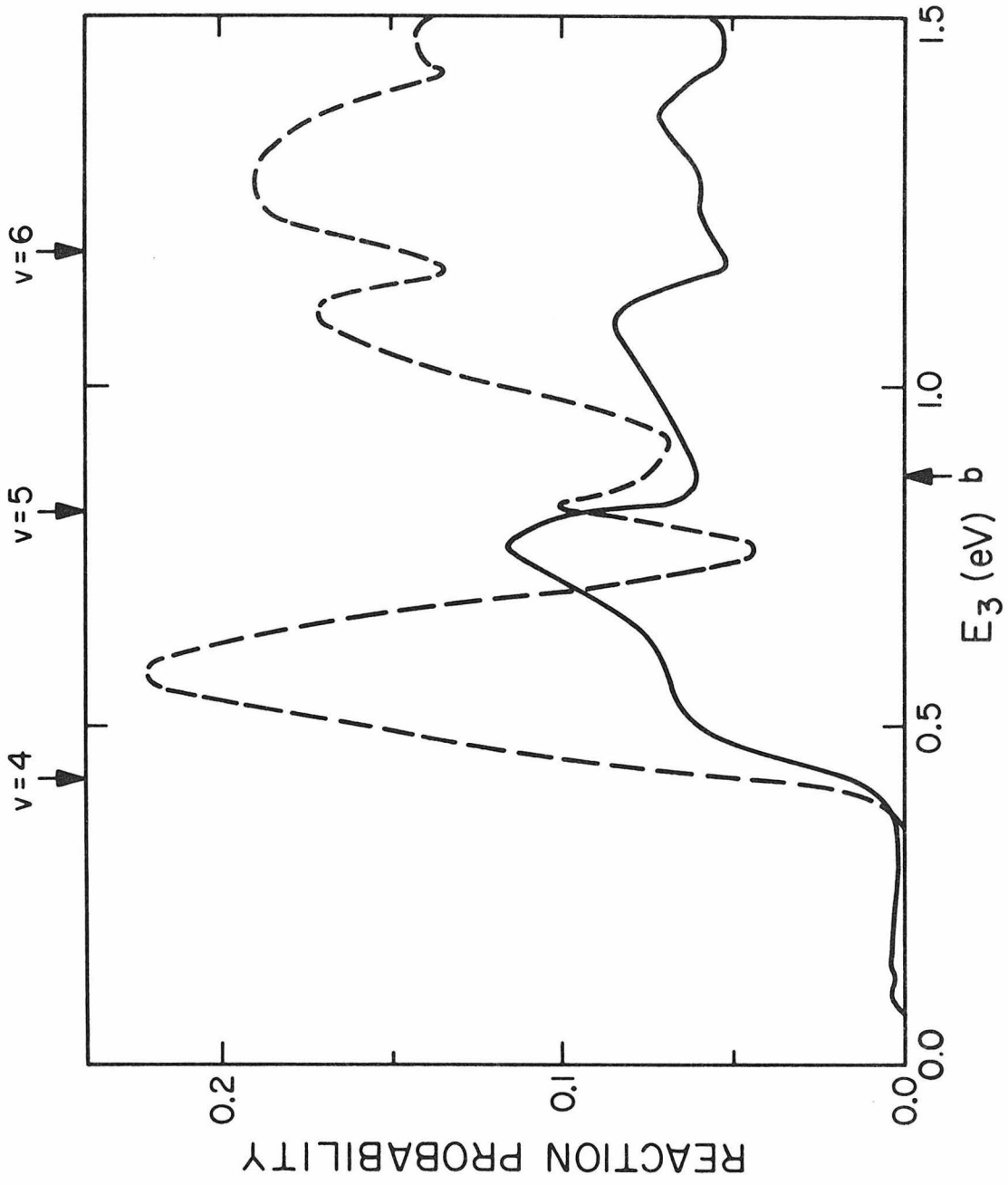

Fig. 11.

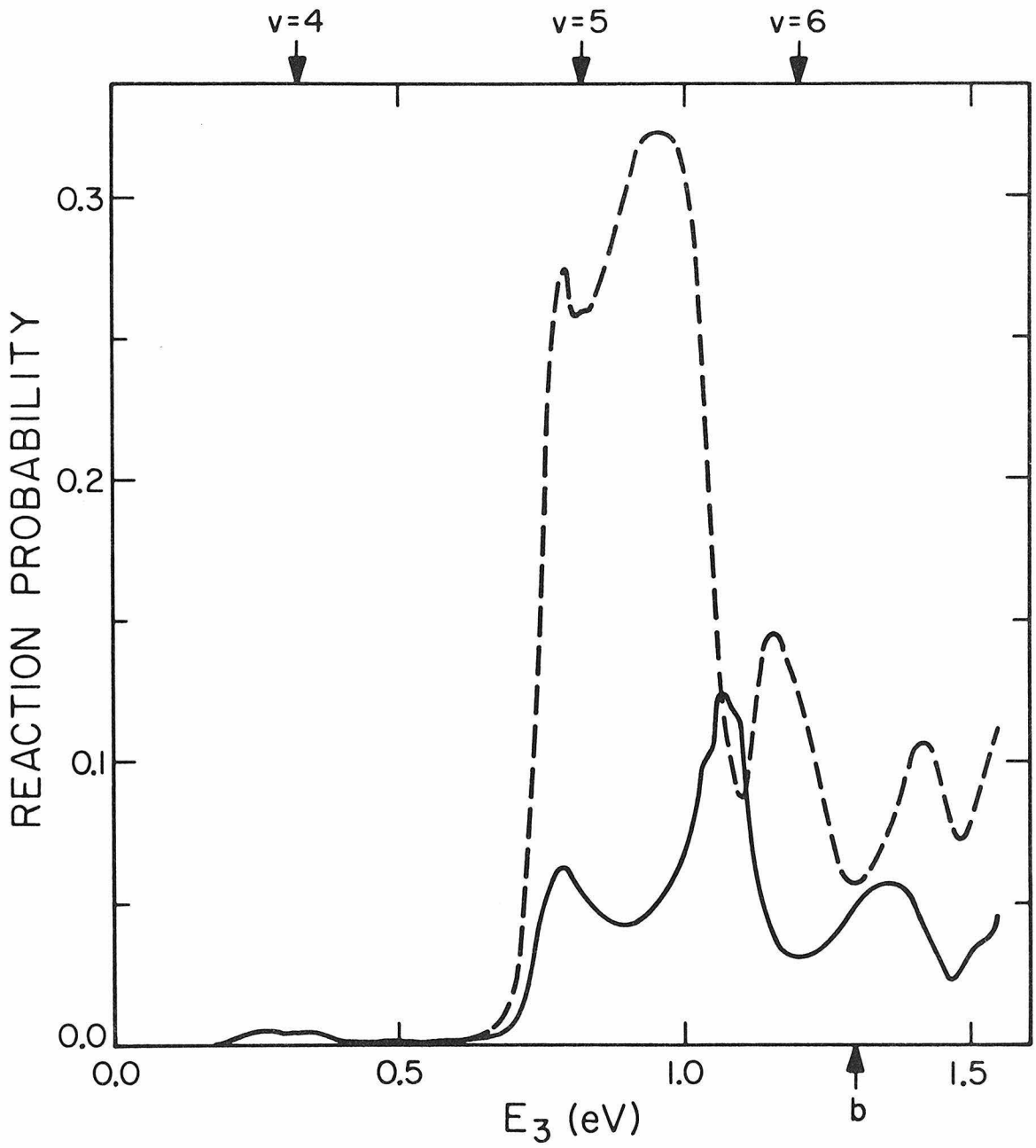

Fig. 12.

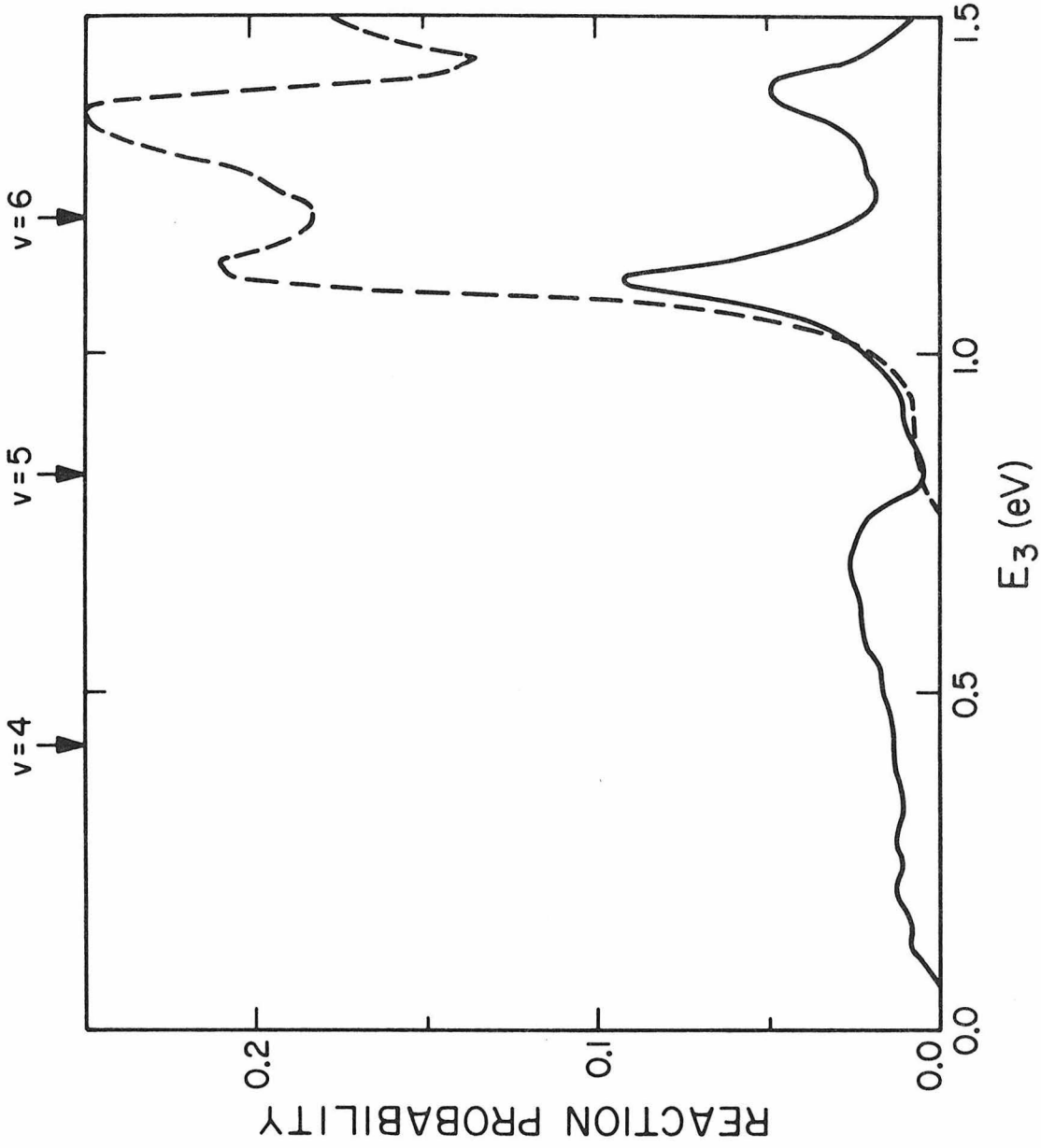

Fig. 13.

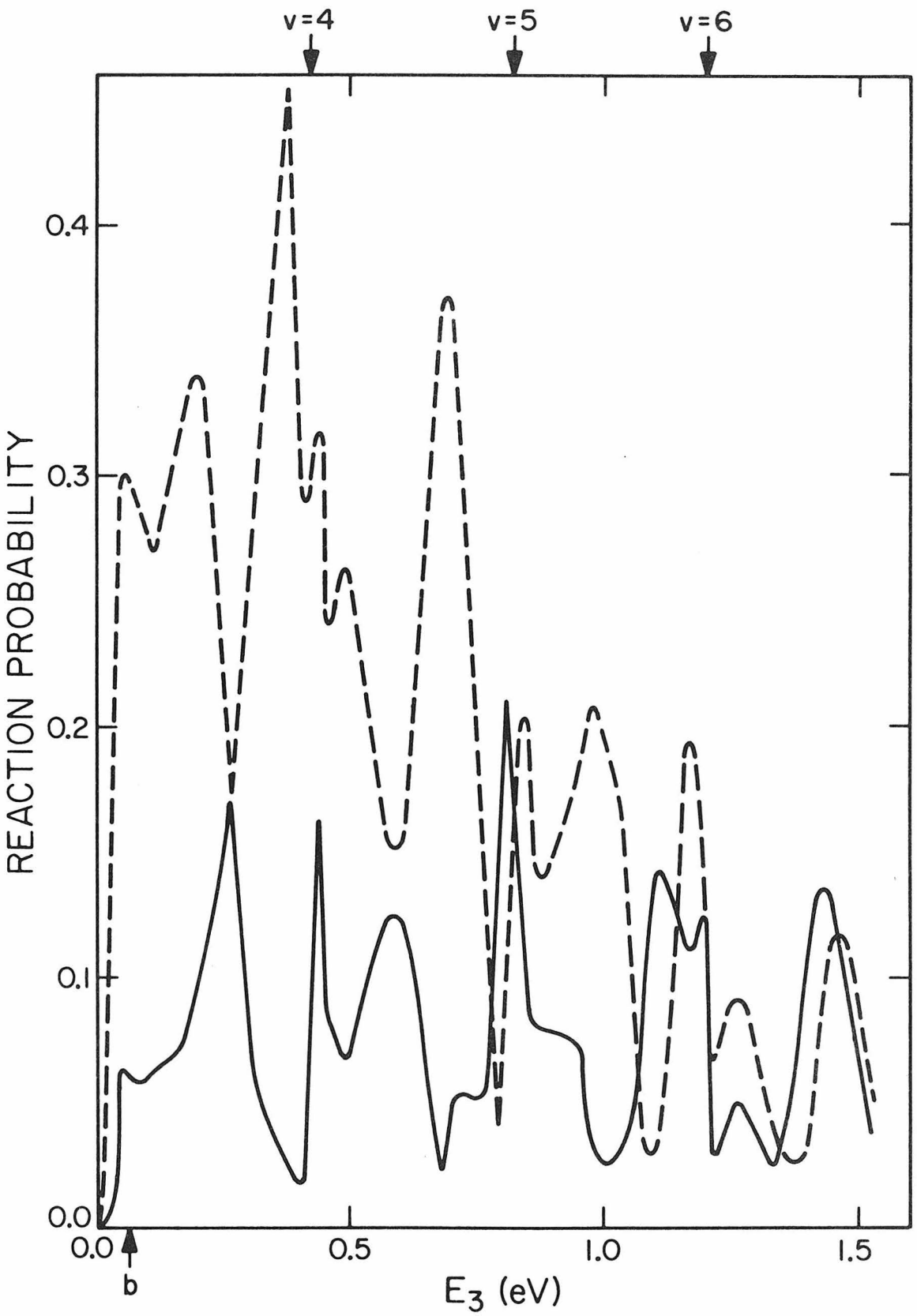

Fig. 14.

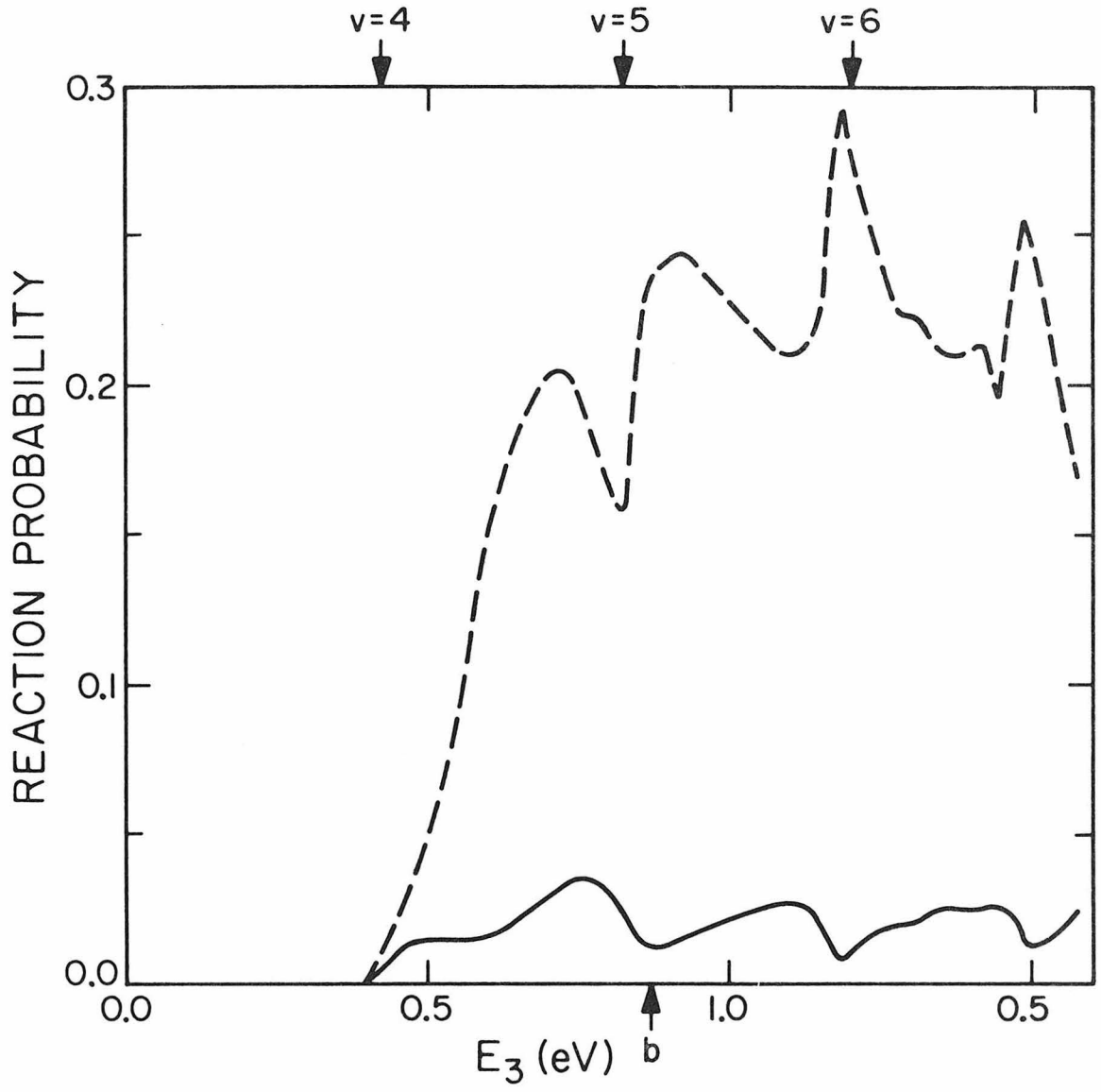

Fig. 15.

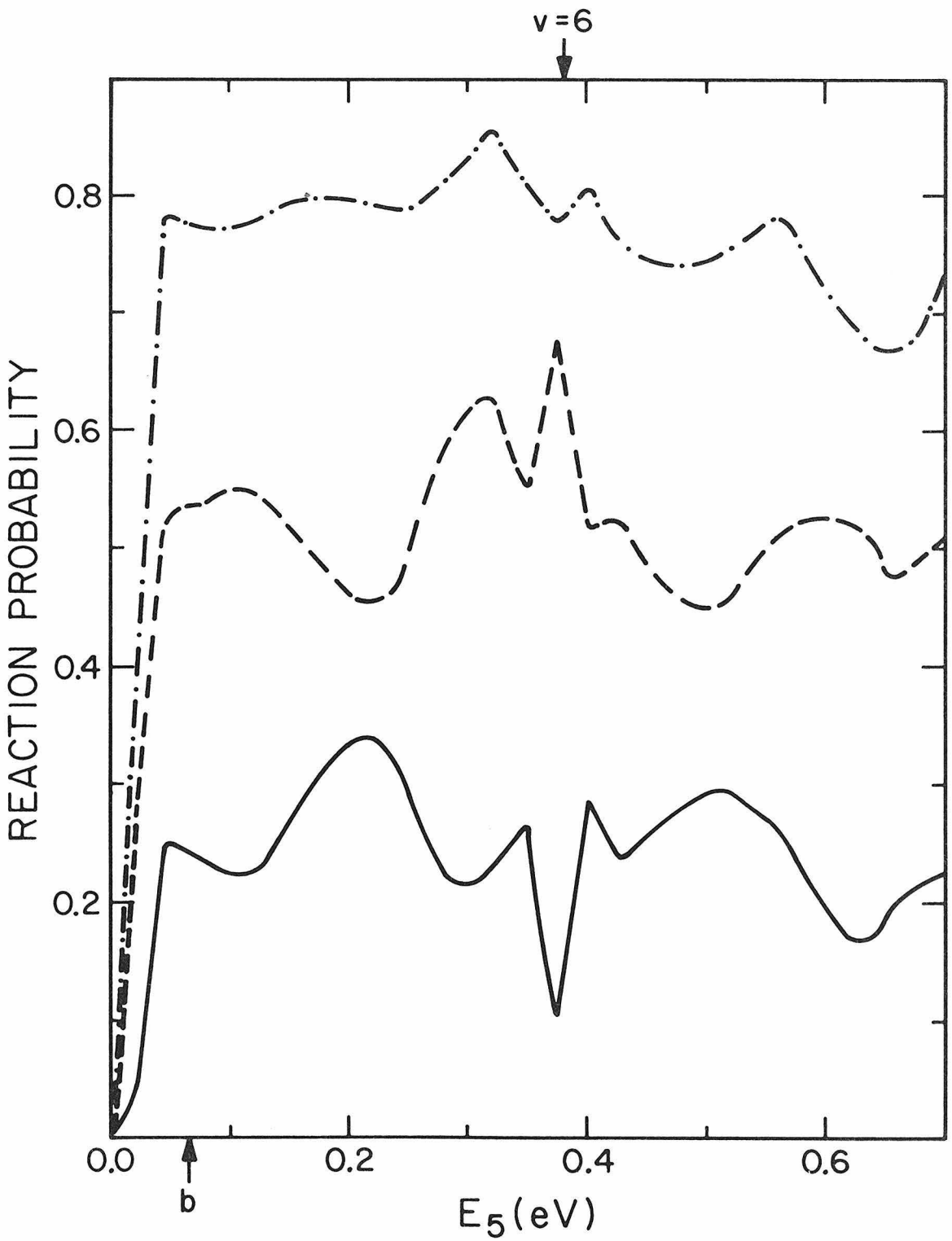

Fig. 16.

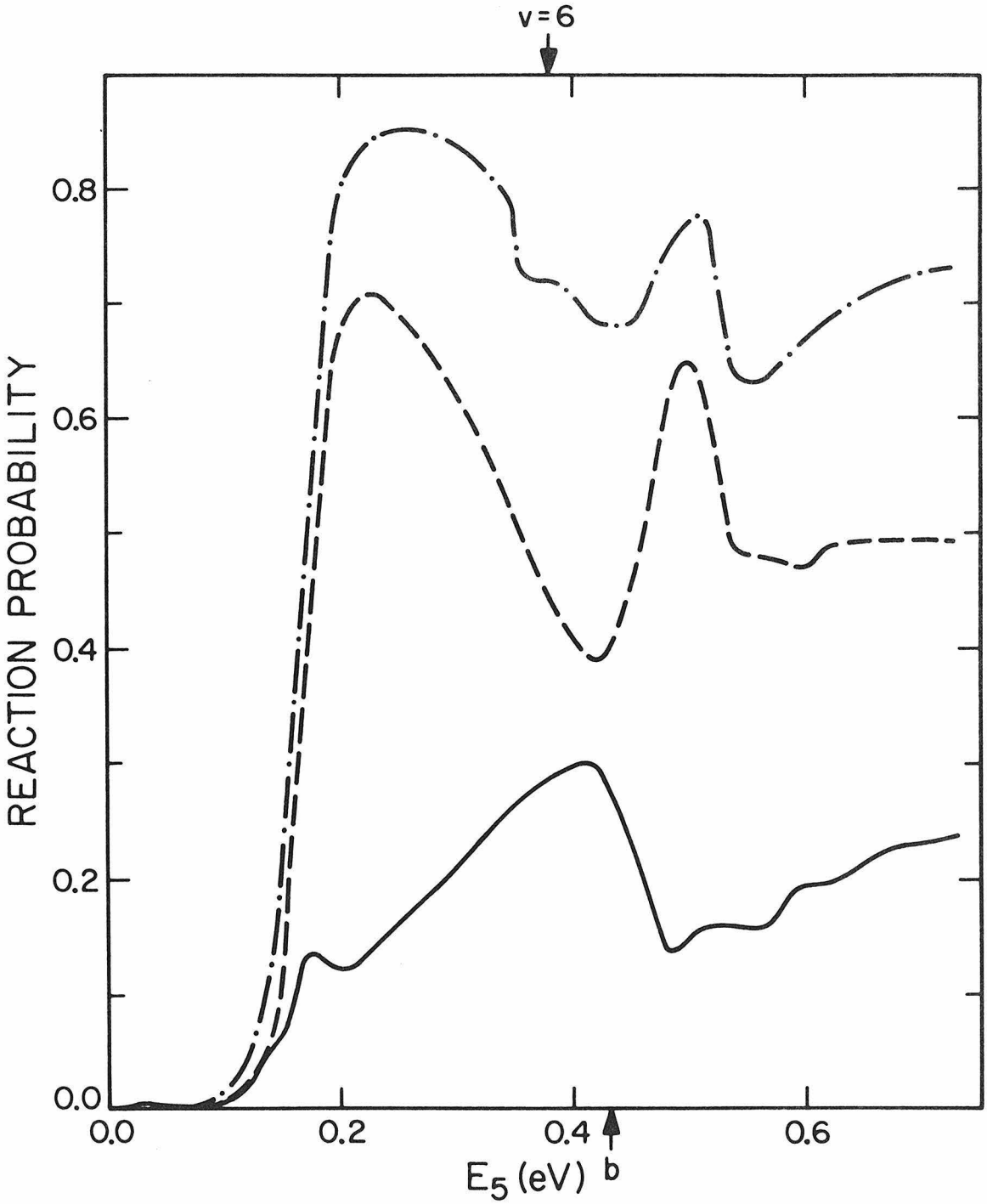

Fig. 17.

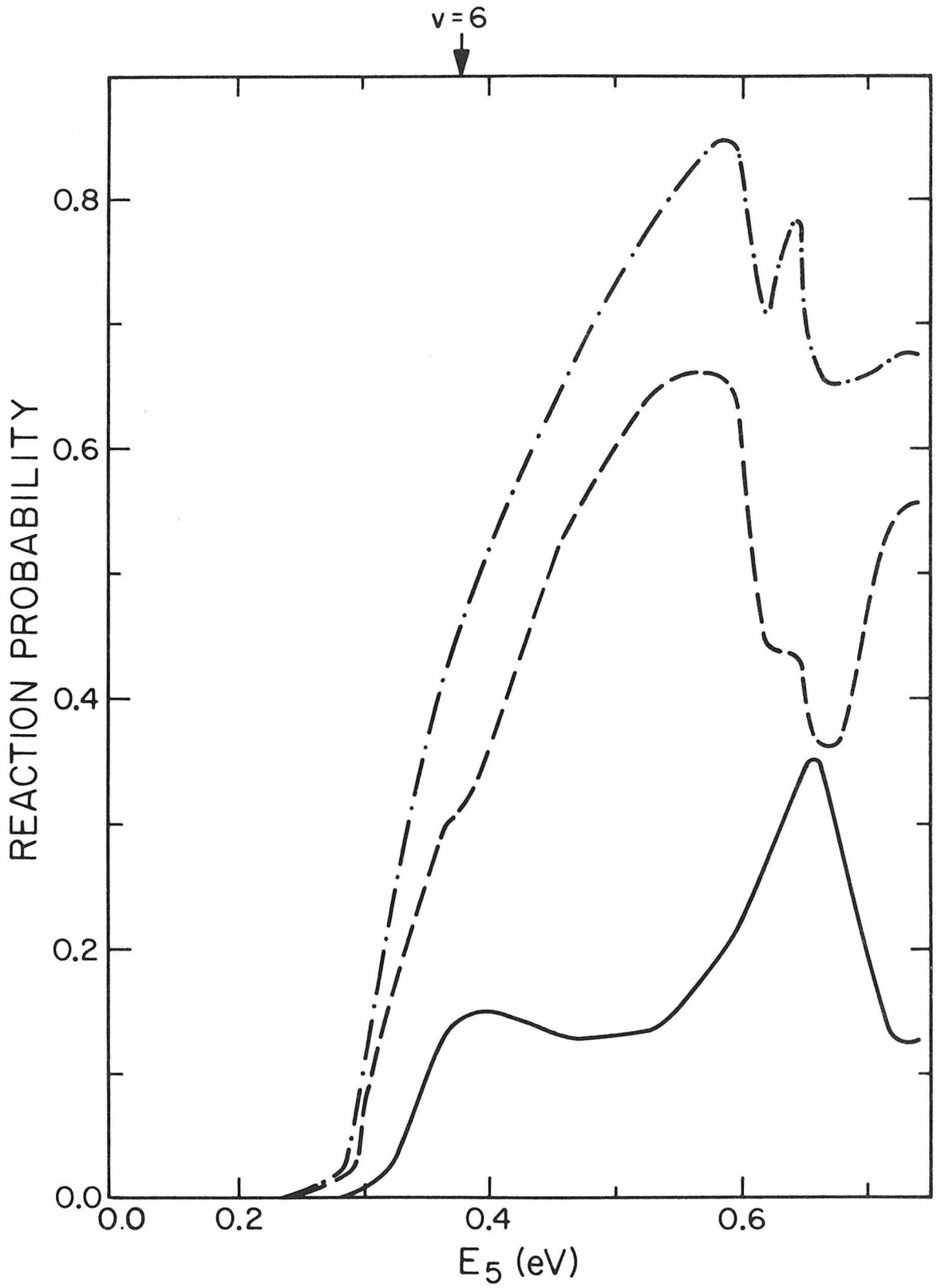

Fig. 18.

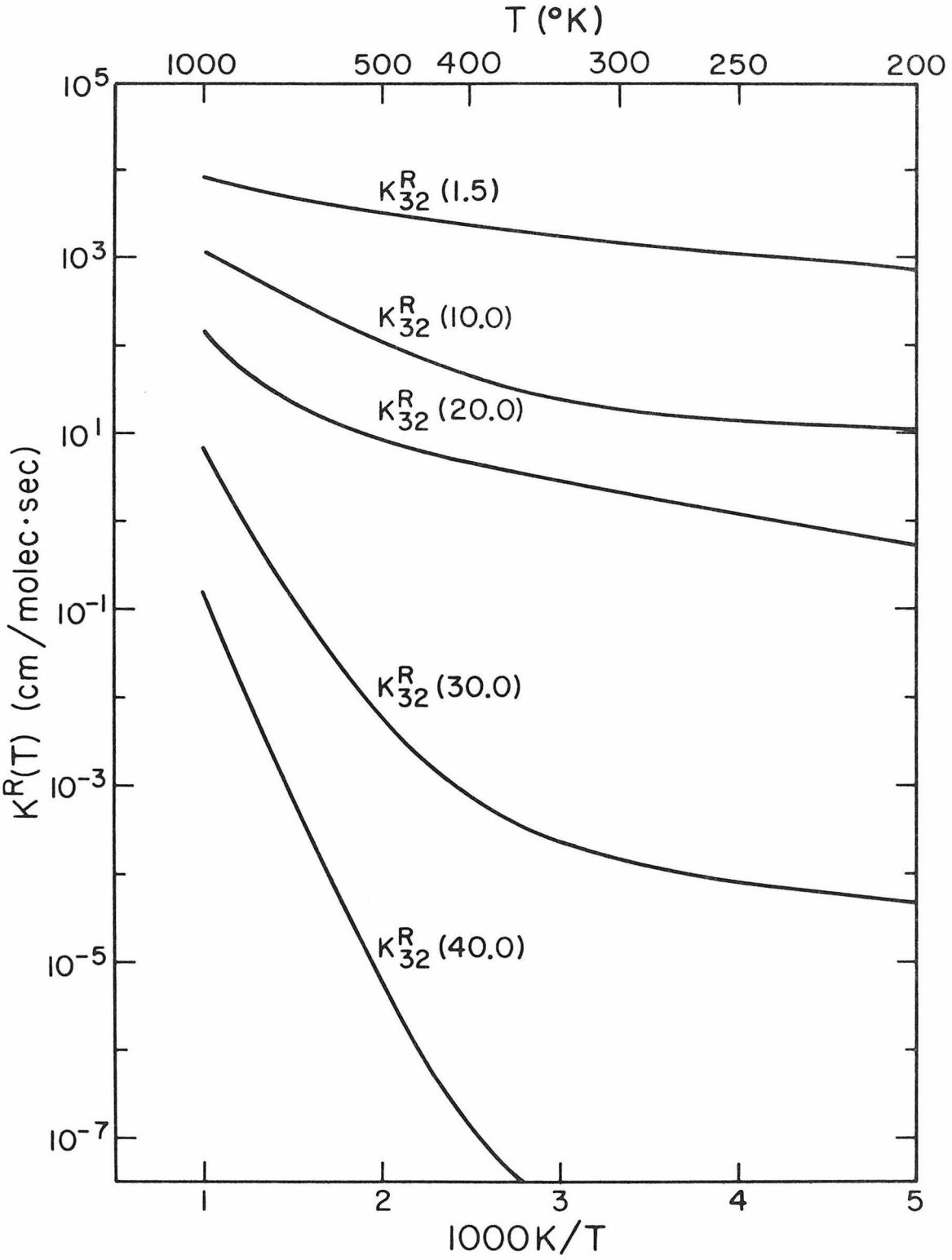
T (°K)
1000
500
400
300
250
200
10^5
10^3
10^1
10^{-1}
10^{-3}
10^{-5}
10^{-7}
K^R_{32} (1.5)
K^R_{32} (10.0)
K^R_{32} (20.0)
K^R_{32} (30.0)
K^R_{32} (40.0)
$K^R(T)$ (cm/molec·sec)
1
2
3
4
5
1000K/T

Fig. 19.

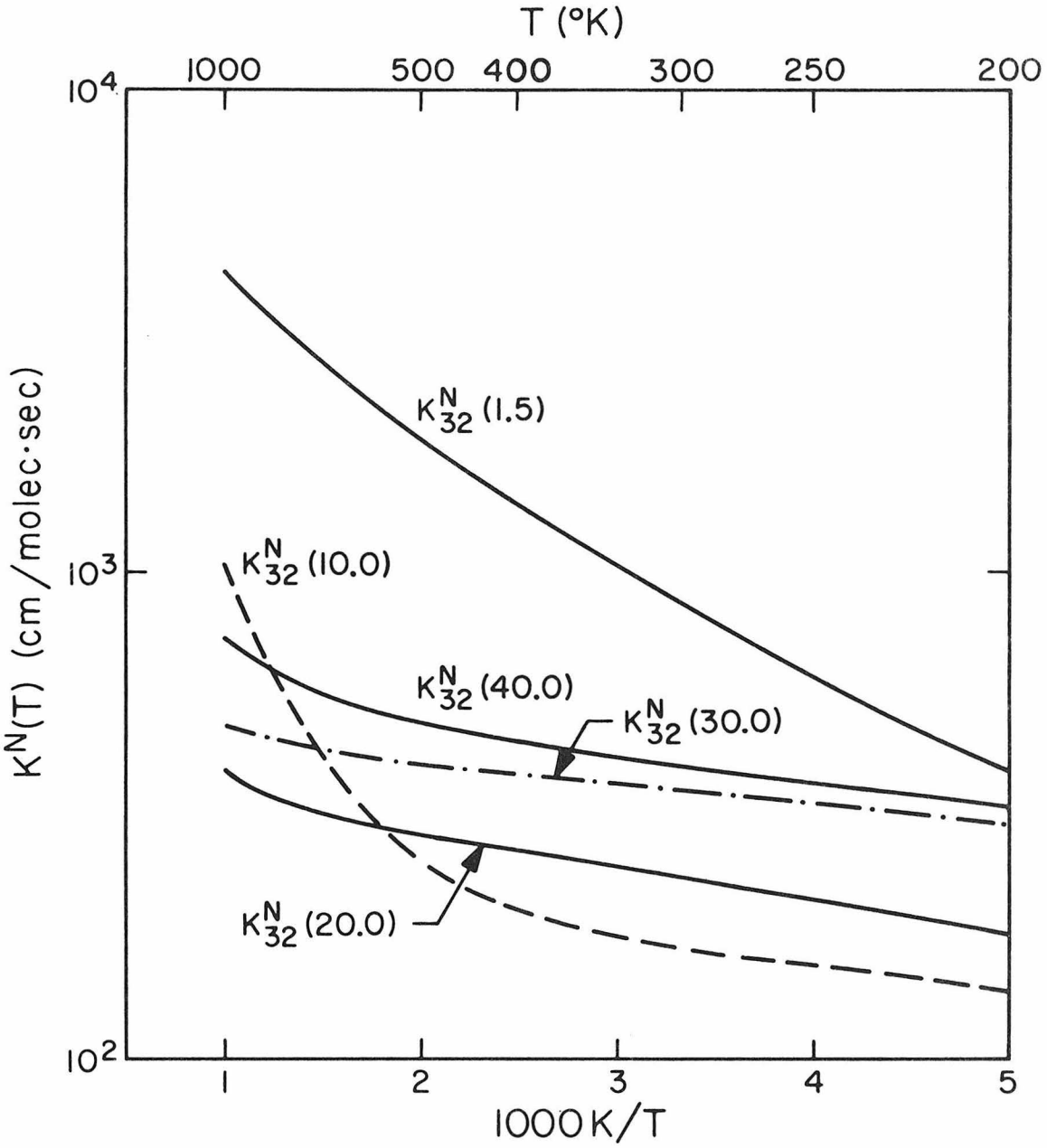
T (°K)
1000
500
400
300
250
200
10^4
10^3
10^2
$K^N(T)$ (cm/molec·sec)
K^N_{32} (1.5)
K^N_{32} (10.0)
K^N_{32} (40.0)
K^N_{32} (30.0)
K^N_{32} (20.0)
1
2
3
4
5
1000 K/T

Fig. 20.

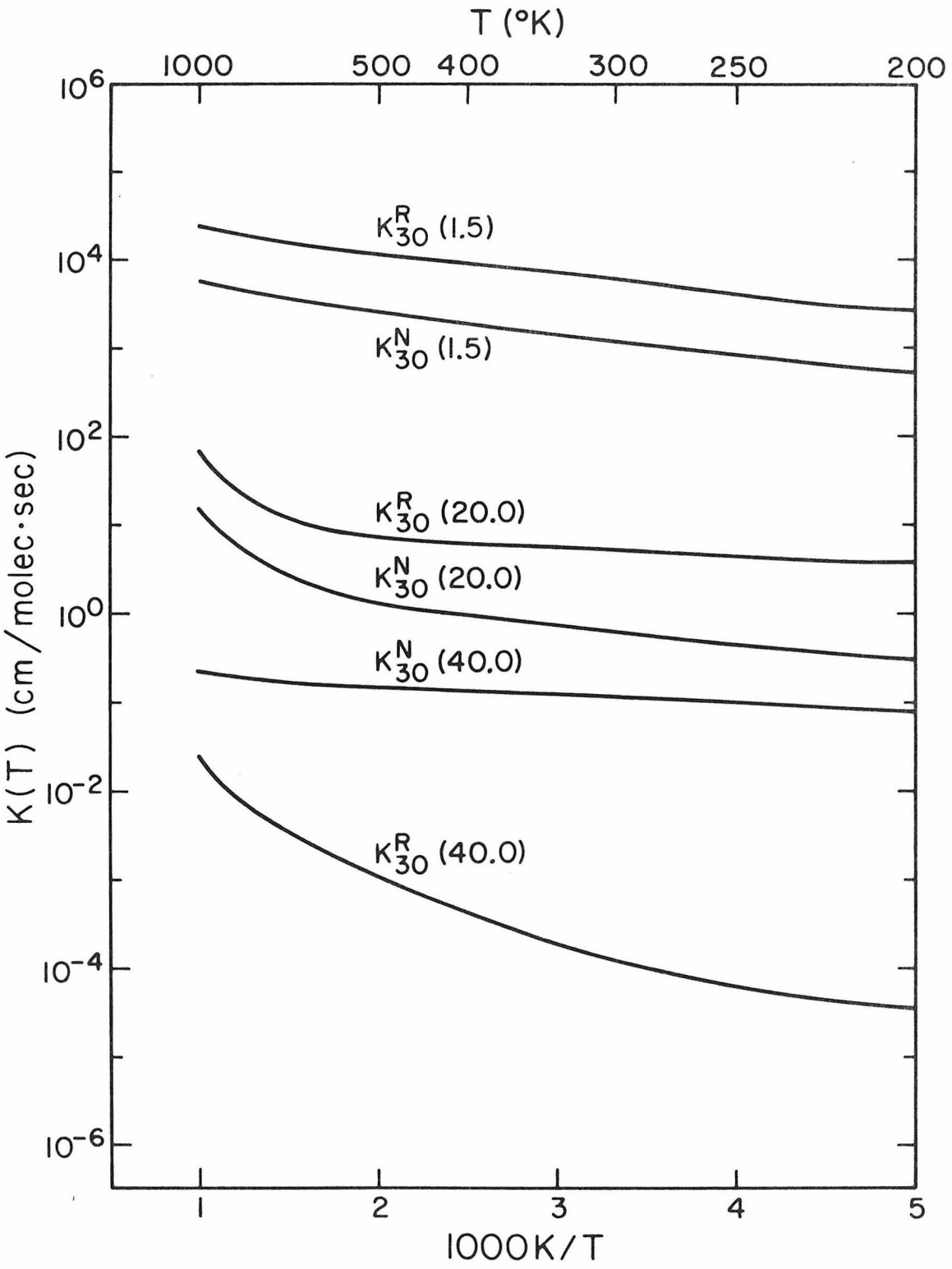
T (°K)
1000
500
400
300
250
200
10^6
10^4
10^2
10^0
10^{-2}
10^{-4}
10^{-6}
K^R_{30} (1.5)
K^N_{30} (1.5)
K^R_{30} (20.0)
K^N_{30} (20.0)
K^N_{30} (40.0)
K^R_{30} (40.0)
K(T) (cm/molec·sec)
1
2
3
4
5
1000K/T

Fig. 21.

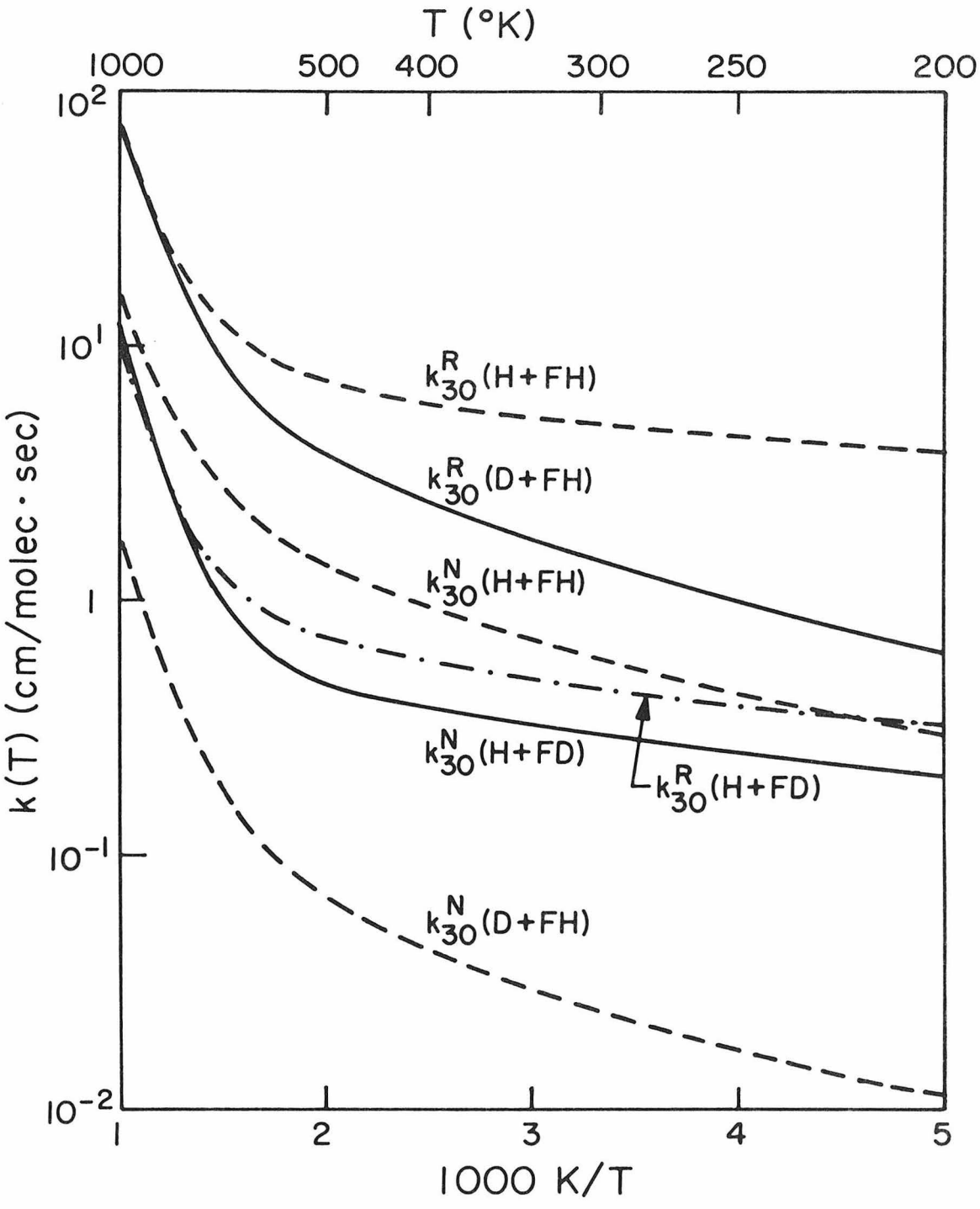
T (°K)
1000
500
400
300
250
200
10^2
10^1
1
10^{-1}
10^{-2}
k(T) (cm/molec · sec)
k_{30}^R(H+FH)
k_{30}^R(D+FH)
k_{30}^N(H+FH)
k_{30}^N(H+FD)
k_{30}^R(H+FD)
k_{30}^N(D+FH)
1
2
3
4
5
1000 K/T

Fig. 22.

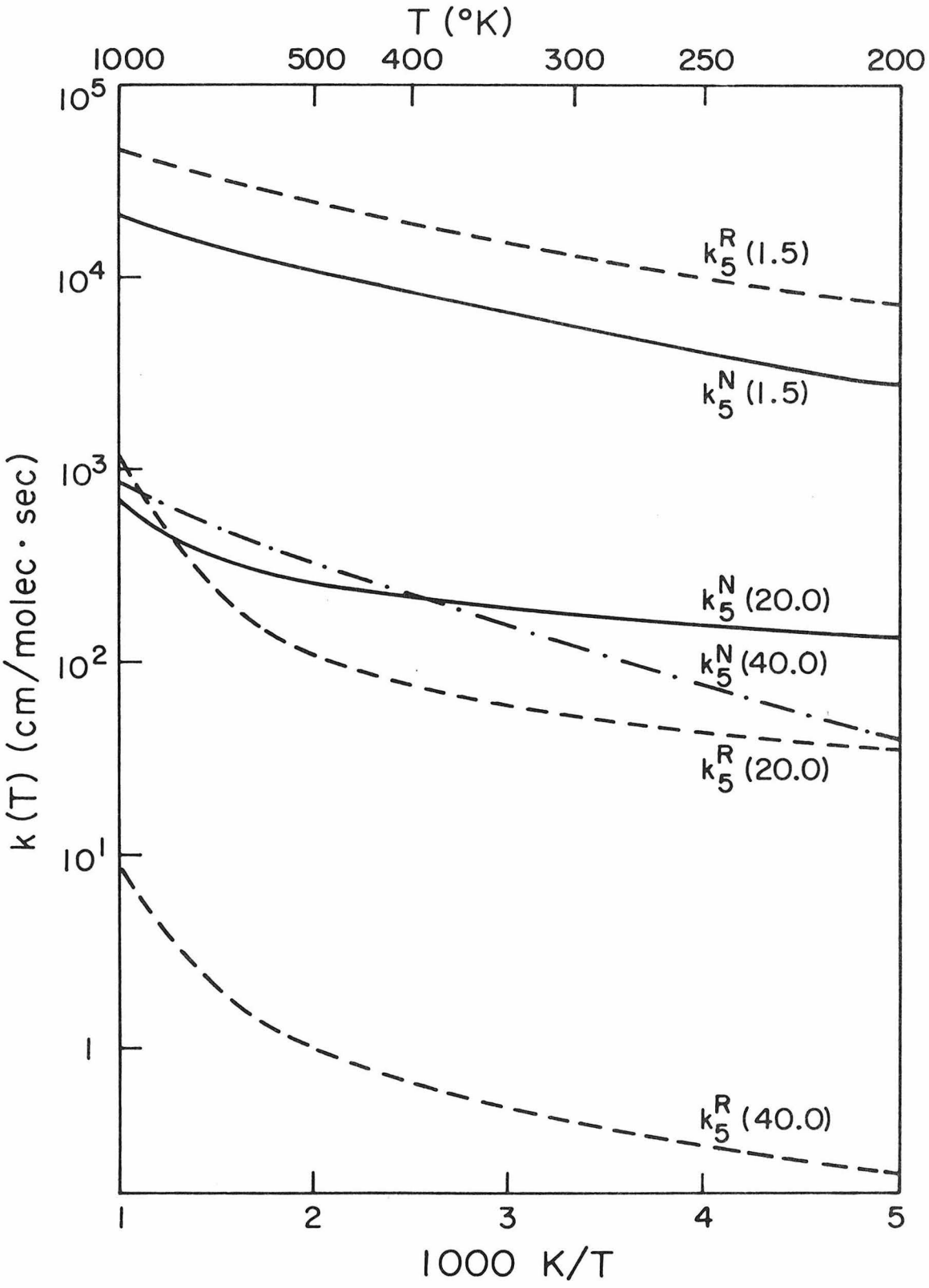
T (°K)
1000
500
400
300
250
200
10^5
10^4
10^3
10^2
10^1
1
k (T) (cm/molec · sec)
k_5^R (1.5)
k_5^N (1.5)
k_5^N (20.0)
k_5^N (40.0)
k_5^R (20.0)
k_5^R (40.0)
1
2
3
4
5
1000 K/T

Fig. 23.

CHAPTER 5.

Breakup Collisions: A Theoretical Framework

I. INTRODUCTION

In recent years there have been several[1] exact quantum mechanical studies of collinear reactive scattering. Most of these (electronically adiabatic) reactions are of the form

$$\begin{aligned} A + B &\rightarrow AB + C \\ &\rightarrow A + BC, \end{aligned}$$

where, in general, the wavefunctions describing these reactions have not included any contributions from the continuum, i.e., the dissociated triatomic system. In order to calculate reliable transition probabilities, only collision energies significantly smaller than dissociation energies have been used.

One recent study[2] outlined a method to calculate collinear quantum mechanical dissociative cross sections, but the author was unable to include reactive scattering (rearrangement collisions) in the formalism and he published no results.

Three questions immediately arise. What are the cross sections for collinear reactions at high (near dissociation) energies? To what degree does the inclusion of the continuum in the calculation affect reactive and nonreactive cross sections? What are the cross sections for dissociation? In Secs. II and III we present a general method to calculate reactive, nonreactive, and dissociative cross sections for the collinear collision of atom A with diatom BC. In Sec. IV we examine the unusual nature of some of these cross sections. Finally, in Sec. V we present preliminary results for the collinear $H + H_2$ reaction using a realistic potential surface.

II. COORDINATE SYSTEMS AND COUPLED EQUATIONS

Consider the collinear arrangement of atoms A, B, and C, where ξ_A, ξ_B, and ξ_C are the respective laboratory coordinates and B is the central atom. The Hamiltonian for this system is

$$\mathcal{H} = \frac{-\hbar^2}{2m_A}\frac{\partial^2}{\partial\xi_A^2} - \frac{\hbar^2}{2m_B}\frac{\partial^2}{\partial\xi_B^2} - \frac{\hbar^2}{2m_C}\frac{\partial^2}{\partial\xi_C^2} + V(\xi_A, \xi_B, \xi_C), \quad (1)$$

where m_A, m_B, and m_C are the masses of atoms A, B, and C, respectively, and V is the adiabatic potential energy surface that determines the nuclear motion.

We can define internuclear coordinates r_1 and r_2 by

$$r_1 = \xi_B - \xi_A$$

$$r_2 = \xi_C - \xi_B$$

and a center of mass coordinate R by

$$R = \frac{m_A\xi_A + m_B\xi_B + m_C\xi_C}{(m_A + m_B + m_C)} \quad .$$

Then the Hamiltonian becomes

$$\mathcal{H} = -\frac{\hbar^2}{2}\left[\frac{1}{m_A}\frac{\partial^2}{\partial r_1^2} + \frac{1}{m_B}\left(\frac{\partial^2}{\partial r_1^2} + \frac{\partial^2}{\partial r_2^2} - 2\frac{\partial^2}{\partial r_1 \partial r_2}\right) + \frac{1}{m_C}\frac{\partial^2}{\partial r_2^2} + \frac{1}{M}\frac{\partial^2}{\partial R^2}\right] + V(r_1, r_2), \quad (2)$$

where

$$M = m_A + m_B + m_C$$

and V is a function of only the internuclear distances because we have assumed there are no external forces. If we let T_{CM} be the kinetic

energy of the center of mass and partition the Hamiltonian by

$$\mathcal{H} = H_0 - \frac{\hbar^2}{2M} \frac{\partial^2}{\partial R^2} \quad , \tag{3}$$

we find that the total wavefunction Ψ may be written as

$$\Psi(r_1, r_2, R) = \psi(r_1, r_2) e^{ikR}, \tag{4}$$

where

$$T_{CM} = \frac{\hbar^2 k^2}{2M}$$

and the plane wave describes the motion of the center of mass. The remaining part, $\psi(r_1, r_2)$, contains the chemistry; it describes the internal motion of the triatomic system. We can transform H_0 to a set of center of mass coordinates by

$$x_2' = r_2$$

and

$$x_1' = r_1 + \frac{\mu_{BC}}{m_B} r_2,$$

where

$$\mu_{BC} = \frac{m_B m_C}{(m_B + m_C)} \quad ,$$

i.e., x_1' is the distance between A and the center of mass of BC. The new Hamiltonian becomes

$$H_0 = \frac{-\hbar^2}{2\mu_{A,BC}} \frac{\partial^2}{\partial x_1'^2} - \frac{\hbar^2}{2\mu_{BC}} \frac{\partial^2}{\partial x_2'^2} + V(x_1', x_2') \ , \tag{5}$$

where

$$\mu_{A,BC} = \frac{m_A(m_B + m_C)}{M} \quad .$$

We now want to transform the Hamiltonian so that it uses only one reduced mass. This transformation, first proposed by Delves[3] and

Jepsen and Hirschfelder,[4] can be written

$$x_1 = \left(\frac{\mu_{A,BC}}{\mu_{BC}}\right)^{\frac{1}{4}} x_1'$$

$$x_2 = \left(\frac{\mu_{BC}}{\mu_{A,BC}}\right)^{\frac{1}{4}} x_2' \ .$$

Then the Hamiltonian becomes

$$H_0 = -\frac{\hbar^2}{2\mu}\left(\frac{\partial^2}{\partial x_1^2} + \frac{\partial^2}{\partial x_2^2}\right) + V(x_1, x_2) \ , \tag{6}$$

where

$$\mu = (\mu_{A,BC}\,\mu_{BC})^{\frac{1}{2}}$$

$$= (\mu_{AB,C}\,\mu_{AB})^{\frac{1}{2}}$$

$$= [(m_A m_B m_C)/M]^{\frac{1}{2}} \ .$$

The Hamiltonian, as we have developed it, is well suited for the arrangement channel A + BC, because one of the coordinates, x_2, is a measure of the internuclear distance of BC. To describe the other arrangement channel (AB + C), we need a new set of coordinates, z_1, z_2, such that

$$z_1' = r_2 + (\mu_{AB}/m_B) r_1$$

$$z_2' = r_1$$

$$z_1 = (\mu_{AB,C}/\mu_{AB})^{\frac{1}{4}} z_1'$$

$$z_2 = (\mu_{AB}/\mu_{AB,C})^{\frac{1}{4}} z_2' \ .$$

In these coordinates the Hamiltonian may be written

$$H_0 = \frac{-\hbar^2}{2\mu}\left(\frac{\partial^2}{\partial z_1^2} + \frac{\partial^2}{\partial z_2^2}\right) + V(z_1, z_2) \quad , \tag{7}$$

where μ is the same reduced mass as before. We can define polar coordinates ρ, α by

$$\rho = (x_2^2 + x_1^2)^{\frac{1}{2}} = (z_2^2 + z_1^2)^{\frac{1}{2}} \tag{8a}$$

$$\alpha = \tan^{-1}(x_2/x_1) \ . \tag{8b}$$

The limits of α are at $r_1 = 0$ and $r_2 = 0$. At $r_1 = 0$, we have $\tan \alpha = (m_B/\mu)$, and at $r_2 = 0$, $\tan \alpha = 0$, so that for H_3, $\alpha_{min} = 0$ and $\alpha_{max} = \pi/3$. Figure 1 shows the semi-empirical Porter-Karplus[5] (PK) H_3 surface (in the collinear configuration) in internuclear (r_1, r_2) coordinates, while Fig. 2 shows it in Delves' (x_1, x_2) coordinates.

In polar coordinates, the Hamiltonian is written

$$H_0 = -\frac{\hbar^2}{2\mu}\left(\frac{1}{\rho^2}\frac{\partial^2}{\partial\alpha^2} + \frac{\partial^2}{\partial\rho^2} + \frac{1}{\rho}\frac{\partial}{\partial\rho}\right) + V(\rho, \alpha) \ , \tag{9}$$

and the corresponding Schrödinger equation at energy E is

$$H_0\psi_j(\rho, \alpha) = E\psi_j(\rho, \alpha) \ , \tag{10}$$

where ψ_j is the j^{th} solution. If we let

$$\psi_j(\rho, \alpha) = \rho^{-\frac{1}{2}} G_j(\rho, \alpha) \ ,$$

the Schrödinger equation becomes

$$\frac{-\hbar^2}{2\mu}\left[\frac{\partial^2 G_j(\rho, \alpha)}{\partial\rho^2} + \frac{1}{\rho^2}\frac{\partial^2 G_j(\rho, \alpha)}{\partial\alpha^2}\right] + \left[V(\rho, \alpha) - \frac{\hbar^2}{8\mu\rho^2}\right] G_j(\rho, \alpha)$$

$$= E G_j(\rho, \alpha) \ . \tag{11}$$

Now we will expand $G_j(\rho, \alpha)$ in a complete set of pseudo-vibrational basis functions, $\phi_i(\bar{\rho}, \alpha)$, such that

$$-\frac{\hbar^2}{2\mu}\frac{d^2\phi_i(\bar{\rho},\alpha)}{d\alpha^2} + \bar{\rho}^2 V(\bar{\rho},\alpha)\,\phi_i(\bar{\rho},\alpha) = \bar{\rho}^2 E_2^{\bar{\rho}}\,\phi_i(\bar{\rho},\alpha)\,, \tag{12}$$

where $\phi_i(\bar{\rho},\alpha)$ is parametrically dependent on $\bar{\rho}$. The boundary conditions are $\phi_i(\bar{\rho},0) = \phi_i(\bar{\rho},\alpha_{max}) = 0$. An example of $V(\bar{\rho},\alpha)$ ($\bar{\rho} = 5.0$ bohr) for the PK H_3 surface is given in Fig. 3 with a corresponding basis function (i = 7). Figure 4 shows the same eigenfunction, but for the DH_2 system. It is important to note that even at energies above dissociation the basis functions are discrete. This is because at α_{min} and α_{max} the potential diverges, which implies that the basis functions are eigenfunctions of an infinitely deep well. In other words, we now have a discrete (albeit infinitely large) representation of the continuum. This is in contrast with the usual basis function expansion which includes only the bound vibrations of the triatomic or (asymptotically) the diatomic molecule.

The eigenfunctions and eigenvalues are found numerically by a finite difference method, specifically the Givens-Householder[6] method for real symmetric matrices. In this paper we will refer to those states whose eigenvalues are below dissociation as bound and those states whose eigenvalues are above dissociation as dissociated.

Expanding $\psi_j(\rho,\alpha)$ in terms of this basis, we get

$$\psi_j(\rho,\alpha) = \rho^{-\frac{1}{2}} G_j(\rho,\alpha) = \rho^{-\frac{1}{2}} \sum_{i=1}^{\infty} g_{ij}(\rho,\bar{\rho})\,\phi_i(\bar{\rho},\alpha)\,, \tag{13}$$

where g_{ij} depends parametrically on $\bar{\rho}$, although ψ_j does not. Rigorously, the number of terms is infinite, but in practice only a sufficient number of terms are included to achieve a preset degree of convergence. Substituting Eqs. (12) and (13) into Eq.(11) gives

$$-\frac{\hbar^2}{2\mu}\sum_i \frac{d^2 g_{ij}(\rho,\bar{\rho})}{d\rho^2}\phi_i(\bar{\rho},\alpha) + (\bar{\rho}^2/\rho^2)\sum_i g_{ij}(\rho,\bar{\rho})[E_i^{\bar{\rho}} - V(\bar{\rho},\alpha)]\,\phi_i(\bar{\rho},\alpha)$$

$$+\left[V(\rho,\alpha) - \frac{\hbar^2}{8\mu\rho^2}\right]\sum_i g_{ij}(\rho,\bar{\rho})\phi_i(\bar{\rho},\alpha) = E\sum_i g_{ij}(\rho,\bar{\rho})\phi_i(\bar{\rho},\alpha)\ . \qquad (14)$$

If we premultiply by $\phi_{i'}(\bar{\rho},\alpha)$ and integrate over the range of α, we get the following coupled equations in the single variable ρ,

$$\frac{-\hbar^2}{2\mu} g''_{ij}(\rho,\bar{\rho}) + \left[(\bar{\rho}^2/\rho^2)E_i^{\bar{\rho}} - \frac{\hbar^2}{8\mu\rho^2} - E\right] g_{ij}(\bar{\rho},\rho) + \sum_{i'}[V_{ii'}(\rho,\bar{\rho})$$

$$- (\bar{\rho}^2/\rho^2)V_{ii'}(\bar{\rho})]\ g_{i'j}(\rho,\bar{\rho}) = 0\ , \qquad (15)$$

where

$$V_{ii'}(\rho,\bar{\rho}) = \int_0^{\alpha_{max}} \phi_i(\bar{\rho},\alpha)V(\rho,\alpha)\phi_{i'}(\bar{\rho},\alpha)d\alpha \qquad (16a)$$

and

$$V_{ii'}(\bar{\rho}) = \int_0^{\alpha_{max}} \phi_i(\bar{\rho},\alpha)V(\bar{\rho},\alpha)\phi_{i'}(\bar{\rho},\alpha)d\alpha\ . \qquad (16b)$$

In matrix notation this can be written

$$\underset{\approx}{g}'' = \underset{\approx}{U}(\rho)\underset{\approx}{g}(\rho)\ , \qquad (17)$$

where

$$\underset{\approx}{U} = (2\mu/\hbar^2)\left[\underset{\approx}{V}(\rho,\bar{\rho}) - (\bar{\rho}^2/\rho^2)\underset{\approx}{V}(\bar{\rho}) + (\bar{\rho}^2/\rho^2)\underset{\approx}{E}^{\bar{\rho}} - \left(\frac{\hbar^2}{8\mu\rho^2} + E\right)\underset{\approx}{1}\right] \qquad (18)$$

and $\underset{\approx}{E}^{\bar{\rho}}$ is a diagonal matrix whose elements are $E_i^{\bar{\rho}}$. Equation (17) represents the coupled equations that must be solved. When the solutions are known asymptotically, they are used to calculate the scattering matrix (S-matrix) and, ultimately, the cross sections. The next section details a method for solving these equations.

III. METHOD OF SOLUTION

An efficient method to solve coupled second-order differential equations like Eq.(17) has been developed by Gordon.[7] The method uses the (matrix) function g and its first derivative g′ at $\rho = \rho_\ell$ and propagates them to $\rho = \rho_r$. The accuracy of the method increases as the step size $\rho_r - \rho_\ell$ decreases. To do the propagation, the effective potential $\underset{\approx}{U}(\rho)$ is approximated by an analytical reference potential. The usual choice is a linear approximation,

$$[U_0(\rho)]_{ii'} = \left[U_{ii}(\rho_c) + (\rho - \rho_c) \frac{dU_u(\rho)}{d\rho}\bigg|_{\rho=\rho_c} \right] \delta_{ii'} , \tag{19}$$

where ρ_c is the midpoint of the interval $\rho_r - \rho_\ell$. Because the reference potential has a simple analytical form, the solutions to

$$\underset{\approx}{g}''(\rho) = \underset{\approx}{U}_0(\rho)\underset{\approx}{g}(\rho) \tag{20}$$

are easily found. If the reference potential is a constant over the interval; the solutions are sines and cosines, if the potential is linear, the solutions are Airy functions; if the potential is quadratic, the solutions are parabolic cylinder functions. Normally we chose the linear approximation as a compromise between efficiency and accuracy. However, at large values of ρ, the potential becomes flat and it is often necessary to use a constant reference potential.

The exact solutions to Eq.(17) can be written as

$$\underset{\approx}{g} = \underset{\approx}{A}\underset{\approx}{a} + \underset{\approx}{B}\underset{\approx}{b} \tag{21a}$$

and

$$\underset{\approx}{g}' = \underset{\approx}{A}'\underset{\approx}{a} + \underset{\approx}{B}'\underset{\approx}{b} , \tag{21b}$$

where $\underset{\approx}{A}$ and $\underset{\approx}{B}$ are the Airy function solutions of Eq.(20), and $\underset{\approx}{a}$ and

$\underset{\approx}{b}$ are slowly varying functions of ρ. Because they are slowly varying, $\underset{\approx}{a}$ and $\underset{\approx}{b}$ can be accurately found by the first-order expansions,

$$\underset{\approx}{a}(\rho_r) = \underset{\approx}{a}(\rho_\ell) + (\rho_r - \rho_\ell)\langle d\underset{\approx}{a}/d\rho\rangle \tag{22a}$$

and

$$\underset{\approx}{b}(\rho_r) = \underset{\approx}{b}(\rho_r) + (\rho_r - \rho_\ell)\langle d\underset{\approx}{b}/d\rho\rangle \quad . \tag{22b}$$

At very small values of ρ, all three atoms are very close together and the potential is strongly repulsive. In this classically forbidden region, the wavefunction ψ must have zero amplitude, which implies that $\underset{\approx}{g} = 0$. Using this initial condition, the solution matrix $\underset{\approx}{g}$ is propagated to larger ρ. When $|\rho - \bar{\rho}|$ is small, fewer states are required to accurately describe ψ_j than when the difference is large. In order to keep the number of basis functions to a minimum, the basis set is recalculated at new values of ρ as $\underset{\approx}{g}$ is propagated radially. This requires a transformation of $\underset{\approx}{g}$ and $\underset{\approx}{g}'$ every time a new basis is calculated. Because both ψ_j and its derivative $(d\psi_j/d\rho)$ are continuous,

$$\frac{d\psi_j}{d\rho} = \sum_{i=1}^{\infty} g'^{\,old}_{ij}(\rho,\bar{\rho}_{old})\phi_i^{old}(\bar{\rho}_{old},\alpha) = \sum_{i=1}^{\infty} g_{ij}^{new}(\rho,\bar{\rho}_{new})\phi_i^{new}(\bar{\rho}_{new},\alpha) \tag{23}$$

and

$$\frac{d\psi_j}{d\rho} = \sum_{i=1}^{\infty} g'^{\,old}_{ij}(\rho,\bar{\rho}_{old})\phi_i^{old}(\bar{\rho}_{old},\alpha) = \sum_{i=1}^{\infty} g'^{\,new}_{ij}(\rho,\bar{\rho}_{new})\phi_i^{new}(\bar{\rho}_{new},\alpha). \tag{24}$$

If we left-multiply both sides of each equation by $\phi_k^{new}(\bar{\rho}_{new},\alpha)$, integrate over the range of α and recall that the ϕ_i's are orthonormal, we get

$$\sum_{i=1}^{\infty} g_{ij}^{old}(\rho,\bar{\rho}_{old})O_{ki}(\bar{\rho}_{new},\bar{\rho}_{old}) = \sum_{i=1}^{\infty} g_{ij}^{new}(\rho,\bar{\rho}_{new})\delta_{ki}$$

and

$$\sum_{i=1}^{\infty} g'^{old}_{ij}(\rho,\bar{\rho}_{old})O_{ki}(\bar{\rho}_{new},\bar{\rho}_{old}) = \sum_{i=1}^{\infty} g'^{new}_{ij}(\rho,\bar{\rho}_{new})\delta_{ki} ,$$

where

$$O_{ki} = \int \phi_k^{new}(\bar{\rho}_{new},\alpha)\,\phi_i^{old}(\bar{\rho}_{old},\alpha)\,d\alpha .$$

In matrix notation,

$$\underset{\approx}{O}\,\underset{\approx}{g}^{old}(\rho,\bar{\rho}_{old}) = \underset{\approx}{g}^{new}(\rho,\bar{\rho}_{new}) \tag{25}$$

and

$$O\,\underset{\approx}{g}'^{old}(\rho,\bar{\rho}_{old}) = \underset{\approx}{g}'^{new}(\rho,\bar{\rho}_{new}) \ . \tag{26}$$

To avoid loss of particle flux, $\underset{\approx}{O}$ should be orthogonal, which is rigorously satisfied if both the new and old basis sets are complete, but is approximately satisfied otherwise. The smaller the difference $\bar{\rho}_{new} - \bar{\rho}_{old}$, the closer $\underset{\approx}{O}$ will be to satisfying this orthogonality condition.

At this point it is appropriate to discuss a rigorous decoupling procedure for symmetric (A + BA) systems. Because the potential $V(\rho,\alpha)$ is symmetric about the line $\alpha = (\alpha_{max}/2)$, the eigenfunctions of Eq.(12) are alternately symmetric and antisymmetric. This implies that every other term in the potential matrix $\underset{\approx}{V}$ [Eq.(16)] vanishes. Alternatively, $\underset{\approx}{V}$ may be written so that it is block diagonal, which implies that the solutions, $\underset{\approx}{g}^{s}(\rho,\bar{\rho})$, associated with the symmetric eigenfunctions (see Fig. 3), may be solved independently from the solutions, $\underset{\approx}{g}^{a}(\rho,\bar{\rho})$, associated with the antisymmetric eigenfunctions. In other words, one set of solutions is given by

$$\psi_j = \sum_i g^s_{ij}(\rho,\bar{\rho})\phi_i^s(\bar{\rho},\alpha)$$

and another by

$$\psi_j = \sum_i g^a_{ij}(\rho,\bar{\rho})\phi^a_i(\bar{\rho},\alpha) \ .$$

This decoupling of the equations reduces the computation time that increases with the cube of the number of basis functions. For nonsymmetric systems, the equations remain fully coupled as long as the propagation is in polar coordinates.

As ρ becomes large, one intuitively expects the equations to decouple further, whether there is symmetry or not. This is because the barrier between the two arrangement channels is wide (several bohr) and high (perhaps a couple of eV larger than the translational energy). This implies that there is no interaction or coupling between the two arrangement channels if ρ is large enough. This is clearly shown in Fig. 4 where the amplitude of one eigenfunction is almost completely localized in one arrangement channel. Of course, the dissociative part of the wavefunction (i.e., that part associated with basis functions whose eigenvalues are above the continuum threshold) is not decoupled in this way. The dissociative eigenfunctions span the complete range of α and have nonzero coupling with the bound eigenfunctions in both arrangement channels. A discussion of the decoupling of the dissociative wavefunctions from the bound wavefunctions is given in Appendix A.

When the arrangement channels become decoupled, that is, when the elements in the potential matrix which couple different arrangement channels become sufficiently small, we switch from polar coordinates (ρ,α) to rectangular coordinates (x_1, x_2) and (z_1, z_2) for A + BC and AB + C, respectively. To do this we must project each solution ψ_j and its derivative $d\psi_j/dx_i$ $(d\psi_j/dz_i)$ onto a new basis set of the coordinate

$x_2(z_2)$. Because the wavefunction is continuous, we have in the A + BC arrangement channel

$$\sum_i h^I_{ij}(x_1,\bar{x}_1)\chi^I_i(\bar{x}_1,x_2) = \sum_i g_{ij}(\rho,\bar{\rho})\phi^I_i(\rho,\alpha) \ , \tag{27}$$

where h^I_{ij} is a solution of

$$-\frac{\hbar^2}{2\mu} h^{I''}_{ij}(x_1,\bar{x}_1) + (E_i^{\bar{x}_1} - E)h^I_{ij}(x_1,\bar{x}_1) + \sum_{i'} [V_{ii'}(x_1,\bar{x}_1) - V_{ii'}(\bar{x}_1)]h^I_{i'j}(x_1,\bar{x}_1) = 0 \tag{28}$$

and is to be propagated in the coordinate x_1'. χ^I_i is a basis function that is a solution of

$$-\frac{\hbar^2}{2\mu}\frac{d^2}{dx_2'^2}\chi^I_i(\bar{x}_1,x_2) + V(\bar{x}_1,x_2)\chi^I_i(\bar{x}_1,x_2) = E_i^{\bar{x}_1}\chi^I_i(\bar{x}_1,x_2) \ . \tag{29}$$

Solving for h^I_{ij} we get

$$h^I_{ij}(x_1,\bar{x}_1) = \int \sum_m g^I_{mj}(\rho,\bar{\rho})\phi^I_m(\bar{\rho},\alpha)\chi^I_i(\bar{x}_1,x_2)dx_2 \ , \tag{30}$$

when ρ and α are related to x_2 by Eqs. (8a) and (8b). The limits on the integral are determined by the classically forbidden regions of the potential where χ^I_i vanishes.

Similarly, the derivative of the wavefunction must be continuous:

$$\sum_i h^{I'}_{ij}(x_1,\bar{x}_2)\chi^I_i(\bar{x}_1,x_2) = (\partial/\partial x_1)\sum_i g^I_{ij}(\rho,\bar{\rho})\phi^I_i(\bar{\rho},\alpha) \ , \tag{31}$$

which gives

$$h^{I'}_{ij}(x_1,\bar{x}_1) = \int \sum_m \Big[g^{I'}_{mj}(\rho,\bar{\rho})(\partial\rho/\partial x_1)\phi_m(\bar{\rho},\alpha) + g^I_{mj}(\rho,\bar{\rho})\phi^{I'}_m(\bar{\rho},\alpha) \times (\partial\alpha/\partial x_1)\Big]\chi^I_i(\bar{x}_1,x_2)dx_2 \ , \tag{32}$$

where the prime indicates differentiation with respect to the explicit variable.

Equation (28) and the analogous one in the AB + C arrangement channel can be solved using the Gordon method, as before. Solutions are propagated until there is no more coupling between the different states in each arrangement channel. The dissociative states are never projected, but are propagated in polar coordinates.

IV. CROSS SECTIONS

Asymptotically, there is no coupling and Eq. (15) takes the form of a Riccati-Bessel[8] equation. The j^{th} solution, ψ_j, becomes

$$e^{-ik_j^I x_1}\chi_j^I(x_2) + \sum_{n=1}^{N} S_{nj}^I (k_j^I/k_n^I)^{\frac{1}{2}} e^{ik_n^I x_1}\chi_n^I(x_2) + \sum_{n=1}^{M} S_{nj}^{II}(k_j^I/k_n^{II})^{\frac{1}{2}}$$

$$\times e^{ik_n^{II} z_2}\chi_n^{II}(z_2) + \rho^{-\frac{1}{2}} e^{ik^{III}\rho} \sum_{n=1}^{\infty} S_{nj}^{III}(k_j^I/k^{III})^{\frac{1}{2}}\chi_n^{III}(\alpha) , \qquad (33)$$

where I, II, and III denote arrangement channels A + BC, AB + C, and A + B + C, respectively, and we have assumed for the purpose of illustration that the j^{th} solution has type I incident flux. The wave numbers are defined by

$$k_n^I = [(2\mu/\hbar^2)(E - E_n^I)]^{\frac{1}{2}} ,$$

$$k_n^{II} = [(2\mu/\hbar^2)(E - E_n^{II})]^{\frac{1}{2}} ,$$

and

$$k^{III} = [(2\mu/\hbar^2)E]^{\frac{1}{2}} .$$

The S_{nj}'s are the scattering matrix (S-matrix) elements that are calculated in the usual way (see Appendix B).

It is important to note that the discrete basis set has provided a discrete S-matrix. If we make the approximation that the infinite sum can be truncated, we will be able to calculate cross sections for dissociation.

The cross sections for reactive and nonreactive scattering (i.e., bound-to-bound transitions) are given by

$$\sigma_{nj} = \frac{J_n(y_1)}{J_j(y_1')} \quad , \tag{34}$$

where $J_n(J_j)$ is the outgoing (incoming) flux in vibrational state n(j) and in direction $y_1(y_1')$. In physical coordinates (x_1', x_2') the flux in the A + BC arrangement channel is given by

$$\vec{j}(x_1', x_2') = \hat{x}_1' \hbar \, \mathrm{Im}[\psi^*(1/\mu_{A,BC})(\partial\psi/\partial\psi/\partial x_1')] + \hat{x}_2' \hbar \, \mathrm{Im}[\psi^*(1/\mu_{BC})(\partial\psi/\partial x_2')] \quad . \tag{35}$$

If we define $J(x_1')$ as the total flux in direction x_1',

$$J(x_1') = \lim_{x_1' \to \infty} \int \vec{j}(x_1', x_2') \cdot \hat{x}_1' \, dx_2' ,$$

then

$$J(x_1') = \lim_{x_1' \to \infty} (\hbar/2\mu_i) \int [\psi^*(\partial\psi/\partial x_1) - \psi(\partial\psi^*/\partial x_1)] \, dx_2$$

$$= \sum_n |S_{nj}|^2 (k_j^I \hbar/\mu) \quad . \tag{36}$$

The outgoing flux in each vibrational state n is given by

$$J_n(x_1') = |S_{nj}|^2 (k_j^I \hbar/\mu) \quad . \tag{37}$$

Because the incoming flux $J_j = (\hbar k_j^I/\mu)$, the nonreactive j→n cross section from initial arrangement channel A + BC is just

$$\sigma_{nj} = |S_{nj}^I|^2 \quad . \tag{38}$$

Similarly, for reaction to arrangement channel II (AB + C)

$$\sigma_{nj} = |S_{nj}^{II}|^2 \quad . \tag{39}$$

For dissociation from an initially bound state, the cross sections

are more complicated. First we will show that the distribution of translational energy among the dissociated atoms A, B, and C is a function of the final scattering angle α in configuration space. Let v_1 be the relative velocity of atom A to the center of mass of BC and v_2 be the velocity of B relative to C. Because

$$(x_1'/x_2') = (v_1/v_2) \text{ as } r \to \infty \qquad (r^2 = x_1'^2 + x_2'^2)$$

and

$$\tan \alpha = (\mu_{BC}/\mu_{A,BC})^{\frac{1}{2}}(x_2'/x_1') ,$$

we get

$$\tan \alpha = (\mu_{BC}/\mu_{A,BC})^{\frac{1}{2}}(v_2/v_1) \text{ as } r \to \infty .$$

From this it follows that

$$V_C = v_1(m_A/M) + v_2 m_B/(m_B + m_C) , \tag{40a}$$

$$V_B = v_1(m_A/M) - v_2 m_C/(m_B + m_C) , \tag{40b}$$

and

$$V_A = -v_1(m_B + m_C)/M , \tag{40c}$$

where V_A, V_B, and V_C are the center of mass velocities of atoms A, B, and C, respectively. Because the total kinetic energy is

$$E_T = \tfrac{1}{2}(m_A V_A^2 + m_B V_B^2 + m_C V_C^2)$$

$$= \tfrac{1}{2}(v_1^2 \mu_{A,BC} + v_2^2 \mu_{BC}) ,$$

the fraction of the total energy for each of atoms A, B, and C is given by

$$E_A/E_T = [(m_B + m_C)/M] \cos^2 \alpha \tag{41a}$$

$$E_B/E_T = [m_B/(m_B + m_C)] [(m_A/M)^{\frac{1}{2}} \cos \alpha - (m_C/m_B)^{\frac{1}{2}} \sin \alpha]^2 \tag{41b}$$

and

$$E_C/E_T = [m_C/(m_B + m_C)][(m_A/M)^{\frac{1}{2}}\cos\alpha + (m_B/m_C)^{\frac{1}{2}}\sin\alpha]^2, \qquad (41c)$$

respectively. Graphs of these ratios as a function of α are shown in Fig. 5 for the H_3 surface. As one might expect, E_B/E_T is a symmetric function and $\frac{E_A}{E_T}(\alpha) = \frac{E_C}{E_T}(\pi/3 - \alpha)$. The derivation has assumed that $V(\alpha) = 0$ for all α, which is valid in the limit $\rho = \infty$.

Because the energy distribution is a function of α, it is useful to find the probability of a transition from a bound state j to an angle α at $\rho = \infty$. The total radial flux between α and $\alpha + d\alpha$ is given by

$$(\hbar/\mu)\,\mathrm{Im}[\psi^*(\partial\psi/\partial\rho)]\rho d\alpha$$

$$= (\hbar/\mu)k_j\,\mathrm{Im}\left[i\sum_n\sum_{n'}\chi_n^{III}(\alpha)\chi_{n'}^{III}(\alpha)S_{nj}^{III*}S_{n'j}^{III}\right]d\alpha.$$

The cross section is

$$\mathrm{Re}\left[\sum_n\sum_{n'}\chi_n^{III}(\alpha)\chi_{n'}^{III}(\alpha)S_{nj}^{III*}S_{n'j}^{III}\right]d\alpha\ .$$

For a given total energy E_T, only one of E_A, E_B, and E_C is independent and it is necessary only to determine the cross section for particle A to have final energy between E_A and $E_A - dE_A$. From Eq. (41a)

$$E_A^{max} = \frac{E_T(m_B + m_C)}{M}\ ,$$

which implies that $E_A/E_A^{max} = \cos^2\alpha$ or $\alpha = \cos^{-1}(E_A/E_A^{max})^{\frac{1}{2}}$. Therefore, the cross section for a transition from a bound state j to three dissociated atoms with atom A having energy between E_A and $E_A - dE_A$ is

$$\frac{\mathrm{Re}\left\{\sum_{n}\sum_{n'} \chi_{n}^{III}[\cos^{-1}(E_A/E_A^{max})^{\frac{1}{2}}]\,\chi_{n'}^{III}[\cos^{-1}(E_A/E_A^{max})^{\frac{1}{2}}]\,S_{nj}^{III*}S_{n'j}^{III}\right\}dE_A}{2[E_A(E_A^{max}-E_A)]^{\frac{1}{2}}}\,.$$

V. APPLICATION TO THE H_3 SYSTEM

In principle, this method of calculating cross sections is applicable to any collinear atom-diatom system, if the potential surface is known. In choosing a suitable system, we should consider several factors. First, the system should be simple. A difficult system, one with a large exothermicity or a deep diatomic potential, might require an excessive number of basis functions for convergence, making it difficult to assess the limitations of the method. Second, to test a new method, a system for which comparable exact results are available should be chosen. Agreement between the results of different methods is a necessary condition for their validity. Third, although it is not essential, it might be useful to use a realistic potential surface. The results might have some physical meaning, particularly if the "true" reaction is collinearly dominated. Finally, it would be very helpful if there were symmetries in the reaction, because such symmetries help to locate errors and reduce the computing time. The H_3 surface fits all of the above criteria. In addition, the small masses involved will make the quantum effects more pronounced.

Although more accurate surfaces are available,[11] we have chosen the Porter-Karplus H_3 surface[5] because it is reasonably accurate, easy to calculate, and has been used by previous investigators.[1d] The potential does have an anomaly at very small internuclear distances that is, however, easily resolved.[12]

Before examining the results, one should note that in the collinear world, cross sections are dimensionless and equal to probabilities. We will let P_{ij}^{R} and P_{ij}^{N} denote the reactive and nonreactive transition

probabilities from state i to state j. For any numerical calculation there are a number of adjustable parameters. Among these are the number of basis functions, the number of points used in calculating the basis functions, and the beginning and stopping points of the integration. All of the results presented here are converged with respect to these parameters. The values for some of these parameters are listed in Table I. Another criterion of reliability is found in the unitary condition, $S^{\dagger}S = 1$. We required that the sum of the squares of absolute values of any column or row of the S matrix be within 1% of unity.

The results presented herein are for low translational energies, with up to three open vibrational states. In Fig. 6, P_{00}^{R} (the circles) is plotted as a function of translational energy and compared with the results (the x's) of Schatz, Bowman, and Kuppermann[1d] for the same system. For low energies ($E_0 < 0.65$ eV), the agreement is excellent, which indicates that the method is at least successful in determining bound-to-bound transition probabilities. At larger energies, there is some discrepancy, sometimes as large as 14%. Because the present work was converged, the work by Schatz et al. was repeated with more basis functions, more points per basis function, etc. The results were invariant to the parameter changes. It was felt that the major difference between the method of Schatz et al. and the present work was that they assumed the dissociative region to be energetically infinitely high, while we considered it to have its correct finite value. For very low collision energies, this difference should have an insignificant effect. When Schatz's method was repeated with more of the correct dissociative region included, the results were unaltered.

The only other possible source of error that might be energy-dependent is the projection [see Eqs.(27)-(32)]. In order to do the integral in Eq.(30), one must know each $g^I(\rho,\bar{\rho})$ and $\phi^I(\bar{\rho},\alpha)$ at each point along the line $x_1 = \bar{x}_1$. To do this exactly would require knowledge of each g^I and ϕ^I at ~150 points (see Table I), more than is needed in the rest of the entire calculation. To facilitate this, we assumed that each ϕ^I is roughly constant throughout the projection region ($\Delta\rho \sim 1$ bohr) and that each g^I could be found through a fifth-order Taylor expansion about a known value of g^I. The Taylor expansion appears adequate, because a fourth-order expansion gives the same results. However, it is clear that the basis functions change significantly over a distance of 1 bohr. In fact, to assure accuracy, the basis sets are recalculated every 0.3 bohr in the rest of the calculation. The approximation of constant ϕ^I will be worse at higher energies because higher basis functions will become more and more important in the calculation. To date we have not made the modifications necessary to test this source of error.

In spite of the discrepancies between the two curves, one can see that there is good qualitative agreement throughout the energy range and that the resonances are well reproduced.

There is some interest in cross sections at very low translational energies. Figure 7 is a semilog plot of P_{00}^R for the results of Ref. 1d and the present work, and one can see that the agreement between them is very good. Using these results, we have calculated rate constants for the reactive $0 \rightarrow 0$ transition. The rate constants are given by[1e]

$$k_{ij}(T) = (2\mu_{A,BC}\pi k_b T)^{-\frac{1}{2}} \int_0^\infty P_{ij}^R(E_i) e^{-E_i/k_b T} dE_i ,$$

where k_b is Boltzmann's constant, T is the temperature in K, and E_i is the translational energy of the system with the initial diatomic BC in vibrational state v = i. The range of E_i used in calculating the integral was 0.003 eV to 1.0 eV. Using energies outside this range did not alter the rate constants. In Table II one can see that there is some disagreement at very low temperatures ($\sim$ 4%) but that it all but vanishes at high temperatures.

From the above comparisons, we conclude that this method of calculating collinear bound-to-bound transition probabilities is satisfactory and promises to be useful for dissociative collisions. With the general validity of the method established, we will be able to ascertain the importance of closed dissociative eigenfunctions for bound-to-bound transition probabilities.

Rather than use the PK surface to examine dissociative transitions, it might be more instructive to use a surface that has far fewer bound states ($\sim$ three or four). This would permit one to reach dissociative energies with much less computational effort than if the PK surface were used. Such a shallow surface could easily be created by using the Bowman-Kuppermann[13] modification to the Wall-Porter[14] method of rotating Morse functions.

APPENDIX A

To show that dissociative eigenfunctions decouple from bound eigenfunctions, we need to show that [see Eq. (15)]

$$V_{ii'}(\rho,\bar{\rho}) - (\bar{\rho}^2/\rho^2)V_{ii'}(\bar{\rho}) \tag{A.1}$$

vanishes. The integrals in these matrices have the form

$$\int \phi^B(\bar{\rho},\alpha)V(\rho,\alpha)\phi^D(\bar{\rho},\alpha)d\alpha ,$$

where B denotes a bound eigenfunction and D a dissociative eigenfunction.

Let us assume the ρ is always within a neighborhood ϵ_{max} of $\bar{\rho}$; that is, $\rho = \bar{\rho} + \epsilon$, where $|\epsilon| < \epsilon_{max}$. If we expand $V_{ii'}(\rho,\bar{\rho})$ in a Taylor's expansion, we get (neglecting higher order terms)

$$V_{ii'}(\bar{\rho} + \epsilon,\bar{\rho}) = V_{ii'}(\bar{\rho}) + V'_{ii'}(\bar{\rho})\epsilon , \tag{A.2}$$

where the prime denotes a derivative with respect to ρ evaluated at $\bar{\rho}$. Expanding $(\bar{\rho}^2/\rho^2)$ gives

$$(\bar{\rho}^2/\rho^2) = [1 - \epsilon/\bar{\rho} + \epsilon^2/\bar{\rho}^2 - \ldots]^2 = 1 - 2\epsilon/\bar{\rho} . \tag{A.3}$$

Substituting Eqs. (A.3) and (A.2) into (A.1) gives

$$V_{ii'}(\bar{\rho}) + V'_{ii'}(\bar{\rho})\epsilon - V_{ii'}(\bar{\rho}) + (2\epsilon/\bar{\rho})V_{ii'}(\bar{\rho}) = V'_{ii'}(\bar{\rho})\epsilon$$

as $\rho \to \infty$. Therefore, to show (A.1) vanishes, we need only show that $V_{ii'}(\bar{\rho})$ becomes a constant asymptotically. For simplicity we will assume that the potential is symmetric and of the form

$$V(\bar{\rho},\alpha) = \infty , \qquad \alpha < 0,\ \alpha > \alpha_{max}$$

$$V(\bar{\rho},\alpha) = V_0 , \qquad 0 < \alpha < \alpha',\ \alpha_{max} - \alpha' < \alpha < \alpha_{max},\ \text{and } V_0 < 0$$

$$V(\bar{\rho},\alpha) = 0 \qquad \text{elsewhere.}$$

If both the eigenfunctions are either symmetric or antisymmetric [otherwise Eq.(A.1) trivially vanishes], the integral becomes

$$2V_0 \int_0^{\alpha'} \phi^B(\alpha)\phi^D(\alpha)d\alpha .^*$$

As $\bar{\rho}$ becomes very large, the range of the integral becomes smaller and smaller. When α' is sufficiently small, ϕ^D will have no oscillations within the range of the integrand and is, therefore, essentially a constant for $0 < \alpha < \alpha'$. The integral now becomes

$$C'' \int_0^{\alpha'} \phi^B(\alpha)d\alpha \ ,$$

where C'' is a constant. For the potential we have chosen

$$\phi^B(\alpha) = A \sin \beta\alpha \ ,$$

$$\beta = \frac{2\mu(E - V_0)}{\hbar^2}^{\frac{1}{2}} .$$

Thus we have as $\bar{\rho} \to \infty$

$$V_{ii'}(\bar{\rho}) = C' \int_0^{\alpha'} \sin \beta\alpha \, d\alpha$$

$$= C \cos \beta\alpha' .$$

As $\alpha' \to 0$, this integral converges to a constant C, which is what we wanted to show.

---

* The upper limit on the integral is not strictly accurate. In fact, the bound eigenfunction dies off exponentially for $\alpha > \alpha'$. However, this does not affect the argument given here.

APPENDIX B

Asymptotically, the general numerical solution to the Schrödinger equation is

$$\psi_j = \sum_{i=1}^{M} g_{ij}^{I}(x_1)\chi_i^{I}(x_2) + \sum_{i=1}^{N} g_{ij}^{II}(z_1)\chi_i^{II}(z_2) + \rho^{-\frac{1}{2}} \sum_{i=1}^{L} g_{ij}^{III}(\rho)\chi_i^{III}(\alpha) \ . \qquad (B.1)$$

The g's may be written as linear combinations of exponentials (incoming and outgoing parts) but are usually written as linear combinations of sines and cosines to avoid complex arithmetic:

$$\begin{aligned} \underset{\approx}{g}^{I} &= \underset{\approx}{\sin}\, k^{I}x_1 \underset{\approx}{B}^{I} + \underset{\approx}{\cos}\, k^{I}x_1 \underset{\approx}{A}^{I} , \\ \underset{\approx}{g}^{II} &= \underset{\approx}{\sin}\, k^{II}z_1 \underset{\approx}{B}^{II} + \underset{\approx}{\cos}\, k^{II}z_1 \underset{\approx}{A}^{II} , \\ \underset{\approx}{g}^{III} &= \underset{\approx}{\sin}\, k^{III}\rho \underset{\approx}{B}^{III} + \underset{\approx}{\cos}\, k^{III}\rho \underset{\approx}{A}^{III} , \end{aligned} \qquad (B.2)$$

and

and $\underset{\approx}{\sin}\, k^{I}x_1$, $\underset{\approx}{\cos}\, k^{I}x_1$, etc., are diagonal matrices of the form

$$\begin{pmatrix} \sin k_1^{I}x_1 & & & 0 \\ & \sin k_2^{I}x_1 & & \\ & & \ddots & \\ 0 & & & \sin k_M^{I}x_1 \end{pmatrix} .$$

Because there are K = L + M + N solutions, $\underset{\approx}{g}^{I}$ is an M × K matrix, $\underset{\approx}{g}^{II}$ is an N × K matrix, and $\underset{\approx}{g}^{III}$ is an L × K matrix. We can define square K × K matrices as follows:

$$\underset{\approx}{\sin}\, k\rho = \begin{pmatrix} \underset{\approx}{\sin}\, kx_1 & 0 & 0 \\ 0 & \underset{\approx}{\sin}\, kz_1 & 0 \\ 0 & 0 & \underset{\approx}{\sin}\, k\rho \end{pmatrix}$$

$$\underset{\approx}{g} = \begin{pmatrix} \underset{\approx}{g}^{I} \\ \underset{\approx}{g}^{II} \\ \underset{\approx}{g}^{III} \end{pmatrix} \qquad \underset{\approx}{A} = \begin{pmatrix} \underset{\approx}{A}^{I} \\ \underset{\approx}{A}^{II} \\ \underset{\approx}{A}^{III} \end{pmatrix} .$$

Analogous matrices exist for $\cos k\rho$, $\underset{\approx}{g}'$, and $\underset{\approx}{B}$. We can now write

$$\underset{\approx}{g} = \sin k\rho \; \underset{\approx}{A} + \cos k\rho \; \underset{\approx}{B} \tag{B.3}$$

and

$$\underset{\approx}{g}' = \underset{\approx}{k} \cos k\rho \; \underset{\approx}{B} - \underset{\approx}{k} \sin k\rho \; \underset{\approx}{A} , \tag{B.4}$$

where $\underset{\approx}{k}$ is the diagonal matrix

$$\begin{pmatrix} k_1^I & & & & & & & & \\ & k_2^I & & & & & & & \\ & & \ddots & & & & & & \\ & & & k_M^I & & & & & \\ & & & & k_1^{II} & & & & \\ & & & & & \ddots & & & \\ & & & & & & k_N^{II} & & \\ & & & & & & & k_1^{III} & \\ & & & & & & & & \ddots \\ & & & & & & & & & k_L^{III} \end{pmatrix}$$

Solving for $\underset{\approx}{A}$ and $\underset{\approx}{B}$ gives

$$\underset{\approx}{A} = \cos k\rho \; \underset{\approx}{g} - \underset{\approx}{k}^{-1} \sin k\rho \; \underset{\approx}{g}' \tag{B.5}$$

and

$$\underset{\approx}{B} = \sin k\rho \, \underset{\approx}{g} + \underset{\approx}{k}^{-1} \cos k\rho \; \underset{\approx}{g}' . \tag{B.6}$$

Because the physical wavefunction has the form

$$\underset{\approx}{g} = \underset{\approx}{k}^{-\frac{1}{2}} (\cos k\rho + \sin k\rho \; \underset{\approx}{R}) , \tag{B.7}$$

we must take linear combinations of (B.3) to fit (B.7):

$$\underset{\approx}{g} = (\sin k\rho \; \underset{\approx}{B} + \cos k\rho \; \underset{\approx}{A}) \; \underset{\approx}{P} .$$

This implies that

$$\underset{\approx}{A} \, \underset{\approx}{P} = \underset{\approx}{k}^{-\frac{1}{2}} , \qquad \underset{\approx}{B} \, \underset{\approx}{P} = \underset{\approx}{k}^{-\frac{1}{2}} \underset{\approx}{R}$$

and

$$\underset{\approx}{R} = \underset{\approx}{k}^{\frac{1}{2}}\underset{\approx}{B}\underset{\approx}{A}^{-1}\underset{\approx}{k}^{-\frac{1}{2}}.$$

The scattering matrix is given by[9,10]

$$\underset{\approx}{S} = (\underset{\approx}{1} + i\underset{\approx}{R})(\underset{\approx}{1} - i\underset{\approx}{R})^{-1}.$$

TABLE I. Parameters for numerical integration.

Number of basis functions in each arrangement channel	10-14
Number of points/basis function - polar coordinates	350
Number of points/basis function - rectangular coordinates	150-190
Beginning point of integration	1.5 bohr
Projection point	7.0 bohr
Stopping point of integration	10.0-15.0 bohr
Distance between basis sets	0.3 bohr

TABLE II. Rate constants $k_{00}(T)$ (cm/molecule-sec).

Temperature, K	Ref. 1d	This Work[a]
200	9.42 (-1)	9.86 (-1)
300	3.16 (1)	3.25 (1)
400	2.23 (2)	2.27 (2)
500	7.73 (2)	7.83 (2)
600	1.83 (3)	1.85 (3)
700	3.47 (3)	3.50 (3)
800	5.66 (3)	5.70 (3)
900	8.37 (3)	8.42 (3)
1000	1.15 (4)	1.16 (4)

[a] Numbers in parentheses are the powers of 10 by which each number should be multiplied.

REFERENCES

1. Only a few papers are listed (all on the H_3 surface). (a) S. F. Wu, B. R. Johnson, and R. D. Levine, Mol. Phys. 25, 609 (1973); (b) B. Johnson, Chem. Phys. Lett. 13, 172 (1972); (c) D. Diestler, J. Chem. Phys. 54, 4547 (1971); (d) G. Schatz, J. Bowman, and A. Kuppermann (unpublished); (e) D. Truhlar and A. Kuppermann, J. Chem. Phys. 56, 2232 (1972).
2. G. Wolken, Jr., J. Chem. Phys. 63, 528 (1975).
3. (a) L. Delves, Nucl. Phys. 9, 391 (1959); (b) ibid. 20, 275 (1960).
4. D. Jepsen and J. O. Hirschfelder, Proc. Natl. Acad. Sci. USA 45, 249 (1959).
5. R. N. Porter and M. Karplus, J. Chem. Phys. 40, 1105 (1964).
6. Mathematical Methods for Digital Computers, A. Ralston and H. Wilf, Eds. (John Wiley & Sons, Inc., New York; 1967), Vol. 2, p. 94.
7. R. G. Gordon, J. Chem. Phys. 51, 14 (1969).
8. Handbook of Mathematical Functions, M. Abramowitz and I. Stegen, Eds. (Dover Publications, Inc., New York, 1970), p. 361.
9. A. M. Lane and R. G. Thomas, Rev. Mod. Phys. 30, 257 (1958).
10. T. Teichmann and E. P. Wigner, Phys. Rev. 87, 123 (1952).
11. B. Liu, J. Chem. Phys. 58, 1925 (1973).
12. For $\rho < 3.0$ bohr and $\alpha < 3°$ (Delves' coordinates), a deep (~ 25 eV) well appears. In fact, the potential should be strongly repulsive, and it is just set to +30 eV.
13. J. M. Bowman and A. Kuppermann, Chem. Phys. Lett. 34, 523 (1975).
14. F. T. Wall and R. N. Porter, J. Chem. Phys. 36, 3256 (1962).

FIGURE CAPTIONS

FIG. 1. The lines are equipotentials of the collinear PK H_3 surface in internuclear (r_1, r_2) coordinates. The zero of energy is dissociation. The dashed lines represent contours of the potential for energies below dissociation, while the solid lines are for values above dissociation. The abscissa and ordinate are in bohr and the contours in eV.

FIG. 2. The lines are equipotentials of the collinear PK surface in mass-scaled (x_1, x_2) coordinates. Units and designations are identical to Fig. 1.

FIG. 3. A cut of the collinear PK DH_2 potential $V(\bar{\rho}, \alpha)$ is plotted at $\bar{\rho} = 5.0$ bohr, with an associated eigenfunction $\phi\ (\bar{\rho}, \alpha)$. The abscissa is measured in units of $\alpha_{max} = 50.77°$, the ordinate in eV. The solid horizontal line indicates the position of the corresponding eigenvalue.

FIG. 4. A cut of the collinear PK H_3 potential $V(\bar{\rho}, \alpha)$ is plotted at $\bar{\rho} = 5.0$, with an associated $\phi\ (\bar{\rho}, \alpha)$. The abscissa is in degrees and the ordinate in eV. The solid horizontal line indicates the position of the corresponding eigenvalue.

FIG. 5. A plot of the fraction of the relative kinetic energy partitioned among the dissociated atoms A, B, and C as a function of α in the limit $\rho = \infty$, for the collinear PK H_3 system.

FIG. 6. Plot of the $0 \rightarrow 0$ reactive probability (P_{00}^{R}) calculated by two methods. The x's are from Ref. 1d. The circles are from the present work. The abscissa is in translational energy (eV).

FIG. 7. Compares the results from Ref. 1d and the present work at low energies on a semilog scale. The abscissa is in translational energy (eV).

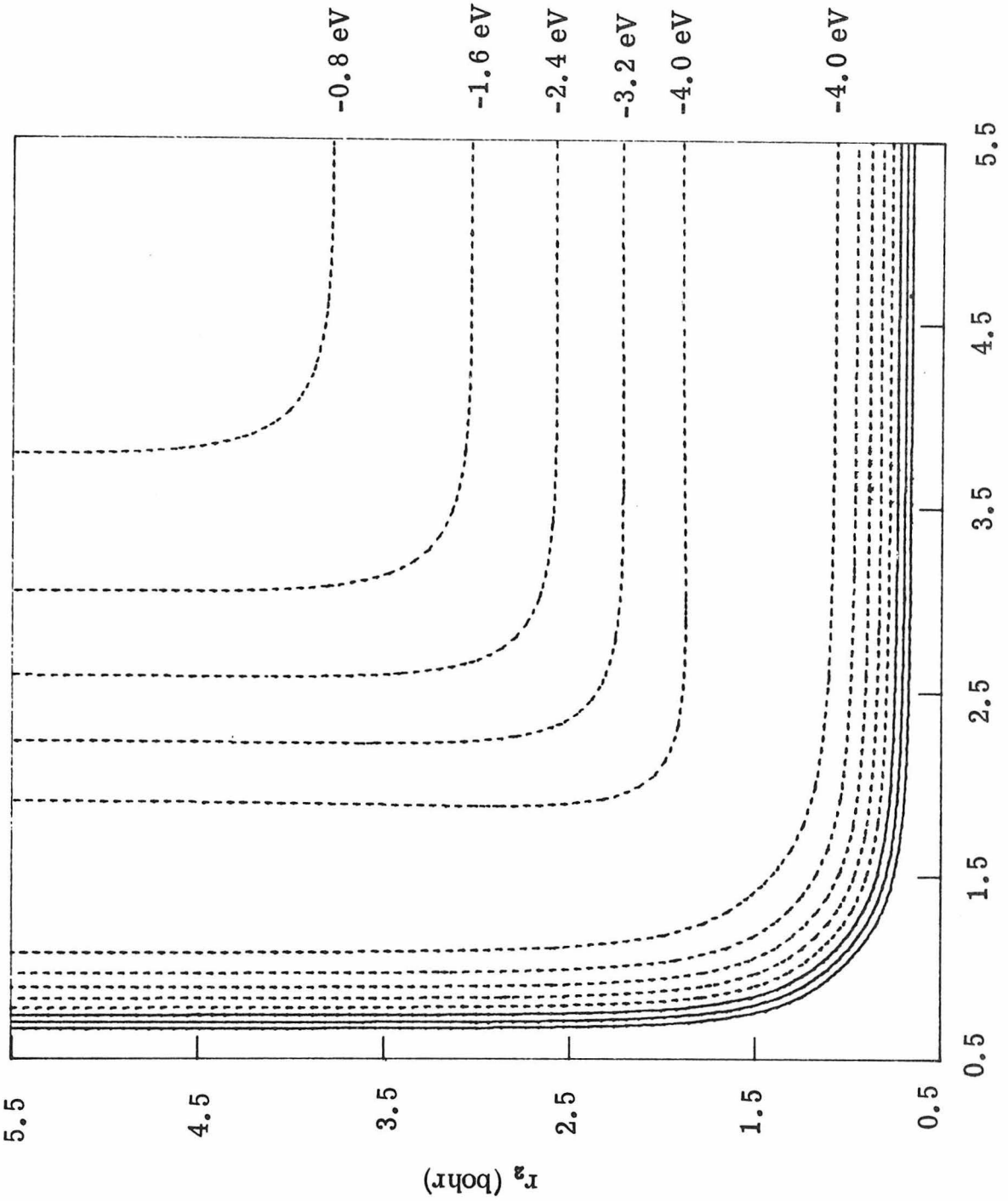
-0.8 eV
-1.6 eV
-2.4 eV
-3.2 eV
-4.0 eV
-4.0 eV
5.5
4.5
3.5
2.5
1.5
0.5
r₂ (bohr)
0.5
1.5
2.5
3.5
4.5
5.5
r₁ (bohr)

Fig. 1.

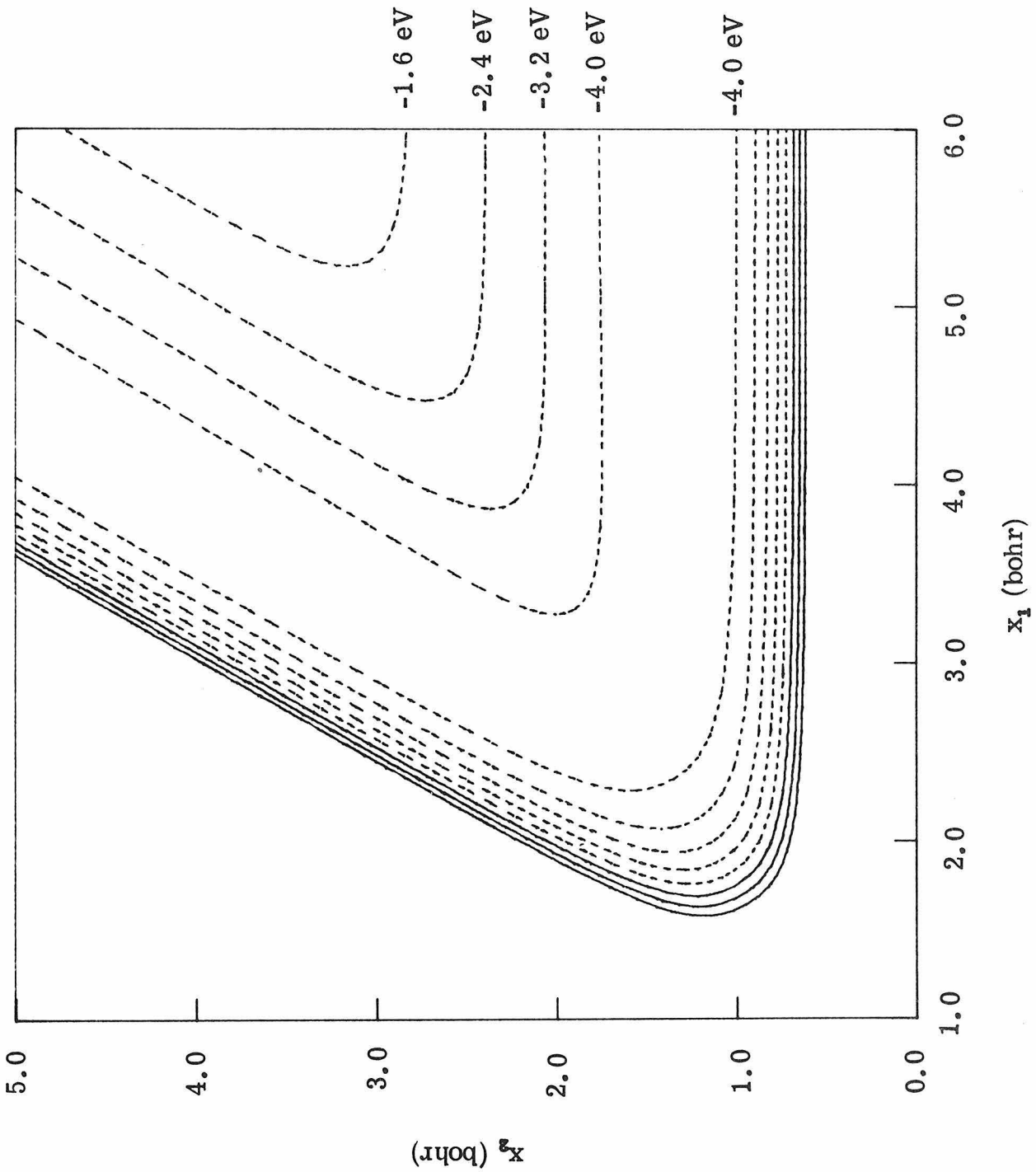
-1.6 eV
-2.4 eV
-3.2 eV
-4.0 eV
-4.0 eV
5.0
4.0
3.0
2.0
1.0
0.0
x_2 (bohr)
1.0
2.0
3.0
4.0
5.0
6.0
x_1 (bohr)

Fig. 2.

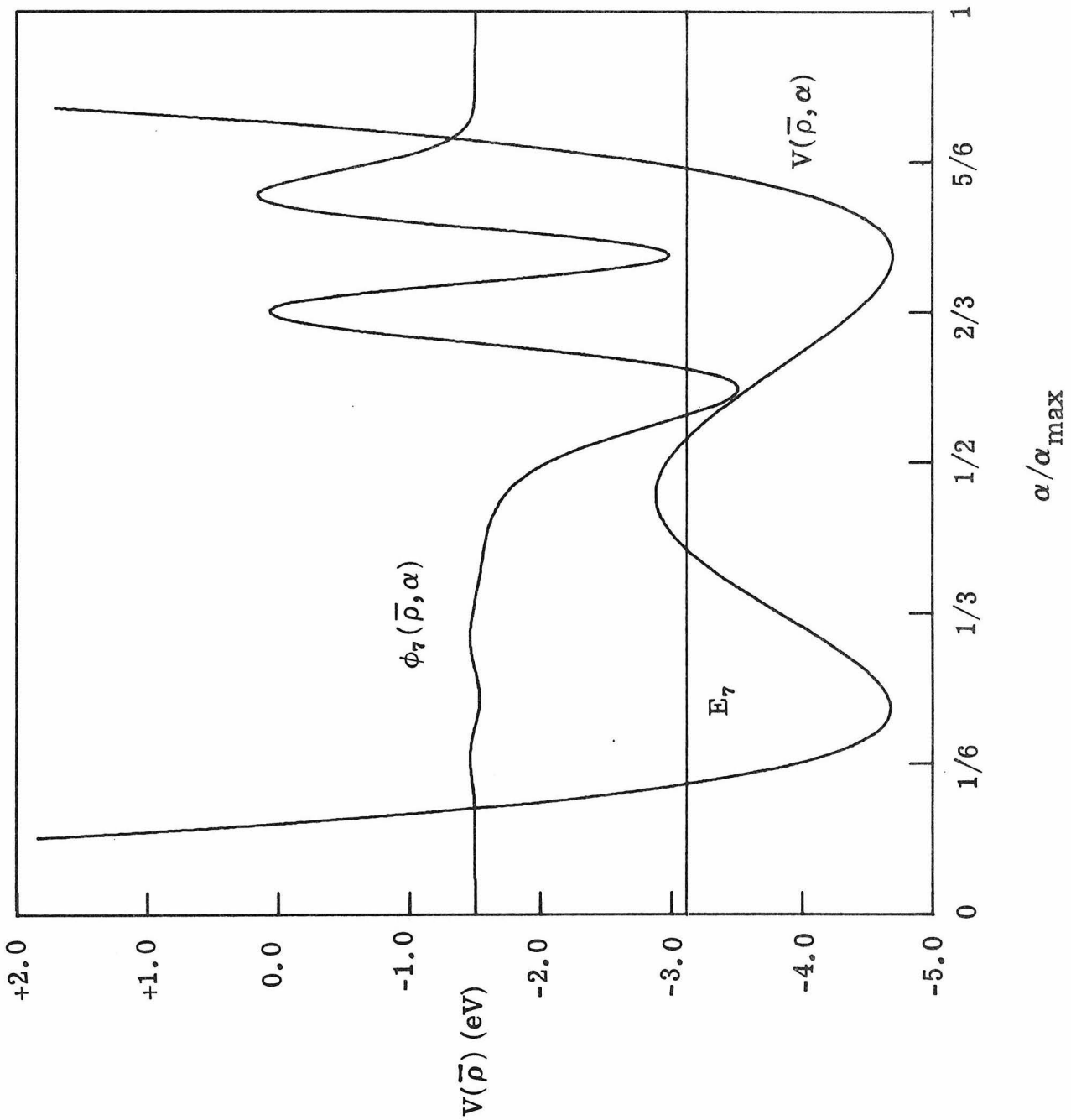

Fig. 3.

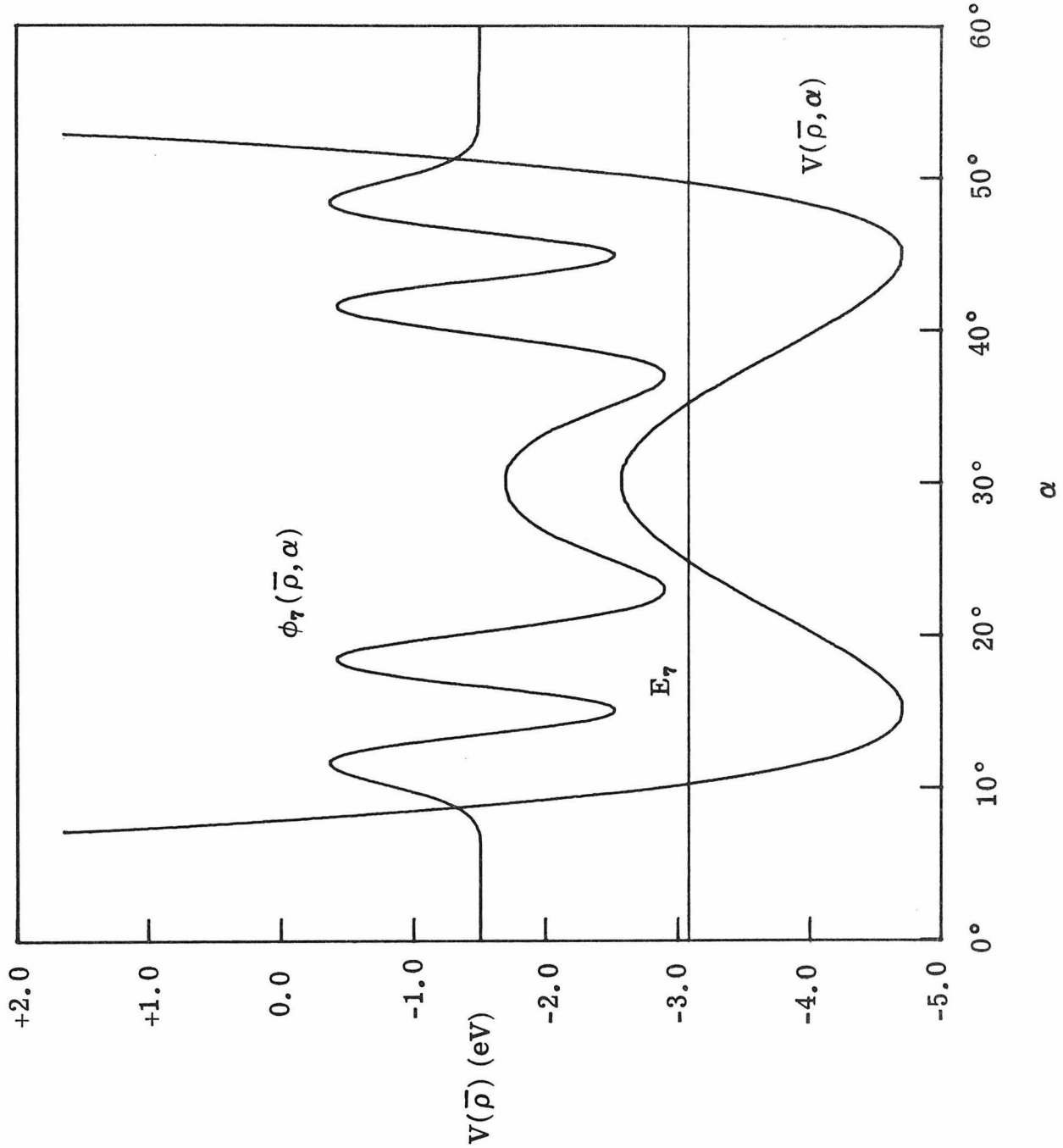

Fig. 4.

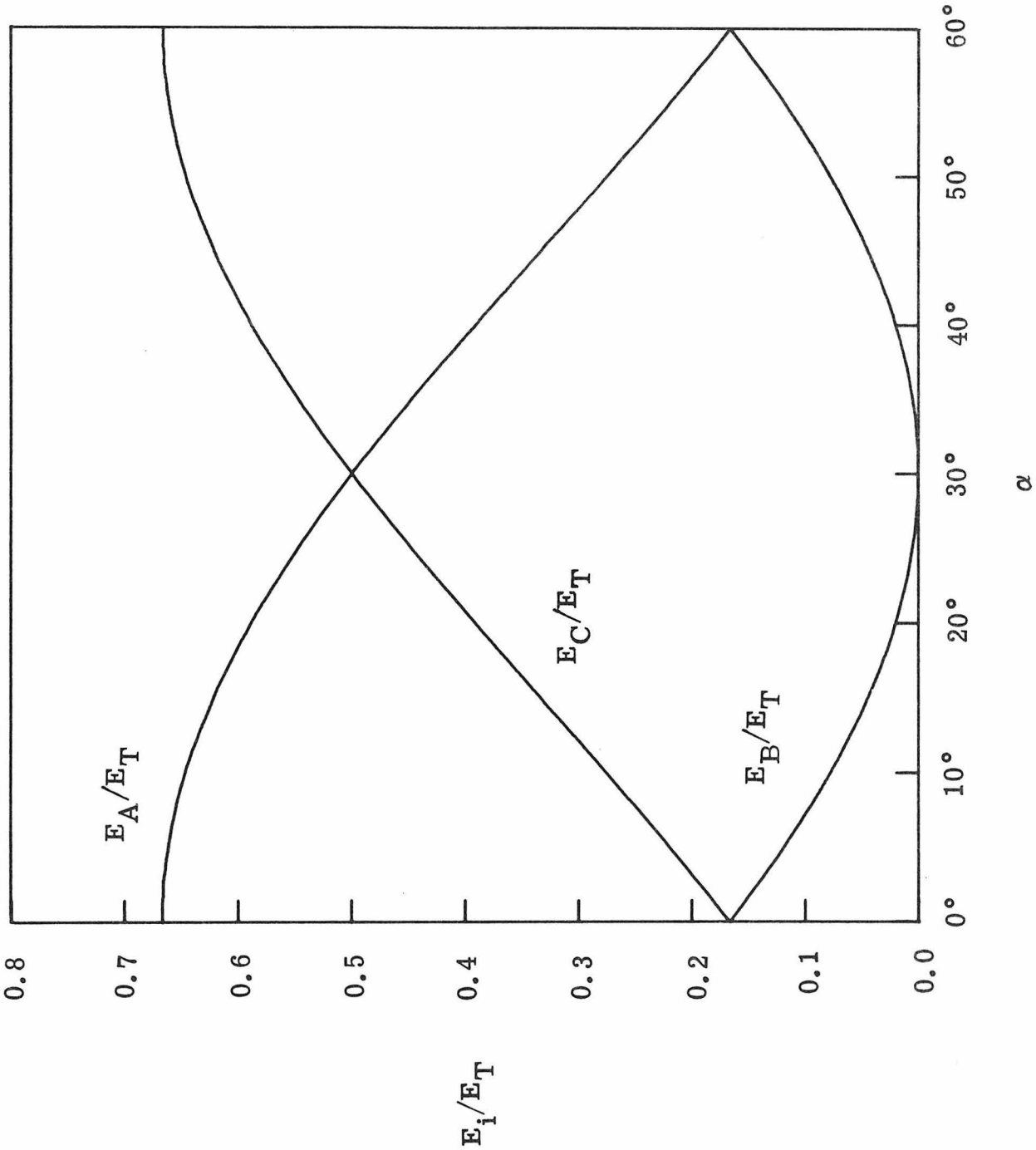
E_A/E_T
E_C/E_T
E_B/E_T
E_i/E_T
0.8
0.7
0.6
0.5
0.4
0.3
0.2
0.1
0.0
0°
10°
20°
30°
40°
50°
60°
α

Fig. 5.

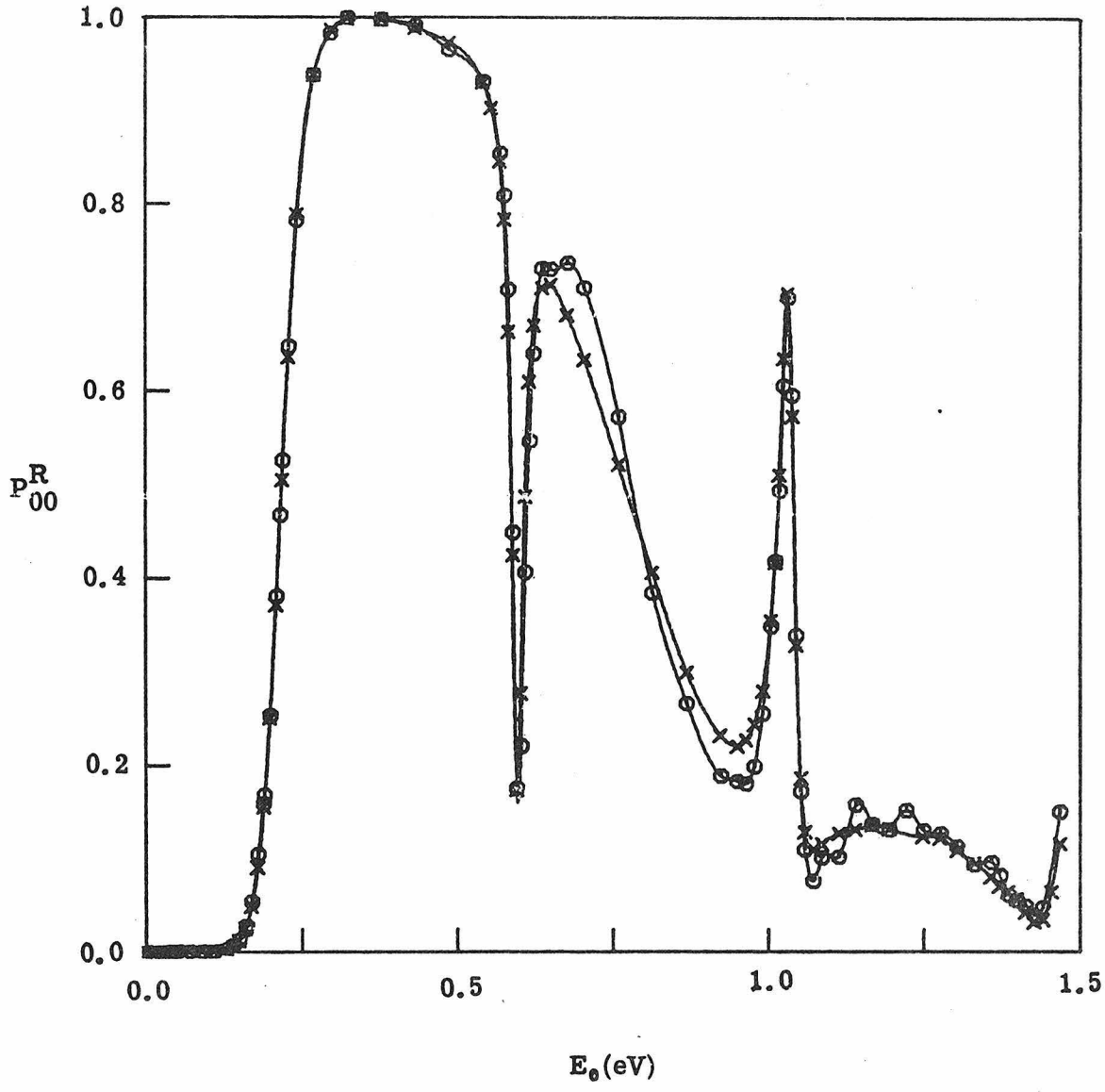

Fig. 6.

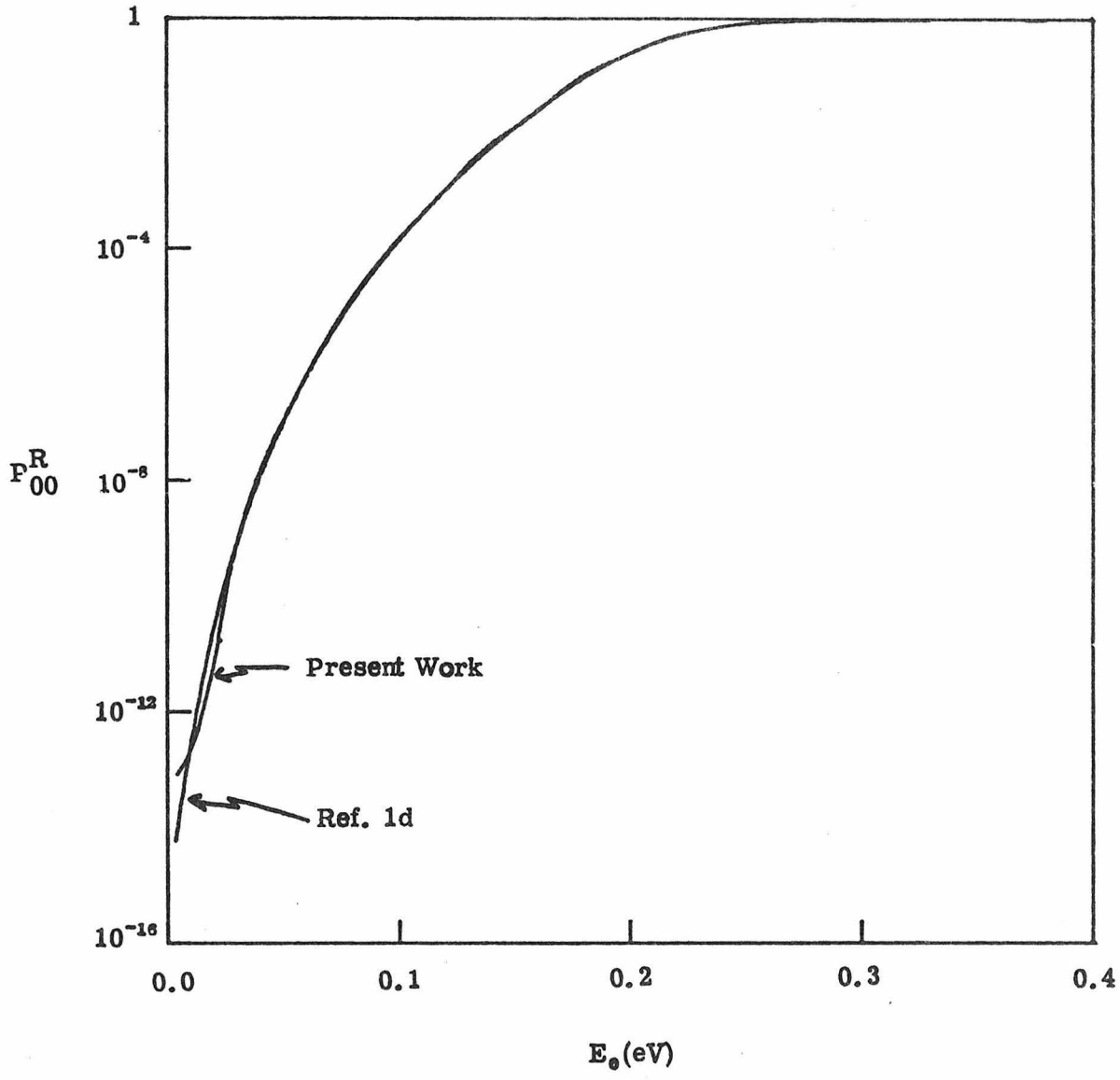

Fig. 7.

CHAPTER 6.

A Comparison of Two Exact Quantum Mechanical Calculations of a Three-Dimensional Reactive System

I. INTRODUCTION

There is considerable interest in studying three-dimensional reactive scattering using an exact quantum mechanical formulation. If a reliable calculation on a chemical system were made, one would be able to compare the results with those of approximate theories and to find the limits of validity and the degree of accuracy. Recently, two papers[1,2] have been published which give results on the H + H_2 system. In each case, an exact quantum mechanical formulation was used, and the same potential energy surface[3] was used. However, the results do not agree. The purpose of this paper is to examine the two methods and sets of results more closely and to discover why the discrepancy exists.

One paper, by Elkowitz and Wyatt[1] (hereafter called I), gives para-to-ortho integral cross sections in the energy range of 0.55 to 0.85 eV total energy. The second paper, by Schatz and Kuppermann[2] (hereafter called II), reports calculations done from a total energy of 0.40 eV to 0.70 eV. As reported in II, the cross sections from the two methods of the lowest para-to-ortho transition agree to within 20% over the energy range 0.60 eV to 0.70 eV. However, the cross sections on the next para-to-ortho transition differ by a factor of 2.5 over the same energy range.

In Sec. II we will briefly examine the two methods of calculation for differences which might affect the results. In Sec. III we present reaction probabilities at 0.60 eV from each of the methods and a third set calculated by using the potential surface actually used by Elkowitz and Wyatt in the computer program used by Schatz and Kuppermann.

Using these results we will draw some conclusions about the validity of the two methods.

II. METHODS OF CALCULATION

As reported in I, Elkowitz and Wyatt express the Hamiltonian operator in natural collision coordinates and divide it into three parts. The first describes motion along the reaction coordinate, the second vibration (using a local Morse potential), and the third internal rotation as well as tumbling of the triatomic plane. The wavefunction is expanded in a basis formed from the products of (local) Morse oscillators and (local) hindered asymmetric top states. The close-coupled differential equations were solved at several values of E and for many partial waves. At energies less than or equal to 0.60 eV, the basis included 12 rotations in the v = 0 vibrational state, six in the v = 1 state, and four in the v = 2 state. At higher energies the basis was partitioned 30/16/4. Ostensibly, the potential surface used was the Porter-Karplus[3] (PK) semi-empirical surface. However, that surface was not used directly. Instead, the potential was written as the sum of four terms.[5] The first is just the translational potential along the reaction path. The second term is a local Morse potential fit to the collinear PK surface. The third term is the rotational potential and is fit to an analytical expression. The fourth term is the deviation from the PK surface. It is assumed to be small and is ignored. In this treatment there is no coupling between rotational and vibrational states. When the Hamiltonian for this method was derived,[4] four kinetic energy terms were neglected. All of these terms vanish for large values of the reaction coordinate. One of these

couples the translational motion and the tumbling motion, but has no contribution for total angular momentum, J = 0, which is the value of J for the results presented herein.

Schatz and Kuppermann develop their method of reactive scattering in one paper[5] and apply the method to the PK surface in II. Unlike Elkowitz and Wyatt, they do not use natural collision coordinates, but use just center of mass, mass-scaled coordinates. The wavefunction is expanded in partial waves and then in a vibration-rotation basis set. As with I, the basis set is a local basis. The resulting close-coupled differential equations are solved and the scattering matrix calculated. The basis that was used differed depending on which partial wave was being calculated, but typically it had four vibrations with 30 rotations for v = 0 and v = 1, and 20 rotations for v = 2 and v = 3. For J = 0, the basis had five vibrations and eight rotations in each vibration. In Table III of II, Schatz and Kuppermann present results which demonstrate the convergence of the results with respect to the number of vibrational basis functions. In Table I we present results which show that the results are converged with respect to the number of rotational functions as well as vibrational functions. The potential surface used was ostensibly, as with Elkowitz and Wyatt, the PK surface. Actually, the potential was expanded in a series of Legendre polynomials. In practice, only a small number of terms is used in the expansion. Convergence with respect to the number of terms was shown in Table IV of II. For the PK surface, three terms were usually sufficient to insure accuracy of $\sim 5\%$.

III. RESULTS AND DISCUSSION

In Fig. 1 we present nonreactive and reactive transition probabilities for three types of calculations. All were done at 0.60 eV total energy and for J = 0 using the PK surface. The transitions ($vjm_j \rightarrow v'j'm'_j$) are for $v = v' = 0$, $m_j = m'_j = 0$, and $j = 0$ to all possible values of j'. Type 1 are the results from the Elkowitz and Wyatt formulation. Type 2 are the results from the Schatz and Kuppermann formulation. The third type requires some explanation. The scattering program used is from Schatz and Kuppermann. The potential surface is from Elkowitz and Wyatt (EW) and was expanded in Legendre polynomials (as was the PK surface in II). As Table II shows, more terms were required for convergence (five rather than three), indicating that PK and EW surfaces are not identical. A comparison of Type 1 and Type 2 reactive and nonreactive probabilities show that over a broad range of values the two methods give quite different results. For large j' (and therefore low values of the probability) the ratio of Type 1 and Type 2 nonreactive probabilities can be several orders of magnitude, but even at small j' values the ratio is as large as 6.5. For small j' reactive transitions, the ratio of Type 1 to Type 2 probabilities is as large as 1.6, but for large j', it is again several orders of magnitude. Thus the only point of close agreement is for reactive $0 \rightarrow j'$ ($j' \leq 2$) transitions. This difference can be accounted for in two ways. Either the potentials used are different (and we have seen above that, at least superficially, this is true) or the two methods produce different results. To see if the methods differ, we used the EW potential and the Schatz and Kuppermann formulation, i.e., Type 3 results.

For nonreactive results, the Type 1 and Type 3 calculations agree over a broad range of j′ (and hence probabilities) to within a factor of three. For $j' \leq 2$, the reactive transitions agree to within a factor of 1.5, and for $j' \geq 3$, all but one of the corresponding transitions agree to within a factor of six. This indicates that the formulations are indeed different. That is, they give quantitatively different results.

To see if the potential surfaces used differ, one should compare Type 2 and Type 3 calculations. For all nonreactive transitions, the agreement between Type 2 and Type 3 is substantially worse than the agreement between Type 1 and Type 3. For all but the highest j′, the Type 3 reactive transitions agree with the Type 2 results to within a factor of three.

To summarize, for nonreactive transitions, changing the potential has the most pronounced effect. For reactive transitions, changing either the potential or the formulation changes the results drastically, with the larger change due to the formulation.

It is worthwhile to consider the rotational distributions of reactive transitions. In II this was considered, and low j to j′ distinguishable atom cross sections were found to have a temperature-like distribution. For three-dimensional collisions the (J = 0) transition probability between rotational states j and j′ (and v = v′ = 0) may be written

$$P^{R}_{0,0j0\rightarrow 0j'0} = A_j(E)(2j'+1)p(E^{tr}_{j'})\exp[-E_{j'}/kT_j(E)] \quad ,$$

where T_j and A_j are the independent parameters. E_j is the energy of the product rotational state and $E^{tr}_{j'} = E - E_{j'} - E^0$, i.e., the product translational energy relative to state j′. E^0 is the v′ = j′ = 0 zero point

energy. If we plot $P_{0,0j0 \rightarrow 0j'0}/p(E_{j'}^{tr})(2j'+1)$ on a logarithmic scale as a function of $E_{j'}$, the resulting curve should be linear with a slope inversely proportional to T_j, if the distribution of product rotational states is temperature-like. In Fig. 2 we see that for the results calculated by Elkowitz and Wyatt (Type 1), the calculated temperature is 490°K. The results reported by Schatz and Kuppermann (Type 2) give a value of 275°K. This again clearly demonstrates the differences between the two calculations. The Type 3 results (the EW potential in the Schatz and Kuppermann formulation) give a temperature of 296°K. The close agreement between the Type 2 and Type 3 temperature parameters and the large difference between the Type 1 and Type 3 parameters emphasizes that the difference between the Type 1 and Type 2 reactive calculations lies not in the potential but in the formulation.

IV. SUMMARY

We have briefly examined two formulations for reactive scattering as applied to $H + H_2$ which give different results. We have shown that the two calculations did not use the same potential but that this only affected the nonreactive results. We have demonstrated that one set of results (Type 2) were converged with respect to the number of terms in the rotation-vibration basis set. The other set of results (Type 1) were apparently not tested for convergence. In addition, Type 1 results were calculated using a much smaller basis. The Type 2 formulation used all of the terms of the Hamiltonian in the calculation. The Type 1 formulation neglected some Coriolis terms and the effect of ignoring such terms was not investigated. We demonstrated that for reactive collisions the major difference between Type 1 and Type 2 calculations was not the potential surface but the formulation. Because the Type 2 results were shown to be converged, we conclude that the Type 1 results are in error.

TABLE I. Nonreactive and reactive transition probabilities for E = 0.6 eV. Type 1 calculation.

Transition ($vj \rightarrow v'j'$) J = 0, $m_j = m'_j = 0$	Reactive or Nonreactive	Basis Set	
		(N = 40)[a]	(N = 60)[b]
00 → 02	N	0.740	0.739
01 → 03	N	0.226	0.227
00 → 00	R	0.0249	0.0248
00 → 01	R	0.0418	0.0420
01 → 01	R	0.0715	0.0709

[a] Four vibrations, eight rotations/vibration ($j_{max} = 7$).

[b] Six vibrations, ten rotations/vibration ($j_{max} = 9$).

TABLE II. Convergence of nonreactive and reactive transition probabilities with respect to the number of terms used in the expansion of the EW potential at E = 0.6 eV.

(vj → v′j′)	Nonreactive or Reactive	Number of Terms 3	4	5	6
00 → 00	N	0.139	0.253	0.243	0.243
00 → 02	N	0.427	0.255	0.307	0.306
00 → 04	N	0.200	0.218	0.204	0.205
00 → 06	N	0.146(-3)	0.127(-3)	0.987(-4)	0.103(-3)
00 → 00	R	0.312(-1)	0.349(-1)	0.320(-1)	0.320(-1)
00 → 01	R	0.506(-1)	0.591(-1)	0.530(-1)	0.528(-1)
00 → 02	R	0.268(-1)	0.321(-1)	0.293(-1)	0.293(-1)
00 → 03	R	0.776(-2)	0.102(-1)	0.861(-2)	0.859(-2)
00 → 04	R	0.796(-3)	0.110(-2)	0.806(-3)	0.801(-3)
00 → 05	R	0.153(-4)	0.133(-4)	0.682(-5)	0.613(-5)
00 → 06	R	0.616(-6)	0.479(-6)	0.220(-6)	0.281(-6)

TABLE III. Nonreactive and reactive transition probabilities for E = 0.6 eV. Type 3 calculation (five-term expansion).

Transition ($vj \rightarrow v'j'$) $J=0$ $m_j = m'_j = 0$	Reactive or Nonreactive	Basis Set	
		$(N = 40)^a$	$(N = 60)^b$
$00 \rightarrow 02$	N	0.307	0.306
$01 \rightarrow 03$	N	0.304	0.304
$00 \rightarrow 00$	R	0.0320	0.0324
$00 \rightarrow 01$	R	0.0528	0.0531
$01 \rightarrow 01$	R	0.0864	0.0877

[a] Four vibrations, eight rotations/vibration ($j_{max} = 7$).

[b] Six vibrations, ten rotations/vibration ($j_{max} = 9$).

REFERENCES

1. A. B. Elkowitz and R. E. Wyatt, J. Chem. Phys. 62, 2504 (1975).

2. G. C. Schatz and A. Kuppermann, J. Chem. Phys. 65, 4668 (1976).

3. R. N. Porter and M. Karplus, J. Chem. Phys. 40, 1105 (1964).

4. R. E. Wyatt, J. Chem. Phys. 56, 390 (1972).

5. G. C. Schatz and A. Kuppermann, J. Chem. Phys. 65, 4642 (1976).

FIGURE CAPTIONS

FIG. 1. A plot of reactive (top) and nonreactive (bottom) transition probabilities for the 000 → 0j'0 transition, j' = 0 - 6. The energy is 0.60 eV and J = 0. The (——○——) are Type 1 results, the (--□--) are Type 2 results, and the (—·Δ—·) are Type 3 results.

FIG. 2. A plot of $P_{0,000\rightarrow 0j'0}/p(E_{j'}^{tr})(2j'+1)$ versus $E_{j'}$ on a log scale at a total energy of 0.60 eV. The (——○——) are Type 1 results, the (--□--) are Type 2 results, and the (—·Δ—·) are Type 3 results.

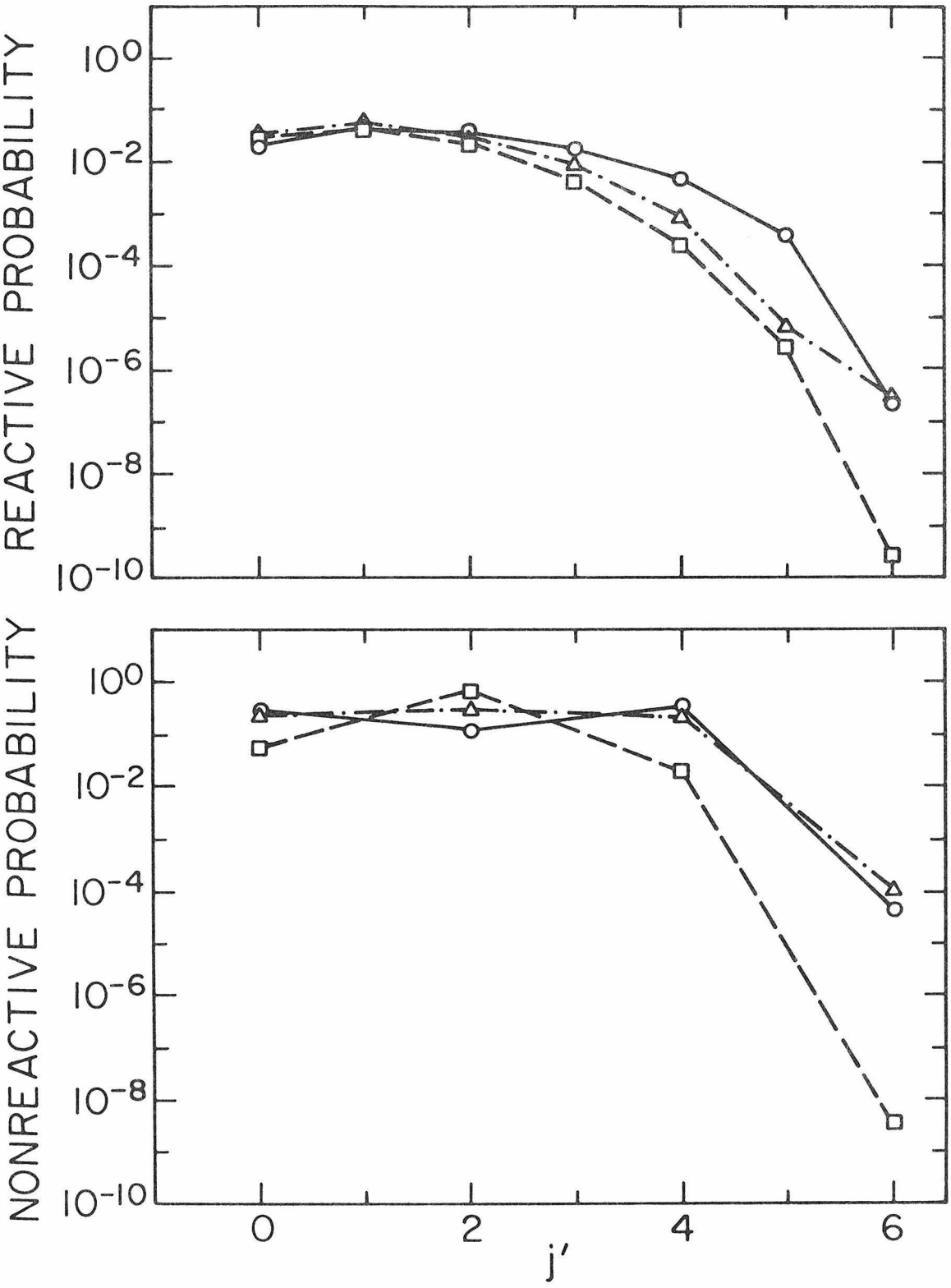
REACTIVE PROBABILITY
NONREACTIVE PROBABILITY
10^0
10^-2
10^-4
10^-6
10^-8
10^-10
0
2
4
6
j'

Fig. 1.

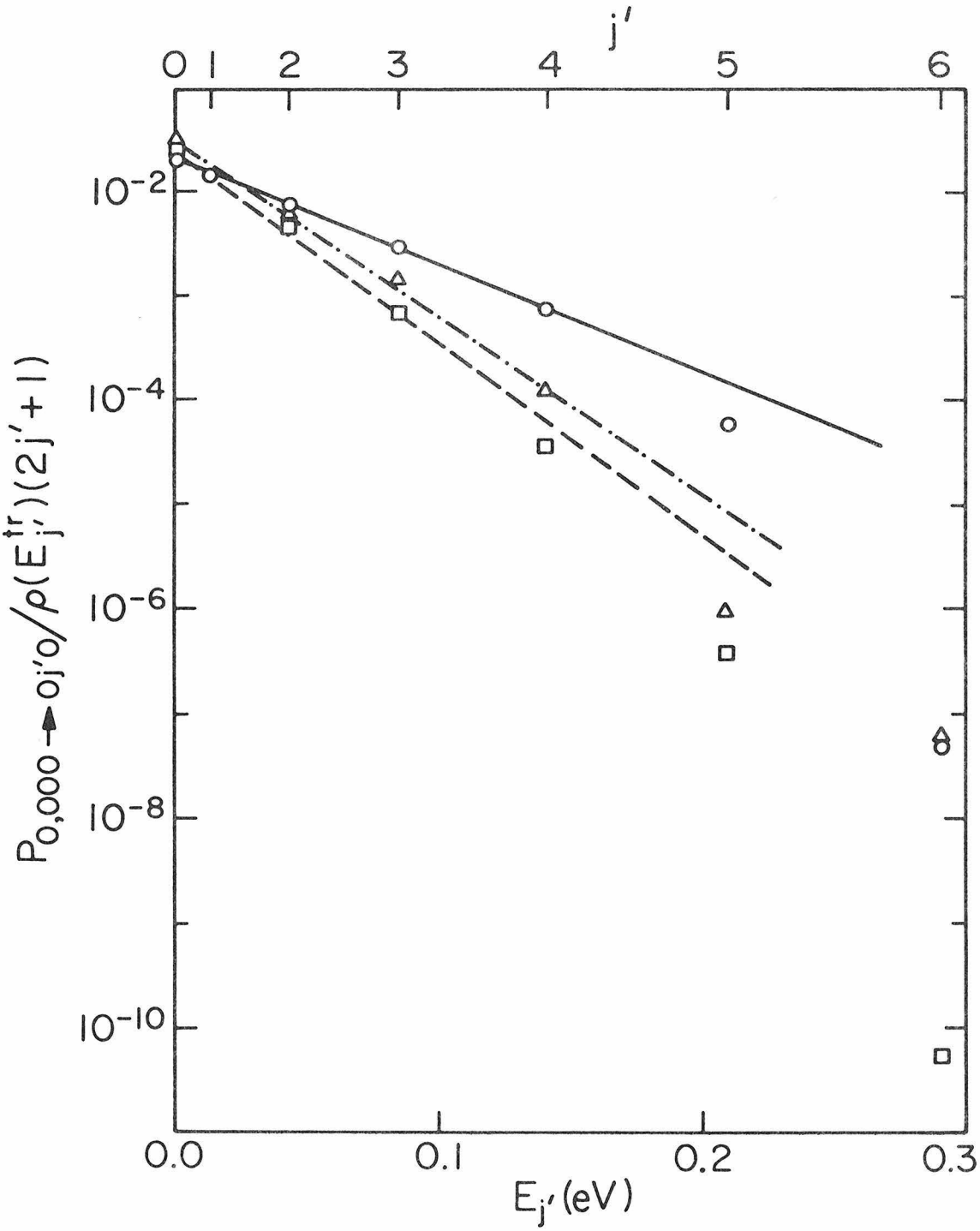
j'
0 1 2 3 4 5 6
10^{-2}
10^{-4}
10^{-6}
10^{-8}
10^{-10}
$P_{0,000 \rightarrow 0j'0}/\rho(E^{tr}_{j'})(2j'+1)$
0.0 0.1 0.2 0.3
$E_{j'}$ (eV)

Fig. 2.

CHAPTER 7.

Angular Momentum Decoupling Approximation in Reactive Scattering: Application to $H + H_2$

I. Introduction

There have been some recent attempts[1-5] to calculate accurate quantum mechanical cross sections for three-dimensional reactive atom-diatom collisions. In one paper (hereafter referred to as I), Schatz and Kuppermann[2] developed the theory and method necessary to solve the Schrödinger equation for these systems. The technique, called close-coupling, involves expanding the wavefunction in vibration-rotation basis functions, generating solutions of the coupled equations in each of the three arrangement channels, and smoothly matching these solutions at the boundary between the channels. The smoothly matched solutions are then used to calculate the scattering matrix (S-matrix) from which transition probabilities and cross sections are obtained. In another paper[3] (hereafter referred to as II), they present results for the $H + H_2$ reaction using the Porter-Karplus[6] potential energy surface. Using a different close-coupling formulation based on natural collision coordinates, Elkowitz and Wyatt[4,5] have also reported results on the $H + H_2$ system.

The computer time necessary to calculate fully converged reactive and nonreactive cross sections can be enormous. Schatz and Kuppermann[2] have reported that one partial wave at one energy can require as much as 47 minutes (on an IBM 370/158) just to integrate the coupled equations. In order to calculate converged nonreactive differential cross sections, as many as 34 partial waves may be required (reactive cross sections require about 15 partial waves for convergence). Clearly, an approximate method that requires considerably less computer time but preserves the current level of accuracy ($\sim 5\%$) is urgently needed.

In order to find accurate scattering solutions to the Schrödinger equation, one must use large vibration-rotation basis sets which may total 100 states. We will see later that some of these states are not coupled to others, thus reducing the dimensionality of the problem. Even so, it is often necessary to solve 30 coupled equations simultaneously. It is the manipulation of these large (30×30) matrices which slows the computation. Because the computation time increases with the cube of the number of states, one can see that it would be more efficient to solve the Schrödinger equation ten times, three states at a time, than to solve it once with 30 states. Therefore, to reduce significantly computation times, one should develop an approximation which uncouples many of the states.

One idea is to use an angular momentum decoupling (tumbling decoupling) approximation. In a triatomic system there is a quantum number, call it Ω, that is associated with the tumbling of the triatomic plane. (In this paper Ω will often be called the projection of the rotational quantum number, j.) The central idea of the tumbling decoupling approximation is to neglect the coupling in the Hamiltonian between states of different Ω.

Because the number of projections, Ω increases linearly with the number of rotational states included in the basis set, this approximation can be used effectively in one of two ways. The smaller number of coupled equations allows one to include more vibrational and rotational basis functions and, therefore, to investigate higher energies or systems that require more basis functions. On the other hand, one can use

the same basis and perform the calculations with significantly smaller computer times and, therefore, be able to sample more energies within a certain range. We have chosen the latter approach in order to investigate the validity of the approximation for reactive and nonreactive scattering.

In Sec. II we discuss the basic idea of the tumbling decoupling approximation and formulate it in two different schemes. We compare these schemes with previous attempts in nonreactive and reactive scattering. In Sec. III we present an analysis of the computation time saved by the approximations. Section IV contains the results, probabilities and cross sections from the $H + H_2$ reaction using the Porter-Karplus surface. A careful comparison with the fully coupled Schatz and Kuppermann results[3] is included. In Sec. V we give a summary of the more significant findings and the limits of the approximations.

II. Theory

In this section we will present the ideas and equations necessary to develop two tumbling decoupling approximations, called simple decoupling (SD) and proper decoupling (PD). A complete treatment of the fully coupled problem is given in I. First we will consider the solution of the Schrödinger equation for an atom-diatom collision.

The notation used here is identical to the notation in I. Consider a triatomic system with atoms A_α, A_β, and A_δ. Following I, $\underset{\sim}{r}_\lambda$ is the mass-scaled[7,8] position vector from A_ν to A_κ, $\underset{\sim}{R}_\lambda$ is the mass-scaled position vector from the center of mass of $A_\nu A_\kappa$ to A_λ, and γ is the angle from $\underset{\sim}{r}_\lambda$ to $\underset{\sim}{R}_\lambda$, where $\lambda\nu\kappa$ is any cyclic permutation of $\alpha\beta\delta$. In arrangement channel λ coordinates, where atom A_λ is far from diatom $A_\nu A_\kappa$, the Schrödinger equation can be written

$$\left\{ \frac{-\hbar^2}{2\mu} (\nabla^2_{\underset{\sim}{R}_\lambda} + \nabla^2_{\underset{\sim}{r}_\lambda}) + V^\lambda(r_\lambda, R_\lambda, \gamma_\lambda) - E \right\} \psi^\lambda(\underset{\sim}{r}_\lambda, \underset{\sim}{R}_\lambda) = 0 , \quad (2.1)$$

where

$$\mu = [m_\lambda m_\nu m_\kappa / (m_\lambda + m_\nu + m_\kappa)]^{\frac{1}{2}} \quad (2.2)$$

and $m_\nu, m_\lambda, m_\kappa$ are the masses of A_ν, A_λ, and A_κ, respectively. We may write an analogous equation for each of the other two arrangement channels, κ and ν. ψ^λ is expanded in simultaneous eigenfunctions of $\underset{\sim}{J}^2$, J_Z, and the Hamiltonian to give

$$\psi^\lambda(\underset{\sim}{r}_\lambda, \underset{\sim}{R}_\lambda) = \sum_{J=0}^{\infty} \sum_{M=-J}^{J} C_{JM} \psi^\lambda_{JM}(\underset{\sim}{r}_\lambda, \underset{\sim}{R}_\lambda) . \quad (2.3)$$

In space-fixed coordinates, xyz (with the origin at the center of mass of the triatomic system), the polar and azimuthal angles of $\underset{\sim}{R}_\lambda$ and $\underset{\sim}{r}_\lambda$ are denoted as $\theta_\lambda, \varphi_\lambda$ and $\theta_{r_\lambda}, \varphi_{r_\lambda}$, respectively. As explained in I, body-

fixed coordinates can be defined by rotating the space-fixed axes through the Euler angles, $\alpha = \varphi_\lambda, \beta = \theta_\lambda$, and $\gamma = 0$. The resulting body-fixed z_λ axis is chosen to lie along $\underset{\sim}{R}_\lambda$. The angle ψ_λ defines the tumbling of the triatomic system around $\underset{\sim}{R}_\lambda$. We expand each partial wave in (2.3) in elements of Wigner rotation matrices as follows:

$$\psi^\lambda_{JM}(\underset{\sim}{r}_\lambda, \underset{\sim}{R}_\lambda) = \sum_{\Omega_\lambda=-J}^{J} D^J_{M\Omega_\lambda}(\varphi_\lambda, \theta_\lambda, 0)\psi^\lambda_{J\Omega_\lambda}(r_\lambda, R_\lambda, \gamma_\lambda, \psi_\lambda), \quad (2.4)$$

where Ω_λ, the tumbling quantum number in arrangement channel λ, is the component of the total angular momentum J around $\underset{\sim}{R}_\lambda$. When Eqs. (2.4) and (2.3) are substituted into Eq.(2.1), we get

$$H^{J\lambda}_{\Omega_\lambda,\Omega_\lambda}\psi^\lambda_{J\Omega_\lambda} + H^{J\lambda}_{\Omega_\lambda,\Omega_\lambda+1}\psi^\lambda_{J\Omega_\lambda+1} + H^{J\lambda}_{\Omega,\Omega_\lambda-1}\psi^\lambda_{J\Omega_\lambda-1} = E\psi^\lambda_{J\Omega_\lambda}, \quad (2.5)$$

where

$$H^{J\lambda}_{\Omega_\lambda,\Omega_\lambda} = \frac{-\hbar^2}{2\mu}\left(\frac{1}{r_\lambda}\frac{\partial^2}{\partial r_\lambda^2}r_\lambda + \frac{1}{R_\lambda}\frac{\partial^2}{\partial R_\lambda^2}R_\lambda\right) + \frac{j_\lambda^2}{2\mu r_\lambda^2}$$

$$+ \frac{1}{2\mu R_\lambda^2}[J(J+1)\hbar^2 - 2\Omega_\lambda\hbar j_\lambda + j_\lambda^2] + V^\lambda(r_\lambda, R_\lambda, \gamma_\lambda), \quad (2.6)$$

$$H_{\Omega_\lambda,\Omega_\lambda\pm1} = \frac{-\hbar}{2\mu R_\lambda^2}[J(J+1) - \Omega_\lambda(\Omega_\lambda \pm 1)]^{\frac{1}{2}} j_\lambda^{\mp}, \quad (2.7)$$

and $j_\lambda^{\mp}$ are the lowering and raising operators of the rotational angular momentum j_λ.

Now $\psi^\lambda_{J\Omega_\lambda}$ is expanded in spherical harmonics which are simultaneous eigenfunctions of j_λ^2 and $j_{\lambda z_\lambda}$,

$$\psi^\lambda_{J\Omega_\lambda}(r_\lambda, R_\lambda, \gamma_\lambda, \psi_\lambda) = \sum_{j_\lambda=|\Omega_\lambda|}^{\infty} Y_{j_\lambda\Omega_\lambda}(\gamma_\lambda, \psi_\lambda) w^\lambda_{Jj_\lambda\Omega_\lambda}(r_\lambda, R_\lambda). \quad (2.8)$$

A little more manipulation and integration finally gives

$$(t^{J\lambda j_\lambda}_{\Omega_\lambda,\Omega_\lambda} - E)w^\lambda_{Jj_\lambda\Omega_\lambda}(r_\lambda,R_\lambda) + \sum_{j'_\lambda=|\Omega_\lambda|}^{\infty} V^{\lambda\Omega_\lambda}_{j_\lambda j'_\lambda} w^\lambda_{Jj'_\lambda\Omega_\lambda}(r_\lambda,R_\lambda)$$

$$+ t^{J\lambda j_\lambda}_{\Omega_\lambda,\Omega_\lambda+1} w_{j_\lambda\Omega_\lambda+1}(r_\lambda,R_\lambda) + t^{J\lambda j_\lambda}_{\Omega_\lambda,\Omega_\lambda-1} w^\lambda_{Jj_\lambda\Omega_\lambda-1}(r_\lambda,R_\lambda) = 0, \quad (2.9)$$

where

$$t^{J\lambda j_\lambda}_{\Omega_\lambda,\Omega_\lambda} = \frac{-\hbar^2}{2\mu}\left[\frac{1}{R_\lambda}\frac{\partial^2}{\partial R_\lambda^2}R_\lambda + \frac{1}{r_\lambda}\frac{\partial^2}{\partial r_\lambda^2}r_\lambda\right] + \frac{j_\lambda(j_\lambda+1)\hbar^2}{2\mu r_\lambda^2}$$

$$+ \frac{\hbar^2}{2\mu R_\lambda^2}[J(J+1) - 2\Omega_\lambda^2 + j_\lambda(j_\lambda+1)], \quad (2.10)$$

$$t^{J\lambda j_\lambda}_{\Omega_\lambda,\Omega_\lambda\pm1} = \frac{-\hbar^2}{2\mu R_\lambda^2}[J(J+1) - \Omega_\lambda(\Omega_\lambda\pm1)]^{\frac{1}{2}}[j_\lambda(j_\lambda+1) - \Omega_\lambda(\Omega_\lambda\pm1)]^{\frac{1}{2}}$$

$$|\Omega_\lambda| \le J, j_\lambda, \quad (2.11)$$

and

$$V^{\lambda\Omega_\lambda}_{j_\lambda j'_\lambda}(r_\lambda,R_\lambda) = \langle j_\lambda\Omega_\lambda|V^\lambda(r_\lambda,R_\lambda,\gamma_\lambda)|j'_\lambda\Omega_\lambda\rangle. \quad (2.12)$$

Here the Ω_λ coupling is explicit. One can see that it occurs only in the kinetic terms and that the potential coupling is diagonal in Ω_λ. We can now make the angular momentum decoupling approximation. We will neglect the terms $t^{J\lambda j_\lambda}_{\Omega,\Omega\pm1}$. This is the central approximation for both decoupling schemes presented here; the differences between the two will be detailed in a discussion of the matching.

This decoupling scheme has been used extensively by other workers in nonreactive scattering,[9-11] and quite recently in reactive scattering.[12] However, many of these workers further approximate terms in Eq.(2.10)

(see Appendix). In nonreactive scattering,

$$\frac{\hbar^2}{2\mu R_\lambda^2}\left[J(J+1) - 2\Omega_\lambda^2 + j_\lambda(j_\lambda+1)\right]$$

has been replaced by $\hbar^2 J(J+1)/2\mu R_\lambda^2$ (Pack[10]) or $\hbar^2 \ell_\lambda(\ell_\lambda+1)/2\mu R_\lambda^2$ (McGuire and Kouri[9]). McGuire and Kouri found that decoupled integral cross sections of elastic collisions (in the He-H_2 system) differed from the fully coupled results by less than 1%, while inelastic integral cross sections were in error by 4%.

Elkowitz and Wyatt[12] have recently reported results using a J_z-conserving approximation for the reactive H + H_2 system. The method was adapted from their fully coupled formulation and incorporates the J_z-conserving ideas of McGuire and Kouri and Pack. They report total cross sections for $j \rightarrow j'$ transitions which agreed with their fully coupled results to about 7%. However, they did not report any differential cross sections, cross sections of individual (i.e., $\Omega_j \rightarrow \Omega_j'$) transitions, or any nonreactive cross sections.

With the neglect of Ω_λ coupling, each set of equations with a different Ω_λ may be integrated in each arrangement channel separately. (In the H_3 system, each of the three arrangement channels are identical and the coupled equations are solved in only one of the channels.) In the fully coupled calculation positive and negative Ω_λ are uncoupled by a unitary transformation. This so-called parity decoupling,[3] which is rigorous and is normally applicable to any triatomic system, cannot be used here. The decoupling approximation has uncoupled all Ω_λ from each other; to say that positive and negative Ω_λ are also uncoupled is redundant.

Because the target diatom (H_2) is homonuclear, there is no coupling between even and odd j_λ in arrangement channel λ. This symmetry decoupling,[3] which is rigorous, further reduces the number of equations that must be solved simultaneously. It can be used simultaneously with the decoupling approximation. Because $V^{\lambda\Omega_\lambda}_{j_\lambda j'_\lambda}$ and the diagonal part of the kinetic energy, $t^{J\lambda j_\lambda}_{\Omega_\lambda,\Omega_\lambda}$, are independent of the sign of Ω_λ [see Eqs. (2.8), (2.10), and (2.12)], only $\Omega_\lambda \geq 0$ need be considered in the calculation.

As described in I, we must now relate the wavefunction $w^\lambda_{J\Omega_\lambda}$ in arrangement channel λ coordinates to the wavefunction $w^\nu_{J\Omega_\nu}$ in arrangement channel ν coordinates. This can be written using Wigner rotation matrices,

$$w^\lambda_{J\Omega_\lambda} = \sum_{\Omega_\nu} D^J_{\Omega_\nu\Omega_\lambda}(0,\Delta_{\nu\lambda},0)\, w^\nu_{J\Omega_\nu}, \tag{2.13}$$

where $\Delta_{\nu\lambda}$ is the angle between R_ν and R_λ. The ν and κ channels and the κ and λ channels are analogously related. The important thing to notice is that this equation allows mixing between states of different Ω in different arrangement channels. In the simple decoupling procedure we set

$$D^J_{\Omega_\nu\Omega_\lambda}(0,\Delta_{\nu\lambda},0) = \delta_{\Omega_\nu,\Omega_\lambda}. \tag{2.14}$$

This assumption forces the scattering matrix to be diagonal in Ω. In the proper decoupling procedure, as in the fully coupled procedure, this assumption is not made, and the mixing occurs. There is no significant difference in the computation times for the two approximations.

Once the coupled equations have been solved in each arrangement channel and the resulting solutions smoothly matched, one can calculate

the S-matrix, $\underset{\approx}{S}_J$. The S-matrix is related to transition probabilities and scattering amplitudes, which are related to differential and integral cross sections. The reactive (nonreactive) transition probability from state vjm_j[13] to state $v'j'm'_{j'}$ with total angular momentum J is defined to be

$$P^{R(N)}_{J,\,vjm_j \to v'j'm'_{j'}} = \left| S^{R(N)}_{J,\,vjm_j \to v'j'm'_{j'}} \right|^2 .$$

Reactive (nonreactive) differential cross sections are given by

$$\sigma^{R(N)}_{vjm_j \to v'j'm'_{j'}}(\theta) = \frac{1}{4\bar{k}^2_{vj}} \left| \sum_{J=0}^{\infty} (2J+1) d^J_{m'_{j'} m_j}(\theta) T^{R(N)}_{J,\,vjm_j \to v'j'm'_{j'}} \right|^2 ,$$

where $\underset{\approx}{T}_J$ is the transition matrix and is defined by

$$\underset{\approx}{T}_J = \underset{\approx}{1} - \underset{\approx}{S}_J ,$$

$$d^J_{m_j m'_{j'}}(\theta) = D^J_{m_j m'_{j'}}(0, \theta, 0)$$

(Wigner rotation matrices[14]), $\bar{k}_{vj}$ is the wave number, and θ is the scattering angle, which is defined as the angle between the velocity vector of the incident atom and the velocity vector of the product atom. The differential cross section may be integrated over the polar angles to yield integral cross sections,

$$Q^{R(N)}_{vjm_j \to v'j'm'_{j'}} = \frac{\pi}{k^2_{vj}} \sum_{J=0}^{\infty} (2J+1) \left| T^{R(N)}_{J,\,vjm_j \to v'j'm'_{j'}} \right|^2 .$$

The cross sections as written are nonphysical; they describe a distinguishable-atom triatomic system. For our application, $H + H_2$, the atoms are indistinguishable and we must convert the cross sections to physical ones by post-antisymmetrization.[2]

It was shown in I that the nonreactive scattering amplitude, $f^{N}_{vjm_j \to v'j'm'_{j'}} = 0$, if j-j' is odd. This implies that all nonreactive cross sections will vanish for j-j' odd.

III. Computation Times

An analysis of Table II in II indicates that the computation times for the integration of the coupled equations increase with the cube of the number of channels. These equations can be decoupled rigorously by two procedures. Parity decoupling, which can be used on any triatomic system, can be used to decouple equations labelled by $\Omega_\lambda \geq 0$ from those labelled $\Omega_\lambda < 0$. The second procedure, symmetry decoupling, can be used only on those arrangement channels in which the diatom is homonuclear (i.e., H_2). In an example considered by Schatz and Kuppermann, a certain choice of vibrational and rotational quantum numbers led to a ($J \geq 4$) basis of 100 channels. Using symmetry and parity decoupling, the 100 channel basis can be divided into four uncoupled parts, two with 30 channels and two with 20 channels. If the compute time t is given by

$$a \sum_i n_i^3 = t \ , \tag{3.1}$$

where n_i is the number of channels for a given solution (i.e., 30), and a is the time constant, we find that $a = 6.7 \times 10^{-4}$ min. If we examine the same problem (i.e., 100 channels) using the angular momentum decoupling approximation (and applying symmetry decoupling), we find that it divides into ten solutions, two with each of two, four, six, eight, and ten channels. (Recall that the scattering matrix is invariant to the sign of Ω_λ and therefore only $\Omega_\lambda \geq 0$ need be considered.) Using Eq.

(3.1) we see that t = 2.4 min, which is a factor of 20 faster than the exact calculation.

Table I gives a more detailed comparison of times from paper II, actual computation times with the simple and proper decoupling methods and the potential computation times using Eq.(3.1). The reasons for the difference in columns four and five are twofold. First, the alterations for decoupling made to the computer program used in II were made in the most expedient but not in the most efficient manner possible. Second, the computation time increases as n^2 for small n. There were virtually no differences in the time required for matching for the fully coupled, proper decoupled, or simple decoupled methods. For the fully coupled calculation, the integration was roughly 77% of the total compute time necessary for calculating the S matrix. Using the decoupling approximation, that percentage has been reduced to as little as 36%.

IV. Results

In this section we will examine transition probabilities, phases of S-matrix elements, total cross sections, and differential cross sections of individual transitions, i.e., transitions between states labelled by vjm_j. We will also consider transition probabilities and cross sections that have been summed over final projections and averaged over initial projections. These states are identified by the quantum numbers vj. We will consider nonreactive, reactive, and antisymmetrized transitions and will denote them by N, R, and A, respectively. The energy range considered is from 0.3 to 0.7 eV total energy in which only one vibrational state is open.

In Fig. 1, the reactive probability, $P^R_{2,000\to010}$ (i.e., J = 2), is plotted as a function of total energy E for the three types of calculations, the fully coupled method, the proper decoupled method, and the simple decoupled method. One can see that the agreement between the approximations and the exact method is generally good even though the probability changes 15 orders of magnitude. The phase of the S-matrix element is defined to be

$$\phi = \tan^{-1}\left(\frac{S_{imag}}{S_{real}}\right)$$

for any individual transition. In Fig. 2 we have plotted the phases of the same reactive transition, $\phi^R_{2,000\to010}$, as a function of energy. The figure shows that over the range of energies considered, the phase changes by ten radians. For most energies, the error for both approximations is less than 0.10 radians. These two figures together indicate that for $m_j = 0$ to $m'_j = 0$ transitions, both the proper and simple

decoupling methods can accurately reproduce the exact S-matrix element. The largest error for both methods in the magnitude and phase of the S-matrix element is at the lowest energy, 0.30 eV.

$P^{R}_{J,000\rightarrow010}$ is plotted as a function of total angular momentum J in Fig. 3 for two different energies. One can see that for both energies the PD calculation gives results in better agreement with the full calculation than does the SD calculation for an $m_j = 0$ to $m'_{j'} = 0$ transition. This figure clearly demonstrates another point. For J = 0, the two approximations agree with the fully coupled calculation exactly. When J = 0, the maximum absolute value of Ω (or m_j) is zero, and there is no decoupling of different Ω. [This is explained in I, where $|\Omega| \leq \min(J, j)$.] Another important point is that reactive probabilities tail off around J = 9 for energies at or below 0.60 eV. Figure 4 illustrates the same points at E = 0.60 eV for a different transition, $010 \rightarrow 020$. It is apparent from these two figures that the SD probabilities are usually larger than the exact probabilities and that the PD results are usually smaller. Figure 5 is a plot of the phases corresponding to the transitions in Figs. 3 and 4, and Fig. 6 contains the errors of the PD and SD phases with the exact phases. First, even though the PD probabilities are significantly better than the SD probabilities, the phases of both approximations have about the same error. Second, as J is increased, the error in the phases increases (indicating some sort of cumulative effect), and at large J ($J \sim 9$), it can be as large as 1.5 radians. Third, the phases of the approximate S-matrix elements are always less than the exact phases.

As shown in the last section, probabilities are weighted by $2J+1$ in calculating cross sections. Figure 7 is a plot of $(2J+1) \times P^{R}_{J,000\rightarrow010}$ versus J at 0.60 eV. This figure more correctly emphasizes the differences between the PD and SD methods. From this we expect that the cross sections for individual $m_j = 0$ to $m'_{j'} = 0$ transitions will be too large by the SD method and too small (with a smaller absolute error) by the PD method.

Because there is no mixing between Ω_λ and Ω_ν in the SD method, probabilities and cross sections of reactive transitions between m_j and $m'_{j'}$, where $m_j \neq -m'_{j'}$, will vanish. However, in the PD method, there is mixing and nonzero probabilities exist for all transitions. Figure 8 illustrates a comparison of the fully coupled calculations with the PD calculation at E = 0.6 eV for the transition $P^{R}_{J,011\rightarrow000}$. Note that the PD method gives probabilities that are in error of up to two orders of magnitude. Equally important is that the transition probabilities are over an order of magnitude smaller than those for $m_j = m'_{j'} = 0$. This is what makes the decoupling approximation useful. Summed and averaged probabilities and cross sections will be dominated by the $m_j = m'_{j'} = 0$ transition. Because the decoupling methods give good results for that transition, the summed and averaged cross sections (which are the experimental observables) should be reasonably accurate. Figure 9 is a plot of the reactive transition probability $P^{R}_{J,011\rightarrow01-1}$ as a function of J. Although the error between the approximations and the full calculation is large (with SD giving better results), the fully coupled result is very small compared with the $m_j = m'_{j'} = 0$ transition. This transition is not expected to contribute strongly to the summed and averaged cross section.

Figure 10 is a plot of the summed and averaged 00→01 reactive transition probabilities at E = 0.60 eV. It shows that the SD probabilities are larger than the fully coupled results and that the PD results are smaller. This is the same ordering as in the 000→010 reactive transition (see Fig. 3). However, the error in the PD results has increased (to a maximum of 14%) while the error in the SD results decreased ~ 35% . This indicates that transitions other than $m_j = m'_{j'} = 0$ do not contribute strongly to a summed and averaged probability, but that they are not negligible.

Nonreactive transitions behave differently. Figure 11 is a plot of $P^N_{J,000\to020}$ versus J at 0.60 eV for all the three methods. The figure shows that the two approximations are in close agreement with each other over a wide range of J, but that both are in quite poor agreement with the fully coupled calculation. The figure also indicates that non-reactive transition probabilities are non-negligible over a wide range of J, which is different from reactive transitions. Figure 12 shows $P^N_{011\to01-1}$ at 0.60 eV. Previously, we found that the corresponding reactive transition probabilities (see Fig. 9) did not contribute strongly to the summed and averaged result. For nonreactive transitions, it is clear that $P^N_{J,011\to01-1}$ is as important as $P^N_{J,010\to010}$. Figure 13 shows that the summed and averaged probabilities $P^N_{J,00\to02}$ for the PD approximation agree very well with the fully coupled calculation, much better than the corresponding reactive transition $P^R_{00\to01}$ (see Fig. 10).

As discussed previously,[15] nonreactive collisions span a wider range of atom-molecule distances than do reactive collisions, which

increases the importance of kinematic coupling. A method which decouples the angular momentum terms will give individual, nonreactive results which are poorer than the reactive results. Nonreactive transition probabilities from $m_j = 0$ to $m_j' \neq 0$ are orders of magnitude too small in the PD approximation. This, plus the fact that the summed and averaged results agree quite well, indicates that in the approximations all flux is transferred from different m_j', to $m_j' = 0$ for the same j.

We now turn our attention to integral cross sections. First we will consider reactive and nonreactive (distinguishable atom) cross sections. Figure 14 is a plot of $Q^R_{000\rightarrow010}$ for all three methods and a plot of the relative error of the decoupling approximations with the exact calculation. It reflects the information in Figs. 1 and 3 in three ways. One, the PD method is significantly better than the SD method. Two, the cross sections agree remarkably well as Q changes by 14 orders of magnitude. Three, the error is largest at the lowest energy, 0.30 eV. In Fig. 15 one can see that the summed and averaged cross section $Q^R_{00\rightarrow01}$ is best reproduced by the PD method, although the error for the SD method is smaller than it was for $Q^R_{000\rightarrow010}$. Figures 16 and 17 show $Q^R_{000\rightarrow020}$ and $Q^R_{00\rightarrow02}$ (note, j = 2 is closed at E = 0.30 eV). For the individual transition, the PD results are clearly better, but the quality of the SD results is significantly improved (and the PD results worsened) by summing and averaging. In Fig. 17, neither approximation is significantly better. In short, the PD method gives significantly better reactive integral cross sections for individual transitions than does the SD method, but sometimes only slightly better when the cross sections are summed and averaged.

One can deduce from the nonreactive probability plots (see Figs. 11 and 12) that individual SD and PD nonreactive cross sections will agree quite poorly with the full calculation. However, summed and averaged nonreactive integral cross sections, $Q^{N}_{00\rightarrow02}$ (see Fig. 18), agree at least as well as the reactive cross sections of Figs. 15 and 17.

The reactive and nonreactive cross sections shown assume that the atoms are distinguishable, which they are not. The physical, or antisymmetrized, cross sections allow us to look at ortho-to-para, para-to-ortho, ortho-to-ortho, and para-to-para transitions. In Fig. 19 we have plotted summed and averaged integral cross sections for a para-to-ortho transition ($00 \rightarrow 01$) and for the para-to-para transition ($00 \rightarrow 02$). The top plot $Q^{A}_{00\rightarrow01}$ ($p \rightarrow o$) shows nothing new because it is equal to $3 \times Q^{R}_{00\rightarrow01}$. Because $Q^{N}_{00\rightarrow02}$ is much larger than $Q^{R}_{00\rightarrow02}$, $Q^{A}_{00\rightarrow02}$ ($o \rightarrow o$) (the bottom plot) looks very similar to Fig. 18. Figure 20 is a plot of an ortho-to-para transition, $Q^{A}_{01\rightarrow00}$, and an ortho-to-ortho transition, $Q^{A}_{01\rightarrow03}$. The first one is exactly equal to $Q^{R}_{01\rightarrow00}$ and gives no new information. The second one, $Q^{A}_{01\rightarrow03}$, is strongly dominated by the nonreactive S-matrix elements. At 0.60 eV, the error is large ($\sim 30\%$) compared with the quality of the rest of the calculations.

In the remainder of this section we will consider differential cross sections (DCS), in particular, $j = 0$ to $j' = 1$ and $j = 0$ to $j' = 2$ at $E = 0.60$ eV. Because para-to-ortho and ortho-to-para transitions are proportional to the corresponding reactive cross sections, we will look only at the antisymmetrized $j = 0$ to $j' = 1$ transition.

In Fig. 21 we compare the PD and SD methods with the fully coupled calculation for the individual differential cross section

$\sigma^{A}_{000\rightarrow010}(\theta_R)$. ($\theta_R$ is defined as the angle between the velocity vector of the product molecule and the velocity vector of the incident atom.) Near $\theta_R = 180°$, the error between the PD cross section and the fully coupled cross section is large ($\sim 25\%$). At angles below $\theta_R = 135°$, the agreement is much better. The SD calculation gives better results near $\theta_R = 180°$, but below $\theta_R = 150°$ the PD results are superior.

In calculating integral cross sections from differential cross sections, $\sigma(\theta_R)$ is weighted by $\sin\theta_R$. Figure 22 is a plot of $\sigma^{A}_{000\rightarrow010} \times \sin\theta_R$ and illustrates that even if the SD results are better than the PD results at $\theta_R \sim 180°$, the PD method will produce better integral cross sections. A comparison of Fig. 23 [$\sigma^{A}_{00\rightarrow01}(\theta_R)$] with Fig. 21 reveals that the SD error is smaller after summing and averaging, whereas the PD error is slightly larger. However, weighting by $\sin\theta_R$ (Fig. 24) shows that the PD results are still better.

In Fig. 25 we have plotted the reactive differential cross section $\sigma^{R}_{000\rightarrow020}(\theta_R)$ at 0.60 eV. One can see that both the SD and PD cross sections are in poor agreement with the fully coupled cross sections. The summed and averaged results (Fig. 26) are no improvement. In fact, Fig. 27 shows that the SD results are better than the PD results when weighted by $\sin\theta_R$. This is a reflection of Fig. 17, where we saw that $Q^{R}_{00\rightarrow02}$ (SD) was significantly better than $Q^{R}_{00\rightarrow02}$ (PD) at 0.60 eV.

However, these large errors are irrelevant for observable cross sections because the antisymmetrized results are completely dominated by the nonreactive portion. Figure 28 shows a DCS for the same individual transition at 0.60 eV. As expected from probability plots, there is no agreement between the PD method and the fully coupled calculation.

Even the shape of the DCS is not preserved, as it was for reactive transitions. However, Fig. 29 shows that the two methods agree well throughout the entire 0-π range of θ for $\sigma^{N}_{00\to02}$.

As mentioned before, other workers[9,10] have studied nonreactive systems using an angular momentum decoupling method. As outlined in the Appendix, the central idea is to replace the L^2 operator by the eigenvalue $\bar{\ell}(\bar{\ell}+1)\hbar^2$, thus neglecting diagonal terms (which we have included). In their original paper,[9] McGuire and Kouri identified $\bar{\ell}$ with the final orbital angular momentum ℓ, while Pack[10] set $\bar{\ell}=J$. Since then, Kouri and McGuire[16,17] have used $\bar{\ell}=J$ and $\bar{\ell}=J-j$. These calculations were less successful than the original choice of $\bar{\ell}=\ell$, and recently several papers[18-24] have appeared that support the original[9] choice for $\bar{\ell}$. In each of these, theoretical or computational arguments are made for the best choice of $\bar{\ell}$. There are no arguments given for neglecting other diagonal contributions to L^2.

The nonreactive systems that were studied by this method included He + H_2 and He + HCℓ. The elastic scattering integral cross sections differed from exact close coupling results by less than 1% and inelastic (low j) cross sections by less than 4%.[9] These results are a little more accurate than the results presented in this paper. The major difference in quality between the two sets of results is in the DCS. As shown in Ref. 9, there is perfect agreement between the decoupled results and the exact results for $\theta > 150°$, and the agreement becomes better at lower angles as the energy is increased. This is in contrast to the results in Fig. 29, which show that the agreement is generally good at all angles but never perfect for any finite range of θ. This difference is

either caused by the atom-diatom interaction or the decoupling methods. Because the number of partial waves necessary to describe nonreactive scattering is about the same for $H + H_2$ and $He + H_2$,[22] the difference may lie with the decoupling methods. Future work must determine which method is more appropriate for reactive scattering.

V. Summary

Exact quantum mechanical solutions to atom-molecule scattering problems can require substantial computation times. We found that the major reason was the large number of coupled equations to be solved. If some of the states could be uncoupled from each other, the number of equations to be solved simultaneously (and the computation time required to solve them) would be reduced. When the Schrödinger equation is written in the coupled equation form, it is apparent that the potential matrix is diagonal in the tumbling quantum number, Ω. This, and the weakness of centrifugal coupling, led to an angular momentum decoupling approximation in which terms in the Hamiltonian that coupled states of different Ω were neglected. This approximation, which has been used successfully in nonreactive scattering, has been applied in this paper to reactive scattering.

Two slightly different decoupling schemes, called proper decoupling and simple decoupling, have been presented. They differ, not in the integration of the Schrödinger equation, but in the matching procedure. One method (PD) allows mixing between states of different Ω and in different arrangement channels, whereas the other (SD) does not.

It was shown in II that for atom-diatom systems which preferentially react in the collinear orientation (of which $H + H_2$ is an example) there is a quasi-selection rule; $m_j = m'_{j'} = 0$ reactive transition probabilities are much larger than other reactive probabilities. Because Ω-coupling has been neglected (except between arrangement channels) by both decoupling approximations, one expects $m_j = m'_{j'} = 0$ reactive transition probabilities to also be dominant. These two facts together

insure that the decoupled $P^{R}_{J,vj0\to v'j'0}$ will agree closely with the corresponding exact result. For all transitions the PD results are in error by less than 7% and the SD results by as much as 60%, which indicates the importance of Ω-mixing between different arrangement channels. Nearly all of the PD probabilities were smaller than the corresponding exact ones, and nearly all of the SD results were larger. For other reactive transitions, both the SD and PD results were in error by as much as several orders of magnitude.

The integral cross sections corresponding to the above probabilities showed similar trends. While the cross section $Q^{R}_{vj0\to v'j'0}$ changed 14 orders of magnitude, the PD results agreed with the exact to better than 10%, except at low energies. The SD results, while preserving the shape of the cross section curve, were in error of up to 60%. For $j \to j + 1$ transitions, the summed and averaged results had about the same accuracy. For $j \to j + 2$ transitions, which are dominated by nonreactive contributions in calculating the antisymmetrized (or physical) cross section, the summed and averaged PD and SD results were in error by about 20%. Reactive differential cross sections were similar in that $j \to j + 1$ ($m_j = m'_{j'} = 0$) transitions were best reproduced by the PD method.

We found that all individual nonreactive transition probabilities were poorly reproduced by either approximation. This is not surprising, because nonreactive collisions involve orientations besides the collinear one. However, summed and averaged probabilities agreed well, with errors less than 3%. Because nonreactive $j \to j + 2$ cross sections are much larger than the corresponding reactive ones, the antisymmetrized

cross sections are almost identical to the nonreactive cross sections. We found that at most energies the summed and averaged nonreactive (or antisymmetrized) integral PD cross sections agreed with the exact ones to better than 10%. The corresponding DCS had the correct shape and had a maximum error of 10%.

The computation times for the two decoupling methods are identical, and the savings over the exact method can be as high as a factor of 20.

Appendix

In this Appendix we will examine the differences between the fully coupled and several decoupled formalisms. In arrangement channel λ, the Hamiltonian operator may be written

$$H(\underset{\sim}{R}_\lambda, \underset{\sim}{r}_\lambda) = \frac{-\hbar^2}{2\mu} \frac{1}{R_\lambda} \frac{\partial^2}{\partial R_\lambda^2} R_\lambda + \frac{L^2_{R_\lambda}}{2\mu R_\lambda^2} + h_\lambda(r_\lambda) + \Delta V(R_\lambda, r_\lambda, \gamma_\lambda),$$

where

$$h_\lambda(r_\lambda) = \frac{-\hbar^2}{2\mu} \frac{1}{r_\lambda} \frac{\partial^2}{\partial r_\lambda^2} r_\lambda + \frac{L^2_{r_\lambda}}{2\mu r_\lambda^2} + v_\lambda(r_\lambda) ,$$

$$v_\lambda(r_\lambda) = \lim_{R_\lambda \to \infty} V_\lambda(R_\lambda, r_\lambda, \gamma_\lambda),$$

and

$$\Delta V(R_\lambda, r_\lambda, \gamma_\lambda) = V_\lambda(R_\lambda, r_\lambda, \gamma_\lambda) - v_\lambda(r_\lambda).$$

In the decoupling formalism, the only term that will be changed will be $(L^2_{R_\lambda}/2\mu R_\lambda^2)$. In terms of other operators, $L^2_{R_\lambda}$ may be written as

$$L^2_{R_\lambda} = J^2 + L^2_{r_\lambda} - 2J_z^2 - (L^-_{r_\lambda} - \hbar \cot\gamma_\lambda) J_\lambda^+ - (L^-_{r_\lambda} + \hbar \cot\gamma_\lambda) J_\lambda^- ,$$

where

$$J^2 = \hbar^2 \left[\frac{-\partial^2}{\partial\theta_\lambda^2} - \cot\theta_\lambda \frac{\partial}{\partial\theta_\lambda} - \frac{1}{\sin^2\theta_\lambda} \left(\frac{\partial^2}{\partial\phi_\lambda^2} + \frac{\partial^2}{\partial\psi_\lambda^2} \right) + \frac{2\cos\theta_\lambda}{\sin^2\theta_\lambda} \frac{\partial^2}{\partial\phi_\lambda \partial\psi_\lambda} \right] ,$$

$$L^2_{r_\lambda} = -\hbar^2 \left[\frac{1}{\sin^2\gamma_\lambda} \frac{\partial^2}{\partial\psi_\lambda^2} + \frac{1}{\sin\gamma_\lambda} \frac{\partial}{\partial\gamma_\lambda} \left(\sin\gamma_\lambda \frac{\partial}{\partial\gamma_\lambda} \right) \right] ,$$

and

$$J_{Z_\lambda}^2 = -\hbar^2 \frac{\partial^2}{\partial \psi_\lambda^2} \quad .$$

The last two terms of $L_{R_\lambda}^2$ contain all of the Ω-coupling information. The approximation we have used is to neglect the last two terms. That is, our approximation may be written

$$L_{R_\lambda}^2 = J^2 + L_{r_\lambda}^2 - 2J_Z^2 \quad .$$

The approximation used by Pack is simply $L_{R_\lambda}^2 = J^2$. The approximation used by McGuire and Kouri is only a part of the J^2 operator,

$$L_{R_\lambda}^2 = -\hbar^2 \left[\frac{\partial^2}{\partial \theta_\lambda^2} + \cot \theta_\lambda \frac{\partial}{\partial \theta_\lambda} + \frac{1}{\sin^2 \theta_\lambda} \frac{\partial^2}{\partial \phi_\lambda^2} \right] \quad .$$

TABLE I.

J	N[a]	Integration Times (IBM 370/158)		
		Full Calculation[b, c]	Proper and Simple Decoupling	Potential Times
0	40	11	11	11
1	90	42	13	9
2	88	37	8	3.7
3	92	36	7	2.4
4	100	47	8	2.4

[a] N is the number of total channels for a given partial wave, J.

[b] These numbers are taken from II.

[c] The computation times are in minutes.

References

1. A. Kuppermann and G. C. Schatz, J. Chem. Phys. 62, 2502 (1975).
2. G. C. Schatz and A. Kuppermann, J. Chem. Phys. 65, 4642 (1976).
3. G. C. Schatz and A. Kuppermann, J. Chem. Phys. 65, 4668 (1976).
4. A. B. Elkowitz and R. E. Wyatt, J. Chem. Phys. 62, 2504 (1975).
5. A. B. Elkowitz and R. E. Wyatt, J. Chem. Phys. 63, 702 (1975).
6. R. N. Porter and M. Karplus, J. Chem. Phys. 40, 1105 (1964).
7. L. M. Delves, Nucl. Phys. 9, 391 (1959); ibid. 20, 275 (1960).
8. D. Jepsen and J. O. Hirschfelder, Proc. Natl. Acad. Sci. USA 45, 249 (1959).
9. P. McGuire and D. J. Kouri, J. Chem. Phys. 60, 2488 (1974).
10. R. T Pack, J. Chem. Phys. 60, 633 (1974).
11. R. B. Walker and J. C. Light, Chem. Phys. 7, 84 (1975).
12. A. B. Elkowitz and R. E. Wyatt, Mol. Phys. 31, 189 (1976).
13. v is the vibrational quantum number, j is the rotational quantum number and m_j is the tumbling quantum number. The final $m'_{j'} = \Omega_{j'}$, but the initial $m_j = -\Omega_j$.
14. A. S. Davydov, Quantum Mechanics, translated by I. Schensted (NEO Press, Ann Arbor, Michigan, 1966), Chap. 6.
15. A. Kuppermann, G. C. Schatz, and J. P. Dwyer, Chem. Phys. Lett. 45, 71 (1977).
16. D. J. Kouri and P. McGuire, Chem. Phys. Lett. 29, 414 (1974).

17. P. McGuire, Chem. Phys. 13, 81 (1976).

18. Y. Shimoni and D. J. Kouri, J. Chem. Phys. 65, 3372 (1976).

19. R. Goldflam and D. J. Kouri, J. Chem. Phys. 66, 542 (1977).

20. S. Green, L. Monchick, R. Goldflam, and D. J. Kouri, J. Chem. Phys. 66, 1409 (1977).

21. R. T Pack, J. Chem. Phys. 66, 1557 (1977).

22. Y. Shimoni and D. J. Kouri, J. Chem. Phys. 66, 2841 (1977).

23. G. A. Parker and R. T Pack, J. Chem. Phys. 66, 2850 (1977).

24. L. Monchick and S. Green, J. Chem. Phys. 66, 3085 (1977).

Figure Captions

FIG. 1. $P^R_{2,\,000\to010}$ versus total energy E (in eV). The solid line represents results of the fully coupled calculation (from paper II), the open triangles are results of the SD method, the open squares are results of the PD method, and the darkened squares are overlapping results of the PD and SD methods.

FIG. 2. The upper graph is a plot of the phases $\phi^R_{2,\,000\to010}$ (in radians) of the reactive S-matrix element $S^R_{2,\,000\to010}$ (the same transition as in Fig. 1) as a function of total energy. Designations are the same as in Fig. 1. The lower graph is a plot of the absolute error (versus E) of the PD and SD phases with the exact phase. SD results are denoted by (-·Δ-·) and PD results by (--□--).

FIG. 3. $P^R_{J,\,000\to010}$ versus total angular momentum J for all three methods at two energies, 0.60 and 0.50 eV. The fully coupled results are denoted by (——○——). The other designations are identical to Fig. 2.

FIG. 4. $P^R_{J,\,010\to020}$ versus J at 0.60 eV for all three methods. The designations in this figure and all following figures are identical to those in Fig. 3.

FIG. 5. The phases of the S-matrix elements versus J for the transitions in Figs. 3 and 4. The PD and SD results are denoted by (--□--).

FIG. 6. The error between the approximate and exact phases plotted in Fig. 5.

FIG. 7. $(2J+1) \times P^R_{J,\,000\to010}$ as a function of J for the three methods at E = 0.60 eV.

FIG. 8. $P^{R}_{J,\,011\rightarrow000}$ versus J for the PD method and the fully coupled method at E = 0.60 eV.

FIG. 9. $P^{R}_{J,\,011\rightarrow01\text{-}1}$ versus all three methods at E = 0.60 eV.

FIG. 10. The summed and averaged $P^{R}_{J,\,00\rightarrow01}$ versus J at E = 0.60 eV for all three methods.

FIG. 11. $P^{N}_{J,\,000\rightarrow020}$ versus J at E = 0.60 eV for all three methods.

FIG. 12. $P^{N}_{J,\,011\rightarrow01\text{-}1}$ versus J at E = 0.60 eV for all three methods.

FIG. 13. $P^{N}_{J,\,00\rightarrow02}$ versus J at E = 0.60 eV for the PD and fully coupled methods.

FIG. 14. The upper graph is a plot of the reactive integral cross section (in bohr^2) $Q^{R}_{000\rightarrow010}$ versus E (in eV) for all three methods. The lower graph is a plot of the relative error between each approximation and the exact calculation.

FIG. 15. The upper graph is a plot of $Q^{R}_{00\rightarrow01}$ versus E for all three methods. The lower graph is a plot of the relative errors in the approximations.

FIG. 16. The upper graph is a plot of $Q^{R}_{000\rightarrow020}$ versus E for all three methods. The lower graph is a plot of the relative errors in the approximations.

FIG. 17. The upper graph is a plot of $Q^{R}_{00\rightarrow02}$ versus E for all three methods. The lower graph is a plot of the relative errors of the approximations.

FIG. 18. The upper graph is a plot of $Q^{N}_{00\rightarrow02}$ versus E for the PD and

exact methods. The relative error of the PD method is in the lower graph.

FIG. 19. The upper graph is a plot of a para-to-ortho integral cross section, $Q^{A}_{00\rightarrow01}$ versus E for all three methods. The lower graph is a plot of a para-to-para integral cross section $Q^{A}_{00\rightarrow02}$ versus E for the PD and exact methods.

FIG. 20. The upper graph is a plot of an ortho-to-para integral cross section $Q^{A}_{01\rightarrow00}$ versus E for all three methods. The lower graph is a plot of an ortho-to-ortho integral cross section $Q^{A}_{01\rightarrow03}$ versus E for the PD and exact methods.

FIG. 21. The differential cross section $\sigma^{A}_{000\rightarrow010}$ (in bohr^2/sterad) at 0.60 eV as a function of reactive scattering angle θ_R (in degrees) for all three methods.

FIG. 22. $\sigma^{A}_{000\rightarrow010} \times \sin\theta_R$ versus θ_R at 0.60 eV for all three methods.

FIG. 23. $\sigma^{A}_{00\rightarrow01}$ versus θ_R at 0.60 eV for all three methods.

FIG. 24. $\sigma^{A}_{00\rightarrow01} \sin\theta_R$ versus θ_R at 0.60 eV for all three methods.

FIG. 25. $\sigma^{R}_{000\rightarrow020}$ versus θ_R at 0.60 eV for all three methods.

FIG. 26. $\sigma^{R}_{00\rightarrow02}$ versus θ_R at 0.60 eV for all three methods.

FIG. 27. $\sigma^{R}_{00\rightarrow02} \sin\theta_R$ versus θ_R at 0.60 eV for all three methods.

FIG. 28. $\sigma^{N}_{000\rightarrow020}$ versus θ at 0.60 eV for the PD and exact methods.

FIG. 29. $\sigma^{N}_{00\rightarrow02}$ versus θ at 0.60 eV for the PD and exact methods.

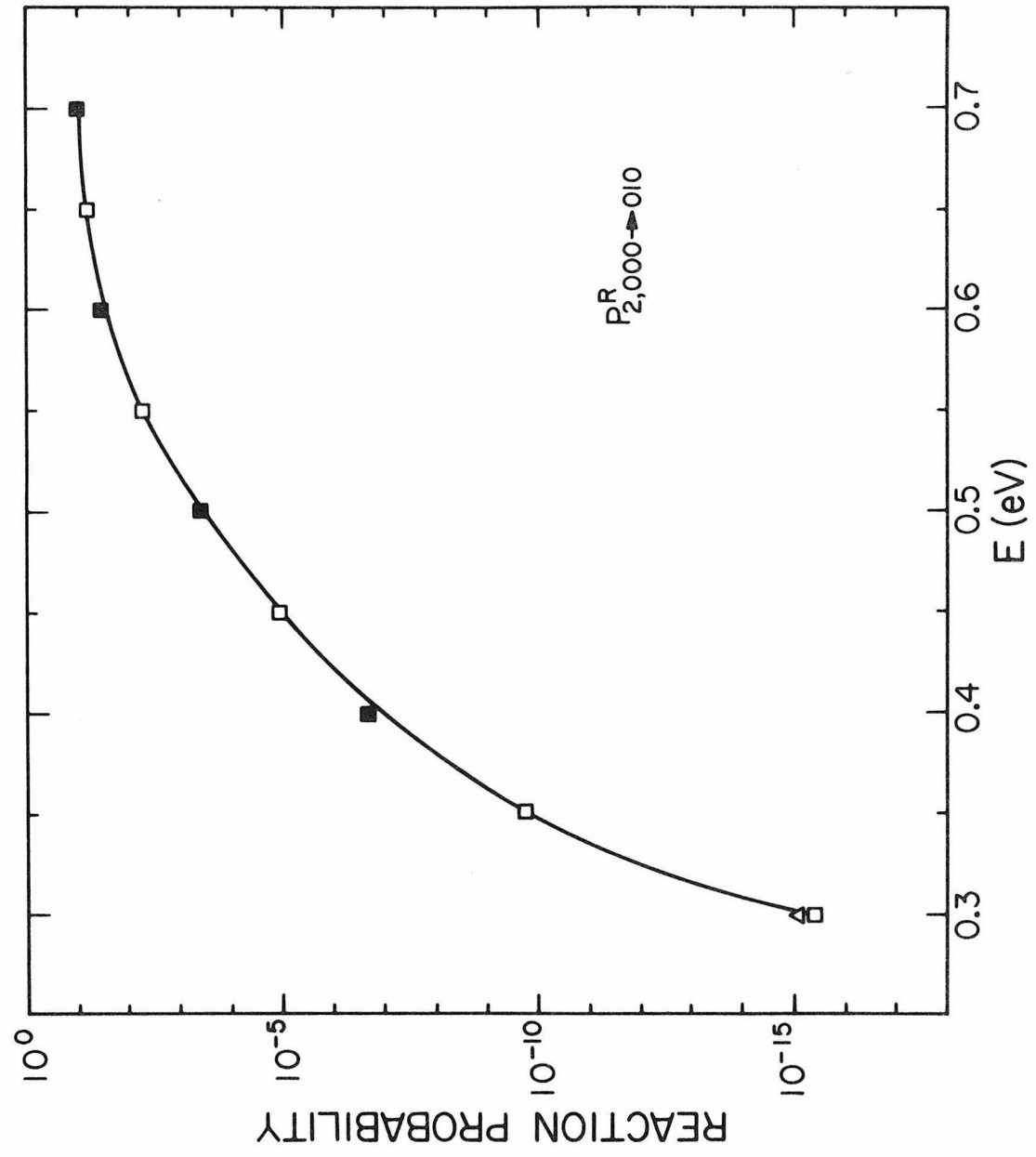
REACTION PROBABILITY
10^{0}
10^{-5}
10^{-10}
10^{-15}
$P^{R}_{2,000\rightarrow 010}$
0.3
0.4
0.5
0.6
0.7
E (eV)

Fig. 1.

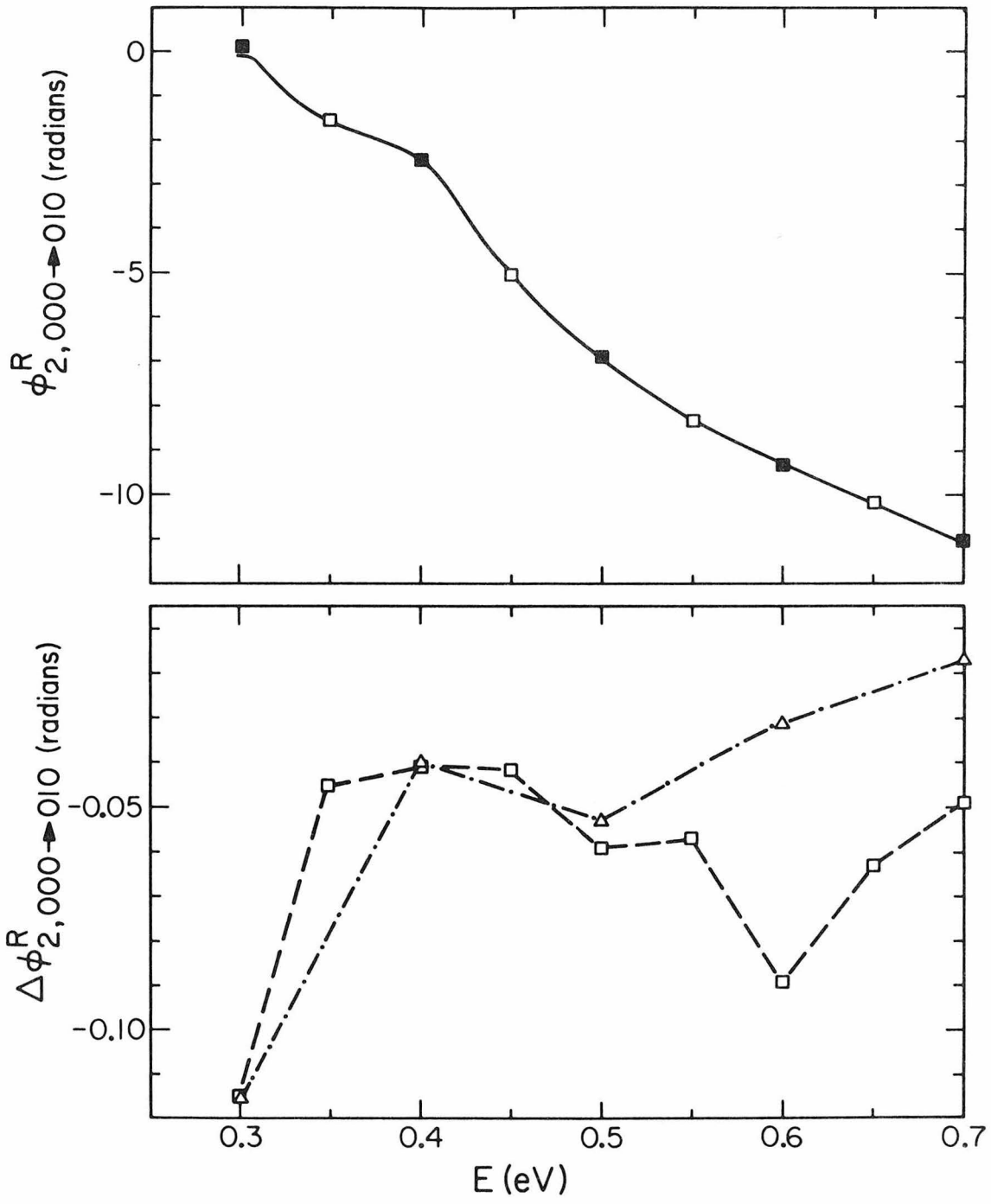
0
-5
-10
$\phi^R_{2,000\rightarrow 010}$ (radians)
-0.05
-0.10
$\Delta\phi^R_{2,000\rightarrow 010}$ (radians)
0.3
0.4
0.5
0.6
0.7
E (eV)

Fig. 2.

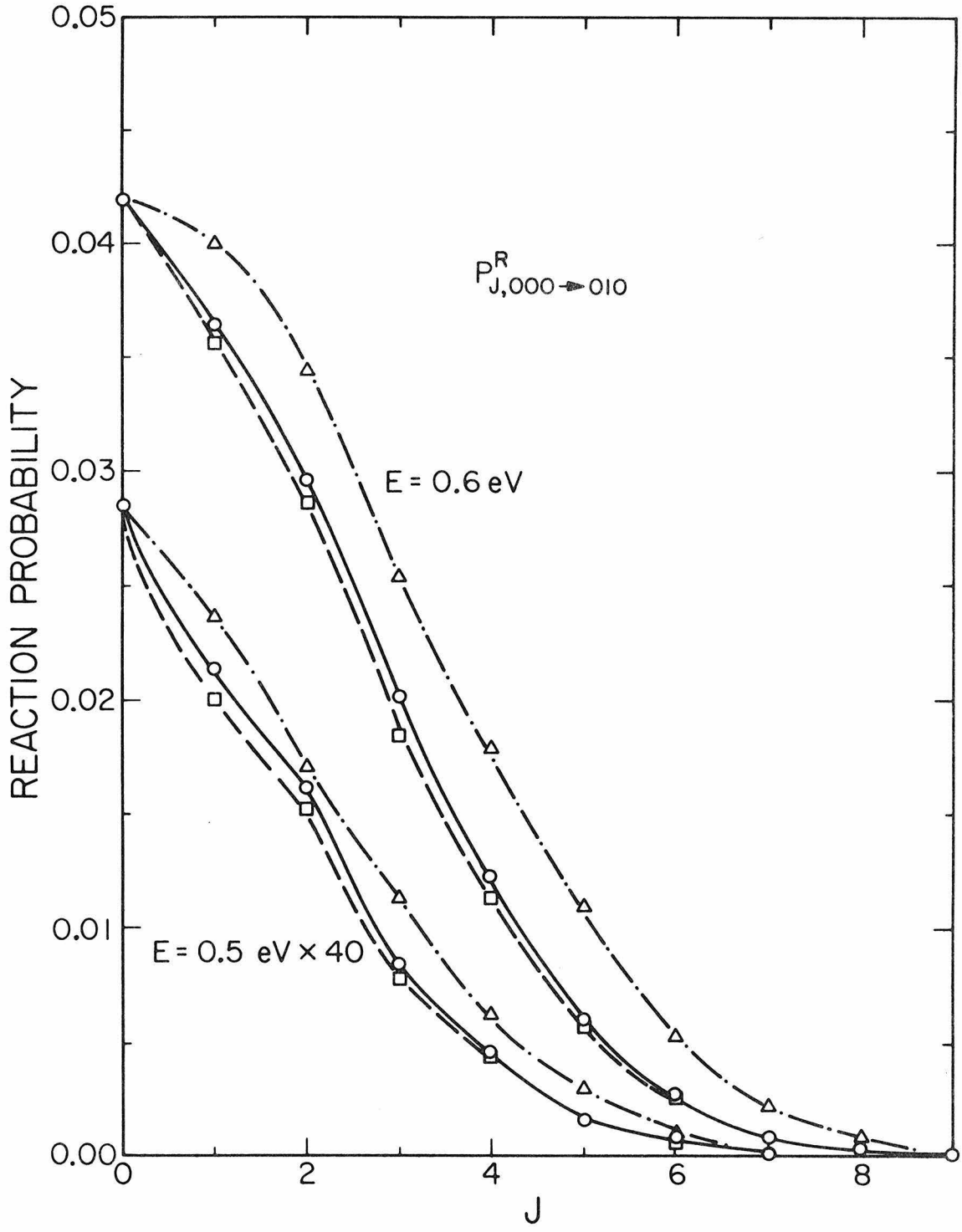
0.05
0.04
0.03
0.02
0.01
0.00
REACTION PROBABILITY
$P^R_{J,000\rightarrow 010}$
E = 0.6 eV
E = 0.5 eV × 40
0
2
4
6
8
J

Fig. 3.

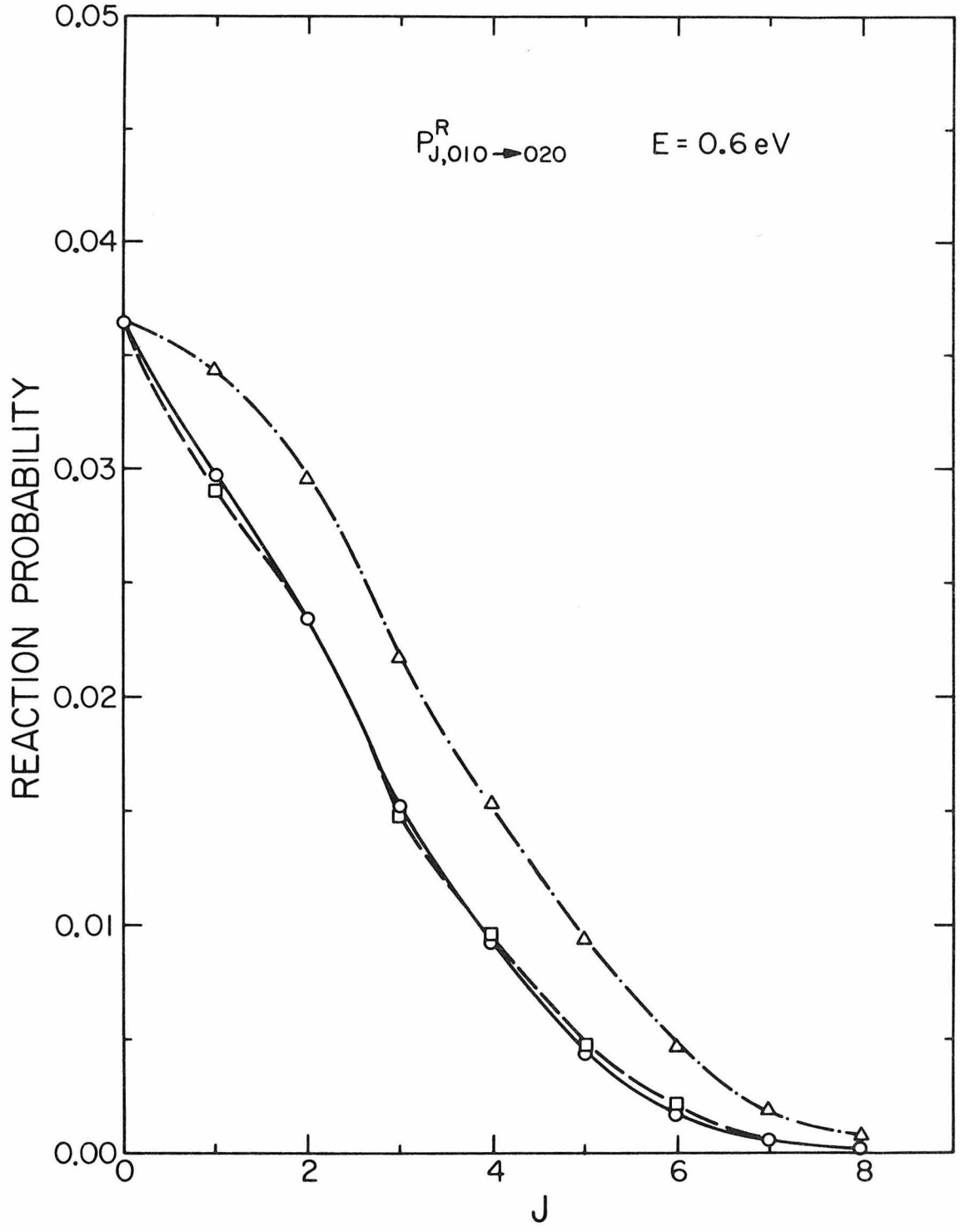
0.05
0.04
0.03
0.02
0.01
0.00
REACTION PROBABILITY
$P^R_{J,010\rightarrow020}$
E = 0.6 eV
0
2
4
6
8
J

Fig. 4.

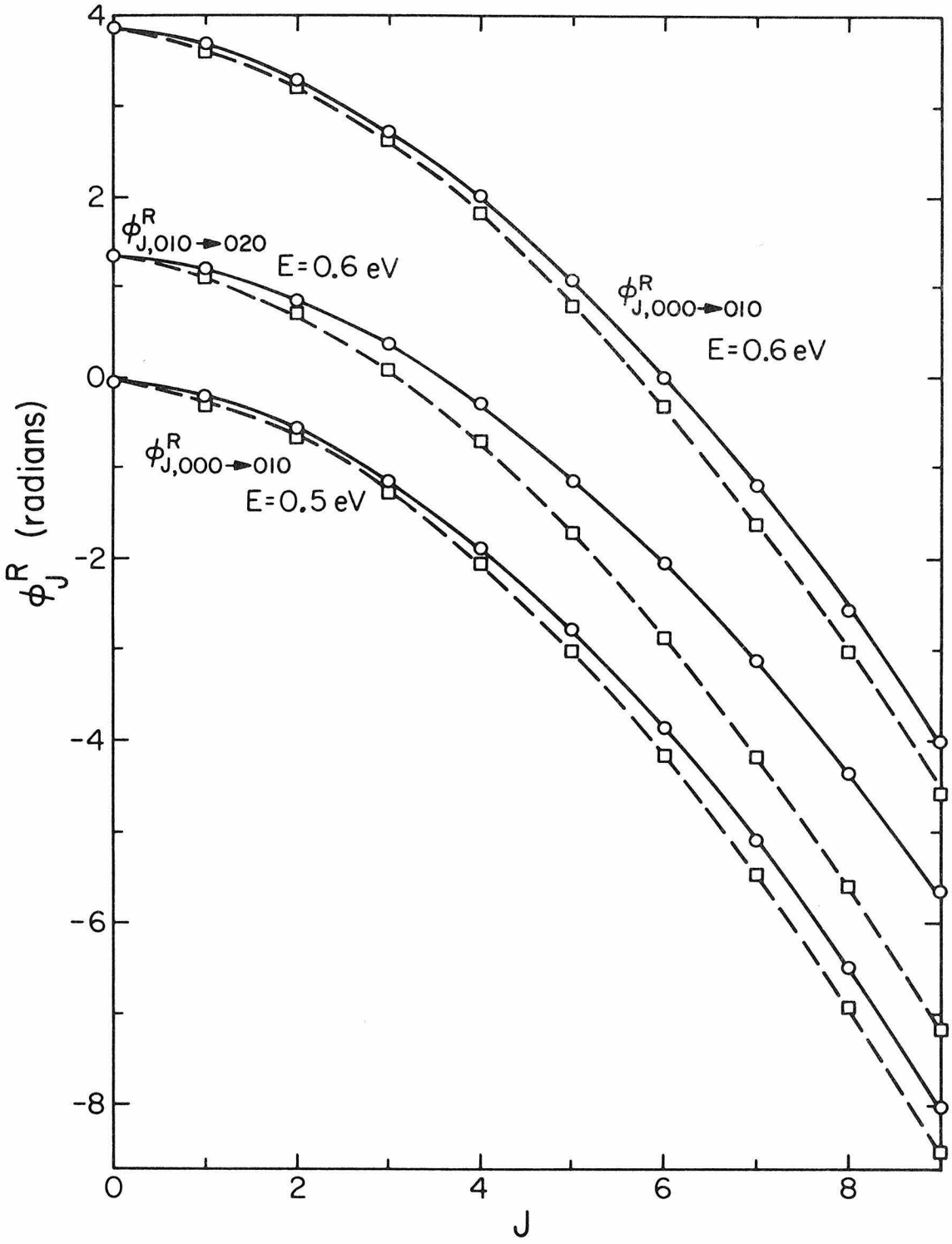
4
2
0
-2
-4
-6
-8
0
2
4
6
8
J
ϕ_J^R (radians)
$\phi^R_{J,010\to020}$
E=0.6 eV
$\phi^R_{J,000\to010}$
E=0.6 eV
$\phi^R_{J,000\to010}$
E=0.5 eV

Fig. 5.

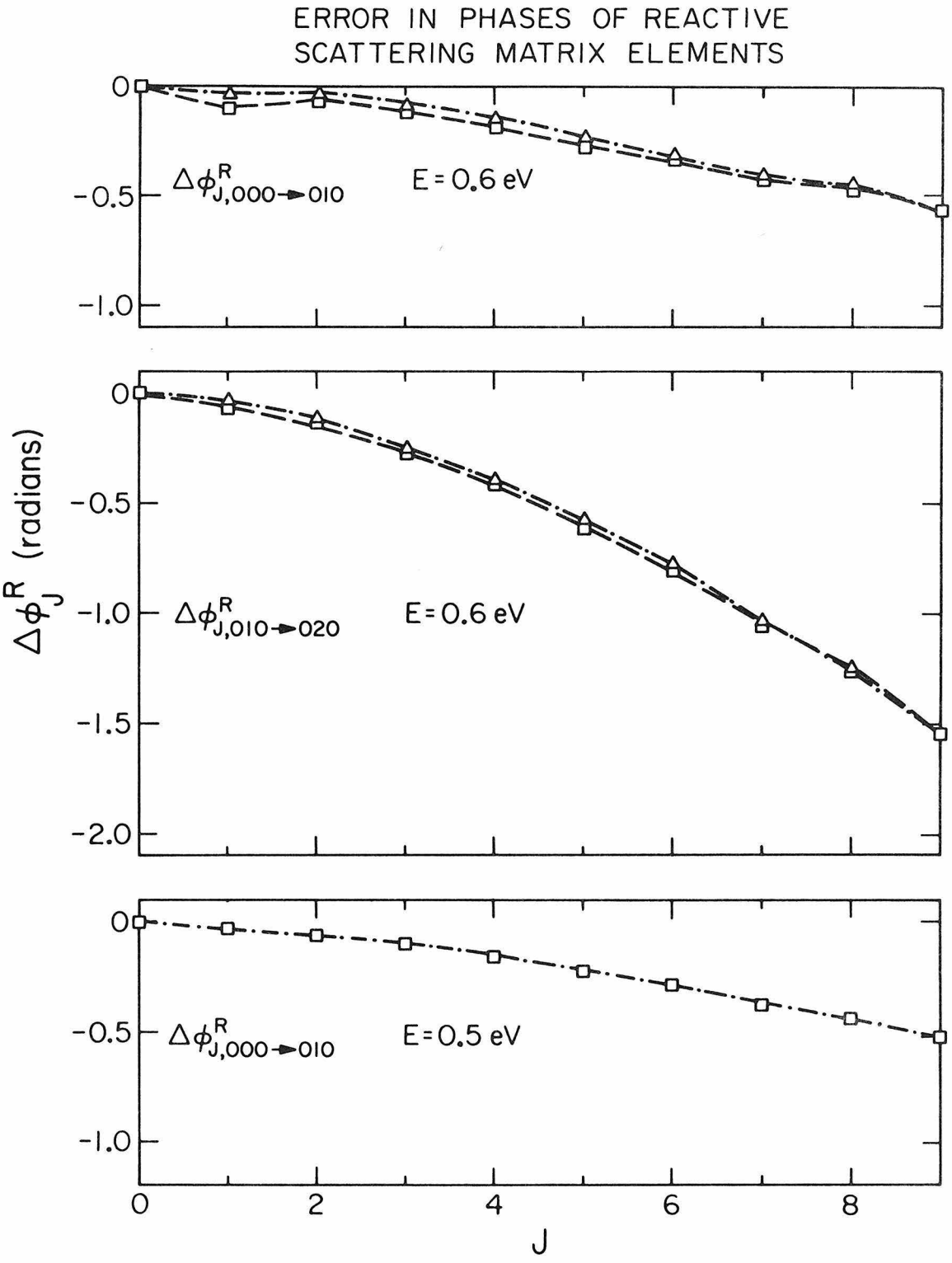
ERROR IN PHASES OF REACTIVE
SCATTERING MATRIX ELEMENTS
$\Delta\phi^R_{J,000\to010}$
E = 0.6 eV
$\Delta\phi^R_{J,010\to020}$
E = 0.6 eV
$\Delta\phi^R_{J,000\to010}$
E = 0.5 eV
$\Delta\phi^R_J$ (radians)
J
0
-0.5
-1.0
-1.5
-2.0
2
4
6
8

Fig. 6.

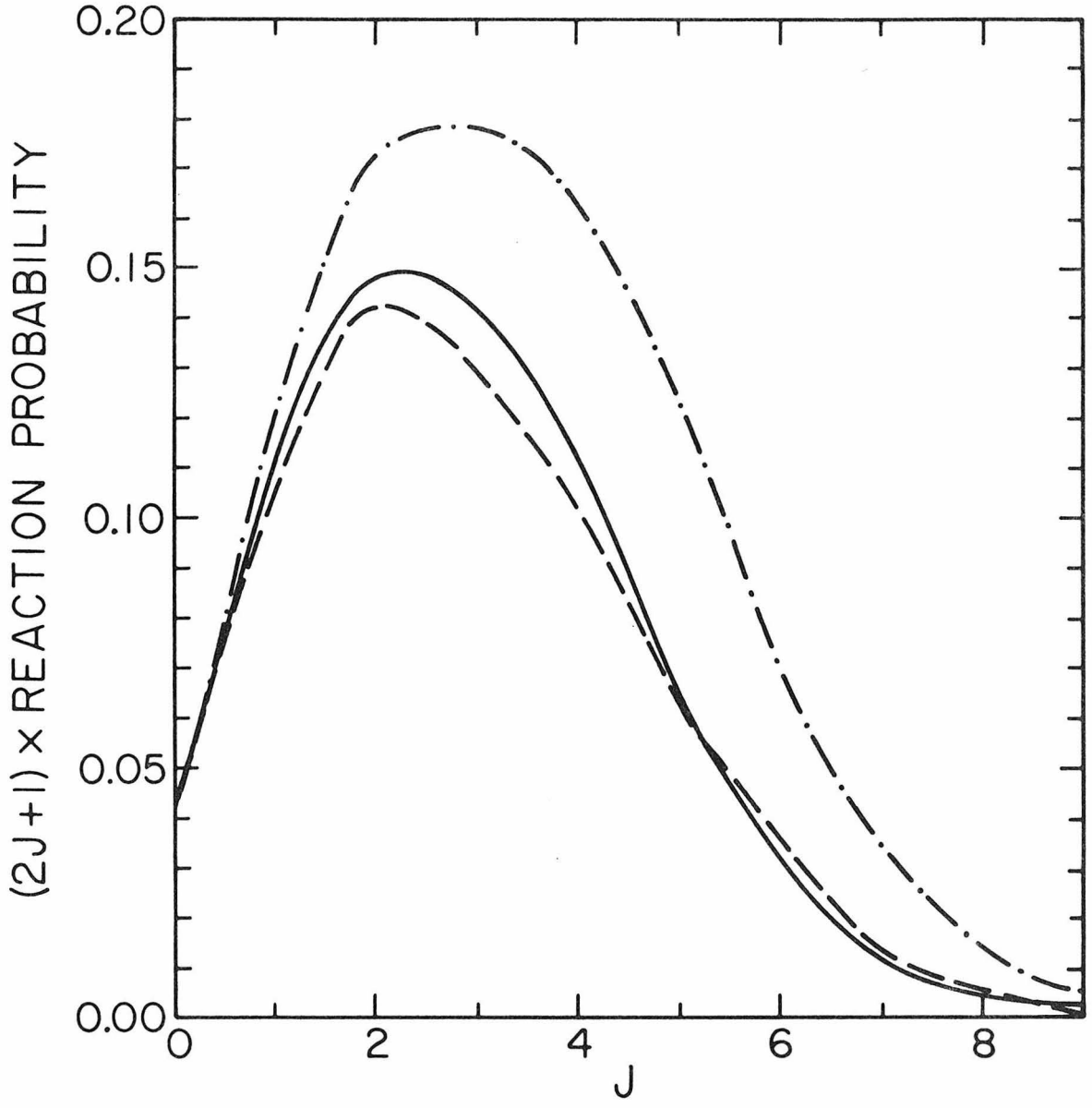

Fig. 7.

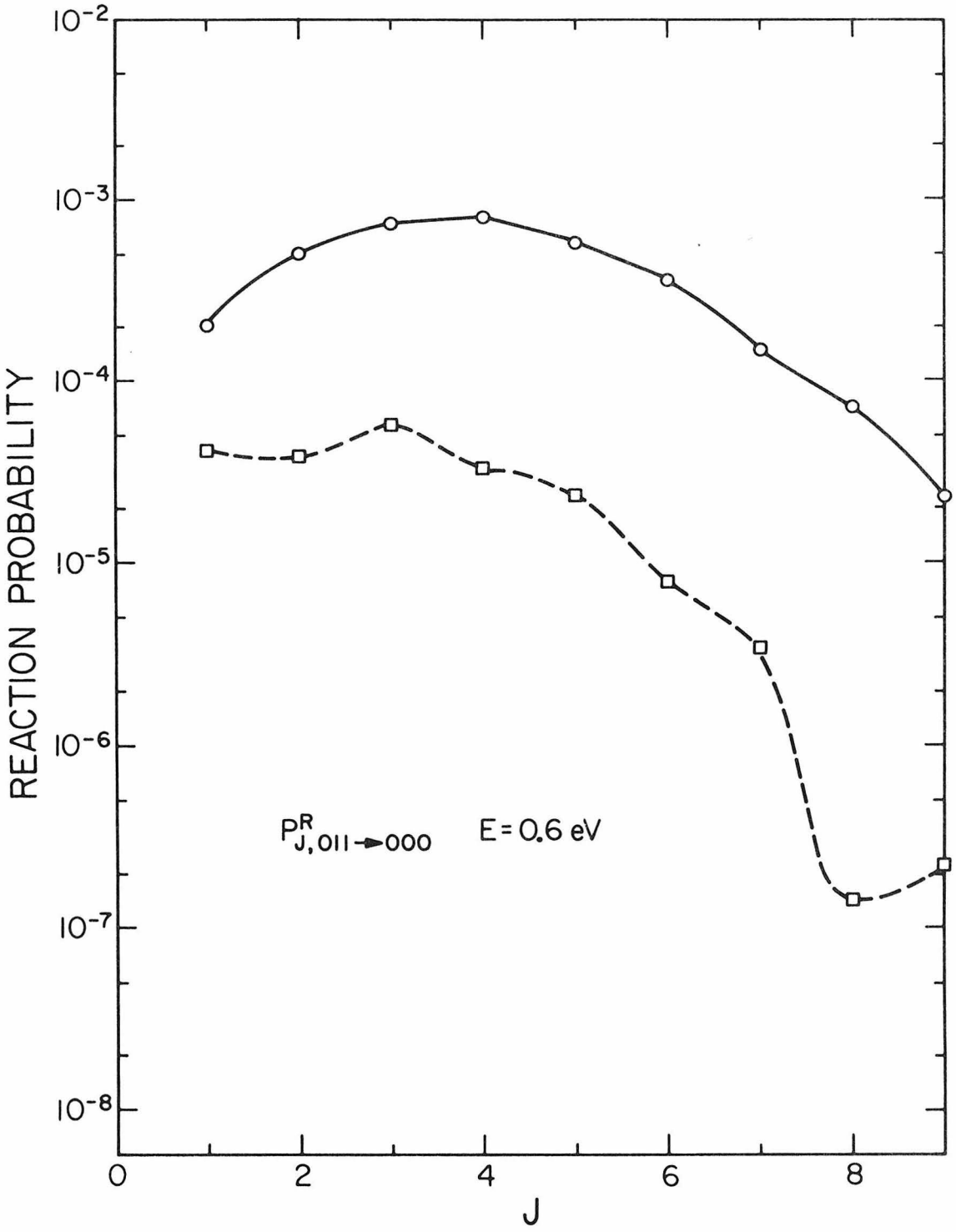
REACTION PROBABILITY
10^{-2}
10^{-3}
10^{-4}
10^{-5}
10^{-6}
10^{-7}
10^{-8}
$P^{R}_{J,011\rightarrow000}$
E = 0.6 eV
0
2
4
6
8
J

Fig. 8.

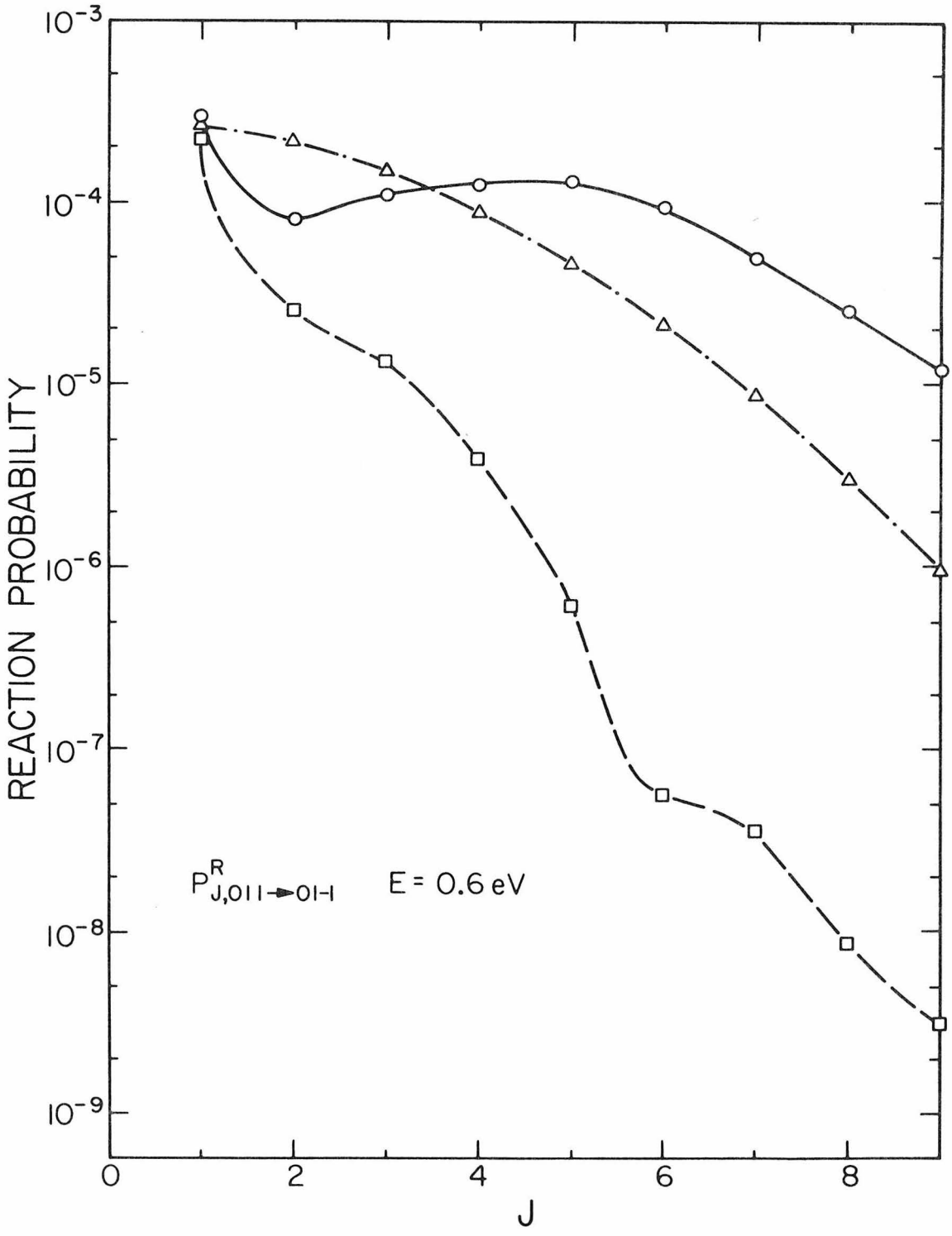
REACTION PROBABILITY
10^{-3}
10^{-4}
10^{-5}
10^{-6}
10^{-7}
10^{-8}
10^{-9}
$P^{R}_{J,011\rightarrow 01\text{-}1}$
E = 0.6 eV
0
2
4
6
8
J

Fig. 9.

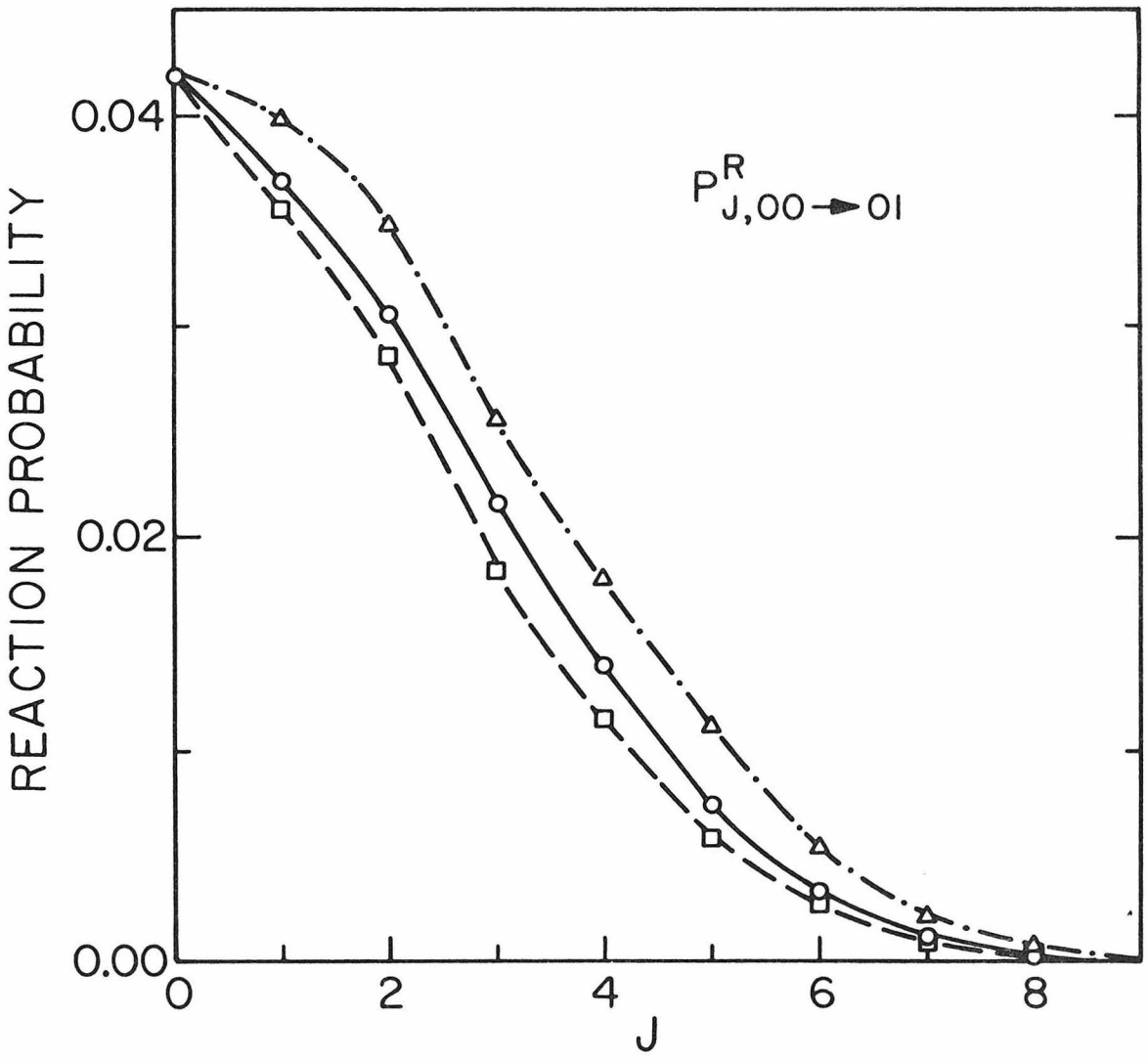
REACTION PROBABILITY
0.04
0.02
0.00
0
2
4
6
8
J
$P^R_{J,00\rightarrow 01}$

Fig. 10.

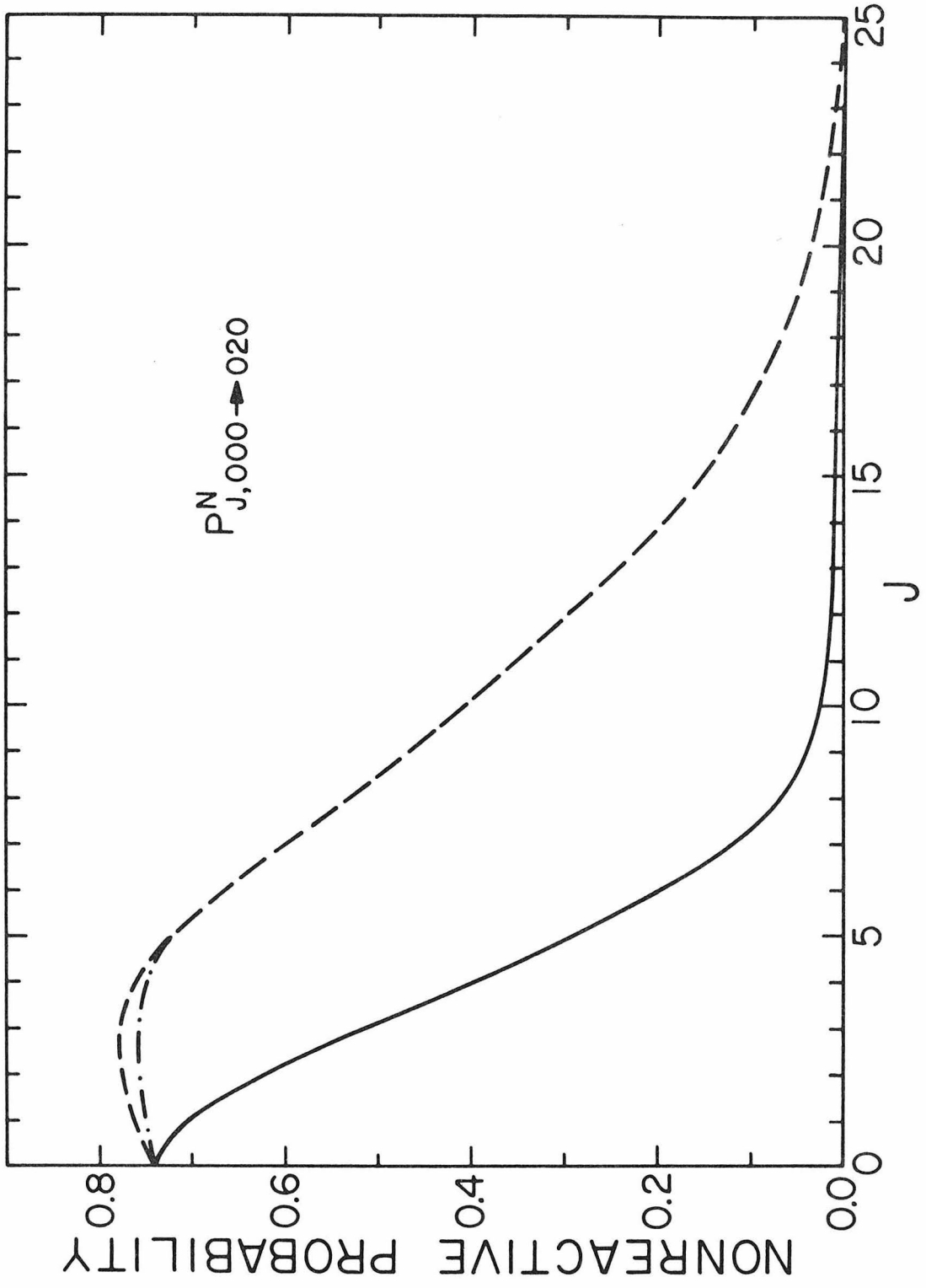
NONREACTIVE PROBABILITY
0.0
0.2
0.4
0.6
0.8
0
5
10
15
20
25
J
$P^N_{J,000\to020}$

Fig. 11.

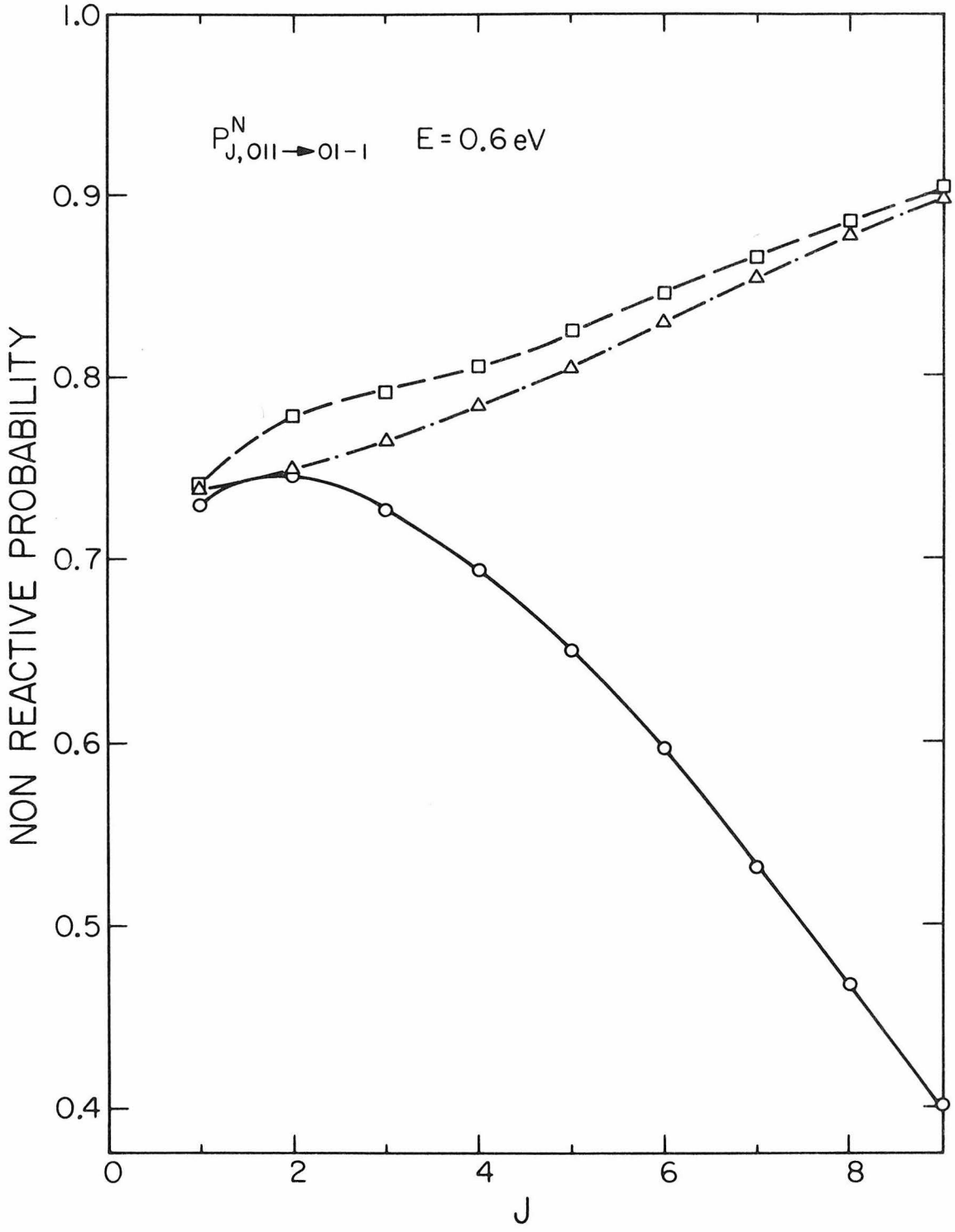
1.0
0.9
0.8
0.7
0.6
0.5
0.4
NON REACTIVE PROBABILITY
$P^N_{J,011 \rightarrow 01-1}$
E = 0.6 eV
0
2
4
6
8
J

Fig. 12.

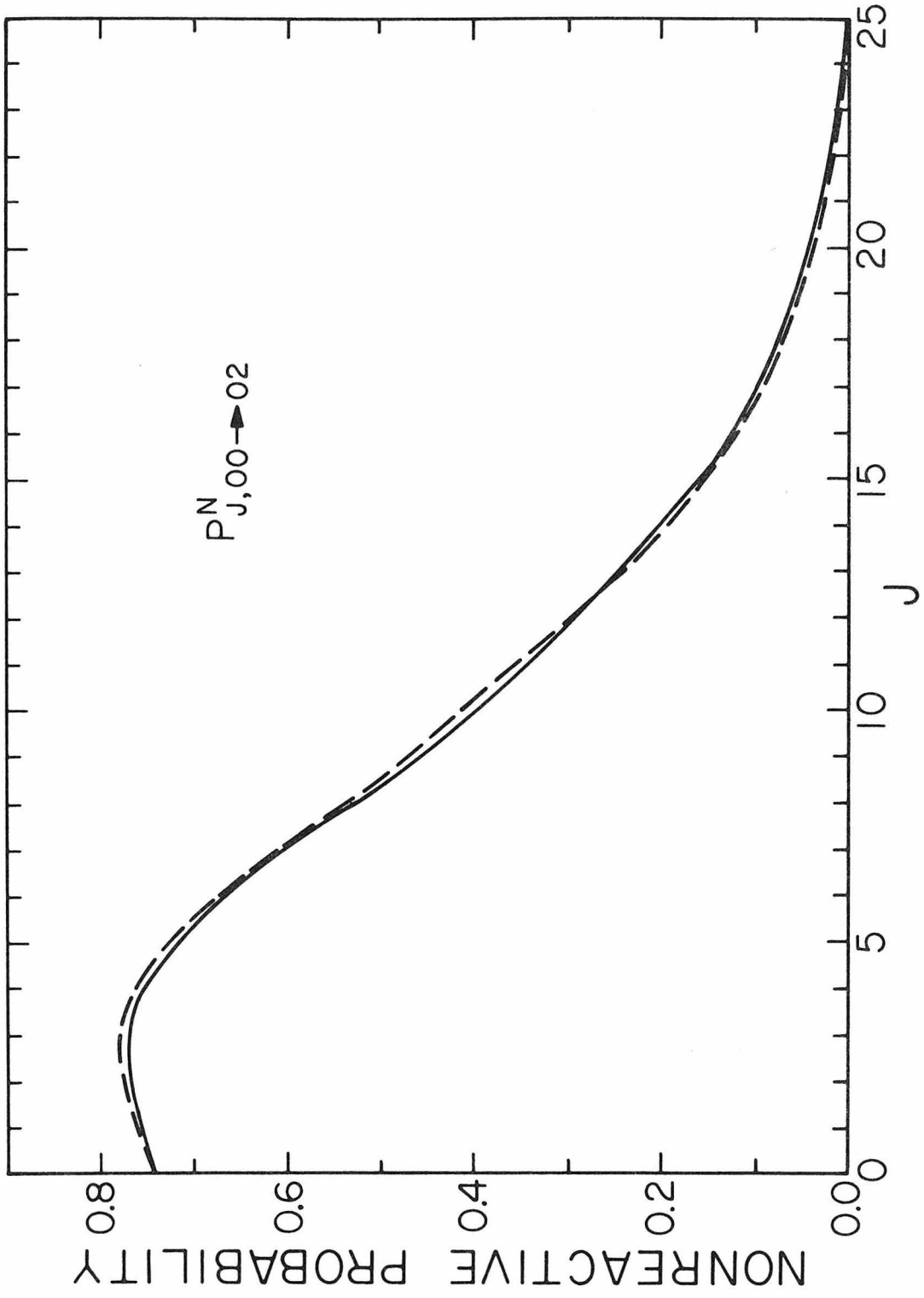
NONREACTIVE PROBABILITY
0.0
0.2
0.4
0.6
0.8
0
5
10
15
20
25
J
$P^N_{J,00\to 02}$

Fig. 13.

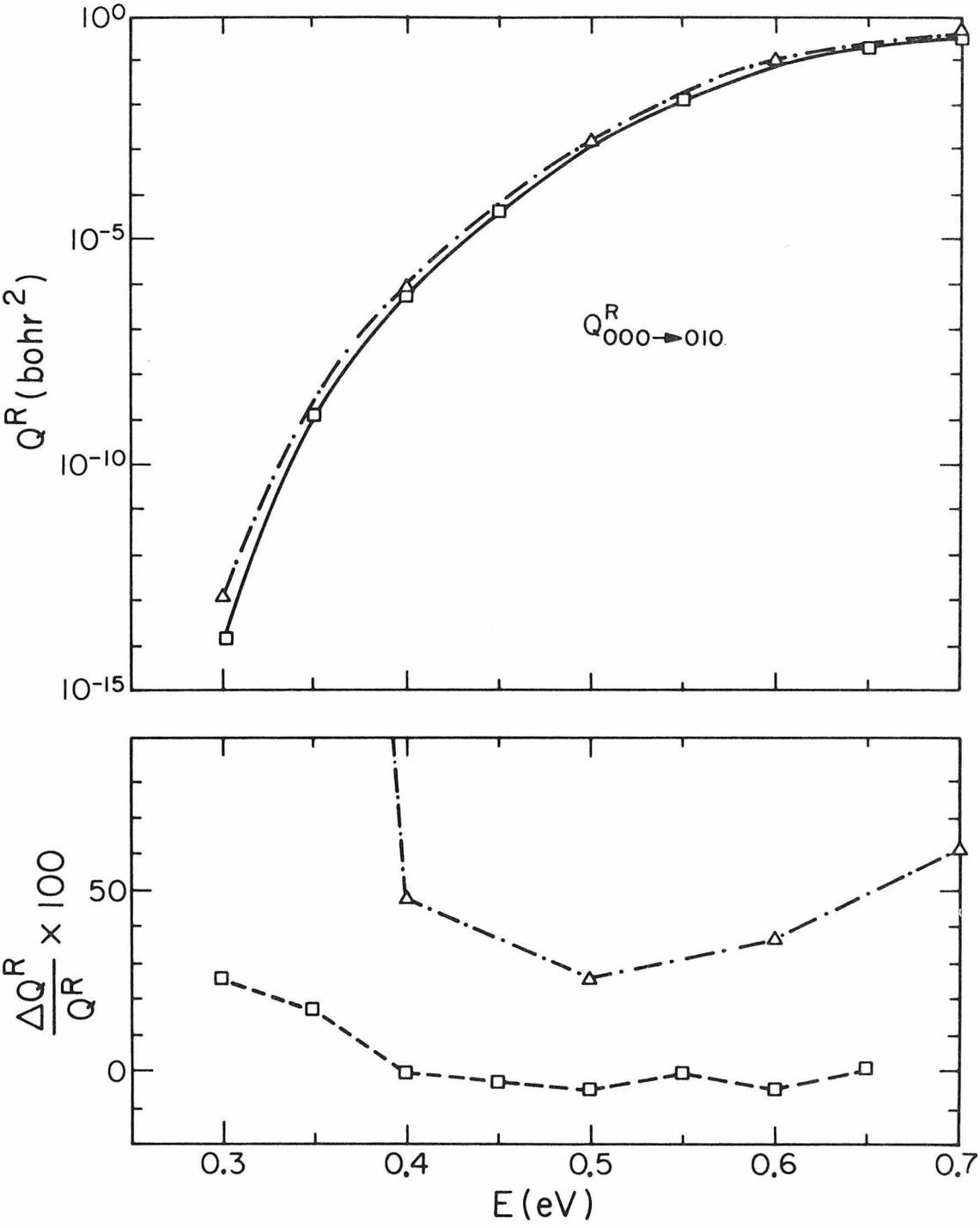
10^{0}
10^{-5}
10^{-10}
10^{-15}
Q^R (bohr^2)
$Q^R_{000\rightarrow 010}$
$\frac{\Delta Q^R}{Q^R} \times 100$
50
0
0.3
0.4
0.5
0.6
0.7
E (eV)

Fig. 14.

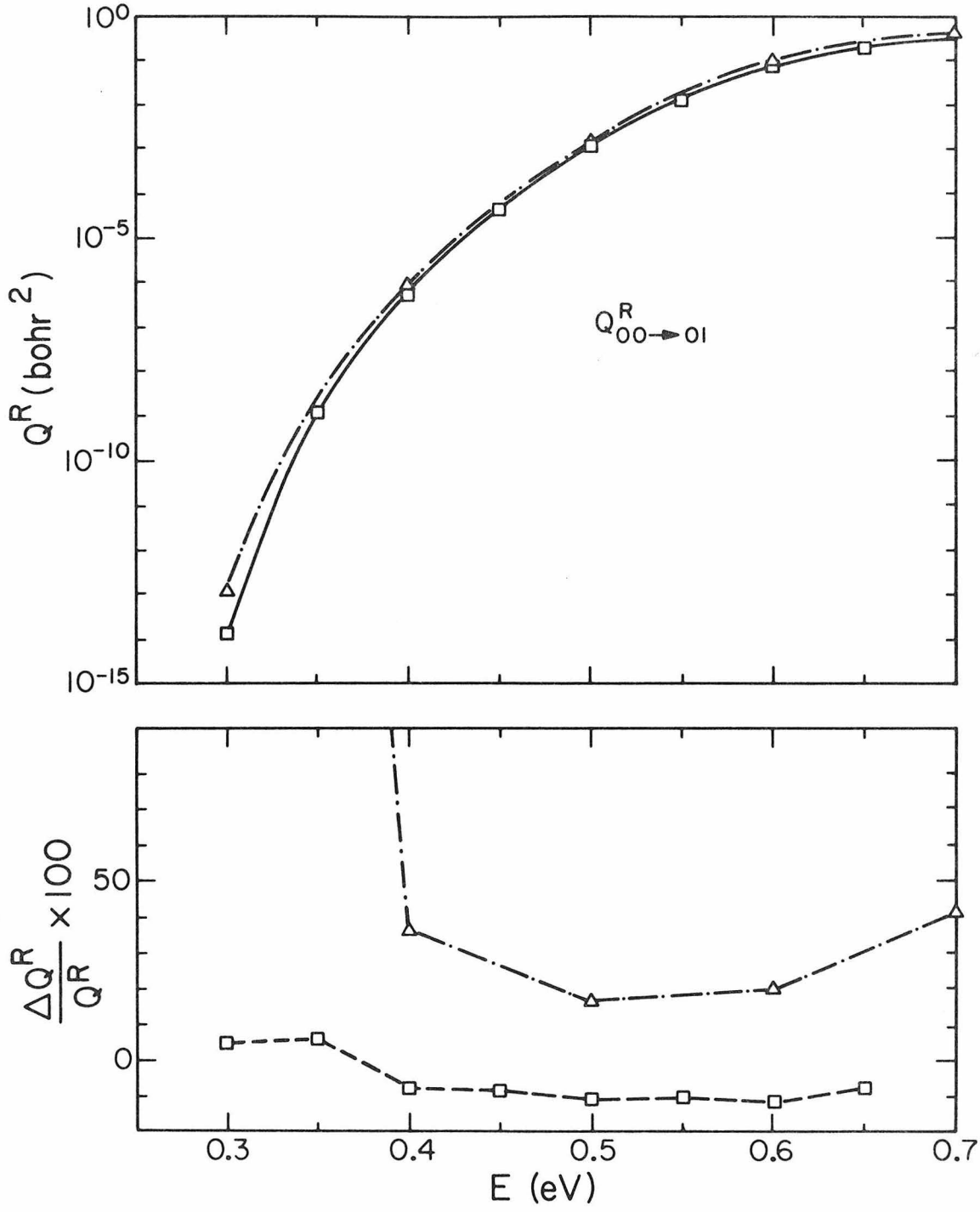
10^{0}
10^{-5}
10^{-10}
10^{-15}
Q^R (bohr^2)
$Q^R_{00\rightarrow 01}$
$\frac{\Delta Q^R}{Q^R} \times 100$
50
0
0.3
0.4
0.5
0.6
0.7
E (eV)

Fig. 15.

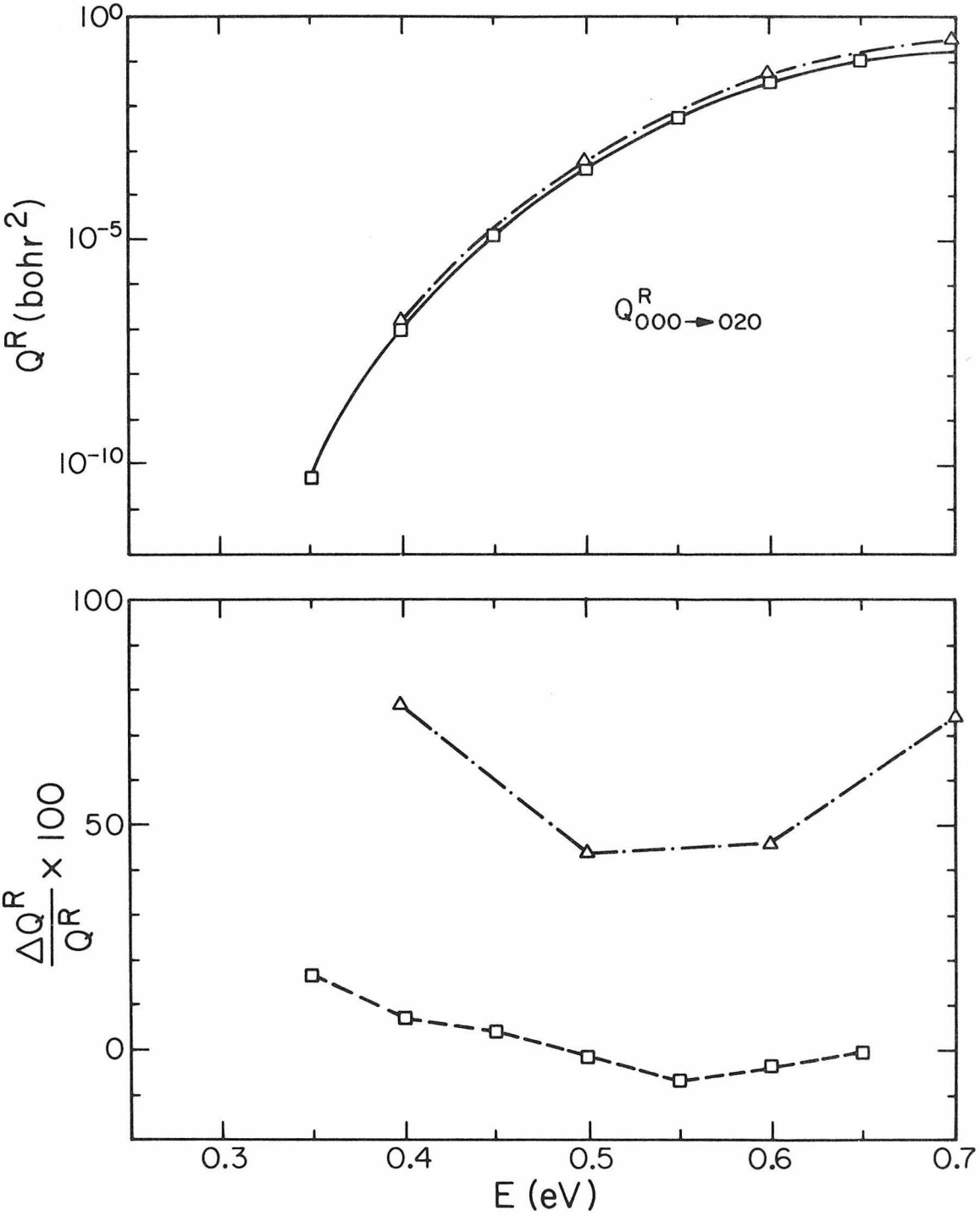
10^0
10^{-5}
10^{-10}
Q^R (bohr^2)
$Q^R_{000\rightarrow 020}$
100
50
0
$\frac{\Delta Q^R}{Q^R} \times 100$
0.3
0.4
0.5
0.6
0.7
E (eV)

Fig. 16.

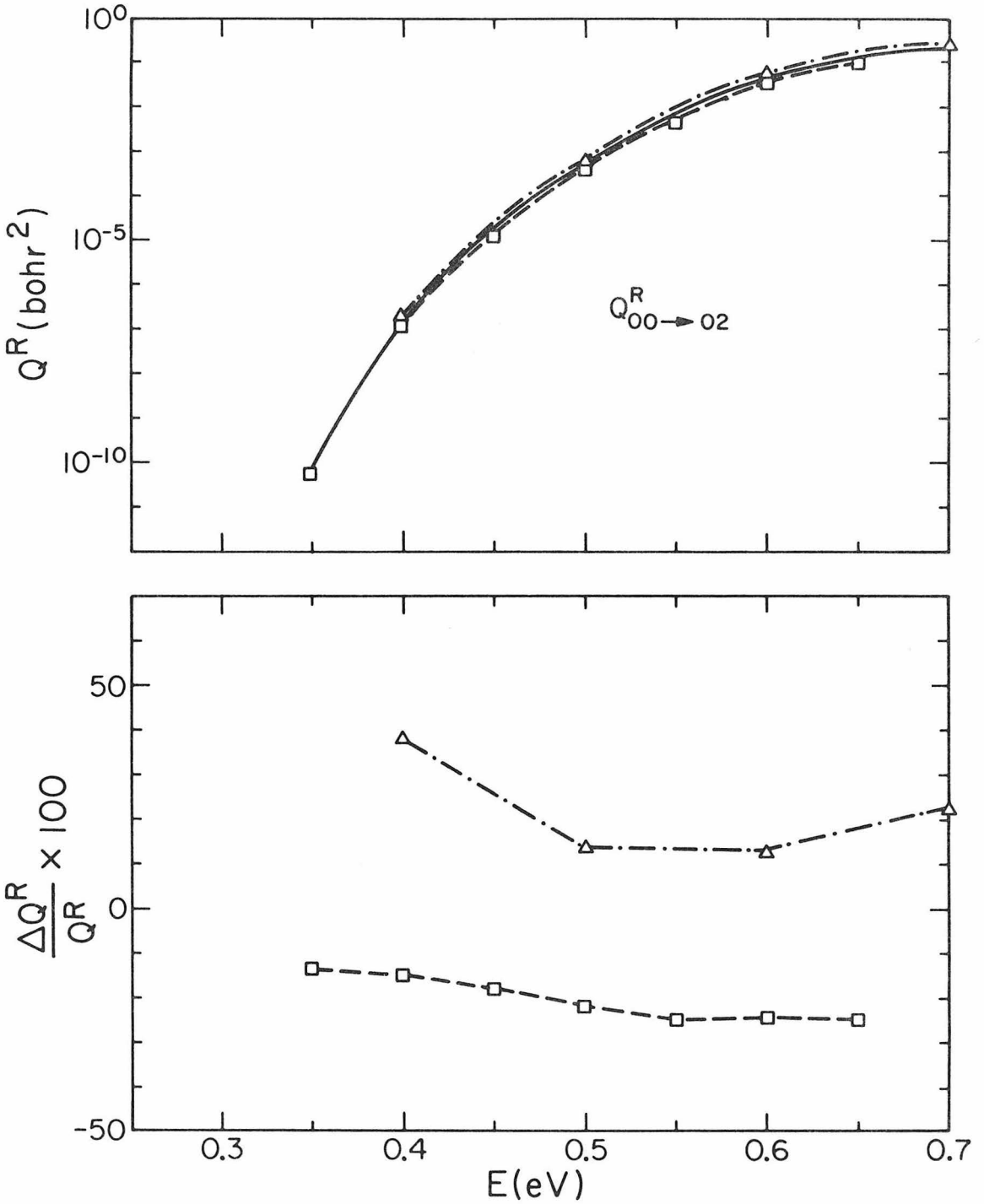
10^0
10^{-5}
10^{-10}
Q^R(bohr^2)
$Q^R_{00\rightarrow 02}$
50
0
-50
$\frac{\Delta Q^R}{Q^R} \times 100$
0.3
0.4
0.5
0.6
0.7
E(eV)

Fig. 17.

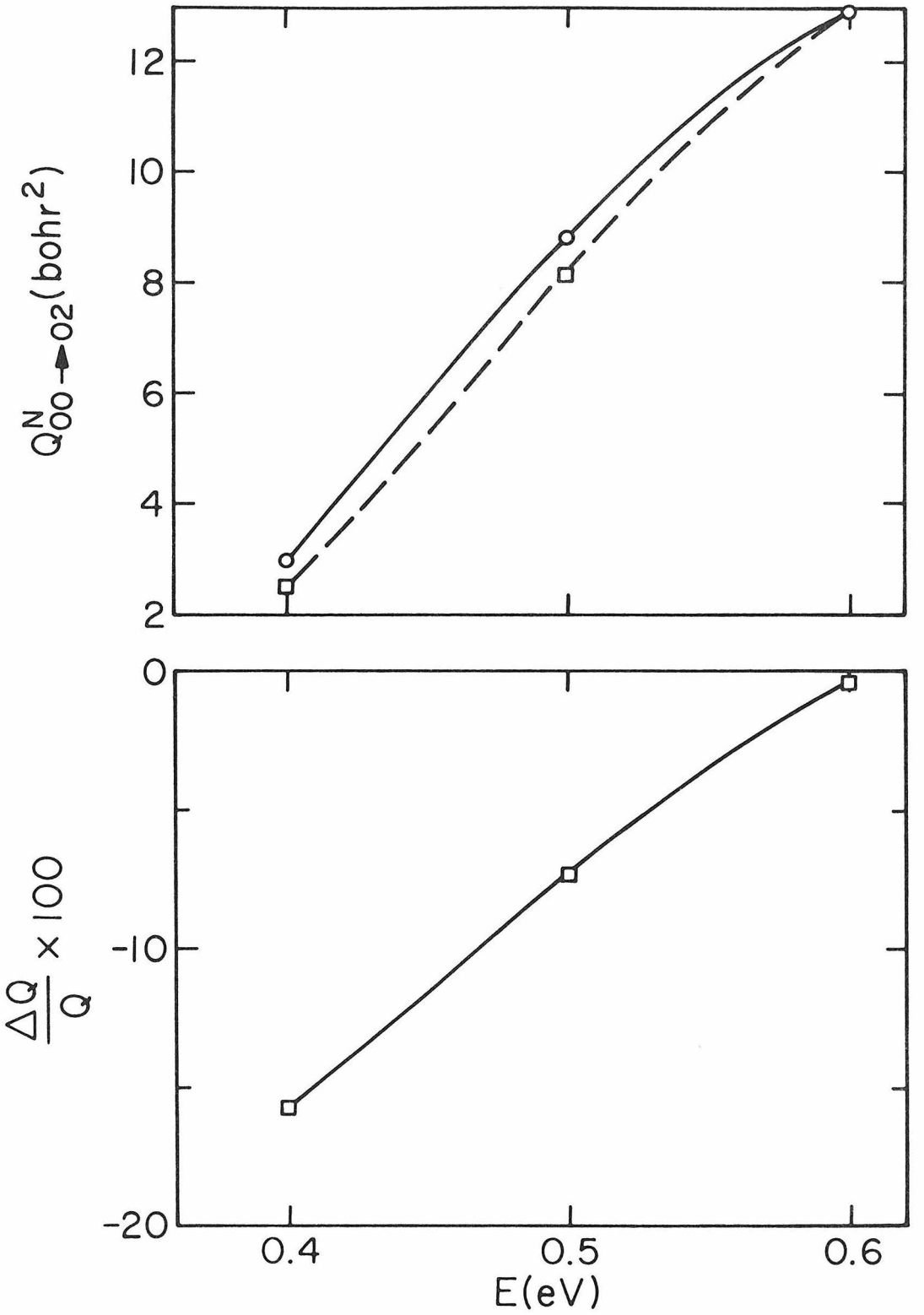
12
10
8
6
4
2
$Q^N_{00\rightarrow 02}$(bohr^2)
0
-10
-20
$\frac{\Delta Q}{Q} \times 100$
0.4
0.5
0.6
E(eV)

Fig. 18.

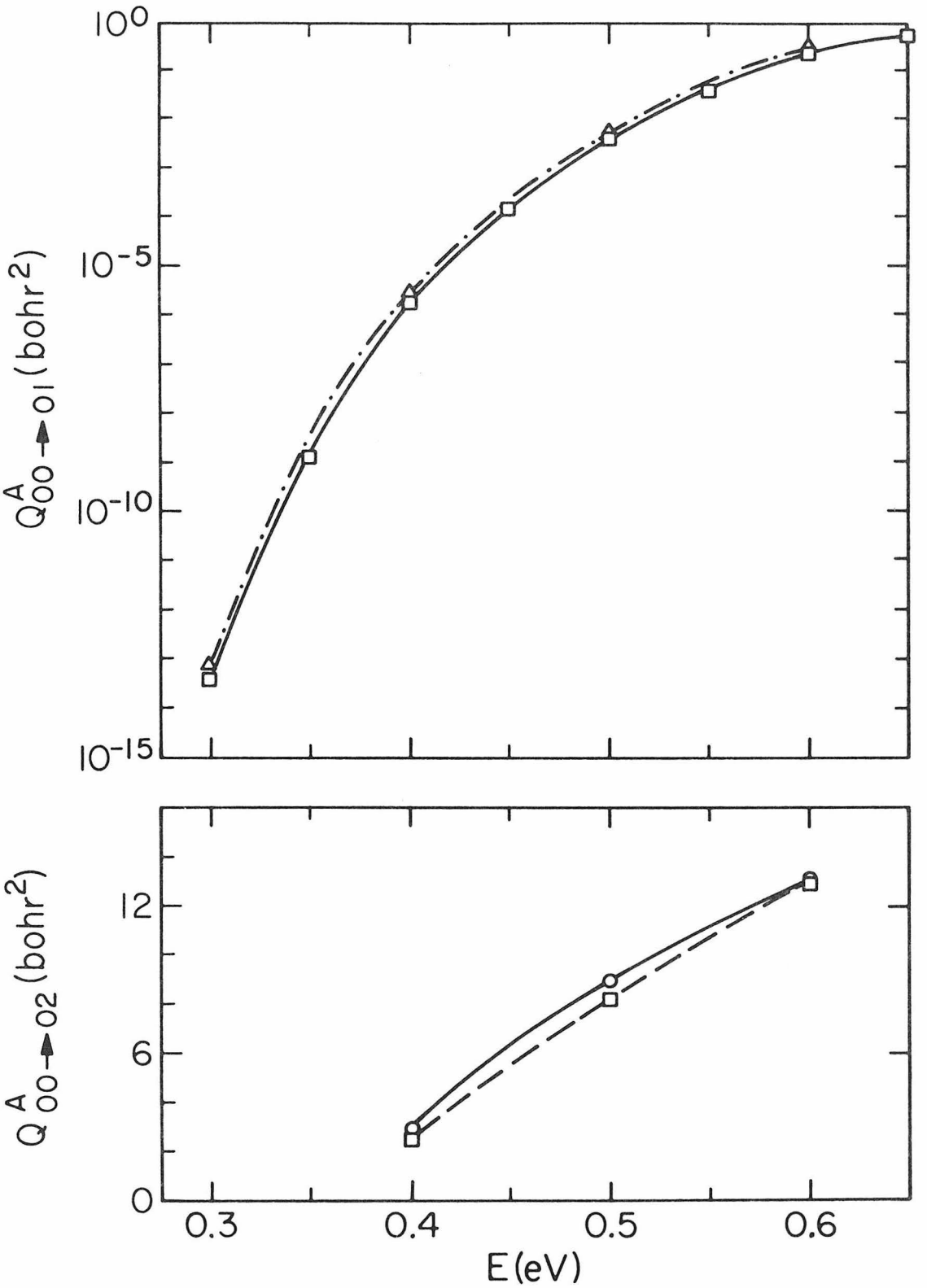
10^0
10^{-5}
10^{-10}
10^{-15}
$Q^A_{00\rightarrow 01}$ (bohr^2)
12
6
0
$Q^A_{00\rightarrow 02}$ (bohr^2)
0.3
0.4
0.5
0.6
E(eV)

Fig. 19.

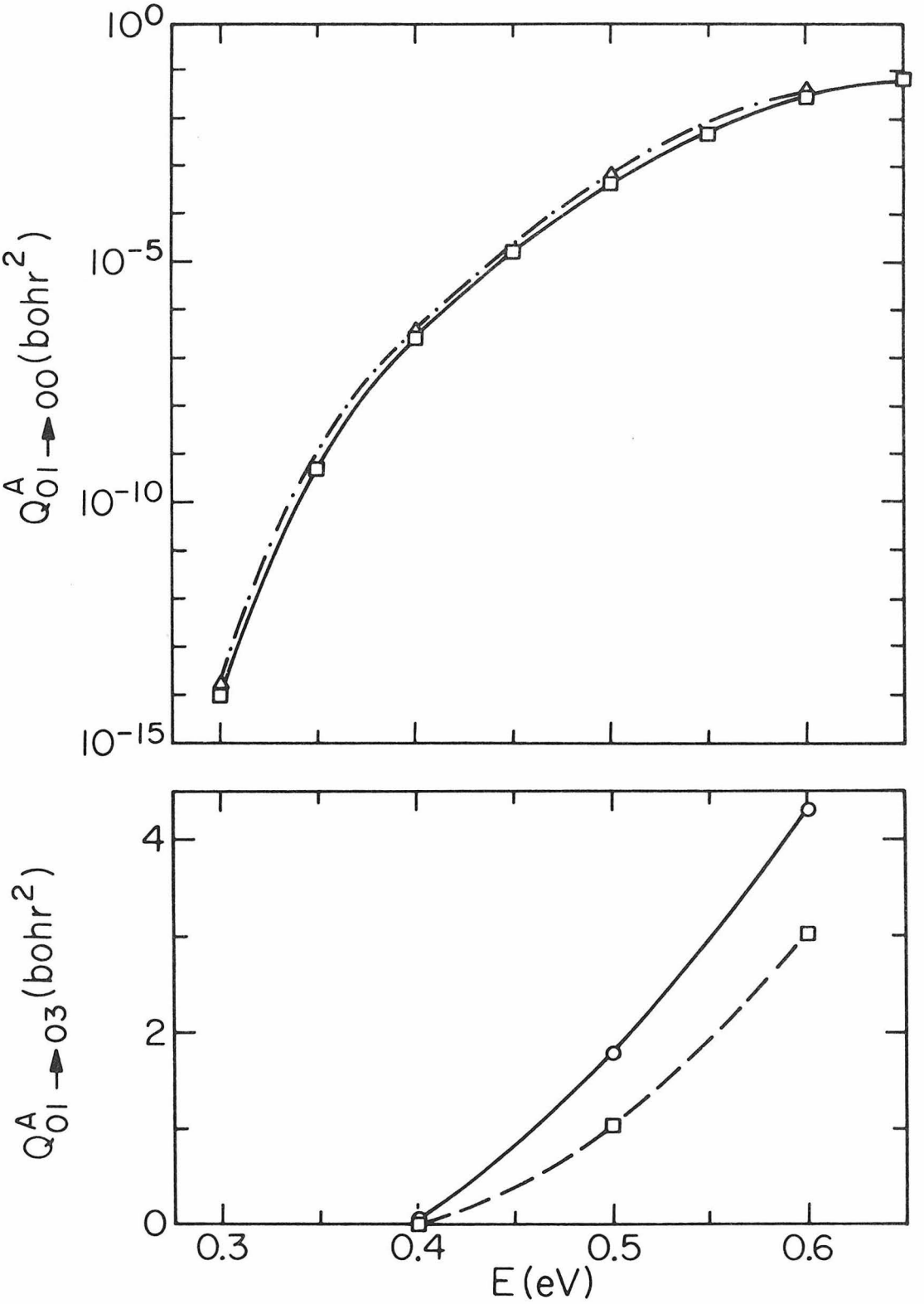
10^0
10^{-5}
10^{-10}
10^{-15}
$Q^A_{01\rightarrow 00}(\text{bohr}^2)$
4
2
0
$Q^A_{01\rightarrow 03}(\text{bohr}^2)$
0.3
0.4
0.5
0.6
E(eV)

Fig. 20.

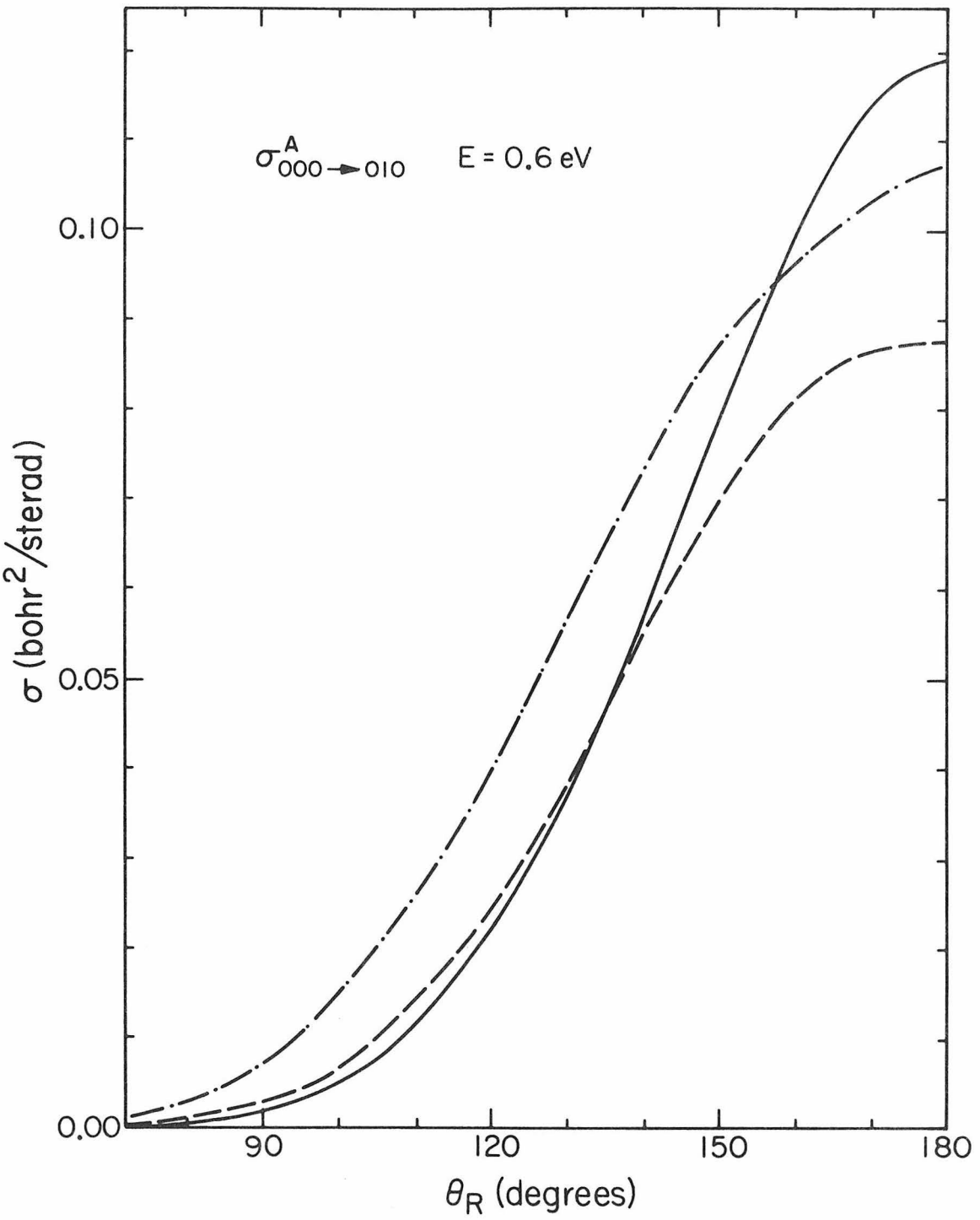
$\sigma^{A}_{000 \rightarrow 010}$ E = 0.6 eV
0.10
0.05
0.00
σ (bohr²/sterad)
90
120
150
180
θ_R (degrees)

Fig. 21.

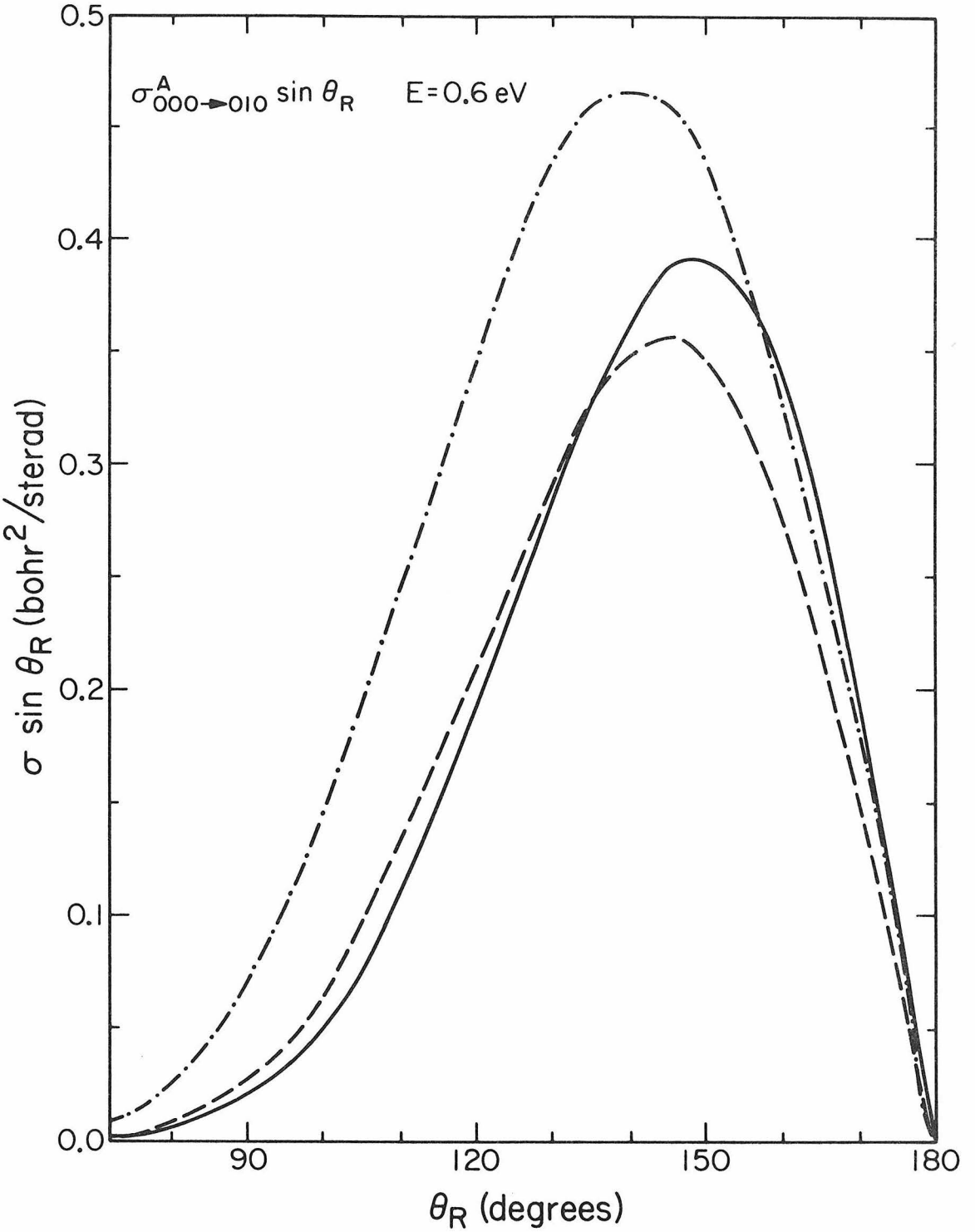
0.5
0.4
0.3
0.2
0.1
0.0
$\sigma^{A}_{000\rightarrow010}$ sin θ_R
E=0.6 eV
σ sin θ_R (bohr^2/sterad)
90
120
150
180
θ_R (degrees)

Fig. 22.

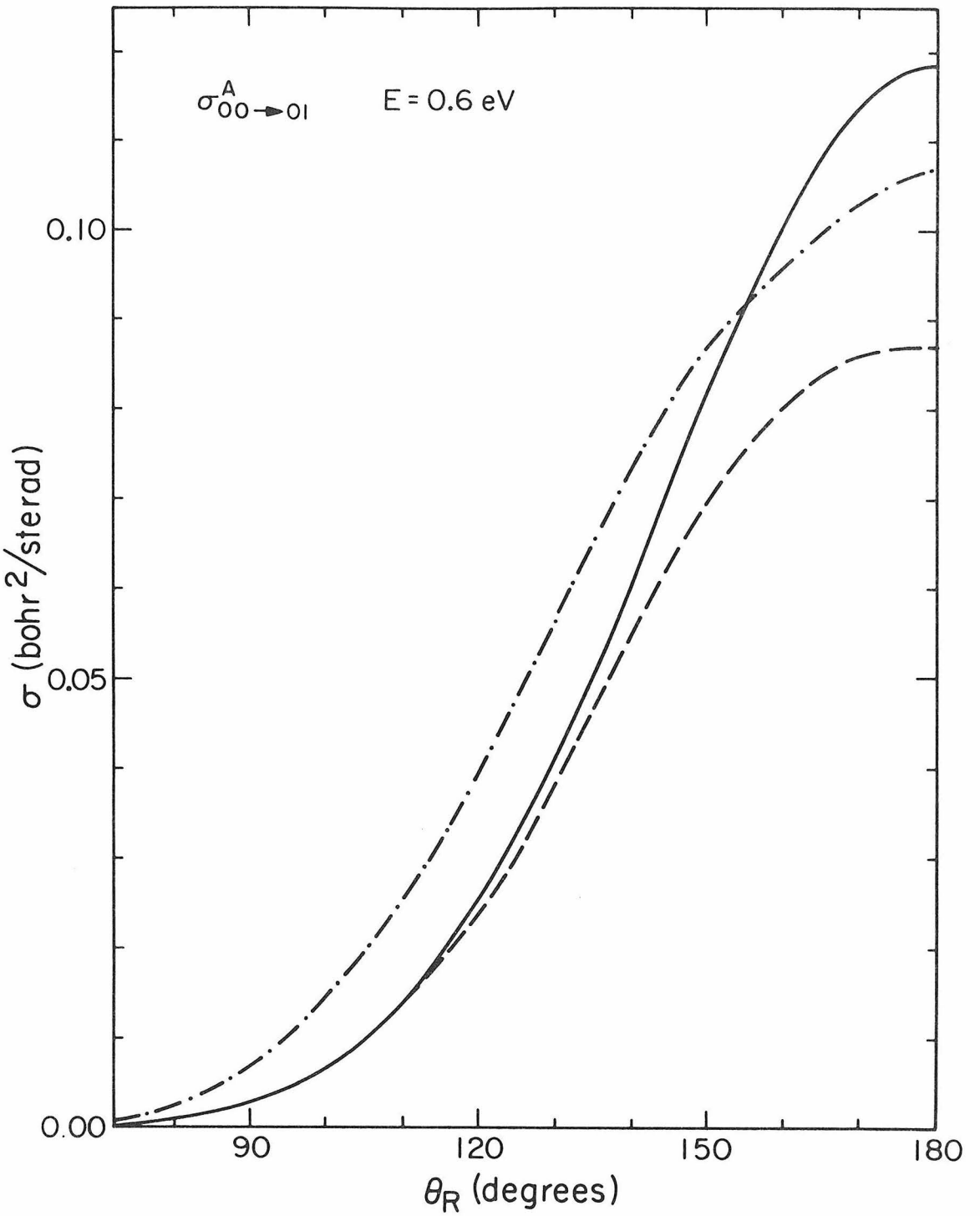
$\sigma^{A}_{00\rightarrow 01}$
E = 0.6 eV
0.10
0.05
0.00
σ (bohr²/sterad)
90
120
150
180
θ_R (degrees)

Fig. 23.

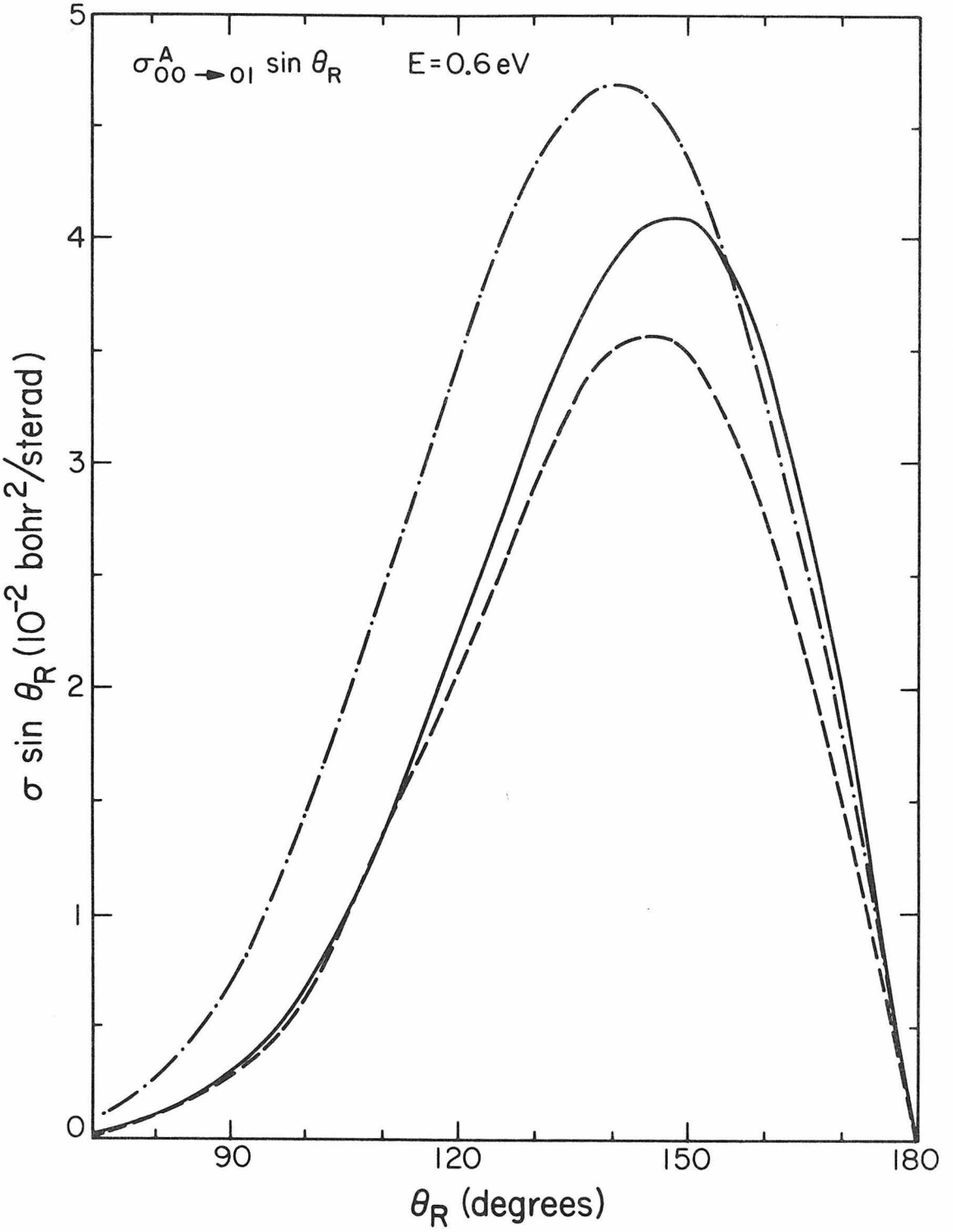
$\sigma^{A}_{00 \rightarrow 01}$ sin θ_R
E = 0.6 eV
σ sin θ_R (10^{-2} bohr^2/sterad)
θ_R (degrees)
0
1
2
3
4
5
90
120
150
180

Fig. 24.

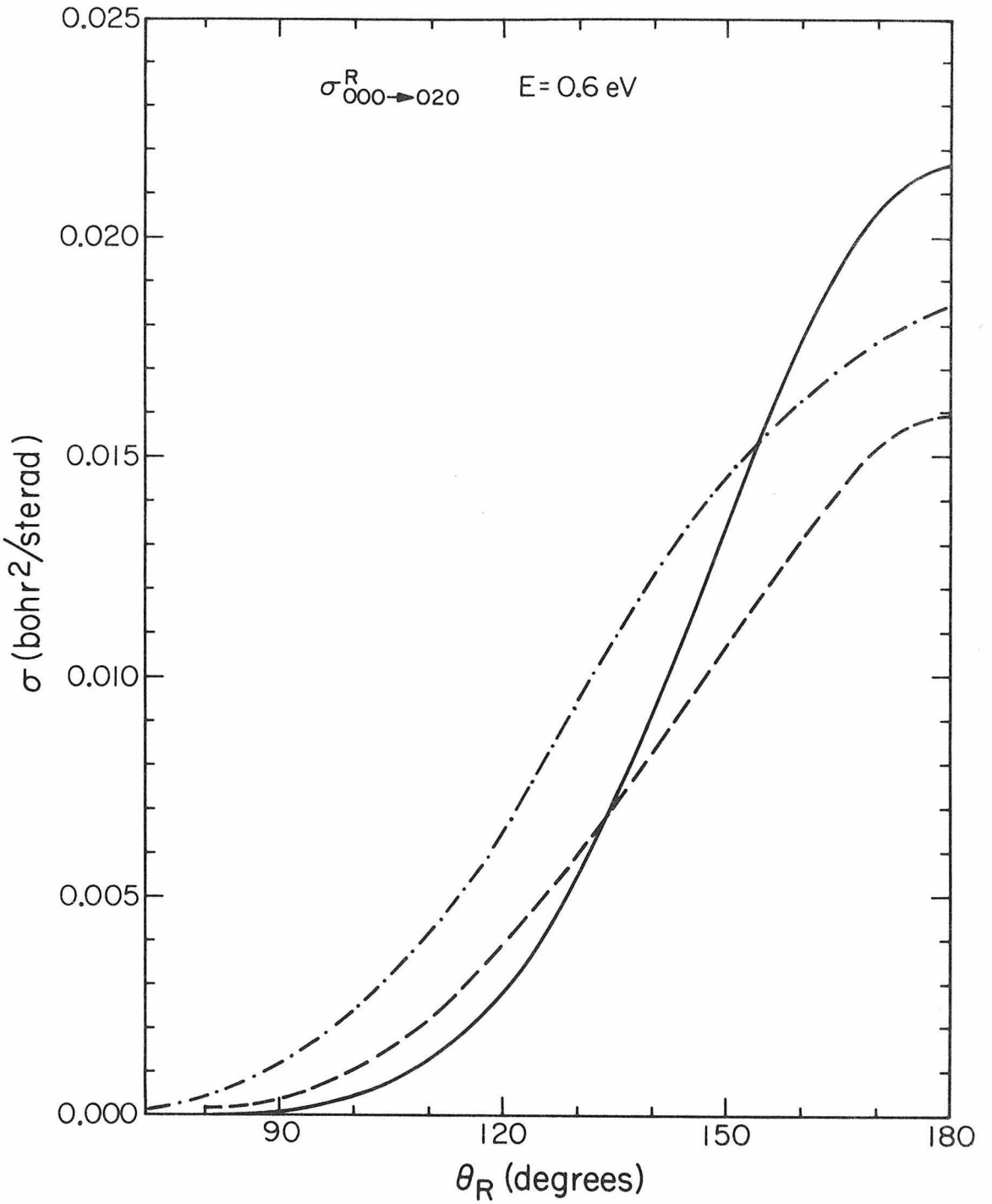
0.025
0.020
0.015
0.010
0.005
0.000
$\sigma^{R}_{000\rightarrow020}$
E = 0.6 eV
σ (bohr²/sterad)
90
120
150
180
θ_R (degrees)

Fig. 25.

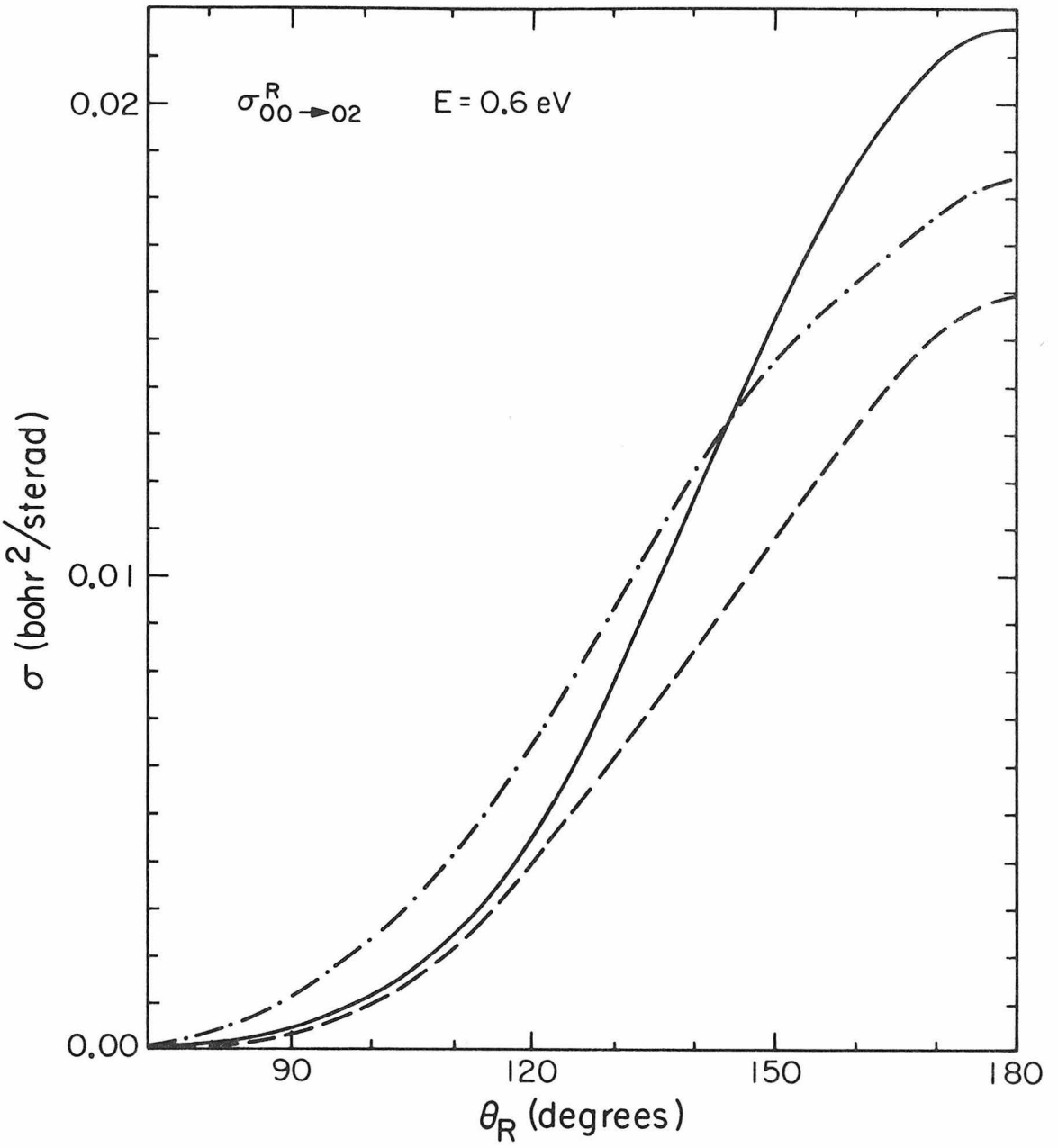
$\sigma^{R}_{00\rightarrow02}$
E = 0.6 eV
0.02
0.01
0.00
σ (bohr²/sterad)
90
120
150
180
θR (degrees)

Fig. 26.

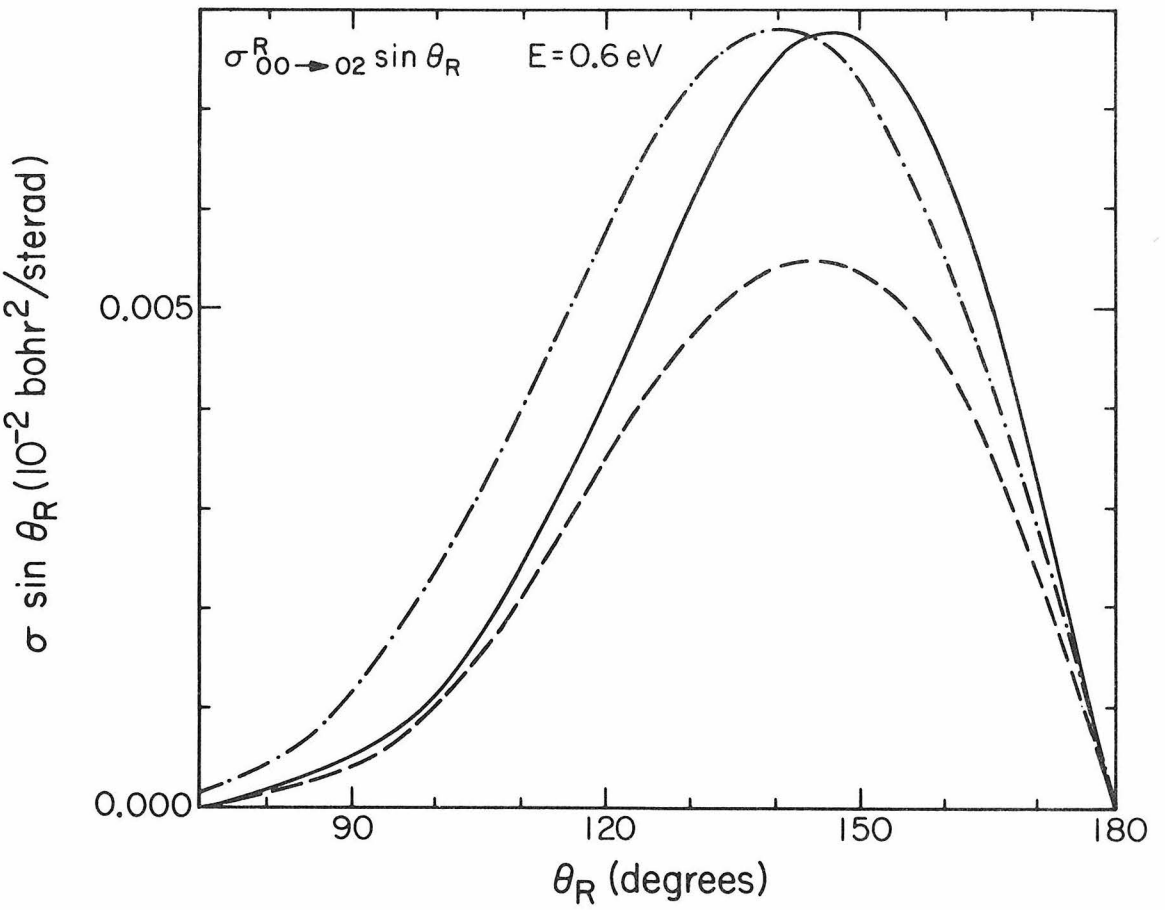
$\sigma^{R}_{00\rightarrow 02}\sin\theta_R$
E=0.6 eV
$\sigma \sin\theta_R$ (10^{-2} bohr^2/sterad)
0.005
0.000
90
120
150
180
θ_R (degrees)

Fig. 27.

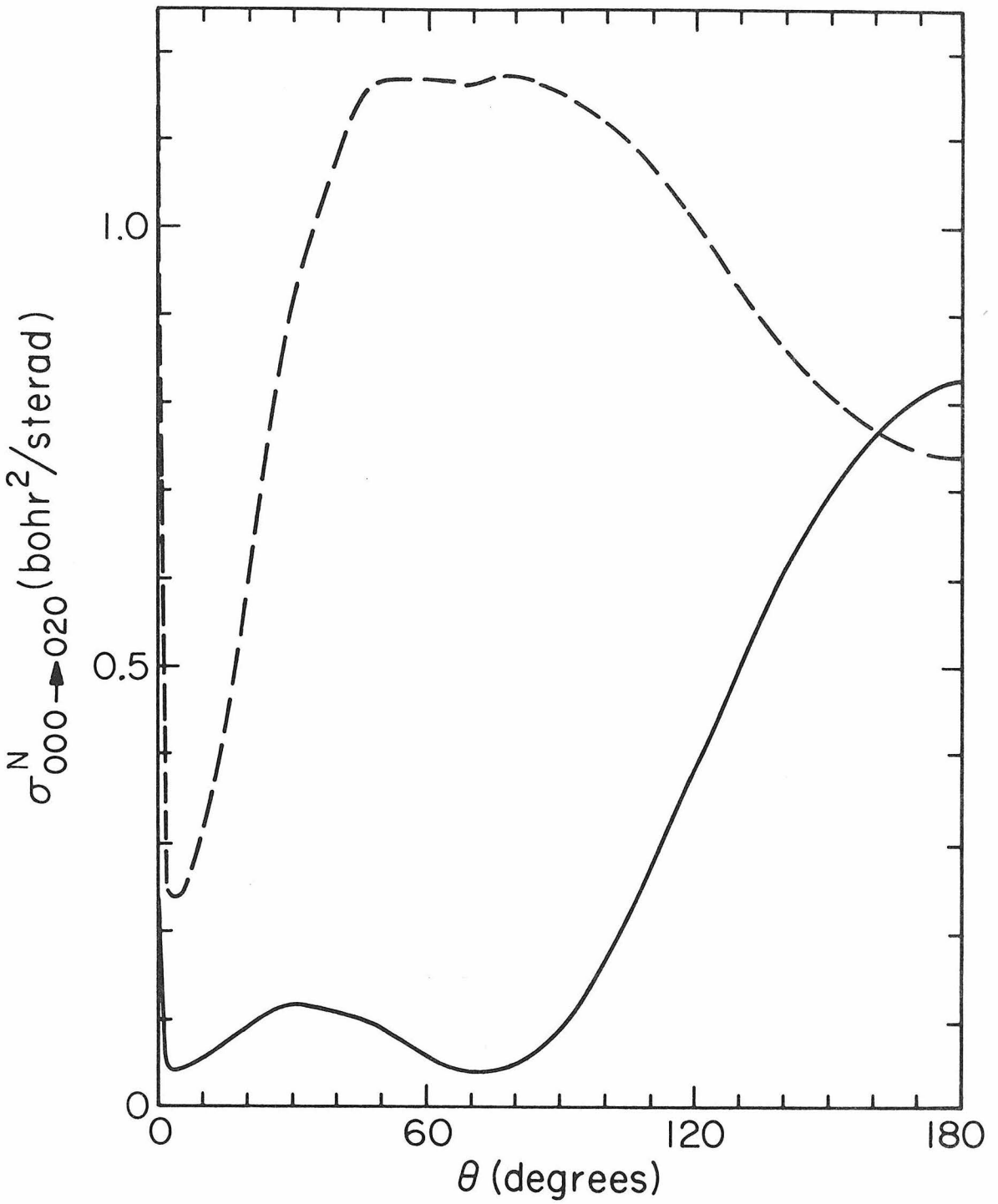
1.0
0.5
0
0
60
120
180
θ (degrees)
$\sigma^{N}_{000\rightarrow 020}$(bohr^2/sterad)

Fig. 28.

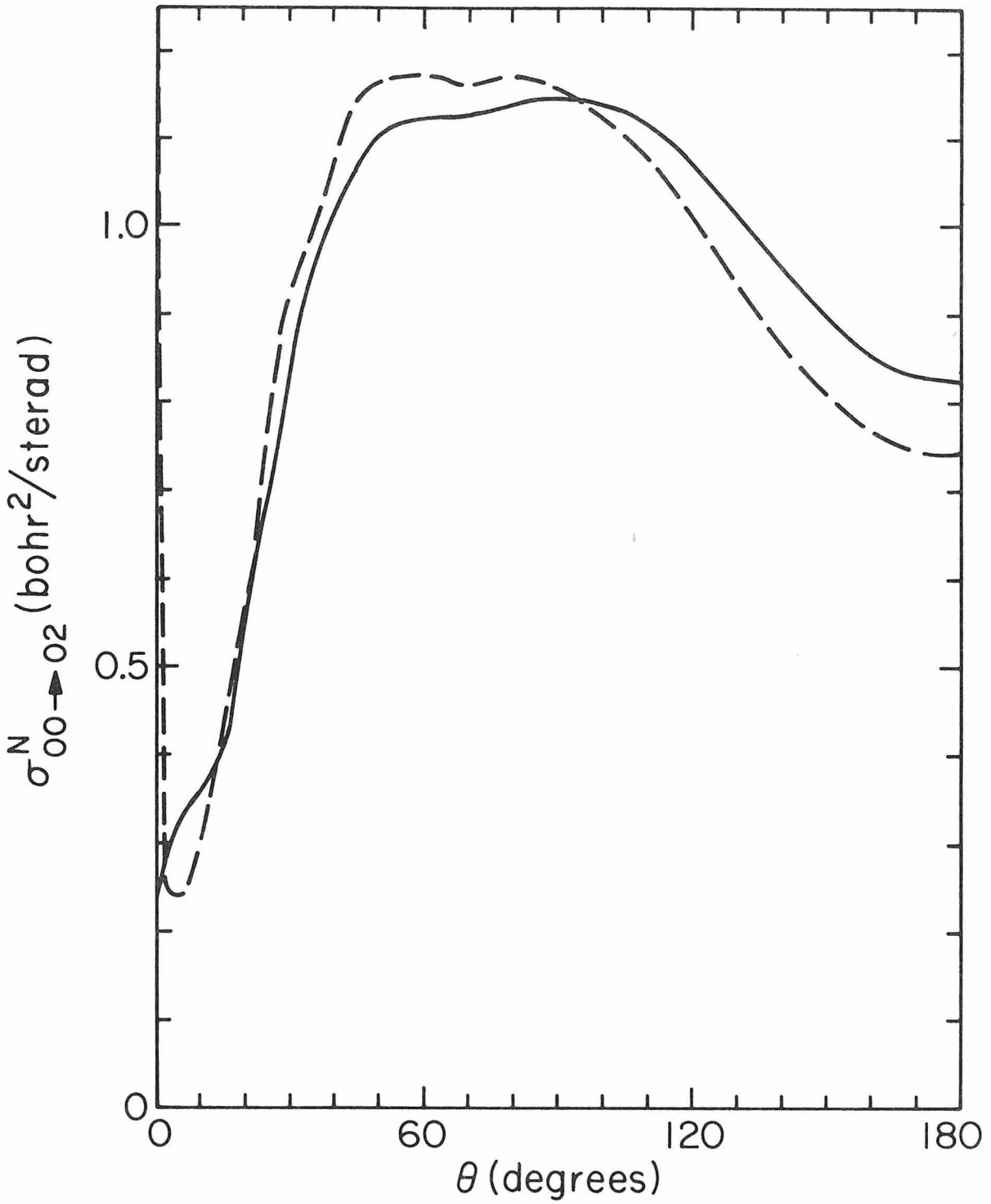

Fig. 29.

PROPOSITION 1

Abstract

It is proposed to calculate transition probabilities for a model collinear electronically nonadiabatic (ENA) reaction using an exact quantum mechanical formulation. In order to study the effects of changing the coupling between two potential energy surfaces we will use a series of parameterized coupling surfaces. In this manner we will study the effect of coupling strength, position and range. We expect to determine whether accurate coupling surfaces are necessary to calculate accurate reaction cross sections for ENA reactions.

PROPOSITION 1

A basic assumption in much of theoretical chemical scattering is the Born-Oppenheimer (BO) approximation.[1] The validity of this assumption rests on the fact that bound electrons have kinetic energies comparable to the nuclei, have masses at least three orders of magnitude smaller than the nuclei, and therefore have much greater velocities than the nuclei. Because of this, one can assume, usually to a very good approximation, that the electronic and nuclear motions are uncoupled. Physically, this means that the electrons adjust instantaneously to the motion of the nuclei.

This may be described mathematically by writing the wavefunction for a molecular system as

$$\Psi(r,R) = \sum_i \psi_i(R)\ \phi_i(r;R) \qquad (1)$$

where ψ and ϕ are the nuclear and electronic wavefunctions, respectively, R denotes all of the nuclear coordinates and r denotes all of the electronic coordinates. Note that each ϕ_i is parametrically dependent on the nuclear coordinates. When one substitutes eq. (1) into the time independent Schrödinger equation, premultiplies by ϕ_i and integrates over all r, one gets the following set of coupled equations[2] (for a two-atom system)

$$\sum_i \left[S_{ij}\left(-\frac{1}{2\mu}\nabla_R^2 - E\right) + V_{ij}(R) + \frac{J_{ij}}{\mu} - \frac{\vec{K}_{ij}}{\mu}\cdot\vec{\nabla}_R\right]\psi_i(R) = 0\ , \qquad (2)$$

where

$$
\begin{aligned}
S_{ij} &= \langle \phi_i | \phi_j \rangle \\
V_{ij} &= S_{ij}(Z_1 \cdot Z_2/R) + \langle \phi_i | H_{el} | \phi_j \rangle \\
\vec{K}_{ij} &= \langle \phi_i | \vec{\nabla}_R | \phi_j \rangle \\
J_{ij} &= \langle \phi_i | -\frac{1}{2} \nabla_R^2 | \phi_j \rangle
\end{aligned}
\tag{3}
$$

and H_{el} is the electronic Hamiltonian.

One approach is to choose molecular wavefunctions for the basis ϕ_i, i.e., eigenfunctions of H_{el}. This basis can be made orthonormal and

$$S_{ij} = \delta_{ij} \quad , \qquad V_{ij} = E_i(R)\, \delta_{ij}$$

where $E_i(R)$ is defined by

$$H_{el}\phi_i(r,R) = E_i(R)\phi_i(r,R) \tag{4}$$

The various E_i are called electronic potential surfaces or adiabatic surfaces. It is on these surfaces that one normally visualizes nuclear motion.

The coupling between different electronic states is given by the terms J_{ij} and $\vec{K}_{ij}$ of equation (2). In most atom-molecule or molecule-molecule scattering calculations to date, theorists have been interested only in collisions on one surface (adiabatic collisions). That is, they have assumed that the coupling terms J_{ij} and $\vec{K}_{ij}$ are negligible. For many years, theoretical chemists and physicists have studied atom-atom collisions involving more than one electronic surface,[2-6] i.e., electronically nonadiabatic (ENA) reactions. More complex

molecular collisions were largely ignored because the necessary tools (high-speed computers and fast numerical techniques) were not available. Now that theoretical chemists have developed techniques for solving electronically adiabatic molecular reactions,[7-9] they have begun to consider ENA molecular reactions. As with electronically adiabatic collisions, the ENA calculations fall into three broad categories: quasiclassical, semiclassical and quantum formulations.

Using a quasiclassical framework, Preston, Tully and coworkers[10-13] have developed a trajectory surface hopping (TSH) model. The model assumes that all degrees of freedom (except electronic) may be treated classically. One begins a trajectory in an asymptotic region (i.e., the distance between the reagents is large and they do not interact) on the ground state electron surface and follows it until an avoided crossing with an excited electronic surface is reached. At this point one calculates the probability on "hopping" from one surface to another. Then the original and new trajectories, each on a different surface, are continued with appropriate velocity corrections until another avoided crossing is reached, where the probability calculation is repeated. Ultimately, each of these trajectories must reach an asymptotic region on one of the surfaces. Each of the trajectories is weighted according to the probability calculation made in midreaction. When enough trajectories have been calculated, total cross sections for reaction on each surface are calculated.

Tully and Preston[12] and Krenos et al.[16] applied this model to the exchange reaction

$$H^+ + D_2 \rightarrow HD + D^+$$
$$\rightarrow H + D_2^+$$
$$\rightarrow HD^+ + D$$

and its isotopic variants. They were able to compare their results with experiments[14-16] and found qualitative agreement. A major difficulty in comparing the calculations with experiment is the potential surfaces used. Because the first excited state and the coupling terms were not well known in the systems they studied, Tully and coworkers calculated the surfaces and coupling terms with the diatomics in molecules with zero overlap (DIMZO) method.[17] Although it is easy to calculate surfaces this way, they are not very accurate.[10] More importantly, the DIMZO method has no adjustable parameters and is inflexible.

Other work has been done using a semiclassical formulation. Restricting the atom-diatom collision to a fixed plane, DeVries and George[18] studied the nonreactive quenching of fluorine by H_2. The three electronic surfaces they used were calculated by the DIMZO method similar to Tully et al.[19] Instead of choosing basis functions which diagonalized the electronic Hamiltonian (an adiabatic representation) they chose a basis which diagonalized $H_{el} + H_{so}$ (spin-orbit Hamiltonian) asymptotically(a diabatic representation). Their reason was that either representation is adequate, and that the diabatic one requires much less computation time.[20] They did not compare their results with either experiments or other calculations, but were able to conclude that for processes with the same threshold, crosslengths were ordered inversely proportional to the magnitude of the energy defect. In

another study Laing et al.[21] calculated transmission probabilities on a one-dimensional surface using semiclassical techniques. Their results showed that transmission probabilities are significantly altered by the inclusion of energetically inaccessible electronic states.

Using a quantum formulation, Rebentrost and Lester[22] calculated the quenching of fluorine by H_2. The calculation used a diabatic representation and restricted the H_2 to a fixed bond length, and thus studied the competition between electronic-rotational and electronic translational energy transfer. They found that the nonresonant (j=0 to j=0) transition agreed roughly with the quasiclassical results of Tully,[19] but that the resonant (j=0 to j=2) transition dominated by over an order of magnitude.

Bowman[23] calculated reaction probabilities (all other semiclassical and quantum results have not allowed reaction) for a model collinear atom-diatom ENA system using an exact quantum foundation. Rather than choosing a diabatic basis and calculating surfaces and coupling terms, Bowman merely chose two surfaces which crossed (which were, implicitly, the choice of some diabatic representation) and a mathematically convenient form for the coupling potential. The coupled equations which govern this model system are

$$\left[-\frac{1}{2\mu}\left(\frac{\partial^2}{\partial x_1^2}+\frac{\partial^2}{\partial x_2^2}\right)+H_{11}(x_1,x_2)-E\right]\psi_1(x_1,x_2)=-H_{12}(x_1,x_2)\psi_2(x_1,x_2)$$

$$\left[-\frac{1}{2\mu}\left(\frac{\partial^2}{\partial x_1^2}+\frac{\partial^2}{\partial x_2^2}\right)+H_{22}(x_1,x_2)-E\right]\psi_2(x_1,x_2)=-H_{12}\psi_1(x_1,x_2)$$

where x_1 and x_2 are the mass-scaled center of mass coordinates of an atom-diatom system, H_{11} and H_{22} are the two potential surfaces, and H_{12} is the coupling surface. The wavefunction ψ is expanded in a vibrational basis set, and the resulting vibrationally and electronically coupled equations are solved to find transition probabilities. Other workers[26] have since used a very similar method for studying ENA reactions with the DIMZO potential surfaces.

All of this research (classical, semiclassical, and quantum) has been done without an accurate coupling potential. Most of the studies have used potential surfaces without adjustable parameters, which have been shown to be inaccurate.

Because the correct coupling terms have not been calculated in many molecular systems, it is important to understand the effect that changing the coupling potentials has on the reaction dynamics. It is proposed, therefore, to generate a series of coupling surfaces, with adjustable parameters, and study collinear reaction dynamics with each of the coupling surfaces using an exact quantum formulation. Specifically, we propose to study ENA reactions involving two electronic surfaces and a coupling surface. Because this is a model calculation, the actual electronic surfaces used need not be accurate. An adequate choice is the pair of surfaces used by Bowman: two identical Wall-Porter[24] fits to the SSMK[25] surface, with one surface displaced from the other. The coupling surface Bowman used was

$$H_{12} = \gamma \, \mathrm{sech}[\beta(x_{20}-x_2)] \exp[-\alpha(x_{10}-x_1)^2] \qquad x_2 > x_{20}$$

$$= 0 \qquad x_2 < x_{20}$$

where the only restriction was that the coupling surface be located near

the crossing seam. One can see that the coupling surface tails off like a gaussian in the transverse direction and exponentially as the atom and diatom are separated. Near the strong interaction region ($x_2 < x_{20}$) the coupling surface vanishes abruptly.

Because this coupling surface was chosen arbitrarily, we first want to test the effect of changing the shape of the surface. Specifically, use surfaces which behave like x_2^{-2} or $e^{-\beta x_2^2}$ for large x_2. It would probably not be useful to use long range coupling surfaces like x_2^{-1}. Such potentials would require solving the coupled equations to very large values of x_2, thus requiring an extraordinary amount of computation time.

In addition, it is important to study the effect of changing the strength of the coupling surface. In a limited study Bowman found that a reactive nonadiabatic transition probability (between ground vibrational states) increased quadratically with the coupling strength, γ. Krenos et al.[16], on the other hand, estimated that nonadiabatic cross sections were largely insensitive to the probability of a surface hop. Finally, we should study the effect of abruptly truncating the coupling surface and the effect of changing the position of the coupling surface.

Results from these calculations would be very useful. If nonadiabatic transition probabilities are largely insensitive to the strength of the coupling (as Krenos claims) or to the shape of the coupling surface, then accurate scattering calculations would require only a few ab initio points to generate an approximate surface. However,

high sensitivity to the coupling strength or shape implies a need for accurate surfaces to accurately study atom-molecule ENA reactions.

References

1. M. Karplus and R. N. Porter, Atoms and Molecules, W. A. Benjamin, inc., New York, N.Y., 1970. p. 454.
2. C. Melius and W. A. Goddard III, Phys. Rev. A 10 (1974) 1541.
3. E. Stueckelberg, Helv. Phys. Acta 5 (1932) 369.
4. C. Zener, Proc. Roy. Soc. (London) A137 (1936) 696.
5. F. H. Mies, Phys. Rev. A 7 (1973) 942.
6. F. H. Mies, Phys. Rev. A 7 (1973) 957.
7. D. G. Truhlar and A. Kuppermann, J. Chem. Phys. 5 (1972) 2232.
8. G. C. Schatz and A. Kuppermann, J. Chem. Phys. 65 (1976) 4668.
9. B. R. Johnson, Chem. Phys. Lett. 13 (1972) 172.
10. R. K. Preston and J. C. Tully, J. Chem. Phys. 54 (1971) 4297.
11. J. Krenos, R. Preston and R. Wolfgang, Chem. Phys. Lett. 10 (1971) 17.
12. J. C. Tully and R. K. Preston, J. Chem. Phys. 55 (1971) 562.
13. R. K. Preston and R. J. Cross Jr., J. Chem. Phys. 59 (1973) 3616.
14. M. G. Holliday, J. T. Muckermann and L. Friedmann, J. Chem. Phys. 54 (1971) 1058.
15. W. B. Maier, J. Chem. Phys. 54 (1971) 2732.
16. J. R. Krenos, R. K. Preston, R. Wolfgang and J. C. Tully, J. Chem. Phys. 60 (1974) 1634.
17. F. O. Ellison, J. Am. Chem. Soc. 85 (1963) 3540,3544.
18. P. L. DeVries and T. F. George, J. Chem. Phys. 66 (1977) 2421.
19. J. C. Tully, J. Chem. Phys.60 (1974) 3042.
20 I. H. Zimmermann and T. F. George, J. Chem. Phys. 63 (1975) 2109.
21. J. R. Laing, J. M. Yuan, I. H. Zimmermann, P. L. DeVries and T. F. George, J. Chem. Phys. 66 (1977) 2801.

22. F. Rebentrost and W. A. Lester, J. Chem. Phys. 64 (1976) 4223.

23a. J. M. Bowman, Ph.D. Thesis, California Institute of Technology, Pasadena, California, 1974.

b. J. M. Bowman, S. C. Leasure and A. Kuppermann, Chem. Phys. Lett. 43 (1976) 374.

24. F. Wall and R. Porter, J. Chem. Phys. 36 (1962) 3256.

25. Z. Shavitt, R. Stevens, F. Minn and M. Karplus, J. Chem. Phys. 48 (1968) 2700.

26a. Z. H. Top and M. Baer, Chem. Phys. Lett. 39 (1976) 134.

b. Z. H. Top and M. Baer, J. Chem. Phys. 64 (1976) 3078.

c. Z. H. Top and M. Baer, J. Chem. Phys. 66 (1976) 1363.

PROPOSITION 2

Abstract

It is proposed to calculate ab initio the second excited electronic state ($^1\Pi$) of AlH and determine the height of the potential barrier. The proposed method is a generalized valence bond (GVB) calculation, followed by a configuration interaction (CI) calculation. It is further proposed to calculate the predissociation lifetime of the molecule in the $^1\Pi$ state.

PROPOSITION 2

In 1940, Herzberg and Mundie[1] presented evidence that the potential curves of the $^1\Pi$ states of BH, AlD and possibly AlH have relative maxima at the finite internuclear distance R. That is, at large r the potential curves are repulsive and at smaller R they are attractive. They further indicated that the observed barrier heights for AlH and AlD are not the same, and agreed with Olsson[2] that this is caused by a tunneling effect.

Recent theoretical work[3,4] has predicted such a barrier for the $^1\Pi$ state of BH at the internuclear distance that Herzberg and Mundie experimentally found it to exist. A smaller barrier for the $^3\Pi$ state was also predicted theoretically. The only theoretical work[5,6] to date on AlH was restricted to the ground state $^1\Sigma^+$.

We propose to calculate the potential curves for the ground state ($^1\Sigma^+$) and low lying excited states ($^3\Pi$, $^1\Pi$) of AlH. If maxima are found in the potential curves, we further propose to calculate the lifetimes of these states.

The interest in both BH and AlH stems from their similar electronic structure of boron and aluminum. Both have a core of electrons ($1s^2$ and $1s^22s^22p^6$ respectively), and a similar outer shell ($2s^22p^1$ and $3s^23p^1$ respectively). It is this similarity, and previous work on BH, which we should exploit in order to understand AlH.

A. Experimental Evidence

To determine whether a potential maximum exists in an electronic state, Herzberg and Mundie examined the rotational fine structure of

successive vibrational levels. In the emission spectra they observed a breaking off of the rotational fine structure for various vibrational levels. This breaking off occurs because the higher rotational levels are completely unstable.

The effective potential energy can be written

$$U_J(R) = U_o(R) + \frac{\hbar}{2\pi c\mu R^2} J(J+1)$$

where $U_o(R)$ is the rotationless potential energy, and μ is the reduced mass. The effective potential reaches a maximum when $\frac{dU_J(R)}{dR} = 0$, or

$$U_o'(R_{max}) = \frac{\hbar}{2\pi c\mu R_{max}^3} J(J+1)$$

where R_{max} is the position of the maximum. One can plot the maximum of each effective potential curve as a function of J(J+1). For a system in which the rotationless curve does not have a maximum at finite distances, the curve will intersect the ordinate at $U_o(\infty)$. The slope of the curve at the ordinate vanishes, corresponding to a slope of $\hbar/2\pi c\mu R^2$ at $R = \infty$. If the rotationless curve has a maximum, the maximum for successive J will be at approximately the same position. In this case, a plot of the maximum of the effective potential vs. J(J+1) should be approximately a straight line with a slope of $\hbar/2\pi\mu cR_{max}^2$.

In effect, Herzberg and Mundie plotted the energy level from the last observed rotational spectrum [vs. J(J+1)], plotted the first missing energy level and said that the true breaking off point must occur somewhere between the two points. This was done for three (AlD and BH)

or two (AlH) vibrational states. A line fit to the points was linear, and the intersection of the line with the ordinate gave the relative maxima of the potential curve of the rotationless state.

By this method they found that the $^1\Pi$ states of AlH, AlD and BH each had a relative maximum. The value of R_{max} for AlH was within 0.5% of the value for AlD. More interesting is that the observed barrier for AlH is 165 cm^{-1} less than the barrier for AlD, which they attributed to a tunneling effect. Because the difference is quite small, they concluded that the tunneling effect is very slight.

Although the $^1\Pi$ state may have a relative maximum (and therefore a relative minimum), the state might be bound by only a couple of hundred wave numbers, if at all. Herzberg has noted the state at 23763 cm^{-1} above the bottom of the $^1\Sigma^+$ state. This is only 515 cm^{-1} above the dissociation limit[10] of the $^1\Sigma^+$ state (3.01 eV). The uncertainty in this limit ($\pm$ .05 eV) implies the state might be bound by only 111 cm^{-1} (0.013 eV).

B. Theoretical Work

1. BH

Blint and Goddard[3,4] have calculated the low lying electronic states of BH using the generalized valence bond (GVB) method. Each of the $^3\Pi$ and the $^1\Pi$ states was found to have a maximum; the lower lying $^3\Pi$ state was predicted to have a barrier of 0.026 eV and the $^1\Pi$ state a barrier of 0.15 eV. The origin of the barrier lies in the coupling of the orbitals on boron and hydrogen. At large inter-atomic distances the coupling is predominantly intra-atomic and repulsive. As the

atoms are brought closer together, the predominant coupling is interatomic and attractive, corresponding to bond formation.

2. AlH

Previously there have been only two calculations[5,6] on AlH, both on the electronic ground state. Both calculations used a Hartree-Fock method to calculate the potential curve and several molecular properties. One paper noted the similarity between the electronic structures of BH and AlH, noted the previous discovery of temperature independent paramagnetism of BH in the gas phase, and presented results which predicted the same for AlH.

We have made preliminary calculations of the ground and first two excited electronic states of AlH which indicate the limited value of the Hartree-Fock calculations near the equilibrium point. The basis set was of roughly double zeta quality. On aluminum we used 36 Gaussian primitives contracted to 18 functions.[7] To generate a polarization function we used one of the 3d Slater functions from Cade and Huo, and following Dunning[8], converted it to a Gaussian function. For hydrogen we used 4 primitives[9] contracted to 3. We again used a polarization function from Cade and Huo and converted it to a Gaussian.

To calculate an accurate potential surface (more accurate than Cade and Huo[5]) one must do a series of calculations at several internuclear distances. The first calculation is a straight Hartree-Fock (HF). This method determines the wavefunctions by a self-consistent and iterative method. The second calculation is a generalized valence bond (GVB) approach, in which the final orbitals from the HF calculation

are used as starting guesses. In the GVB method, one "splits" lone pairs or bonding pairs of electrons with unoccupied orbitals, which allows the electrons to correlate. Finally, one does a configuration interaction (CI) calculation within the GVB space.

The first set of calculations we made were at the equilibrium distance of the ground state of the AlH molecule. The results, in Table I, demonstrate the inability of the Hartree-Fock method to predict accurately the dissociation energy. The Hartree-Fock calculations are in error by about 22% or 0.65 eV. The GVB results are in error by 2%, or 0.07 eV.

The energy of the first excited state, $^3\Pi$, is plotted as a function of energy in Figure 1b for two types of calculations. The first curve (dashed line) is from a GVB calculation, and has a substantial hump near 4.25 bohr. This calculation was done by splitting the bonding pair with a π_x and a π_y orbital to include angular correlation, and with two σ orbitals to include in/out correlation. We found that at R = 3.114 bohr, in/out correlation had a very little effect.

The second type of calculation is called SOGVB. This calculation can optimize the spin orbit coupling, but does not include all of the correlation effects of a GVB calculation. The results (solid line, Fig. 1b) clearly demonstrate the importance of optimizing this coupling at intermediate internuclear distances, but also illustrate its relatively small effect at large distances. The results for the $^1\Pi$ state (Fig. 1a, solid line SOGVB, dashed line GVB) show similar trends. For both states the GVB calculations on AlH seem to be converging to

the asymptotic values for Al+H, indicating that the calculations are consistent. There is no theoretical evidence that the $^1\Pi$ state is bound, which is in accordance with experiment.

To proceed further one must be careful that the CI calculations on AlH and aluminum atom are consistent with each other. Otherwise, the potential curve of AlH will not converge to the asymptotic value of Al+H.

In the CI calculation we want to include the optimum orbitals from both the GVB and SOGVB calculations. To do this we could use the singly occupied π orbital from the SOGVB calculation and the other virtual π orbitals from the GVB calculation. Of course, all of these orbitals must be mutually orthogonalized. A possible choice of configurations for the CI calculation would be to use all single excitations from each of the GVB configurations.

C. Lifetimes

If a diatomic molecule is in a vibrationally and/or rotationally excited state of an electronic state with a hump, it may decay by one of two competing processes. One is deexcitation to a lower electronic, vibrational or rotational state; and the other is predissociation by tunneling. Following Davydov,[11] an approximate expression for the transmission coefficient is given by

$$D = \exp\left(-\frac{2}{\hbar}\int_{x_1}^{x_2}\sqrt{2\mu(U-E)}\,dx\right)$$

where x_1 and x_2 are defined by $U(x_1) = U(x_2) = E$, μ is the reduced

mass, U is the potential of the rotationless state, and E is the energy. The lifetime is given by

$$\tau = \frac{1}{2} \tau_o / D$$

where τ_o is the period of oscillation.

Table 1

Calculations of $^1\Sigma^+$ State of AlH at R_e = 3.114 bohr

	Hartree Fock[a]	GVB[b]	Experiment[c]
AlH	-242.4634 h	-242.4861 h	-
Al	-241.8765 h	-241.8781 h	-
Dissociation Energy	2.36 eV	2.94 eV	3.01 ± 0.05 eV

[a]From Reference 5

[b]Present work

[c]From Reference 10

References

1. G. Herzberg and L. G. Mundie, J. Chem. Phys. 8 (1940) 263.
2. E. Olsson, Zeits. f. Physik 108 (1938) 322.
3. W. A. Goddard III and R. J. Blint, Chem. Phys. Lett. 14 (1972) 616.
4. R. J. Blint and W. A. Goddard III, J. Chem. Phys. 57 (1972) 5296.
5. P. E. Cade and W. M. Huo, J. Chem. Phys. 47 (1967) 649.
6. E. A. Laws, R. M. Stevens and W. N. Lipscomb, J. Chem. Phys. 54 (1971) 4269.
7. T. Dunning, "Contracted Gaussian Basis Sets for Second Row Atoms", unpublished.
8. T. Dunning, J. Chem. Phys. 55 (1971) 3958.
9. T. Dunning, J. Chem. Phys. 53 (1970) 2823.
10. P. Wilkinson, Astrophys. J. 138 (1963) 778.
11. A. Davydov, Quantum Mechanics (Pergamon Press, 1965), p. 80.

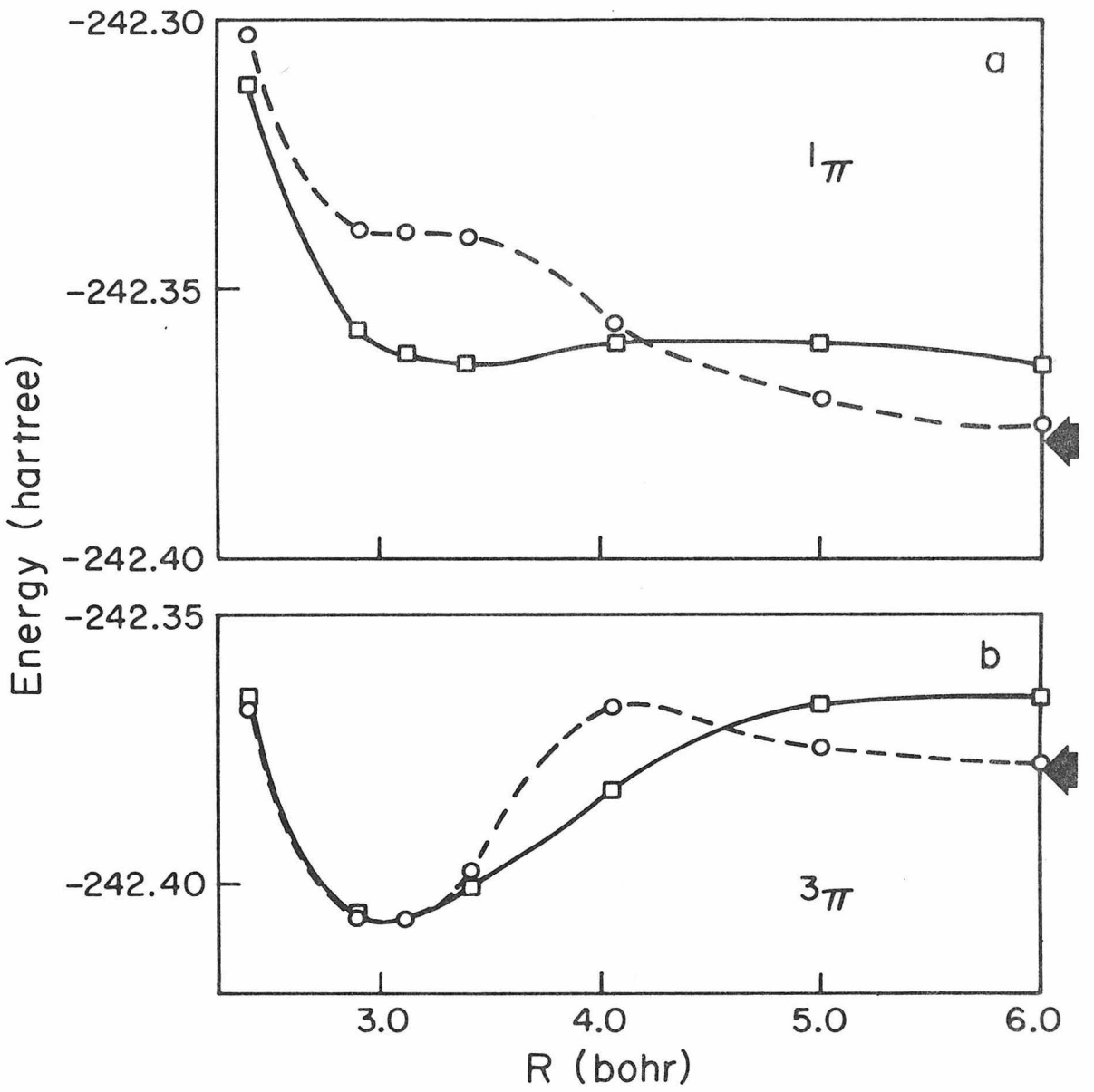

Figure 1. a) The $^1\Pi$ state (in hartrees) of AlH as a function of internuclear distance R (in bohr). The dashed line is the GVB calculation, the solid line the SOGVB. The arrow on the right is the asymptotic GVB limit of Al+H. b) The $^3\Pi$ state of AlH, with markings similar to 1a.

PROPOSITION 3

Abstract

It is proposed to calculate reaction cross sections for the collinear $F+H_2$ reaction with a classical trajectory method. We propose to test a new method to select initial and final conditions of the trajectories in a manner which should satisfy the principle of microscopic reversibility. Because microscopic reversibility is often violated in classical calculations, the proposed resolution should eliminate the ambiguity between "forward" and "reverse" reactions.

PROPOSITION 3

For many years[1] classical trajectory calculations have been a primary tool in understanding the dynamics of chemical reactions. Although exact quantum mechanical calculations have been made for simple atom-diatom reactive systems,[2] classical trajectory methods have already been applied[3] to systems which will always be inaccessible by exact quantum methods. Because classical mechanics is used so frequently to understand phenomena which are fundamentally quantum in nature, it is important to understand the range of validity of trajectory calculations.

Classical calculations are, by their very nature, an unsatisfactory means with which to understand chemical reactions. Rigorously, they can only ascertain whether a trajectory is reactive or not. Many recent trajectory calculations,[4-9] however, have gone further and calculated cross sections for transitions from specific initial vibrational and rotational states to specific final vibrational and rotational states. These so-called quasiclassical calculations are the subject of this proposition.

In order to calculate state to state transition probabilities for simple (atom-diatom) molecular systems, one must be somewhat arbitrary. Classically, vibrational and rotational quantum numbers (v and j, respectively) assume a continuous distribution. However, most trajectory calculations have been made with the assumption that the initial distribution of internal energy is quantal, even if no assumption was made for the final distribution. Then the internal energy of the products

is partitioned between rotation and vibration (which is not rigorous) and finally the continuous distribution of v and j are arbitrarily partitioned to yield only integer values for the quantum numbers. Although seldom acknowledged, this seemingly cavalier approach can lead to meaningless results.

It is not expected, of course, that quasiclassical calculations will be able to describe resonances and other grossly quantal phenomena. The hope is that they will be able to describe the broad features of cross sections or rate constants. At very low temperatures, tunneling is an important mechanism and classical mechanics cannot accurately calculate rate constants. If the temperature is too high, resonances may be important and classical mechanics is again inadequate. It is at medium temperatures ($\sim$ 500-1000°K) that classical rate constants should be most accurate.

In fact, classical mechanics often has great difficulty describing these general features. In a comparison of classical and quantum results on a collinear $H+H_2$ surface, Bowman and Kuppermann[10] found that the general shape of the probability curve was preserved, but that none of the quantum oscillations were reproduced. Oscillations in the classical results were found to have no correspondence to the quantum results. This is perhaps expected, because classical trajectories are not designed to give such detailed (quantum) information. They found that below 900°K the classical rate constants differed from the exact quantum results by more than a factor of 1.25. More importantly, they found that the reaction probability from the v = 1 state to the v = 2

state, P^R_{12}, had nonzero reaction probability at energies below the threshold of the v = 2 state. This bizarre behavior can be attributed to the method of assigning final quantum numbers. Briefly, if the vibrational energy spacing is given by $\Delta E_n = E_{n+1} - E_n$, the trajectory is assigned a vibrational quantum number n whenever its final vibrational energy E_v is in the range

$$E_n - \frac{1}{2}\Delta E_{n-1} \leq E_v \leq E_n + \frac{1}{2}\Delta E_n \qquad (1)$$

This rather arbitrary assignment obviously leads to the above difficulty. In a later paper, Schatz et al.[11] compare classical, semiclassical and quantum results for the collinear $F+H_2$ reaction. One of their more striking results was that microscopic reversibility does not hold for the classical results.[16] That is, transition probabilities, P^R_{ij}, for the forward reaction ($F+H_2 \rightarrow FH+H$) are not equal to transition probabilities, P^R_{ji}, for the reverse reaction ($FH+H \rightarrow F+H_2$). In fact, the energy dependence of the forward and reverse probabilities are not even similar. This result brings into question the validity of any classical trajectory calculations. A priori, one is unable to decide which calculation, the forward or the reverse, is to be considered the classical result. Yet many authors[5a,7] invoke microscopic reversibility without ascertaining its validity.

The origin of this problem is again the assignment of initial and final quantum numbers. The initial quantum conditions (for H_2) are assigned over a very small energy range (in fact, a delta function) and the final conditions (for HF) over an energy range with roughly

the vibrational energy spacing. For the reverse reaction the reverse assignments are made. This lack of symmetry between initial and final conditions will lead to different reaction probabilities, depending on whether forward or reverse trajectories are used.

It is the purpose of this proposition to suggest a method by which a more rational and symmetric assignment of initial and final quantum numbers can be made. By this method, microscopic reversibility will not be grossly violated and the simple ideas of classical mechanics will be retained without the additional complexities. With this new assignment it is proposed to study the collinear $F+H_2$ reaction (both forward and reverse), to test its accuracy both in self-consistency (microscopic reversibility) and as compared with quantum results for the same system. If the collinear classical results are improved, it is further proposed to test the method on 3-D trajectory calculations.

One of the most thorough explanations of the classical mechanical equations describing a reactive atom-diatom system is given by Karplus et al.[1] For collinear calculations the situation is much less complex because there is no need to consider choices for the impact parameter, the orientation of the diatom, or the initial rotational energy. Normally the atom-diatom system is assigned a total energy E, a vibrational state v (with corresponding energy E_v) and implicitly a translational energy $E-E_v$. After the atom and diatom have come together and separated (either from reaction or nonreaction), the internal energy does not correspond directly to any vibrational state. In fact, the internal energy is a continuous distribution. The normal procedure [given in

eq. (1)] utilizes all of the trajectories. It is the partitioning of trajectories into discrete vibrational states which allows one to study energy transfer processes. The procedure suggested herein is to accept only a small fraction of all trajectories as being correct; in particular those whose final internal energy is within some small envelope about the final vibrational energy eigenvalues. Likewise, the initial assignment of internal energy should be made not as a delta function, but as some distribution in an envelope about the desired eigenvalue. The disadvantage of this procedure is the increase in computation time. As the envelope is made smaller, the percentage of unacceptable trajectories increases. The primary advantage is that the straightforward ideas of classical mechanics are retained and microscopic reversibility may no longer be violated. To see the latter point, assume that the only acceptable trajectories were those which began and ended with vibrational energy corresponding exactly to vibrational states. If enough trajectories were run, that is, if the phase angle of each vibration were sufficiently sampled, then the results from trajectories of both the forward and reverse reactions must be identical. This is because each trajectory can be reversed and run until the initial conditions are obtained (assuming no numerical errors). Semiclassical methods,[13] which use such a search procedure, do not violate microscopic reversibility. The condition which is proposed is less severe and correspondingly less accurate. As shown by Miller,[12b] the final (continuous) quantum number is often a smooth function of initial conditions. Thus if one trajectory is found to satisfy the boundary

conditions, it should be much easier to find additional trajectories. In other words, the search process may not be as time consuming as it first appears.

Other workers have suggested alternative methods to resolve the microscopic reversibility problem. Miller[13] and Essen, Billing and Baer[14] suggest averaging over initial as well as final quantum numbers. This process satisfies microscopic reversibility and gives results which agree poorly with the quantum results of one system[13] (collinear $H + H_2$) and moderately well with the quantum results of another[14] (collinear $H + Cl_2$). It appears that in the latter system, total reaction rate constants are adequately predicted.

Another group[15] has suggested that the best way to decide whether to accept quasiclassical forward or reverse reaction calculations is to see which agrees more closely with the prediction of threshold behavior by semiclassical techniques. The method suffers from the fact that one must know the semiclassical results. Additionally, it does nothing to decide the relative worth of the forward and reverse results at energies well above threshold.

Although the method we propose requires more computation time than the usual quasiclassical methods, it is simpler than semiclassical methods and should afford a direct assessment of trajectory calculations. Collinear reactions are a particularly useful beginning point because they do not involve the complications of rotation and require far fewer trajectories than 3-D calculations to achieve "good statistics". Because it is not known a priori how small to make the energy envelopes, it may be necessary to make several calculations with

different envelopes until consistent results are obtained.

If the collinear calculations prove successful, it would be worthwhile to consider 3-D reactions. Because energy levels are more continuous in 3-D reactions (especially if the rotational spacing is small) violations of microscopic reversibility may not be so severe.

References

1. M. Karplus, R. N. Porter and R. D. Sharma, J. Chem. Phys. 43 (1965) 3259.
2. G. C. Schatz and A. Kuppermann, J. Chem. Phys. 65 (1976) 4668.
3. a) M. Karplus and M. Godfrey, J. Amer. Chem. Soc. 88 (1966) 5332.
   b) N. Sathymurthy and L. M. Raff, J. Chem. Phys. 66 (1977) 2191.
4. R. L. Jaffe and J. B. Anderson, J. Chem. Phys. 54 (1971) 2224.
5. a) J. T. Muckermann, J. Chem. Phys. 54 (1971) 1155.
   b) J. T. Muckermann, J. Chem. Phys. 56 (1972) 2997.
6. N. C. Blais and D. C. Truhlar, J. Chem. Phys. 58 (1973) 1090.
7. R. L. Wilkins, J. Chem. Phys. 57 (1972) 912.
8. D. L. Thompson, J. Chem. Phys. 57 (1972) 4170.
9. L. M. Raff, J. Chem. Phys. 60 (1974) 2220.
10. J. M. Bowman and A. Kuppermann, Chem. Phys. Lett. 12 (1971) 1.
11. a) G. C. Schatz, J. M. Bowman and A. Kuppermann, J. Chem. Phys. 63 (1975) 674.
    b) G. C. Schatz, J. M. Bowman and A. Kuppermann, J. Chem. Phys. 63 (1975) 685.
12. a) W. H. Miller, J. Chem. Phys. 53 (1970) 1949.
    b) W. H. Miller, J. Chem. Phys. 53 (1970) 3578.
13. W. H. Miller, J. Chem. Phys. 61 (1974) 1823.
14. H. Essen, G. D. Billing and M. Baer, Chem. Phys. 17 (1976) 443.
15. S. C. Leasure and J. M. Bowman, Chem. Phys. Lett. 39 (1976) 462.
16. There are other examples of this. For example: J. M. Bowman and A. Kuppermann, J. Chem. Phys. 59 (1973) 6524; J. M. Bowman, G. C. Schatz and A. Kuppermann, Chem. Phys. Lett. 24 (1974) 378.

PROPOSITION 4

Abstract

It is proposed to study the scattering of metastable argon (Ar*) off HBr in a crossed molecular beam and to detect the metastable. Cross sections would be measured at collision energies up to 2 eV in order to compare them with values extrapolated from 0.2 eV. In addition we propose a new method of detecting and distinguishing different metastable products from each other. In this way we can measure the branching rates of

$$Ar^* + HBr \longrightarrow Ar^* + HBr$$

and

$$Ar^* + HBr \longrightarrow (ArBr)^* + H$$

to see if the second reaction has contributed to scattered metastable intensities in previous experiments.

PROPOSITION 4

Recent experimental studies[1-8] of collisions of metastable rare gas atoms (lifetimes $\sim$1 sec[11]) with ground state atoms and molecules have demonstrated that the excited atoms behave similarly to ground state alkali atoms. Winicur, Fraites and Bentley[3] have used a crossed molecular beam apparatus to determine the well depth (ε) and position of the attractive well (r_m) between metastable argon (Ar*) and krypton. They found ε and r_m in this system to be the same as ε and r_m in K+ Kr (within experimental error), and substantially different from the parameters in Ar+ Kr. This behavior is not surprising. Rare gas atoms (Rg) form closed shell systems. An electron excited from a p orbital (1s in helium) to an outer s orbital will look much like the corresponding alkali atom with a Z number one larger. The effective radius of the metastable atom will be larger and it should behave as if it has one valence electron. Metastable helium behaves somewhat differently because of the large excitation energy. Often, collisions of He* with other ground state atoms or molecules will cause Penning ionization ($He^* + M \longrightarrow He + M^+ + e^-$) and associative ionization ($He^* + M \longrightarrow HeM^+ + e^-$). Recent cross molecular beam experiments,[5] however, have shown that elastic scattering of He* and Kr is much more similar to Li + Kr than He + Kr. Chen et al[7] report similar results for He* + Ne and He* + Ar. Other work[6] has focused on metastable rare gas atoms scattered by simple diatomics, in particular Ar^* + HBr. Although Ar^* was found to behave quite similarly to K, the experimental data were, in some respects ambiguous.

The usual approach in analyzing crossed beam results is to choose an analytical (parameterized) form for the interaction potential. Usually spherical symmetry is assumed. A quantum scattering calculation is made using this potential to see if the experimental data are reproduced. The parameters are changed iteratively until a good fit with experimental results is obtained. This was done for the Ar* + HBr potential,[6] and it was found that the wide angle data could not be reproduced, although an excellent fit was obtained for low angles. The sharp drop in observed intensity (relative to calculated intensity) was ascribed to quenching of Ar* by HBr.

The ambiguity in this study is twofold. First, the authors were unable to determine what fraction of the scattered events went by the pathway $Ar^* + HBr \longrightarrow (ArBr)^* + H$. The detector they used was only able to detect metastable particles without regard to mass, etc. Second, the authors used several functional forms for the threshold behavior of the the opacity function to describe the quenching cross sections. All of these forms fit the experimental data adequately at the four energies considered, even though at higher energies they behave quite differently.

To resolve these problems it is proposed to study the scattering of Ar* by HBr in a crossed molecular beam apparatus. Following previous workers, a supersonic beam of ground state Ar atoms is to be excited by electron impact and crossed at right angles by a collimated supersonic beam of HBr. We propose to use appropriate detectors which will ascertain whether some of the collisions proceed to (ArBr)* products. We further propose to study the process at higher collision energies so that the correct opacity function can be determined.

Previous quenching experiments have usually focused on the quenching of He(2^1S) and He(2^3S), both of which are metastable, by a ground state atom. In one crossed beam experiment Chen, Haberland Lee[7] studied He(2^1S,2^3S) + Ne and Ar. First they gathered data from He* (85% ^1S, 15% ^3S) + Ar and then they used a lamp to quench all the ^1S to ^3S and repeated the experiment. The difference between the two scattered intensities (normalized by beam composition) gave the ^1S scattered intensity. They used an iterative procedure to calculate a MSV (Morse-Spline-van der Waals) potential[9] from the low angle scattering data for each of the metastable states. They calculated the opacity function for quenching from the classical definition

$$O_b(b,E) = \frac{I_{el}[\theta(b)] - I_{ob}[\theta(b)]}{I_{el}[\theta(b)]} \qquad (1)$$

where I_{ob} is the observed intensity of He* and I_{el} is the expected elastic scattering intensity calculated from the fitted MSV potentials. This implicit one-to-one relationship between the scattering angle and the impact parameter is valid only for angles beyond the rainbow angle. The authors then calculated the total quenching cross section from

$$\sigma(E) = 2\pi \int_0^\infty O_b(b,E) b \, db \quad . \qquad (2)$$

They did not fit the opacity function to an analytical form (as a function of energy) because the experiment was done only at one energy.

In a more recent cross beam experiment, Fraites and Winicur[6] studied elastic collisions of Ar* and HBr. They fitted the low angle scattering data

to a relatively inflexible LJ(12,6) potential, calculated the elastic DCS, and ascribed the wide angle difference between the calculated and observed cross sections to quenching of Ar* to the ground state. They did the experiment at four different collision energies and found that the threshold angle for quenching decreased monotonically with increasing collision energies. They converted the opacity function (which is a function of the impact parameter, b) to one which is a function of the angular momentum quantum number, ℓ. The experimental data were fitted to

$$P(\ell,E) = \frac{P_{lim}}{1 + \exp[(\ell-L_c)/d]} \tag{3}$$

where P_{lim}, L_c, and d are all parameters. They further found that L_c and P_{lim} could be represented as logarithmic functions of the energy E. The quenching cross section is given by

$$\sigma(E) = \left(\frac{\pi h^2}{2\mu E}\right) \sum_{\ell} (2\ell+1)\, P(\ell,E) \tag{4}$$

where μ is the reduced mass of the system.

To get the energy dependence d was assumed to be constant, and $P_{lim} = 1.0$ whenever the function form gave values greater than unity. The quenching cross sections calculated from Eq. (4) fit the experimental cross section at four near-threshold energies quite well. This is not surprising since the opacity function has three adjustable parameters. Without any justification Fraites et al extrapolated the opacity function to 2.0eV (ten times the energy of the fitted points) and plotted the resulting extrapolated quenching cross section. The only previous work[18] (from a flowing pulse-discharge apparatus) gave

thermal quenching cross sections which differ from those of Fraites and Winicur by an order of magnitude. What we propose is to extend the experiment to higher collision energies and find the correct energy dependence of the quenching cross section.

The second half of this proposition is a new technique to distinguish between different types of metastables. In their study Fraites and Winicur detected metastables by the emission of secondary electrons from an electron multiplier. Ground state atoms below 5 eV do not produce secondary electrons and charged particles are deflected beforehand. In this way metastables are detected but are not distinguished from one another. In other words, they were unable to tell what contribution (if any) came from (ArBr)*. As previously noted, Ar* is very similar to K. This behavior extends to the ionization potential (IP) which is 4.3 eV [10] for K and 4.2 eV [11] for Ar* (as opposed to 15.7 eV [10] for Ar). This unique behavior allows us to use a surface-ionizer (SI) detector[11-13] to ionize the metastables. The resulting positive ions can be sent through a mass spectrometer, and thus metastables are distinguished by mass. The success of this technique depends on the low work function of the SI detector, a metal strip or foil which will ionize atoms or molecules of low IP. Thus, ground state atoms and molecules will not be detected. This technique should have wide application in the discrimination of various metastable atoms and molecules.

Finally, we suggest one further improvement. In determining the interaction potential between Ar* and HBr, one should use a Dunham-SPF[14,15] expansion. This potential form has been shown[16,17] to be much

more flexible than the usual Leonard-Jones potential, and will be a more accurate representation of the Ar*-HBr potential.

References

1. R. E. Olson, Chem. Phys. Lett. 13 (1972) 307.
2. D. H. Winicur and J. L. Fraites, J. Chem. Phys. 62 (1975) 63.
3. D. H. Winicur, J. L. Fraites and J. Bentley, J. Chem. Phys. 64 (1976) 1724.
4. D. H. Winicur, J. L. Fraites and J. Bentley, J. Chem. Phys. 64 (1976) 1757.
5. J. Bentley, J. L. Fraites and D. H. Winicur, J. Chem. Phys. 65 (1976) 653.
6. J. L. Fraites and D. H. Winicur, J. Chem. Phys. 64 (1976) 89.
7. C. H. Chen, H. Haberland and Y. T. Lee, J. Chem. Phys. 61 (1974) 3095.
8. D. H. Winicur and J. L. Fraites, J. Chem. Phys. 61 (1974) 1548.
9. P. E. Siska, J. M. Parson, J. P. Shafer and Y. T. Lee, J. Chem. Phys. 55 (1971) 5762.
10. Handbook of Chemistry and Physics, Chemical Rubber Publishing Co., Cleveland, Ohio, 1960, p. 2549.
11. D. H. Stedman and D. W. Setser, Progress in Reaction Kinetics 6 (1971) 193.
12. D. Greene, Proc. Phys. Soc. B 63 (1950) 876.
13. R. D. Rundel, F. B. Dunning, J. S. Howard, J. P. Riola and R. F. Stebbings, Rev. Sci. Instr. 44 (1973) 60.
14. J. L. Dunham, Phys. Rev. 41 (1932) 721.
15. G. Simons, R. G. Parr and J. M. Finlan, J. Chem. Phys. 59 (1973) 3229.
16. R. W. Bickes, Jr. and R. B. Bernstein, J. Chem. Phys. 66 (1977) 2408.
17. M. Keil and A. Kuppermann (in preparation).

18. L. G. Piper, J. E. Velazco and D. W. Sester, J. Chem. Phys. 59 (1973) 3323.

PROPOSITION 5

Abstract

It is proposed to study the rate of collisional deactivation of vibrationally excited HF by He in a crossed molecular beam apparatus. The HF beam is to be excited by an HF laser. Beyond the scattering center the vibrational populations of HF are to be determined by laser induced fluorescence. From this information the relative rates of deexcitation from $v = 2$ to $v = 1$, $v = 1$ to $v = 0$, and $v = 2$ to $v = 0$ can be determined.

PROPOSITION 5

A chemical laser is successful if the pumping of excited vibrational states is rapid compared with the rate of spontaneous or collisional deactivation. In order to fully understand the operation of a chemical laser, one must study the various deactivation processes that may take place. In the $F + H_2$ system, the first three excited vibrational states of HF are populated, and lasing may take place from each of them ($\Delta v = 1$). The HF may be collisionally deactivated by H_2, H, F_3, HF or buffer gases. Reactions with H or F may leave the products in the ground state. A definitive study of deactivation processes in HF may lead to insights as to why (or why not) other chemical systems produce lasing.

Deactivation (or relaxation) processes in diatomics have been extensively studied by other workers. The usual approach is to mix two or more gases (one of which has been vibrationally excited) in a flow system and observe the laser induced fluorescence several centimeters downstream, by which time many collisions have taken place. By varying the partial pressures one can deduce the relaxation rates.

Laser induced fluorescence has been widely used as a tool for determining final state distributions of reaction products. In a study of vibrational populations of OH resulting from $H + NO_2$, Brophy et al[1,2] used a dye laser to excite the various vibrational levels of OH to an excited electronic state. The resulting fluorescence is in the ultraviolet and relatively easy to detect. A similar method (excitation to a higher electronic state and observing the fluorescence) has

been used to monitor the products in the photolysis of ICN[3] and C_2N_2.[4]

In hydrogen halide systems the technique is more difficult to apply because the vibrationally excited diatomics do not have a higher bound electronic state to which they can be excited. One must induce fluorescence directly to lower vibrational states. The fluorescence photons can be monitored directly by commercially available IR detectors. Unfortunately, these are generally very noisy unless cooled to low temperatures. This technique has been used to measure vibrational relaxation of DCl (v = 1) by Cl and Br and HBr (v = 1) by Br,[5] and to monitor the reaction of HCl (v = 1)+ O,H.[6] Deactivation of HF (v = 1) or DF (v = 1) by CO_2,[7,9] hydrogen halides,[8-10,19] $H_2(D_2)$,[11] hydrogen atoms,[12-16] polyatomic molecules,[17] and rare gases[18,31,32] have all been studied in flow systems. In these studies the rate constants for deactivation by rare gas atoms are generally acknowledged to be much smaller than those for deactivation by various diatomics. Some workers[31] could only determine upper limits for the rate constants, while others[18,32] had conflicting results. Room temperature rate constants for deactivation of DF (v = 1) by H_2[10,11] differ by as much as a factor of 6.7, and those for HF (v = 1) deactivation by H[12,15,16] differ by a factor of 100. The reported errors in these experiments range from 10% to 40%. Experimental relaxation rates of HF (v = 1) by HF (v = 0)[16,20] differ by over an order of magnitude. Efforts to measure deactivation from higher vibrational states[13] have been largely unsuccessful. Large errors arise from unknown wall effects, uncertain temperatures (in the case of shock tubes), uncertain pressures, and competing reactions whose rate constants

are poorly known. In many cases, wall effects in flow systems are not taken into account.

Theoretical studies usually have been limited to deactivation of HF or DF by various atoms.[22-25,33] These studies are of limited value because the methods have generally been classical trajectories and the surfaces used have since been shown to be grossly incorrect.[14,21] Calculated vibrational deactivation rate constants of HF are at least an order of magnitude larger than experimental rate constants. An interesting result of these classical calculations and other collinear quantum calculations[26,27] is that multiquantum collisional deactivation transitions are as probable as single quantum transitions, even when the potential surfaces are very different.

This phenomenon has not been observed experimentally. Previous experiments[13,19,28] which examined deactivation from higher vibrational states of HF used kinetic models which allowed only $\Delta v = 1$. It would be interesting, then, to measure experimentally multiquantum deactivation rate constants. The flow systems reviewed above can only measure bulk rate constants and it is often difficult to make them quantitative. A crossed beam experiment, which measures deactivation rate constants from single collisions, has the potential for more quantitative results. Laser induced fluorescence is ideally suited for such an experiment because it allows population measurements in very dilute concentrations.

Because of the aforementioned theoretical work, the most interesting system would be D + HF (v). However, it would first be instructive to try something simpler, like He + HF (v). The advantage would be an

easily generated, clean beam, whereas the former reaction would require some sort of D generation and knowledge of other relaxation rate constants [i.e., D_2+ HF (v)].

Therefore, to determine whether multiquantum transitions are important in the collisional relaxation of diatomic molecules, we propose to study the inelastic scattering of HF and He in a series of experiments in a crossed molecular beam apparatus. In order to determine temperature dependent rate constants, the experiments should be run at several collision energies. There are, in effect, two experiments. The first will entail exciting the HF beam to v = 1, which is subsequently scattered by He, and measuring the resultant vibrational populations. In the second experiment, HF is to be excited to v = 2, scattered by the He and again the final vibrational populations measured. The experiments are to be run at energies low enough so that excited vibrational levels of HF are not collisionally pumped.

HF is to be excited to v = 1 by a pulsed HF laser. This technique has been used in nearly all of the flow systems reviewed above and in some crossed beam experiments.[29] For the second experiment HF can be excited to v = 1 and v = 2 by absorption of radiation from an HF laser operating on (1-0) and (2-1) transitions. This technique has been used by several workers[13,19,28,30] to study excited state deactivation.

The detection system has been used previously, but primarily in flow systems and shock tubes. By irradiating the scattered products with a low resolution HF laser, $\Delta v = 1$ fluorescence can be induced. The resulting IR radiation is collected over a large solid angle and the

photons counted by a commercially available InSb IR detector. Because these detectors are "noisy", it is necessary to cool them to liquid nitrogen temperatures. Even then the signal-to-noise (S/N) is about 1/1 or worse. One group[5] has cooled the detector to liquid He temperatures and achieved S/N ratios of 10/1 before any signal averaging. In spite of the added difficulty of a liquid He cooling system, this is the suggested route for this experiment.

Pulsing the laser is in principle equivalent to chopping the HF beam. However, the laser pulse is generally much better defined and allows a natural way to detect scattered products. The detector should have a gate which opens only when there is fluorescence to be detected, and for an equal time when there is no fluorescence. The modulated laser output, together with signal averaging, may make it possible to increase S/N to as high as 100/1, which is obtainable in bulk experiments.

The first experiment will measure the fluorescence from HF (v = 1) which has not decayed via collisions. The second experiment will measure fluorescence from v = 2 and v = 1. Because v = 1 is being populated as well as depopulated (v = 2 $\rightarrow$ v = 1, v = 1 $\rightarrow$ v = 0), the difference between the fluorescence v = 1 in the two experiments will give the relative rate of v = 2 $\rightarrow$ v = 1. Because fluorescence of v = 2 will give the relative rate of depopulation of v = 2 (to v = 1,0) subtraction of the v = 2 $\rightarrow$ v = 1 rate will give v = 2 $\rightarrow$ v = 0 rate. Implicit in this is a calibration which gives the relative populations of v = 0,1,2 before scattering, detector efficiency, fluorescence efficiency, etc.

This experiment could be extended to v = 3 levels, and if one were particularly ambitious, to deactivation by D atoms. This last experiment would be especially useful in understanding the HF laser which is pumped by

$$F + H_2 \rightarrow HF(v = 1,2,3) + H$$

The proposed experiments are complex but all of the techniques involved have been used previously. The type of information which can be gathered should further the understanding of the relative importance of various deactivation processes in chemical lasers.

References

1. J. H. Brophy, J. A. Silver and J. L. Kinsey, J. Chem. Phys. 62 (1975) 3820.
2. J. A. Silver, W. L. Dimpfl, J. H. Brophy and J. L. Kinsey, J. Chem. Phys. 65 (1976) 1811.
3. M. J. Sabety-Dzvonik and R. J. Cody, J. Chem. Phys. 66 (1977) 125.
4. R. J. Cody and M. J. Sabety-Dzvonik, J. Chem. Phys. 66 (1977) 2145.
5. R. G. Macdonald and C. B. Moore, J. Chem. Phys. 65 (1976) 5198.
6. D. Arnoldi and J. Wolfrom, Chem. Phys. Lett. 24 (1974) 234.
7. R. R. Stephens and T. A. Cool, J. Chem. Phys. 56 (1972) 5863.
8. J. L. Ahl and T. A. Cool, J. Chem. Phys. 58 (1973) 5540.
9. J. F. Bott and N. Cohen, J. Chem. Phys. 58 (1973) 4539.
10. J. J. Hinchen, J. Chem. Phys. 59 (1973) 233.
11. J. F. Bott, J. Chem. Phys. 61 (1974) 2530.
12. R. F. Heidner III and J. F. Bott, J. Chem. Phys. 63 (1975) 1810.
13. R. F. Heidner III and J. F. Bott, J. Chem. Phys. 66 (1977) 2878.
14. J. F. Bott, J. Chem. Phys. 65 (1976) 1976.
15. G. P. Quigley and G. J. Wolga, Chem. Phys. Lett. 27 (1974) 276.
16. M. A. Kwok and R. L. Wilkins, J. Chem. Phys. 60 (1974) 2189.
17. J. F. Bott and N. Cohen, J. Chem. Phys. 61 (1974) 681.
18. J. F. Bott and N. Cohen, J. Chem. Phys. 55 (1971) 3698.
19. R. M. Osgood, Jr., P. B. Sackett and A. Javan, J. Chem. Phys. 60 (1974) 1464.
20. J. F. Bott, J. Chem. Phys. 57 (1973) 96.
21. a) C. F. Bender, B. J. Garrison and H. F. Shaefer III, J. Chem. Phys. 62 (1975) 1188

b) W. R. Wadt and N. W. Winter, "Ab Initio Potential Surface Calculations for the H + H_2O and H + HF Hydrogen Atom Exchange Reactions" 12th International Symposium on Free Radicals, Laguna Beach, CA, January 1976.

22. D. L. Thompson, J. Chem. Phys. 57 (1972) 4164.
23. D. L. Thompson, J. Chem. Phys. 57 (1972) 4170.
24. R. L. Wilkins, J. Chem. Phys. 58 (1973) 3038.
25. R. L. Wilkins, J. Mol. Phys. 29 (1975) 555.
26. G. C. Schatz and A. Kuppermann, Proceedings of Army Symposium on High Energy Lasers: Current Problems in High Energy Transfer Lasers (U.S. Army Missile Command, Redstone Arsenal, Alabama, August 1976), p. 132-142.
27. J. P. Dwyer, Ph.D. Thesis, California Institute of Technology, Pasadena, CA 1977.
28. J. F. Bott, J. Chem. Phys. 65 (1976) 4239.
29. J. G. Pruett and R. N. Zare, J. Chem. Phys. 64 (1976) 1774.
30. J. J. Hinchen and R. H. Hobbs, J. Chem. Phys. 63 (1975) 353.
31. J. K. Hancock and W. H. Green, J. Chem. Phys. 57 (1972) 4515.
32. L. S. Blair, W. D. Breshears and G. L. Schott, J. Chem. Phys. 59 (1973) 1582.
33. K. Smith, S. Ormonde, A. R. Davies and B. W. Torres, J. Chem. Phys. 61 (1974) 2643.